TO THE LORD

"For He will complete what He appoints for me"

QUANTUM CHEMICAL STUDIES OF INTERMEDIATES IN NITROSAMINE CARCINOGENESIS

A Thesis

presented for the degree of

Doctor of Philosophy

in the Faculty of Science of the

University of St. Andrews

by

Christopher Arthur Reynolds, B. Sc.

St. Leonard's College, 1985

I, Christopher Arthur Reynolds hereby certify that this thesis which is approximately 60,000 words in length has been written by me, that it is the record of work carried out by me, and that it has not been submitted in any previous application for a higher degree

date 4th September 1985 signature of candidate

C.A. Reynolds

I hereby certify that the candidate has fulfilled the conditions of the Resolution and Regulations appropriate to the degree of Doctor of Philosophy of the University of St. Andrews and that he is qualified to submit this thesis in application for that degree.

date 4th September 1985 signature of supervisor

C. Thomson

I was admitted as a research student under Ordinance No. 12 on the 6th of December 1982 and as a candidate for the degree of Ph. D. in February 1984; the higher study for which this is a record was carried out in the University of St. Andrews between 1982 and 1985

date 4th September 1985 signature of candidate

C.A. Reynolds

ACKNOWLEDGEMENTS

I would like to thank my supervisor, Dr. Colin Thomson, for the opportunity of carrying out this fascinating research project, for his help, direction and encouragement throughout my time as a research student.

I would also like to acknowledge the help and advice received from both Dr. John Ball and Mr. Colin Edge.

I would also like to thank the National Foundation for Cancer Research, and its supporters, for the award of a research studentship, for the opportunity to attend the Faraday Symposium held in Cambridge in 1984, and also for financial help in attending the 25th International Symposium on Quantum and Quantum Pharmacology, held in Florida in March 1984; I would also like to thank the organisers of this symposium and ICI for the award of a travelling fellowship.

I would also like to thank Prof. J. Pople for providing copies of Gaussian 80 and Gaussian 82, and Dr. Stephen Bell for a copy of MINIT and for several long discussions on the location of transition structures. I would like to express my appreciation to Dr. Butler and Dr. MacCallum of the Chemistry Department and Dr. Goodlad and Dr. Hunter of the Biochemistry Department for helpful discussions and to Mrs. Anne Hughes for preparing diagrams.

Acknowledgements must be given to the University of St. Andrews Computing laboratory for the allocation of computing facilities; in particular to Dr. John Henderson and Dr. Malcolm Bain for advice with programming and to the operators for providing a most helpful service.

Lastly, I would like to thank my wife for her support and encouragement throughout the last three years, and particularly for her help in preparing diagrams and for spending many long hours proofreading.

ABSTRACT

N-Nitrosamines are chemical compounds which are frequently carcinogenic. They may be formed from naturally occurring precursors under a variety of conditions. Despite much experimental study, many of these intermediates in nitrosamine carcinogenesis have not been identified; this thesis describes quantum chemical calculations on these intermediates.

The majority of the calculations have been performed using ab-initio self-consistent-field gradient techniques with a 4-21G split valence basis set. Some calculations have used polarised basis sets; estimates of the correlation energy have also been made. The strategy has been to locate stationary points on the potential energy surfaces for proposed intermediates; the calculation of energies of reaction and energy barriers has made a critical evaluation of alternative pathways possible. A large number of fully optimised ab-initio transition structures are reported.

The nitrosating agent in acidic solution - the nitrous acidium ion - has never been observed. However, calculations show that it may exist as a number of different structures. The nitrosation of tertiary amines by the nitrous acidium ion is discussed. Enzymic activation of nitrosamines usually yields an α-hydroxynitrosamine; the calculations suggest that this decomposes either to the diazohydroxide or to the diazotate. The interconversion of monomethylnitrosamines and methyldiazohydroxides is studied. It is proposed that both the α-hydroxynitrosamines and the diazohydroxides may have sufficient stability to diffuse across the cell. The nature of the alkylating agent is discussed and reasons for reconsidering the diazoalkane are presented. Acid catalysis may be important in the formation of the diazohydroxide. Experiments are suggested which may shed light upon the nature of the alkylating agent.

CONTENTS

INTRODUCTION

It is almost thirty years since nitrosamines were first shown to be carcinogenic [1]. However, despite an enormous amount of research, many of the steps involved in the formation and metabolism of nitrosamines are not known; this is because many of the intermediates have not been identified.

It is the philosophy of the National Foundation for Cancer Research, and particularly of its scientific director, Albert Szent-Györgyi, that progress in fighting cancer will come through basic research into the molecular aspects of biology. Consequently, this study was initiated to shed light on the molecular mechanisms of nitrosamine carcinogenesis. The method of quantum mechanics has been used because it allows for the theoretical study of molecules which are too reactive to be studied experimentally.

The use of theoretical calculations in cancer research has been reviewed by Scribner [2]. He warns of the dangers of using methods which can be applied to molecules only in situations remote from those encountered in the cell. However, he does also point to the value of such calculations, particularly if they can suggest further experiments.

The first chapter in this thesis is an introduction to the chemistry of the formation and metabolism of nitrosamines. In particular, the areas in which there are uncertainties are identified. The second chapter describes the theoretical methods used and outlines many of the approximations which have been made in the course of this work. In the following chapters the results are presented and discussed; some suggestions for further experimental investigations are made. In the final chapter the work is summarised, and the limitations of the results are discussed. Some proposals for further study are also presented.

Although this thesis is concerned with nitrosamine carcinogenesis,

it should also be of interest to many chemists, particularly those with interest in theoretical chemistry, because a large number of fully optimised transition structures have been located.

CHAPTER 1

ASPECTS OF NITROSAMINE CHEMISTRY RELEVANT TO CARCINOGENESIS

1 INTRODUCTION

N-Nitrosamines were first discovered to be carcinogenic by Barnes and Magee in 1956 [1]. Since then there has been an enormous amount of work on nitrosamines to discover how they may be formed and the exact extent of the risk to humans. Their transformation in living creatures to yield the ultimate carcinogen, which is responsible for tumour initiation, has also been the subject of much research. Despite this vast amount of research there are still a number of questions which have not been answered. The theoretical work described in this thesis was initiated in an attempt to shed light on some of these questions. In this chapter an overview of the chemistry of the formation and metabolism of nitrosamines is given and the areas of uncertainty are pointed out. Although this thesis is primarily concerned with nitrosamines, nitrosamides and nitrosoureas have similar properties and their chemistry is discussed where relevant.

2 THE FORMATION OF NITROSAMINES

The usual precursors of nitrosamines are amines and nitrite; nitrosamides and nitrosoureas are formed from the corresponding amides and ureas. A common belief that only secondary nitrosamines can be nitrosated has been refuted many times. Initially, however, the nitrosation of secondary amines by a number of different nitrosating agents is discussed. Nitrite itself is not a nitrosating agent and has to be converted into a carrier of the nitrosonium ion, NO^+ [3]. The nitrosation of other amines, especially tertiary amines, is also discussed.

2.1 Nitrosation in Acidic Solution

In mildly acidic solution (pH 2 - 5), the rate of formation of nitrosamines follows (1.1) for all but the most basic amines.

$$d[R_2NNO]/dt = k[R_2NH][HNO_2]^2 \qquad (1.1)$$

This has led to N_2O_3 being suggested as the nitrosating agent

$$2HONO \longrightarrow N_2O_3 + H_2O \qquad (1.2)$$

The equilibrium constant for reaction (1.2) is $3.02 \times 10^{-3} lmol^{-1}$ [4]. Increasing the acidity increases the concentration of nitrosating agent, but also decreases the amount of unprotonated amine that can react; thus a maximum rate is found at pH = 3.4 [3,4,5,6].

In more acidic solutions, for weakly basic amines such as aromatic amines, amides and ureas (which are not protonated even in strongly acid solution and which are too unreactive to combine with N_2O_3), a different mechanism applies [3,4,5,6].

$$d[R_2NNO]/dt = k[R_2NH][HNO_2][H^+] \qquad (1.3)$$

Aromatic amines may react by attack on the ring, followed by rearrangement [3,4]. In very strong acid, NO^+ itself is a possible nitrosating agent [7], but the nitrosating agent is generally referred to as the nitrous acidium ion and thought to have the structure $H_2NO_2^+$, although it has never been observed experimentally [4]. The general scheme for the above two mechanisms is shown below

$$NO_2^- + 2H_3O^+ + Y \longrightarrow [NOY]^+ + 3H_2O \qquad (1.4)$$

$$R_2NH + H^+ \rightleftharpoons R_2NH_2^+ \qquad (1.5)$$

$$R_2NH + NOY \longrightarrow R_2NNO + HY \qquad (1.6)$$

(where Y is NO_2^- for (1.1) and H_2O for (1.3))

2.2 Nitrosation by Nitrogen Oxide Gases

Just as N_2O_3 derived from NO_2^- is thought to be the nitrosating species in mildly acidic solution, so nitrogen oxide gases including N_2O_3 can nitrosate in the gas phase, in organic solvents and in acid, neutral or alkali aqueous solutions.

Nitric Oxide (NO) is inactive in the absence of air, although under aerobic conditions it can form N_2O_3. Catalysis by I_2 produces NOI, a very reactive nitrosating agent. Gaseous NOCl is also a strong nitrosating agent. Many metal ions can form complexes with NO which can act as nitrosating agents [3,4]; Ag^+ acts as a catalyst by abstracting a hydrogen from R_2NH to form $R_2N^\cdot$ which can react directly with NO, itself an odd-electron species [4]. In simulated urban atmospheres, nitrosamine formation has been attributed to photo dissociation of nitrous acid [3].

$$\text{HONO} \xrightarrow{h\nu} \text{NO}^\cdot + \text{OH}^\cdot \xrightarrow{R_2NH} H_2O + R_2N^\cdot \xrightarrow{NO} R_2NNO \quad (1.7)$$

Dinitrogen trioxide, N_2O_3, however requires no catalyst. In the gas phase and in organic solutions it may react by a radical mechanism involving NO and NO_2 [3,4]. In aqueous alkali, hydrolysis of N_2O_3 also occurs (1.8) but nitrosation is much faster [3,4].

$$N_2O_3 + 2OH^- \longrightarrow 2NO_2^- + H_2O \quad (1.8)$$

In moist air, N_2O_3 will exist as two different isomers, $ONNO_2$ and ONONO, and will be in equilibrium with NO, NO_2, HNO_2 and H_2O [3,4]. No nitramines (R_2NNO_2) are formed from N_2O_3 so the reaction can be considered to involve a nitrosonium ion carrier, NOY. N_2O_4 is similar to N_2O_3 in its reactions, except that nitramines are formed along with nitrosamines; this is due to the equilibrium of $ONONO_2$ with O_2NNO_2.

2.3 Catalysis

Anionic and nucleophilic molecules can act as catalysts in acidic solution by increasing the concentration of NO^+ carriers and by forming nitrosating agents which are more powerful than N_2O_3 [3]. The order of the catalytic effect is $SCN^- > I^- > Br^- > Cl^- > PO_4^-$. These ions also catalyse the acid-catalysed denitrosation of nitrosamines - the reverse of (1.6), but they cannot catalyse the nitrosation of amides ($RCONHR'$) [3,4]. Certain transition metal complexes can react with nitrite to form powerful nitrosating species [8].

The nitrosation reaction in neutral or alkali solution can be catalysed by certain aldehydes and ketones [9]. Simple alcohols can have an inhibitory effect as the nitrite esters, e.g. EtONO, are formed; these are poor nitrosating agents, but 1,2-diols and related compounds can act as catalysts under neutral or alkali conditions.

These results are very relevant to living systems as SCN^- is found in saliva, Cl^- in the stomach, and carbohydrates can function as 1,2-diols [3]. Certain surfactants can catalyse the formation of longer chain dialkylnitrosamines in the micelle phase [10].

2.4 Inhibition of Nitrosamine Formation

Blocking N-nitrosamine formation is one possible strategy in preventing N-Nitrosamine carcinogenesis [11]. For basic nitrosamines, increasing acidity converts the amine substrates to their unreactive conjugate acid, while reducing the acidity converts nitrosating agents to inactive NO_2^-. However, there are drawbacks with these methods, especially in a situation containing many different amines and catalysts. Possibly more useful in this context are scavengers which convert HNO_2 to N_2 or NO, or which bind the NO^+ irreversibly.

One of the most useful molecules in this respect is ascorbic acid (vitamin C) which is effective over a range of pH in aqueous media, as both the free acid and anion can reduce NOY to NO [3]. Another effective agent is α-tocopherol (the chief form of vitamin E), which is most active in the lipid phase, where the solubility of nitrogen oxides is highest [12]. Such reducing agents have to be added in excess to prevent reoxidation. A number of antioxidants contained in foods are also effective in blocking N-nitrosamine formation [12].

2.5 Transnitrosation

Where the N-NO bond is weakened by neighbouring electron withdrawing groups, the Nitroso group can be transferred to other amines; this occurs under acid conditions and probably proceeds via an N-protonated nitrosamine. This is likely with aromatic amines and ureas. Thus even inactive or weakly carcinogenic nitrosamines can cause concern, as their denitrosation can lead to the formation of strongly carcinogenic nitrosamines [3]. Both direct and indirect mechanisms are involved; nucleophilic catalysis implies an indirect denitrosation mechanism via NOY, but in certain solvents free radical mechanisms have been suggested [13].

2.6 The Nitrosation of Primary Amines

Although primary amines usually undergo deamination to produce alcohols, the reaction produces an alkylating agent as an intermediate; if this intermediate is not hydrolysed, it can combine with unreacted amine to form a secondary amine. The mechanism then proceeds as for secondary amines [3,14].

$$RNH_2 + NOY \longrightarrow RNHNO + HY \qquad (1.9)$$

$$RNHNO \longrightarrow R^+ + N_2 + OH^- \qquad (1.10)$$

$$RNH_2 + R^+ \longrightarrow R_2NH + H^+ \qquad (1.11)$$

2.7 The Nitrosation of Tertiary Amines

Although the failure of tertiary amines to react with nitrous acid is a test for tertiary amines, tertiary amines can readily be nitrosated under mildly acidic conditions at physiological temperatures [15 - 23]. This is cause for concern because tertiary and quaternary amines are more abundant in animal and plant tissue than are secondary amines [16]. The extent of the reaction will depend on the conditions, but usually oxidative dealkylation results in the formation of roughly equal amounts of nitrosamine and aldehyde or ketone, provided that an α-hydrogen is present [17]. The rate has been found to follow (1.12) [15].

$$d[R_3N]/dt = k[R_3N][HONO][H^+] \qquad (1.12)$$

Various mechanisms have been proposed [17,18]

a) $$R_2N\text{-}CHR_2 + NO^+ \longrightarrow R_2\dot{N}^+\text{-}CHR_2 + NO \qquad (1.13)$$

$$R_2NNO \longleftarrow R_2NH + R_2C^{\cdot +} \longrightarrow R_2CO$$

b) $$R_2N\text{-}CHR_2 \longrightarrow \left[R_2N(CHR_2)(NO)\right]^+ \longrightarrow R_2N{=}CR_2^+ + HNO \qquad (1.14)$$

$$R_2N{=}CR_2^+ \xrightarrow{H_2O} R_2NH_2^+ + R_2CO$$

$$HNO \longrightarrow 1/2H_2O + 1/2N_2O$$

$$R_2NNO \longleftarrow R_2NH_2^+ + R_2CO$$

c) $R_2N(^{+}CHR_2)(NO) \xrightarrow{OH^-} R_2NNO + R_2CHOH \xrightarrow{HNO_2} R_2CO + N_2O/NO$ (1.15)

d) $R_2N\text{-}CHR_2 \xrightarrow{NO^+} R_2\overset{+}{N}{=}CR_2 + NOH$ (1.16)

e) Omega-1 radical pathway for side products such as alcohols [18].

$n\text{-}Bu_3NNO^+ \rightarrow n\text{-}Bu_3\overset{+}{N}\cdot \rightarrow n\text{-}Bu_2N(H)CH_2CH_2\dot{C}HCH_3^+ \rightarrow$ products (1.17)

Mechanism (a) is not supported by the stoichiometry in the evolved gases found by Smith and Loeppky [17]. Loss of a hydride (d) by NO^+ has been eliminated by the stoichiometry for the nitrosation of mixed tertiary amines RR'R"N, which favours (b) proceeding via a cis-elimination of NOH. Reactions of type (c) have been reported [19]. The preferred products can be predicted from the Newman projections (see I and II), which minimise the steric strain. The products from $(CH_3)_2(PhCH_2)NNO^+$ are preferentially derived from (I), giving $H_2C{=}NCH_3CH_2Ph$ rather than $PhCH{=}N(CH_3)_2$.

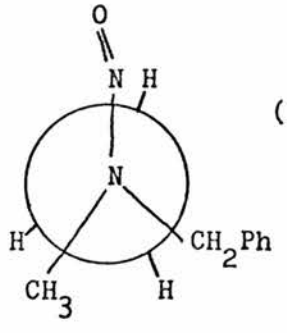

(I)

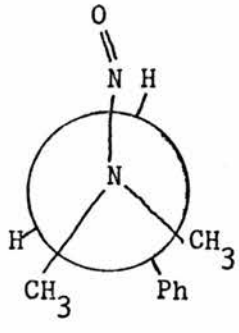

(II)

In certain circumstances, tertiary amines form nitrosamines faster than do secondary amines; these secondary amines might otherwise have been considered as intermediates produced by hydrolysis of the enamines $R_2C{=}NR_2^+$. Thus the reaction may proceed by direct attack of nitrite on

the enamine.

2.8 The Nitrosation of Quaternary Amines

This does not proceed as rapidly as for tertiary amines. Some researchers have found quaternary amines inactive [17], whereas others have observed nitrosamine formation [16]. Tertiary amine N-oxides, which occur in fish, are easily nitrosated [17,23]; possible mechanisms are shown below

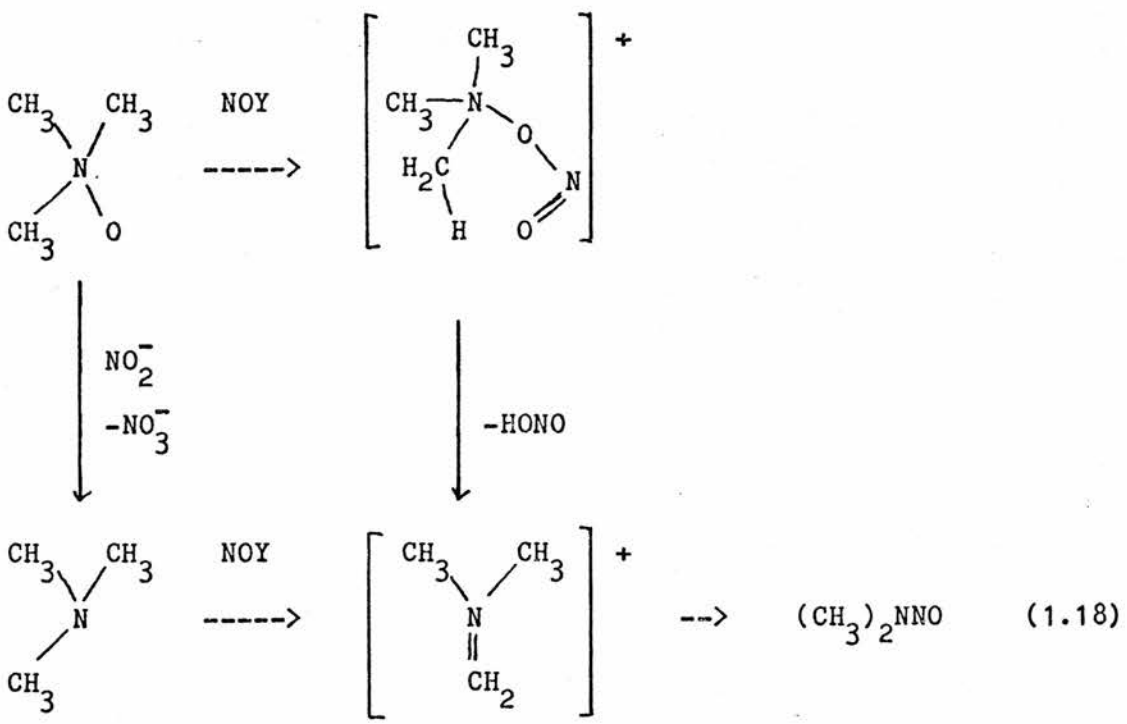

3 HUMAN EXPOSURE TO NITROSAMINES

3.1 Sources of Human Exposure to Exogenous N-Nitrosamines

Exposure to nitrosamines may be of two kinds; exogenous exposure to nitrosamines in the environment and endogenous exposure resulting from the *in vivo* nitrosation of amines.

The most serious incidents of exogenous exposure probably apply where nitrosamines are preformed in the workplace. This is most serious in processes which produce or use amines, such as in the rubber, leather-tanning and metal-working industries. The concentrations of volatile nitrosamines can be of the order of 100 µg/Kg for solids, 100 µg/m^3 for air and 100 µg/l for solutions [24,25].

The greatest non-occupational exposure to nitrosamines comes from tobacco use [25]. Here the nitrosamines are formed partly during processing of tobacco and partly during pyrolysis; they may also be formed *in vivo*. The nitrosamines formed during pyrolysis are in part derived from the nitrate content of tobacco. The nitrosamines are formed partly from residues of agricultural chemicals and partly from tobacco-specific alkaloids, especially nicotine, which is a tertiary amine [26,27].

Various foods can also contain volatile nitrosamines. This appears to be especially true of foods such as cured meat products which contain nitrite as a preservative. Frying bacon does not appear to increase the dimethylnitrosamine content, which probably evaporates, but it does increase the amount of the less volatile N-nitrosopyrrolidine, partly due to increased synthesis at higher temperatures. Dimethylnitrosamine has been found in beer, formed by the drying of malt by direct kilning; the nitrosating agents were found

to be nitrogen oxides formed in the flames [24].

Ethanolamines are used as emulsifiers in many cosmetic and toiletry formulations; as a result nitrosamine contamination up to about 50ppm has been found. The significance of these results lies in the fact that nitrosamines can permeate skin quite freely [24]. There is also concern about drugs which contain secondary or tertiary amino groups, as they can often be administered in quite large doses, up to 500mg, and for long periods of time. In tests, most such drugs have not produced a significant incidence of tumours in test animals, but a small number have [28]. With such drugs, the nitrosamines may be preformed during storage [24] or *in vivo* following administration.

In many areas legal efforts are being made to reduce nitrosamine exposure, for example in pesticides [24].

3.2 Estimating the Risk to Humans of Exposure to Nitrosamines

Some early reports of nitrosamines in human subjects (1977 - 1980) have been refuted by the development of more rigorous analytical procedures for volatile nitrosamines, which were introduced about 1982. However, nitrosamines have short life-times in living creatures, so the total concentration is difficult to assess [29]. Various workers have tried to estimate the risk to humans from nitrosamines by calculating the intake of exogenous nitrosamines, and estimating the extent of endogenous formation from analytically determined levels of nitrite and amines. Some of these models are more sophisticated than others, taking into account the effect of known catalysts and inhibitors of nitrosamine formation [6,29,30].

There appears to be consensus of opinion, recorded in the discussion of the latter two articles [29,30], that such models predict a falsely low risk of carcinogenesis from nitrosamines due to several

factors. Firstly, the models apply to an average population, whereas individual differences, such as the hypoacid stomach or bladder infections, may play a key role in initiating carcinogenesis by increasing the concentration of nitrosating agent. Secondly, the risk is evaluated from our knowledge of the distribution of volatile nitrosamines, simply because these are the only ones for which reliable analytical procedures exist; thus the risk due to non-volatile nitrosamines, nitrosamides and nitrosoureas is unknown and totally ignored. Thirdly, catalysis becomes very important at low levels of nitrite, as the rate of reaction is proportional to the concentration of nitrite, rather than the concentration squared; there may be many unknown catalysts. Finally, the effect of low levels of carcinogens on a population for a long period of time is not known, even though the effect of higher concentrations on experimental animals for a shorter period is known.

Despite an enormous amount of work, the real risk to humans from nitrosamine carcinogenesis is not known. Many workers in the field are greatly concerned that such models may lead to a false sense of security.

4 THE METABOLISM OF NITROSAMINES

Nitrosamines, once they are formed, whether exogenously or endogenously, have the potential to cause tumours. However, the nitrosamines themselves do not form ultimate carcinogens unless they are metabolically transformed. In the following sections, the specific features of nitrosamine carcinogenesis related to metabolic transformation are discussed. The reactions of the metabolically activated nitrosamine, which finally lead to alkylation of DNA (which is thought to be the ultimate cause of tumour initiation), are also

discussed.

4.1 Specific Features of Nitrosamine Carcinogenesis

Nitrosamines are stable and soluble in both aqueous and organic solutions [31]. They can readily permeate biological membranes [12,32] to become distributed throughout a living creature [33]. Nitrosamines are potent carcinogens which can cause tumours following a single dose; for smaller regular doses, however, it is found that the smaller the dose the longer the induction period. Of over 300 N-nitroso compounds tested, over 90% have been found to be carcinogenic, and no test species and few organs have been found to be immune [14].

Nitrosamines show remarkable organ specificity (organotropy), regardless of the route of administration [14,34]. The organ specificity varies from one animal species to another and can even vary between different strains of the same species. Thus intra-peritoneal administration of dimethylnitrosamine in Oslo mice produces lung tumours, whereas in Wistar rats kidney tumours are produced. N-nitroso-N-methyl-n-pentylamine on the other hand produces tumours of the nasal cavity, oesophagus and trachea in Wistar rats. Another general observation is that dialkylnitrosamines usually produce liver tumours, apart from di-n-butylnitrosamine which produces bladder tumours. It is also noted that RMeNNO usually produces tumours of the oesophagus where R contains between 2 and 6 carbon atoms, tumours of the liver where R contains an odd number of carbon atoms between 7 and 11, and bladder tumours where R contains an even number of carbon atoms between 8 and 14. Cyclic nitrosamines are generally active in a broad spectrum of organs, and nitrosoureas tend to exhibit neurotropism. Nitrosamides, which do not require enzymic activation, tend to produce mainly local effects at the site of application. A very full summary

of the organotropism of N-nitroso compounds can be found in reference [14]. The potency and organotropism of nitrosamines make them very useful tools for studying tumours.

4.2 Enzymes Responsible for Activation and Detoxification

The structure-activity relationships of nitrosamines, their organotropy, stability and distribution throughout the whole organism, together with their non-mutagenicity in the Ames test (without an activating system) all point towards enzymic activation in certain tissues being necessary for them to exert their carcinogenic effects (or to selective detoxification in certain tissues only). It was shown about thirty years ago that nitrosamines are almost completely metabolised in the body (to carbon dioxide) [35]. Somewhat later it was shown that metabolism by the microsomal fraction, oxygen and reduced pyridine nucleotides was necessary for nitrosamines to exert their carcinogenic effects [36]. This led to speculation that cytochrome P450 dependent mixed function oxidase was the activating enzyme - a drug metabolising enzyme system located on the endoplasmic reticulum. (The enzyme which acts on dimethylnitrosamine is also referred to as a demethylase).

Various characteristic features of cytochrome P450-dependent enzymes were found to apply to dimethylnitrosamine demethylase, e.g. its inhibition by carbon monoxide and the reversal of this inhibition by monochromatic light of 450nm [37]. Characteristic binding spectra of cytochrome P450 with nitrosamines were observed, providing further evidence that cytochrome P450 could demethylate nitrosamines [38]. Cytochrome P450-dependent enzymes normally function by addition of a single atom of oxygen, and so can convert C-H to C-OH and C=C to epoxides, and can also carry out other reactions [39,40,41].

Concurrent with the enzyme studies, observation of the metabolic products of aldehydes, molecular nitrogen, alcohols and alkylation products led to speculation that the demethylation took place by α-hydroxylation - see figure 1.1, and results in agreement with this may be taken as further evidence for mediation by cytochrome P450.

Several studies have determined the amount of molecular nitrogen evolved, which is a measure of the α-hydroxylation pathway. *In vivo* results gave a higher fraction than *in vitro* results, but the percentage has been found to vary between 5 and 100% [42,43,44]. It thus appears that not all of the metabolism proceeds by this route, and the involvement of other pathways and possibly other enzymes has been proposed.

It soon became apparent that the demethylase is not a classical mixed function oxidase enzyme. It retains its activity for longer than would be expected while it is stored. Nitrosamines do not inhibit the metabolism of other cytochrome P450 substrates. Inhibitors of the enzyme were found not to inhibit the demethylase and even to enhance it in some cases; inducers of the enzyme, some of which were substrates or inhibitors of the monoamine oxidases (which would be found in the microsomal fraction), were also found to inhibit metabolism. Atypical binding spectra have also been observed [45,46,47]. The possible involvement of monoamine oxidases has led to speculation of N-oxidation, rather than α-hydroxylation, as the activating step [46].

There has been much controversy over the abnormal effects of inhibitors and inducers, as some researchers have observed the expected effects, for example see reference [48]. These confusing findings have been clarified by the discovery of several demethylases with different K_m's for substrate binding [46,49]. The high K_m form (low affinity) acts as a typical cytochrome P450 enzyme, being induced by cytochrome P450 inducers, but the low K_m form (high affinity) does not. Only the low K_m form is likely to be active in humans exposed to low levels of

nitrosamines [49].

This low K_m form does however show other cytochrome P450-dependent features, such as a molecular mass similar to that typical of cytochrome P450, a peak at 450.6nm in the CO difference spectrum, and it is dependent upon NADPH-P-450 reductase [49]. Possibly the most convincing evidence for the role of cytochrome P450 in microsomal oxidations comes from studies of six isozymes of microsomal cytochrome P450, isolated and purified from rabbit liver, in reconstituted enzyme systems, which were found to metabolise N-nitroso-2,6-dimethylmorpholine. When antibodies to the two most effective isozymes were added to the microsomal oxidation system, no metabolism was observed [50]. In the metabolism of dimethylnitrosamine, typical monoamine oxidase inhibitors were also found to inhibit these reconstituted cytochrome P450 isozymes. Denitrosation, which was inhibited by superoxide dismutase, was also observed; the relative amount of denitrosation was found to depend upon the particular nitrosamine [51].

The enzymology is clearly not fully understood at present. It is possible that different enzymes may be involved in the metabolism of different nitrosamines [52], and that activation and detoxification may or may not be carried out by the same enzyme. Cytochrome P450 mediated oxidative dealkylation, however, appears to be the main enzymic process involved.

4.3 The Mechanism of Activation and Decomposition of Nitrosamines

The currently accepted activation and detoxification schemes are shown in figure 1.1 [14]. The proposed scheme for activation follows α-hydroxylation, and this is the only scheme considered in this thesis. The nitrosamines are catabolised to carbon dioxide [35]; labelling experiments have shown that both the carbon and nitrogen from nitrosamines are incorporated into tissues throughout the body, either anabolically or by direct alkylation. Elucidation of the pathways has proved difficult because most of the key intermediates have defied isolation, certainly with the simpler dialkylnitrosamines.

The α-hydroxylation pathway is proposed for several reasons. Firstly, nitrosamines fully deuterated in the α-position gave rise to fewer tumours in experimental animals than did the undeuterated nitrosamines. The results are taken to imply a rate determining activation step involving breakage of an α-carbon-hydrogen bond [53,54]. Secondly, increasing branching at the α-carbon results in a significant reduction in carcinogenic potency of nitrosamines. Thirdly, the metabolic products that can be trapped - nitrogen gas [42,43,44], aldehydes [55,56] and alkylation products [57] - are consistent with the decomposition of an α-hydroxynitrosamine. Fourthly, nitrosamides, which decompose spontaneously under physiological conditions, are already oxidised in the α-position [58]. Finally, α-acetoxynitrosamines, which are likewise oxidised in the α-position, produce typical nitrosamine metabolites on solvolysis [59] and are more mutagenic than nitrosamines [60]. (The α-acetoxynitrosamines do not show the same organotropy as nitrosamines, partly because of the ubiquitous nature of the esterases which aid their decomposition [61], hydrolysis of the ester being the rate determining step). In living systems, it appears that the α-hydroxylation occurs trans to the nitroso group [62]. The actual

hydroxylation probably occurs by a radical pathway [40,63].

Not only has the α-hydroxynitrosamine defied isolation, but it has also proved extremely difficult to synthesise [62,64]. The synthesis has been performed, however, and the α-hydroxynitrosamine has been shown to have a very short half-life in aqueous solution at physiological pH's. The half-life can be increased slightly in aqueous acidic media, or quite considerably in aprotic solvents [64].

For nitrosamines other than simple short chain dialkyl derivatives, oxidation at positions other than the α-position is possible; in some cases these oxidation products, which are unlikely to be the ultimate carcinogens, have been isolated. Compounds with long alkyl chains can undergo chain shortening [14].

As mentioned above, several different metabolites of nitrosamine have been trapped: aldehydes, nitrogen gas, alcohols and alkylation products. The aldehydes are assumed to come from the oxidised alkyl group, the alcohols can come from either the alkylation of the solvent [65] or the enzymic reduction of the aldehydes [56]. The consensus of opinion is that the alkyldiazohydroxide is formed from the other alkyl fragment, but there is some doubt as to whether the monoalkylnitrosamine is involved. The monoalkylnitrosamine has been observed spectroscopically at -70°C [66], but at physiological temperatures both compounds are extremely reactive. Moss has suggested that the anti-alkyldiazohydroxide is more stable than the syn isomer [67].

At different times, various compounds were proposed to be the ultimate carcinogen or alkylating agent. Nitrite and formaldehyde were eliminated at an early stage [68]. Rose and Schoental suggested that the diazoalkane was the main alkylating agent [69]; it was assumed that alkylation of DNA was the main cause of neoplastic transformation. (Alkylation of DNA was indeed demonstrated by Magee [70]). This is partly because diazomethane can be prepared by the effect of base

(conc. KOH) on a nitrosourea [71]. However, mass spectral studies using $(CD_3)_2NNO$ found that the main alkylation product had an m/e of 168, corresponding to 7-CD_3-guanine; smaller peaks for 7-CH_3-guanine and 7-CD2H-guanine were also found, but the main conclusion of the author was that other alkylating agents besides diazoalkanes need to be considered, and the carbonium ion was suggested [72]. Similar results were found using diethylnitrosamine-d^{10} [73]. This work was taken to be definitive, ruling out the diazoalkane. It was done on 7-alkylguanine when this was known to be the major alkylation product, but before it was found that 7-methylguanine formation did not correlate with tumour production, and when DNA isolation techniques destroyed O^6-methylguanine. The experiments have not been repeated on the O^6-methylguanine adduct, so it is still possible that the diazoalkane does carry out the all important alkylation of O^6-guanine, especially as there is reason to suspect that different alkylating agents alkylate at different nucleic acid centres (see below).

If a carbonium ion is the alkylating agent, then for higher alkyl carbonium ions rearrangement is likely. This possibility has been studied. In the metabolism of N-nitroso-N-di-n-propylamine, 20 - 40% of the propanol formed was the isopropanol and a similar figure was found for the base catalysed hydrolysis of N-n-propyl-N-nitrosourea. Only 5% of the RNA hydrolysate and 0% of the DNA hydrolysate contained the rearranged product, however, so the authors concluded the alkylation was a bimolecular S_N2 reaction, by the α-hydroxy compound, the diazonium ion, or the alkyldiazohydroxide [65]. However, similar work on the O^6-alkylguanine adduct (both *in vitro* chemical studies, and *in vivo* metabolic studies) showed that the major alkylation product was obtained with rearrangement [74]. The authors suggested that the reaction proceeded via a loose transition structure, with concomitant rearrangement.

Further discussion on the nature of the alkylating agent needs to

take into account the nature of the alkylation products, produced not only by different nitroso compounds, but also by simple alkylating agents such as dimethyl sulphate and methyl methanesulphonate. Alcohols formed by the alkylation of water have been observed [65]. Magee determined at an early stage that proteins are significantly alkylated, along with nucleic acids [70,75]. The most abundant and readily identifiable alkylation site in DNA is N-7 of guanine [76], but advances in analytical techniques have led to the identification of many other sites and their relative abundance [57].

It soon became clear, however, that mutagenicity and tumour induction were not correlated with N-7 alkylation. For example, mutagenic N-nitroso compounds and non-mutagenic simple alkylating agents such as methyl methanesulphonate both gave N-7 guanine as the major alkylation product [77]. Likewise tumour incidence in rats treated with methyl methanesulphonate or N-nitroso compounds did not correlate with the amount of N-7 guanine formed [78]. Such confusion led to suggestions of other modes of tumour induction, besides alkylation, such as cross-linking of macromolecules by bifunctional activated nitrosamines [79], but such theories are no longer pursued.

It has been found that non-mutagenic dimethylsulphate does not methylate O^6 of guanine, whereas the mutagenic and carcinogenic N-methyl-N-nitro-N-nitrosoguanidine does [80]. Loveless also observed this O^6-guanine adduct and suggested that alkylation at O^6 of guanine, rather than at N-7, is the cause of mutations [77]. N-nitroso ethylating agents, which behave differently to methylating agents, have been useful tools in elucidating the importance of various alkylation sites. Thus Swann and Magee were able to show that various ethylating agents (diethylnitrosamine, N-ethyl-N-nitrosourea and ethyl methanesulphonate) produced less N-7 alkylation product than the corresponding methylating agents, even though they were more carcinogenic [81]. Ethylating agents tend to attack oxygen atoms in

DNA bases, whereas methylating agents tend to attack nitrogen [57]. On the basis of the relative abundance of methylated and ethylated nucleic acid bases, and the relative carcinogenicity of the parent nitroso compounds, O^6 alkylguanine has been proposed as the only promutagenic base [82], though it is not the only one that can lead to mis-pairing of the Watson-Crick base pairs [83,84,85].

It has been observed that bimolecular alkylating agents tend to attack nitrogen, but unimolecular alkylating agents tend to attack oxygen. Thus in N-nitrosamine induced methylations, the major alkylating agent would appear to be bimolecular; if it were unimolecular then rearrangement would have been observed at N-7. This would imply that the α-hydroxynitrosamine, the monoalkylnitrosamine, the alkyldiazohydroxide or the alkyldiazonium ion is the alkylating agent. However, the alkylating agent at O^6, which appears to be the ultimate carcinogen, has S_N1 character; this would tend to suggest that a carbonium ion is involved. A loose transition structure midway between S_N1 and S_N2 may suggest that the alkyldiazonium ion is involved.

One of the main questions concerning the alkylating agent is "How can a reactive alkylating agent travel far enough across the cell to enter the nucleus and alkylate DNA ?". The nucleus appears not to contain the necessary activating enzymes, even though it does contain mixed function oxidases [86]. Pegg has suggested that the alkylating agent is able to alkylate the DNA in an adjacent cell [87]. It is probable that one of the intermediates has a sufficiently long life-time to enable it to diffuse across the cell, where it decomposes to a more reactive form; this then reacts immediately.

One other detoxifying mechanism which should be mentioned at this stage is the removal of promutagenic bases. N-methyl-N-nitrosourea normally induces tumours in a variety of organs, including the kidney. However, if rats are fed a low weekly dose, brain tumours are formed.

O^6 methylguanine was found to be removed from renal DNA by repair enzymes, but not from cerebral DNA. Thus tumour induction is also related to the persistence of promutagenic bases, rather than just their formation [88].

5 PREVIOUS RELEVANT QUANTUM CHEMICAL STUDIES

Prior to the commencement of this thesis, very little theoretical work had considered either the pathways involved in the formation of nitrosamines or those involved in the metabolism of nitrosamines. Indeed very few calculations on nitrosamines had been performed, and most of the early work used semi-empirical methods.

Two ab-initio studies had considered the protonation of nitrous acid; the most stable protonated structure is involved in nitrosation by the nitrous acidium ion [89,90]. There has been more intense interest in this recently, and three articles relevant to the structure of $ON(H_2O)^+$ appeared during the progress of this thesis [91,92,93]. Only the latter two articles specifically addressed themselves to determining the structure of the nitrous acidium ion. The work contained in this thesis comprises the most comprehensive study to date of the nitrous acidium ion. Another ab-initio study has investigated catalysis of nitrosation by formaldehyde [94]; this aspect of nitrosation has not been studied in this thesis.

There have been a number of semi-empirical studies of the geometrical and electronic structure of nitrosamines and their barriers to rotation [95,96,97]. The first ab-initio study of nitrosamines considered the electronic structure of H_2NNO [98]. However, none of these studies are directly related to the carcinogenic behaviour of nitrosamines.

The first semi-empirical study of the metabolism of nitrosamines

was published in 1970 [99]. It compared the overall energy changes (for various reactions involved in the metabolism of nitrosamines) for both the carcinogenic methylethylnitrosamine, and the non-carcinogenic diallylnitrosamine, $(CH_2CHCH_2)_2NNO$. It used pyridine as a model for guanine. It was concluded that the final alkylation occurred by an S_N2 mechanism.

$$RN_2^+ + \text{Guanine} \longrightarrow \text{R-Guanine} + N_2 \qquad (1.19)$$

This was because no difference was obtained for ΔE for the two nitrosamines except for reaction (1.19) where ΔE for the diallyl compound was much higher. Ten years elapsed before the next semi-empirical study of the metabolism of nitrosamines [100]. This study was much more thorough, and energy barriers for individual reactions were determined. The results of this study are discussed in the following chapters. However, some of the semi-empirical results are at variance with the ab-initio results reported in this thesis.

The first ab-initio study of the proposed metabolic pathways of nitrosamines was undertaken in this laboratory [101]. The interconversion of the monomethylnitrosamine to the diazohydroxide was studied, and a limited treatment of hydration was included. A high energy barrier was obtained, and it became evident that other routes may be important. This article was followed by an ab-initio study of the geometric and electronic structure of dimethylnitrosamine; a good comparison with experiment was found. The α-hydroxynitrosamine was also studied [102]. This thesis has built upon this and other work carried out in this laboratory.

During the progress of this thesis, another article on the ab-initio structure of nitrosamines has appeared [103]. There has also been an ab-initio study of the decomposition of the α-hydroxynitrosamine [63], and a semi-empirical structure-activity investigation of the pathways involved in the formation and

decomposition of the α-hydroxynitrosamine [104]. A recent semi-empirical study investigated the interaction of nitrosamine derived methylating and ethylating agents with cellular nucleophiles [105]. Even more recently, an ab-initio study has given evidence for alkylation by the alkyldiazohydroxide [106]. These articles will be discussed in the following chapters.

6 SUMMARY

The chemistry of the formation and metabolism of nitrosamines has been outlined above, including areas in which there is uncertainty as to which chemical species are involved. These are the main areas which have been studied theoretically and which will be discussed in the following chapters.

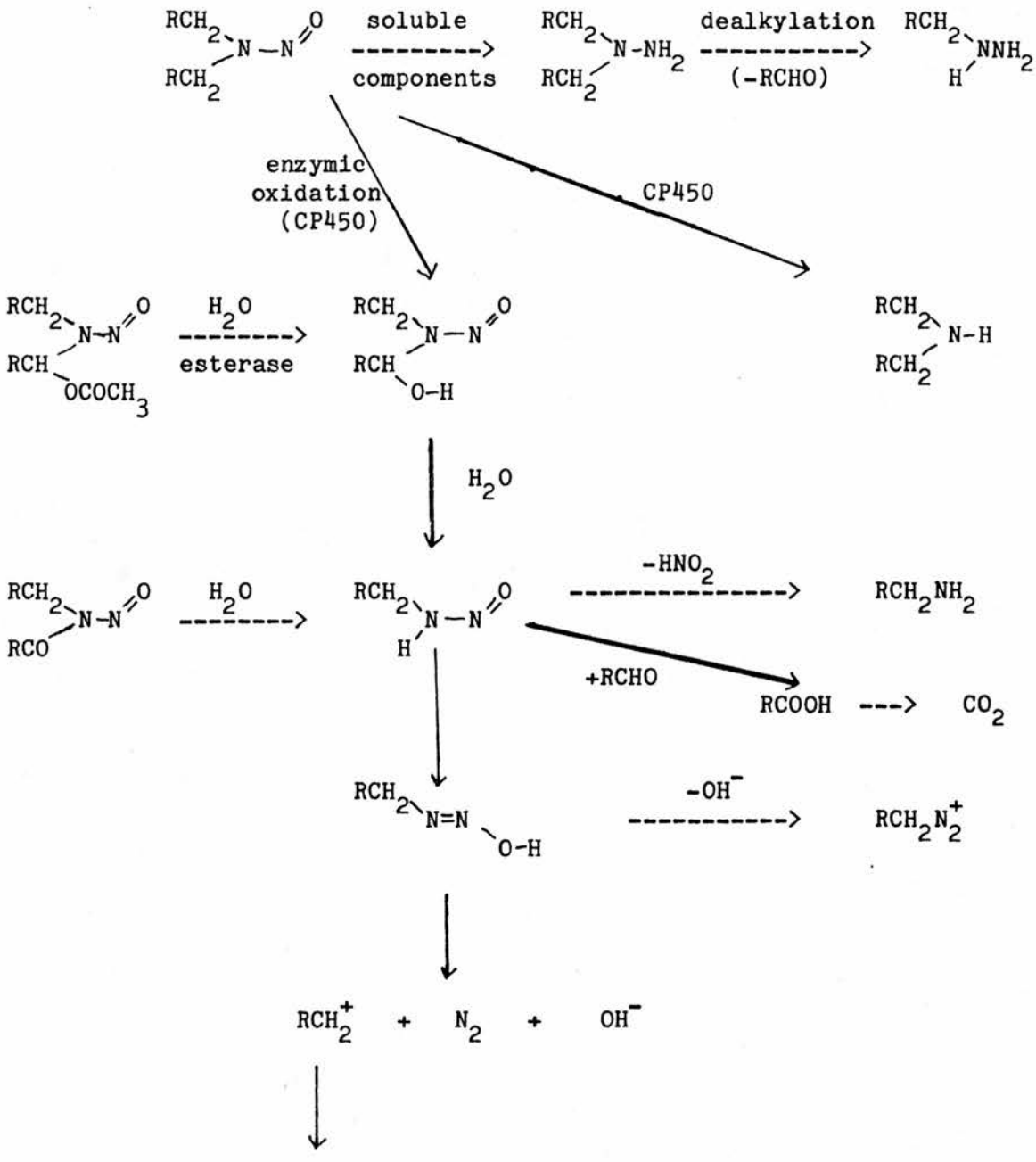

Figure 1.1 Bioactivation and detoxification pathways of N-nitrosamines

CHAPTER 2

THEORETICAL METHODS

1 STRATEGY

There are several areas in the chemistry of the formation and decomposition of nitrosamines in which theoretical methods can be used to shed light on some of the unsolved questions. The main area of concern in nitrosation is the structure of the various nitrosating agents, in particular that of the nitrous acidium ion. There are also many unsolved questions in the area of the decomposition of nitrosamine metabolites.

The overall strategy has been to determine theoretically the structure of the various molecules in fig. 1.1 (along with others), the geometries of the transition states connecting them and the energies of all these stationary points.

The wave function (for a given molecule) can be determined by solving the Schrödinger equation (see below). Solutions of the Schrödinger equation can give the energy, the forces on the nuclei and hence the geometry of stationary points on the surface; other properties also can be determined.

The only chemical species for which the Schrödinger equation can be solved exactly is the hydrogen atom, and so various approximations have to be made. Moreover, these methods become more expensive as the size of the molecule increases and as the desired accuracy increases. This chapter describes the methods used for obtaining these solutions, the approximations involved, and also the steps involved in obtaining other information from the wave function.

2 ENERGY CALCULATIONS

The time-independent Schrödinger equation may be given as

$$H \Psi = E \Psi \tag{2.1}$$

where the Hamiltonian operator, H, is given by

$$H = -\sum_i 1/2\ \nabla_i^2 - \sum_A 1/2M_A\ \nabla_A^2 - \sum_i \sum_A Z_A/r_{iA} + \sum_i \sum_{j>i} 1/r_{ij} + \sum_A \sum_{B>A} Z_A Z_B/R_{AB} \tag{2.2}$$

This form is given in atomic units where

E = total energy in hartrees (1hartree = 2625kJmol^{-1} [107])

Ψ = wave function

M_A = Mass of nucleus A / mass of electron

Z_A = atomic number of nucleus A

∇^2 = Laplacian operator

i,j = index for electrons i = 1,2,....N

A,B = index for nuclei A = 1,2,....M

1 atomic unit of length (Bohr) = 0.529177Å [108]

The Born-Oppenheimer approximation is based on the fact that the mass of the nucleus is very much greater than that of the electron. Consequently, for a small displacement of the nuclei the electrons re-orientate themselves almost immediately. This simplifies equation (2.1); the second term of equation (2.2) is assumed to be negligible, and the final term is treated as a constant, which is simply added to the electronic energy at the end of the calculation. Equation (2.1) then becomes

$$H_{elec.}\ \Psi_{elec.}(r_i; R_A) = E_{elec.}(R_A)\ \Psi_{elec.}(r_i; R_A) \tag{2.3}$$

where $\Psi_{elec.}$ depends explicitly on the electronic coordinates, r_i and parametrically on the nuclear coordinates, R_A. From now on however, the equation will be written in the simplified form of (2.1).

2.1 The Molecular Orbital Method (The Hartree-Fock Method)

Equation (2.1) is solved within the molecular orbital (MO) [109,110] method by building up the N electron wave function, Ψ, as a product of one-electron wave functions, $\psi(r)$; these one-electron wave functions describe the spatial distribution of the electrons as a function of the position coordinate r. To describe the electron fully, however, a spin coordinate is required; this may take one of two values, α or β. The spin-orbital function is then a product of spatial and spin functions

$$\chi(q) = \psi(r)\,\alpha \quad \text{or} \quad \chi(q) = \psi(r)\,\beta \tag{2.4}$$

One of the postulates of quantum mechanics requires the wave function, Ψ, to be antisymmetric with respect to interchange of the (spatial and spin) coordinates, r, of any two electrons i,j

$$\Psi(q_1, \ldots q_i \ldots q_j \ldots q_N) = -\Psi(q_1, \ldots q_j \ldots q_i \ldots q_N) \tag{2.5}$$

This general statement of the Pauli exclusion principle is satisfied by expressing the wave function as a Slater determinant

$$\Psi(q_1 q_2 \ldots q_N) = (N!)^{-1/2} \begin{vmatrix} \chi_i(q_1) & \chi_j(q_1) & \ldots \chi_k(q_1) \\ \chi_i(q_2) & \chi_j(q_2) & \ldots \chi_k(q_2) \\ \vdots & \vdots & \vdots \\ \chi_i(q_N) & \chi_j(q_N) & \ldots \chi_k(q_N) \end{vmatrix} \tag{2.6}$$

where $(N!)^{-1/2}$ is a normalisation factor. Equation (2.6) can be written in shorthand as

$$\Psi = | \chi_i \chi_j \ldots \chi_k | \qquad (i = 1, 2, \ldots N) \tag{2.7}$$

Within the restricted Hartree-Fock framework, the spatial parts of the orbitals with α and β spins are constrained to be equal $\chi_{2i-1} = \psi_i\alpha = \psi_i \quad \chi_{2i} = \psi_i\beta = \bar{\psi}_i$.

$$\Psi = | \psi_1\bar{\psi}_1\psi_2\bar{\psi}_2 \ldots \psi_{N/2}\bar{\psi}_{N/2} | \tag{2.8}$$

Using the above molecular orbital method for the expansion of Ψ, the energy can be written as

$$E = \int \Psi^* H \Psi \, dv \tag{2.9}$$

This can be expressed in Dirac notation as

$$E = \langle \Psi \mid H \mid \Psi \rangle \tag{2.10}$$

(The notation for integrals used in this chapter is defined in reference [110]). The wave functions used in this work are all real, so $\Psi = \Psi^*$. Equation (2.10) can be expanded as

$$E = 2 \sum_i H_i + \sum_{ij} (2J_{ij} - K_{ij}) \tag{2.11}$$

where

$$H_i = \langle \psi \mid H(1) \mid \psi \rangle \tag{2.12}$$

$$J_{ij} = \int \psi_i(1) \psi_i(1) \; 1/r_{ij} \; \psi_j(2) \psi_j(2) \, dv \tag{2.13}$$

$$J_{ij} = \langle \psi_i\psi_i \mid \psi_j\psi_j \rangle = (ii \mid jj) = \langle \psi_j \mid J_i \mid \psi_j \rangle \tag{2.14}$$

$$K_{ij} = \langle \psi_i\psi_j \mid \psi_j\psi_i \rangle = (ij \mid ji) = \langle \psi_j \mid K_i \mid \psi_j \rangle \tag{2.15}$$

where core operator, $H_i(1)$, the coulomb operator, $J_j(1)$, and the exchange operator, $K_j(1)$, can be defined as

$$H_i(1) = 1/2 \; \nabla_i^2 - \sum_A Z_A / r_{iA} \tag{2.16}$$

$$J_j(1)\psi_i(1) = [\int dr_2 \; \psi_j(2) \; 1/r_{12} \; \psi_j(2) \;] \; \psi_i(1) \tag{2.17}$$

$$K_j(1)\psi_i(1) = [\int dr_2 \; \psi_j(2) \; 1/r_{12} \; \psi_i(2) \;] \; \psi_j(1) \tag{2.18}$$

These terms can be interpreted as follows

H_i Describes the kinetic energy of the electrons and the nucleus - electron attraction terms

J_{ij} Describes the coulombic repulsion between electrons i,j

K_{ij} Describes the exchange repulsion between electrons of like spin, and arises out of the antisymmetry principle. It has no classical analogue.

2.1.1 The variational principle

The variational principle states that given a normalised wave function, $| \Psi >$, that satisfies the appropriate boundary conditions, then the expectation value of the Hamiltonian is an upper bound to the exact ground state energy.

If

$$< \Psi | \Psi > = 1$$

then

$$< \Psi | H | \Psi > \geq E_{exact} \tag{2.19}$$

Thus although equation (2.1) cannot be solved exactly, Ψ can be varied to obtain the best energy. This is done by varying the individual MO to find the minimum energy from (2.11) [109]. From (2.11) the following can be obtained

$$\delta E = 2\sum_i \delta H_i + \sum_{ij} (2\delta J_{ij} - \delta K_{ij}) \tag{2.20}$$

$$\begin{aligned} \delta E = {} & 2\sum_i (< \delta\psi_i | H(1) | \psi_i > + < \psi_i | H(1) | \delta\psi_i >) \\ & + \sum_{ij} (< \delta\psi_i | 2J_j - K_j | \psi_i > + < \delta\psi_j | 2J_i - K_i | \psi_j >) \\ & + \sum_{ij} (< \psi_i | 2J_j - K_j | \delta\psi_i > + < \psi_j | 2J_i - K_i | \delta\psi_j >) \end{aligned} \tag{2.21}$$

For real, hermitian, matrices $H_{i,j} = H^*_{i,j}$

$$\delta E = 4\sum_i < \delta\psi_i | H(1) + \sum_j (2J_j - K_j) | \psi_i > \tag{2.22}$$

The energy is minimised by varying the MO subject to the constraint

$$\int \psi_i \psi_j \, d\tau = < i | j > = \delta_{ij} \tag{2.23}$$

(If the original MO are not orthonormal, they can be made orthonormal by a linear transformation).

$$\int \delta\psi_i \psi_j \, dv + \int \delta\psi_j \psi_i \, dv = 0 \tag{2.24}$$

because the MO are real

$$\sum_{ij} \int \delta\psi_i \psi_j \, dv = 0 \tag{2.25}$$

The problem is solved by the method of Lagrangian multipliers; each equation (2.24) is multiplied by the Lagrangian multiplier, $-2\epsilon_{ji}$, and the result is added to equation (2.22)

$$\delta E = 4 \sum_i \int \delta\psi_i \left(\left[H(1) + \sum_j \left(2J_j - K_j \right) \right] \psi_i - \sum_j \psi_j \epsilon_{ji} \right) dv \qquad (2.26)$$

The Fock operator may be defined as

$$F = H(1) + \sum_i \left(2J_i - K_i \right) \qquad (2.27)$$

hence

$$F \psi_i = \sum_j \psi_j \epsilon_{ji} \qquad (2.28)$$

or in matrix form

$$F \psi = \psi \epsilon \qquad (2.29)$$

The ψ can be subjected to a linear transformation to give a diagonal matrix without affecting F hence

$$F \psi_i = \epsilon_i \psi_i \qquad (2.30)$$

2.1.2 The linear combination of atomic orbitals (LCAO) method

In practice the ψ_i are expanded in terms of K basis functions, ϕ_μ

$$\psi_\mu = \sum_\mu C_{\mu i} \phi_\mu \qquad (\mu = 1, 2, \ldots . K) \qquad (2.31)$$

From equation (2.30)

$$F(1) \sum_\nu C_{\nu i} \phi_\nu(1) = \epsilon_i \sum_\nu C_{\nu i} \phi_\nu(1)$$

$$\sum_\nu C_{\nu i} < \phi_\mu(1) \mid F(1) \mid \phi_\nu(1) > = \epsilon_i \sum_\nu C_{\nu i} < \phi_\mu \mid \phi_\nu > \qquad (2.32)$$

where

$$F_{\mu\nu} = < \phi_\mu(1) \mid F(1) \mid \phi_\nu(1) >$$

$$S_{\mu\nu} = < \phi_\mu(1) \mid \phi_\nu(1) >$$

This gives a set of equations

$$\sum_\nu F_{\mu\nu} C_{\nu i} = \epsilon \sum_\nu S_{\mu\nu} C_{\nu i} \qquad (i = 1, 2, \ldots K)$$

or in matrix form

$$F C = S C \epsilon \qquad (2.33)$$

These are the Roothaan equations and can be transformed by a transformation matrix to

$$F\,C = C\,e \tag{2.34}$$

Here the F is still defined in terms of molecular orbitals, ψ, and needs to be defined in terms of basis functions, ϕ_μ. This is done by defining a density matrix, P

$$P_{\mu\nu} = \sum_a C_{\mu a} C_{\nu a} \tag{2.35}$$

This completely specifies the charge density, $\rho(r)$, which is defined as

$$\rho(r) = 2 \sum_a | \psi_a(r) |^2 \tag{2.36}$$

The Fock matrix can then be written as

$$F_{\mu\nu} = H_{\mu\nu} + 2 \sum_{\lambda\sigma} P_{\lambda\sigma} [(\mu\nu | \sigma\lambda) - 1/2 (\mu\lambda | \sigma\nu)] \tag{2.37}$$

The equations (2.30 or 2.34) are not linear as the Fock operator, F, depends on its solutions, ψ, through (2.27), (2.17) and (2.18). They have to be solved iteratively using the self-consistent-field method.

2.1.3 The self-consistent-field (SCF) method

The transformed Roothaan equations can be solved by diagonalising F in (2.34) as part of an iterative procedure.

First of all the geometry of the molecule is set up, then for this geometry the integrals $S_{\mu\nu}$, $H_{\mu\nu}$, and $(\mu\nu|\lambda\sigma)$ are calculated. A transformation matrix, X, is obtained from S. A guess is made at P, and $F_{\mu\nu}$ is calculated. The matrix F is transformed, and diagonalised to obtain C'. The matrix C can then be obtained from C', and a new density matrix, P, is calculated. The iterative procedure is terminated when the r.m.s. convergence on the density matrix is less

than 10^{-6} (10^{-9} for post Hartree-Fock calculations, see below). The total energy is then given by

$$E = \sum_{\mu\nu} P_{\mu\nu} H_{\mu\nu} + 1/2 \sum_{\mu\nu\lambda\sigma} P_{\mu\nu} P_{\lambda\sigma} (\mu\lambda \,||\, \nu\sigma) + V_{nucl.} \qquad (2.38)$$

2.1.4 The unrestricted Hartree-Fock method (UHF)

Where the constraint on the spatial orbitals in (2.8) is removed

$$E = \sum_{i}^{\alpha+\beta} H_i + 1/2 \sum_{i}^{\alpha+\beta} \sum_{j}^{\alpha+\beta} J_{ij} - 1/2 \left(\sum_{i}^{\alpha} \sum_{j}^{\alpha} + \sum_{i}^{\beta} \sum_{j}^{\beta} \right) K_{ij} \qquad (2.39)$$

The coefficients in (2.31) can be satisfied by

$$F^{\alpha} C^{\alpha} = S C^{\alpha} \epsilon^{\alpha} \qquad F^{\beta} C^{\beta} = S C^{\beta} \epsilon^{\beta} \qquad (2.40)$$

where

$$F^{\alpha}_{\mu\nu} = H_{\mu\nu} + \sum_{\lambda}^{} \sum_{\sigma}^{} (P^{\alpha}_{\lambda\sigma} + P^{\beta}_{\lambda\sigma}) (\mu\lambda \,|\, \sigma\nu) - P^{\alpha}_{\lambda\sigma} (\mu\lambda \,|\, \sigma\nu) \qquad (2.41)$$

Similar expressions for the unrestricted density matrices P^{α} and P^{β} to (2.35) can be obtained. The two equations, (2.40), cannot be solved independently of each other, as F^{α} depends on both P^{α} and P^{β}, but can be solved in a similar manner to the restricted equations, (2.34) [111].

The unrestricted solution can be used for radicals, when the restricted solution breaks down [110] (for example for HNO [112] and at long bond lengths [110]) and as a starting point for more accurate solutions [113,114,115].

2.1.5 Limitations of the Hartree-Fock method

There are a number of limitations in the method. One concerns the choice of basis set (basis functions); generally, the larger the basis set, the more accurate the results. In this work it has only been possible to use small finite basis sets - see below. Another limitation arises out of the SCF method whereby the molecular orbital, ψ, is determined within the average field of the other orbitals. Thus no allowance is made for the instantaneous repulsion between electrons, particularly between electrons of opposite spin. Also the restricted formalism does not allow for homogeneous bond cleavage, so dissociation processes are not properly described.

However, as radical mechanisms have not been studied in this thesis, this latter failing is not a problem. Moreover, in reactions where no electron pairs are broken, the Hartree-Fock potential energy surface (at the Hartree-Fock limit) is expected to be parallel to the exact surface. Where the number of electron pairs remains constant, satisfactory results are expected, and even minimal basis sets can give results close to experiment when the number of bonds of each type does not change [116].

2.2 The Correlation Energy

If the molecular orbitals are expanded using an infinite set of basis functions, using (2.31), the above methods yield the Hartree-Fock energy, E_{HF}. This differs from the exact non-relativistic energy, E_{exact} by the correlation energy, E_{corr}

$$E_{corr} = E_{exact} - E_{HF} \qquad (2.42)$$

2.2.1 Configuration interaction (CI)

The exact energy can be calculated by the method of CI, where the exact wave function, $| \Phi >$, can be written as a linear combination of Slater determinants, the coefficients being determined variationally.

$$| \Phi > = c | \Psi > + \sum_{ar} c_{a \to r} | \Psi_{a \to r} > + \sum_{\substack{a<b \\ r<s}} c_{ab \to rs} | \Psi_{ab \to rs} > + \ldots \qquad (2.43)$$

where $| \Psi_{a \to r} >$ represents a determinant where χ_a has been replaced by χ_r in $| \Psi >$. All such excitations are included: $| \Psi_{a \to r} >$ represents a single excitation, and can be written as $| S >$; double, triple and quadruple excitations can be written as $| D >$, $| T >$ and $| Q >$, etc. The exact ground state energy is then found as the lowest eigenvalue of the CI matrix, H, (2.44)

$$Hc = E_{exact} c \qquad \text{or} \qquad \sum H_{st} c_t = E c_s \qquad (s = 0, 1, 2, \ldots) \qquad (2.44)$$

where

$$H = \begin{vmatrix} < \Psi | H | \Psi > & 0 & < \Psi | H | D > & 0 & 0 & \cdots \\ & < S | H | S > & < S | H | D > & < S | H | T > & 0 & \cdots \\ & & < D | H | D > & < D | H | T > & < D | H | Q > & \cdots \\ & & \cdot & \cdot & \cdot & \cdot \end{vmatrix} \qquad (2.45)$$

As shown in (2.45), only double excitations, $| D >$, interact with the ground state, $| \Psi >$, as a consequence of Brillouin's theorem, and the two particle nature of the Hamiltonian. However, the coefficients of $| D >$ in (2.43) are affected by these other excitations. In practice, however, (2.45) is too large for practical computation.

2.2.2 Doubly excited CI (CID)

One degree of truncation is at the level of double excitations. The method which has been used in this work did not consider single excitations [113]. These would have had very little effect on the energy, though they can effect charge densities [110]. In addition, excitations from the core electrons have been excluded, and $|\Psi\rangle$ is based on the UHF method. The matrix H is normally still very large, and has to be solved by an iterative procedure. The iterative procedure due to Pople has the feature of giving the Møller-Plesset (MP) perturbation energies (see below) to second and third order as part of the iterative procedure.

The n-electron Hamiltonian, H, is written as a sum of the one-electron Fock operators, $F_p(1)$, plus a perturbation operator, V, multiplied by a constant, λ, which is later set to unity

$$H = \sum_p F_p(1) + \lambda V \tag{2.46}$$

where

$$V = \sum_{i<j} 1 / r_{ij} - V^{HF}(i) \tag{2.47}$$

and

$$V^{HF}(i) = \sum_p F_p(1) - \sum_p H_p(1) \tag{2.48}$$

The perturbation operator, V, will have matrix elements V_{st}. The matrix U_{st} can be defined by

$$U_{st} = V_{st} - V_{oo}\delta_{st} \tag{2.49}$$

The initial Hartree-Fock energy is

$$E_{UHF} = E_o + V_{oo'} \qquad E_o = \sum_K \epsilon_K \tag{2.50}$$

The CI equations to be solved can be written as

$$\sum_t \left(H_{st}(0) + U_{st} + V_{oo}\delta_{st} \right) c_t = E c_s \tag{2.51}$$

Because H_{st} is diagonal, the equation to be solved iteratively becomes

$$(E_s + V_{oo} - E)\, c_s + w_s = 0 \qquad (2.52)$$

where E is the variational energy obtained at the end of each iterative cycle. A guess is made at the vector c_s, and w_s is formed from

$$w_s = \sum_t U_{st}\, c_t \qquad (2.53)$$

In the first iterative cycle, $E[1] = E_o + V_{oo}$ and is the energy given by first order MP theory. In these terms, the energy correct to second MP order is

$$E_{MP2} = E_o + V_{oo} + \sum_{s>o} |V_{os}|^2 / (E_o - E_s) \qquad (2.54)$$

At the end of each iteration, c[1] is updated by

$$c[m] = w_s[m] / (E[m] - E_s - V_{oo}) \qquad (2.55)$$

until satisfactory convergence is obtained. At the end of the second iteration, E[2] is closely related to EMP3, the third order MP energy; (nth order MP theory is discussed in the next sub-section).

The matrix elements V have to be expressed in terms of two-electron integrals in order to determine the vector w. These integrals are of the form (rs||ab), where

$$(rs \,||\, ab) = \sum_{\mu\nu\lambda\sigma} c_{\mu r} c_{\nu s} c_{\lambda a} c_{\sigma b} (\mu\nu \,||\, \lambda\sigma) \qquad (2.56)$$

This transformation, (2.56), would take N^5 steps and require N^4 locations of mass storage. A particular feature of this CID package is that it avoids explicit transformation of all the two-electron integrals over basis functions.

Truncated CI is not size-consistent, as can be seen from the reaction

$$2A \quad \text{---}> \quad B$$

where only double excitations are taken into account for B, but for A, two double excitations are considered. Size-consistency is important in potential energy surface studies, and so the size consistency

correction of Pople is used [113]; the total energy is denoted as $E_{CI,S}$.

2.2.3 Møller-Plesset perturbation theory

The partitioning of the Hamiltonian in (2.46) - (2.48) was first suggested by Møller and Plesset [117]; the exact energy can be written in a Taylor series in

$$E_{exact} = E(0) + \lambda E(1) + \lambda^2 E(2) + ... \quad (2.57)$$

$$| \Phi > = | \Psi(0) > + \lambda | \Psi(1) > + \lambda^2 | \Psi(2) > + ... \quad (2.58)$$

where E(n) is the n^{th} order energy, and where E(0) and $| \Psi(0) >$ are expected to be reasonably close to E_{exact} and $| \Phi >$ respectively. In this work $| \Psi(0) >$ is taken to be the UHF wave function.

$$E_0 = < \Psi | H_0 | \Psi > = \sum_a \epsilon_a \quad (2.59)$$

where ϵ_n are the occupied orbital energies. The first order correction is

$$E(1) = < \Psi(0) | V | \Psi(0) > = -1/2 < ab || ab > \quad (2.60)$$

and

$$E(1) + E(0) = E_{HF} \quad (2.61)$$

The general result for the second order energy is

$$E(2) = \sum_{n \neq 0} | < \Psi(0) | V | n > |^2 / (E_0(0) - E_n(0)) \quad (2.62)$$

where $| n >$ is of the form $| \Psi_{ab \to rs} >$ and contains only double excitations from the valence orbitals. E(2) is thus given by

$$E(2) = \sum_{\substack{a<b \\ r<s}} | < ab || rs > |^2 / (\epsilon_a + \epsilon_b - \epsilon_r - \epsilon_s) \quad (2.63)$$

The expression for the third order energy is similar [110,115].

A specific feature of the implementation used in this work is the avoidance of the explicit transformation of the two-electron integrals. Møller-Plesset perturbation energy is size-consistent.

Møller-Plesset theory to second order, with a large basis set including polarisation functions, can give 75-84% of the correlation energy [114]. However, Møller-Plesset theory does not perform well at long bond lengths [110], i.e. convergence in (2.57) is slow.

3 BASIS SETS

The set of functions, ϕ_μ, used in (2.31) to determine the molecular orbitals is termed the basis set. In theory any complete set of functions could be used, but the most physically meaningful set are Slater functions which have the form shown below, where $Y_{lm}(\theta,\phi)$ is a spherical harmonic and ζ is the exponent.

$$r^{n-1}e^{-\zeta r}Y_{lm}(\theta,\phi) \tag{2.64}$$

However, the resulting many-centre two electron integrals are difficult to evaluate [118]. In this work the common practice of using gaussian functions, as suggested by Boys [119], has been adopted; these have the form

$$\times x^l y^m z^n e^{-\alpha f^2 r^2} \tag{2.65}$$

where α is the exponent, and f is a scale factor. Integrals over gaussian functions are easily calculated, but a larger set is required to obtain results equivalent to those from Slater functions. In practice, a finite number of gaussian functions is used. Moreover, to prevent the number of spin-orbital coefficients becoming too large, and hence slowing down the SCF procedure, the gaussian functions are normally contracted as follows

$$\phi'_\mu = \sum_k d_k \phi_k \qquad (k = 1,2\ldots K) \tag{2.66}$$

where the coefficients d_k are fixed, and K is the degree of contraction.

For the majority of the work, the 4-21G split-valence basis set

[120] has been used. This has double zeta quality for the basis functions representing the valence orbitals - the inner valence functions are a contraction of two gaussian functions per AO, and the outer valence function is a single gaussian. The inner shell electrons are a contraction of four gaussians. (This basis set was chosen over the more usual 3-21G basis set [120] to give a better description of the core orbitals and for compatibility with earlier work in this laboratory, which used the 4-21G basis set of Pulay [121]). This basis set represents a compromise between the speed, and inherent inferiority of a minimal basis set (which uses a single contraction of gaussians for each atomic orbital), and the extra computational effort that would be required if polarisation functions were added to improve the basis set.

To assess the quality of results that have been obtained, a whole range of basis sets has been used. The sub-minimal STO-2G basis set [122] has been used to generate analytical guesses at the Hessian (the second derivative matrix). The STO-3G basis set [122] has been used for a variety of applications, along with the 3-21G and 4-31G [123] and 6-31G [124] basis sets, which give similar results to the 4-21G basis set. The 4-21G basis set contains atom optimised basis functions; no rescaling of the exponents has been carried out to suit the molecular environment, so the basis set may be particularly relevant in potential energy surface calculations, where atoms may be partly removed from molecules. For quantitative results, polarisation functions are often required. For first row atoms these are 3d functions ($l + m + n = 2$ in (2.65)), which are included in the 6-31G* basis set (heavy atoms only) and in the 6-31G** basis set which also includes 2p functions on hydrogen atoms [125].

3.1 Basis Sets for Anions

Calculations on anions pose particular difficulties because the extra electron is often only weakly bound. Consequently, electron affinities and proton affinities of anions are poorly reproduced, even using large basis sets which include polarisation functions. While geometries and heats of reaction can be reproduced satisfactorily, even using minimal basis sets [126], basis sets often need to be augmented on the heavy atoms (and hydrogens when H^- is involved) with diffuse functions. On first row atoms these are s and p functions, with small exponents; reasonable agreement with experiment can then be obtained [127,128]. In this thesis the 6-31+G basis set [129] has been used for anions.

3.2 Basis Sets for Hydrated Cations

The problems of describing cation-ligand interaction energies have been described by the Pullmans [130]. With minimal basis sets, and the STO-3G basis set in particular, the interaction energy is overestimated. This is due to the basis functions on the cation being utilised by the ligand to improve its own basis set (and vice versa), and is termed the basis-set superposition error. The intermolecular distance is consequently underestimated, and there is a large charge transfer to the cation [130]. In their work on the hydration of NO^+ [91], the Pullmans have used their own (7s,3p) minimal basis set [131], derived from Clementi [132], and have modified the basis functions on the NO^+ by a uniform scale factor of 1.08 on the valence orbitals. Either fortuitously or by design this gives perfect agreement with experiment [133]. This non-variational approach appears to be valid for permanent cations, such as Na^+. However, for the [H_2O - H_3O -

$HONO]^+$ system, where the positive hole can migrate when full optimisation is carried out, this amounts to a semi-empirical approach which has not been well parameterised, and puts an undue restriction on the system. For these reasons we have continued with the 4-21G basis set, and while the above defects can still be observed, the errors are tolerable, and can be estimated from studies using larger basis sets. Unlike the aforementioned basis sets, the (7s,3p) basis set employs different exponents on s and p functions. This results in increased integral and integral derivative evaluation time, and the basis set is only marginally faster than the 4-21G basis set.

4 OTHER INFORMATION DETERMINED FROM THE WAVE FUNCTION

4.1 Derivatives

The forces acting on the nuclei are the negative of the first derivatives of the energy with respect to the nuclear coordinates. These can be calculated numerically, but analytical determination has been used, as suggested by Pulay [134], because this is far more efficient.

$$\partial E/\partial x = \sum_{\mu\nu} P_{\mu\nu} (\partial H_{\mu\nu}/\partial x) + 1/2 \sum_{\mu\nu\lambda\sigma} P_{\mu\nu} P_{\lambda\sigma} (\partial/\partial x) (\mu\nu \,||\, \lambda\sigma) + \partial V_{nuc.}/\partial x$$

$$+ \sum_{\mu\nu} \partial P_{\mu\nu}/\partial x \; H_{\mu\nu} + \sum_{\mu\nu\lambda\sigma} (\partial P_{\mu\nu}/\partial x) P_{\mu\nu} (\mu\lambda \,||\, \nu\sigma) \qquad (2.67)$$

For the first derivatives, the derivatives of the density matrix, P, and hence of the spin-orbital coefficients, $c_{\mu i}$, can be avoided by making use of the derivatives of the orthonormality equation

$$\sum_{\mu\nu} c_{\mu p} S_{\mu\nu} c_{\nu q} = \delta_{pq} \qquad (2.68)$$

$$\partial E/\partial x = \sum_{\mu\nu} P_{\mu\nu} (\partial H_{\mu\nu}/\partial x) + 1/2 \sum_{\mu\nu\lambda\sigma} P_{\mu\nu} P_{\lambda\sigma} (\partial/\partial x) (\mu\nu \,||\, \lambda\sigma) + \partial V_{nuc.}/\partial x$$

$$+ \sum_{\mu\nu} W_{\mu\nu} (\partial S_{\mu\nu})/\partial x) \qquad \text{where } W_{\mu\nu} = \sum_{i} \epsilon_i c_{\mu i} c_{\nu i} \tag{2.69}$$

The derivatives of the integrals $\partial H_{\mu\nu}/\partial x, \partial S_{\mu\nu}/\partial x, (\partial/\partial x)\ (\mu\lambda\,||\,\nu\sigma)$ can be evaluated in a similar manner to the integrals themselves.

The expression for the second derivatives, however, does include the derivatives of the density matrix, and the energy-weighted-density matrix, W. This involves transformation of the integrals (ab||rs), and (ar||st), and so EMP2 can also be readily evaluated. The first derivatives of EMP2 can be evaluated in a similar manner [135].

4.1.1 Frequencies and thermodynamic information

Once the (analytical) second derivative matrix, F (the Hessian), has been determined, at the optimised geometry, the fundamental harmonic vibrational frequencies can be determined as the eigenvalues of the mass-weighted Hessian, $M^{1/2}FM^{1/2}$ ($M^{1/2}$ is a diagonal matrix where M_{11}, M_{22}, M_{33} etc. are the molecular mass of atom one etc). The eigenvectors of this matrix represent the normal modes of vibration; in particular, for transition structures (saddle points), the eigenvector corresponding to the negative eigenvalue is the reaction coordinate for the decomposition of the transition structure [136,137,138].

At the split-valence level (3-21G), these harmonic frequencies are on average 12% higher than the experimentally observed frequencies [135,138]. Improvement of the basis set to the 6-31G* level does not improve the situation significantly. At the MP2/6-31G* level, the error is roughly halved; moreover when the calculated values are compared to experimental harmonic frequencies, the error is reduced to

a third [135,139].

These frequencies can be used to evaluate thermodynamic information [140]. The Gibbs free energy can be evaluated as follows:

$$G(T) = U(0) + V(T) - TS(T) \qquad (2.70)$$

where U(0) is the internal energy at 0K, and is the ab-initio energy plus the zero-point correction; V(T) is the thermal energy correction (this includes a factor RT which is added to the thermal internal energy correction to give the thermal enthalpy correction). S is the entropy and T is the absolute temperature. These can be derived from the molecular partition function, Q

$$Q = \sum_n g_n e^{-\epsilon_n / (kT)} \qquad (2.71)$$

where g_n is the degeneracy and ϵ_n are the energy levels. The interaction between translation, vibration and rotation has been neglected, hence

$$Q = Q_{tr.}\, Q_{vib.}\, Q_{rot.} \qquad (2.72)$$

$Q_{tr.}$ depends primarily on the molecular mass, M, and temperature T. $Q_{vib.}$ depends on the vibrational frequencies, ν_i , and $Q_{rot.}$ depends on the symmetry number, σ , and the rotational constants, A ,B ,C , and hence on the moments of inertia. For molecules with low frequencies, usually corresponding to internal rotations, the internal energy partition function should not be separated into vibrational and rotational parts, but rather the vibration should be treated separately; the treatment depends upon whether the rotation is free or hindered, and therefore upon the barrier height. In line with similar work by G. Loew [141], this refinement has been neglected. The internal energy and entropy can be expressed as a sum of terms due to translation, vibration and rotation

$$V_{tr.}(T) = 5/2\ RT \qquad (2.73)$$

$$V_{rot.}(T) = 3/2\ RT \qquad (2.74)$$

$$V_{vib.}(T) = N/2 \sum_i h\nu_i + N \sum_i h\nu_i \; / \; (\exp(h\nu_i \; / \; kT) - 1) \qquad (2.75)$$

$$S_{tr.}(T) = 5/2 \; RT \; \ln(T) + 3/2 \; R \; \ln(M) + 5/2 \; R - R \; \ln(p) + R \; \ln(\; (2\pi \; / \; N)^{3/2} \; k^{5/2} \; / \; h^3 \;) \qquad (2.76)$$

$$S_{rot.}(T) = R/2 \; (\; 3 \; \ln(T) - \ln(ABC) - 2 \; \ln(\sigma) + \ln(\; \pi (k/hc)^3 \;) + 3 \;) \qquad (2.77)$$

$$S_{vib.}(T) = -R \sum_i g_i \; \ln(\; 1 - \exp(-\nu_i h \; / \; kT) \;) + Rh/(kT \sum_i g_i \nu_i) \; / \; (\exp(\; \nu_i h \; / \; kT) - 1 \;) \qquad (2.78)$$

The thermodynamic information is given at 298.15K and atmospheric pressure, conditions similar to physiological conditions. The symbols R, h and k assume their usual values.

The internal energy will be dependent primarily upon the frequencies, with their inherent errors; the entropies will be fairly accurate as they depend primarily on the geometry.

4.2 Electronic Population Analysis

The Mulliken population analysis for SCF-LCAO-MO wave functions [142] has been used to determine the charges on atoms and the overlap between atoms. For a molecular orbital, ψ , of the form (2.31), the number of electrons in the orbital i is given by

$$N(i) = N(i) \sum_\mu c_{i\mu}^2 + 2N(i) \sum_{\substack{\mu>\nu \\ \nu}} c_{i\mu} c_{i\nu} S_{\mu\nu} \qquad \text{where } S_{\mu\nu} = \langle \phi_\mu \mid \phi_\nu \rangle \qquad (2.79)$$

Summation of elements of the second term between centres k, l over all i gives the total overlap between the two atoms k, l. In determining

the charge on a centre, k, the overlap between k and adjacent centres is partitioned equally between the two atoms; this taken together with the sum of the first term over all i for the orbitals on atom k gives the total electronic charge on atom k.

The charges have been used mainly to predict protonation and hydration sites on molecules. These predictions, however, are only qualitative and may even give incorrect answers, partly due to the arbitrary partitioning of the overlap term [143]. The overlap populations have been used in a study of complexes, and in a study of certain unexpected conformations for nitroso compounds.

4.3 Electrostatic Potentials

The electrostatic potential, introduced by Bonaccorsi [144], is a more reliable guide to chemical reactivity, and is precisely defined as follows

$$V(r) = - \int \rho(r') dr' / | r' - r | + \sum_A Z_A / | R_A - r | \qquad (2.80)$$

Electrostatic potentials have been rigorously calculated on a grid of approximatively 3000 points. These have been displayed (in atomic units) as contour maps. In the majority of calculations, the electrostatic potential has been used to predict protonation sites; however, where the protonated structure has been determined, the electrostatic potential maps have not been shown.

Comparative studies have shown that SCF wave functions can yield reliable qualitative electrostatic potential maps, even when minimal basis sets are used. The order of the relative potential minima is likely to be correct, if the minima are not close together in potential; the precise location and depth of the minima, however, may not be very accurate [143]. Politzer has cited many studies where the

protonation site is correctly predicted by the electrostatic potential, but by way of warning he draws attention to the series of molecules based upon increasing methyl substitution in NH_3 and H_2O; in these molecules the relative proton affinities are not correctly predicted because polarisation and charge transfer effects do not cancel [143]. Thus, for the electrostatic potential to work as a predictive tool for molecular interaction energies, the electrostatic energy has to be the major component of the interaction, or its trend must at least parallel that of the total interaction energy, and the trend of electrostatic potential has to parallel that of the electrostatic energy [145]. (The various components can be evaluated as shown below).

4.4 Energy Decomposition Analysis

In the energy decomposition analysis used [145,146], the interaction energy, INT, is written as a sum

$$INT = ES + EX + PL + CT_{A->B} + CT_{B->A} + MIX + DISP \qquad (2.81)$$

The electrostatic energy, ES, is determined from a wave function which is a product of the isolated monomer wave functions. The polarisation energy, PL, is determined as above, except that the monomer wave functions are allowed to be polarised by the field of the other monomer. (Vacant and occupied orbitals on each monomer are allowed to interact). The exchange energy, EX, is determined by allowing the interaction of occupied orbitals on each monomer, and the charge transfer energy, CT, is calculated by allowing the interaction of occupied orbitals on one monomer with vacant orbitals on the other. MIX represents the higher order coupling terms among various interaction components. DISP represents the induced dipole - induced dipole energy, and cannot be calculated at the RHF level.

This scheme has been applied to the $H_2O.NO^+$ complex. This is a strong complex, and in such cases MIX can become large and obscure the meanings of the other components. In addition, in such cases the deformation energy, DEF, of the monomers in the complex also has to be taken into account. The energy components may be sensitive to basis set, and so they have been determined using a variety of basis sets.

4.5 Ionisation Potentials

Ionisation potentials have been obtained using Koopmans' theorem, which states that the ionisation potential is the negative of the energy of the highest occupied orbital (ϵ_{HOMO} from 2.34). The main approximation involved is that no allowance is made for the relaxation of the orbitals upon the loss of an electron. However, as the relaxation energy is usually accompanied by a decrease in the correlation energy as the number of electrons decreases, the theorem usually works well [110].

4.6 Geometry Optimisations

The majority of energy determinations have been carried out at the optimised geometry, using the 4-21G basis set, unless otherwise stated. Optimised geometries, rather than experimental ones, have been used because many of the species have either not been detected experimentally or the experimental structure is unknown. Hartree-Fock theory is known to reproduce experimental geometries reasonably well [116,147], and so no structure comparisons were undertaken in this work, though the nitrosamine structures themselves do compare well with experiment [102,103]. Instead, comparison of structures (and energies)

using different methods and basis sets have been used, and in the majority of cases favourable results have been obtained - see appendix. Transition structures cannot be determined by experiment and have to be determined by calculation [148].

4.6.1 Optimisation of Minima

The main algorithm that has been used in geometry optimisation is that of Schlegel [149,150], which unlike other optimisation methods has been specifically designed for quantum chemical calculations. The geometry is defined in terms of N internal coordinates: bond lengths, bond angles and dihedral angles. The optimised geometry is found by minimising the forces (gradients) along the internal coordinates using the iterative formula

$$x_{n+1} = x_n - a\,H^{-1} g_n \qquad (2.82)$$

where g_n is the gradient at x_n, x_{n+1} is the improved geometry and H is an approximation to the Hessian. H is usually approximated by a positive definite diagonal matrix derived from experimental values, and is updated at each step of the iteration. The constant, a, is set to unity. The above formula is the standard quasi-Newton method [151]. In addition, Schlegel's method takes the two lowest energy points, x'_{n-1}, x'_n and using the gradient at these points fits a quartic to them, subject to the constraint that d^2E / dx^2 cannot become negative. At the minimum of this curve, x_n, the gradient, g_n, is estimated. The maximum change in geometry is usually restricted. The geometry is deemed to have converged when the maximum and r.m.s. gradients are less than 0.00045 and 0.00030 hartrees/bohr respectively, and when the maximum and r.m.s. changes in geometry are less than 0.0018 and 0.0012 bohrs or radians, which should mean that structures are determined to

approximately 0.001Å or 0.1°. However as H^{-1} is not exact, the errors may be greater than this.

Because of the experimental guess at H^{-1}, and the use of a quartic, the algorithm is usually very fast, and may converge in less than N iterations, where N is the number of internal coordinates. However, because line searches are not performed [151,152] (i.e. a is not determined by calculations along the direction given by $H^{-1}g_n$), and due to the use of the quartic, the algorithm can become unstable ($E_{n+1} > E_n$,) and in certain cases it can inadvertently converge to a saddle point. (In some cases this has been used to advantage). Usually chemical intuition suffices to determine that the structure is indeed a minimum, but this can only be proved by verification that the exact Hessian is positive definite.

Some minima have also been determined using the Murtaugh-Sargent algorithm [153], and the BFS method internal to MINIT - see below; these algorithms are more stable (but much slower). In addition, the BFS method cannot converge to a saddle point because line searches are used [152].

4.6.2 Transition structures - Schlegel's algorithm

Schlegel's algorithm can also be used to find transition structures; these are stationary points on the lowest energy pathway between two minima, and correspond to a maximum in one direction, and a minimum in N-1 directions. They are characterised by one negative eigenvalue of the exact Hessian. Schlegel's algorithm thus searches for a maximum in the direction of the eigenvector corresponding to the negative eigenvalue. The problem becomes one of providing a suitable guess, x_n, in the region of negative curvature, and providing a suitable starting Hessian which contains the appropriate negative

eigenvalue. As the exact calculation of the Hessian is expensive, several procedures have been adopted:

a) A guess at H, based on the Hessian for a similar transition structure.

b) Partial numerical calculation of H for a few important coordinates.

c) Full analytical calculation of H.

The full analytical calculation of H using a cheap basis set appears to be the most satisfactory compromise between speed and accuracy. Whereas the analytical determination of the Hessian using the 4-21G basis set is expensive, especially at points that may be far removed from the true transition structure, it is cheap compared to unfruitful searches.

The choice of starting geometry can be found either by reference to the corresponding minima, or by comparison with similar transition structures. The reaction coordinate method has been used to estimate transition structures and energy barriers, but it is expensive (due to minimisations at every step) and unreliable; it can totally avoid the saddle point and vastly overestimate energy barriers [148,154]. Schlegel's algorithm has also been used to find second order saddle points, which are stationary points with two negative eigenvalues.

4.6.3 Transition structures - MINIT

The other algorithm used in saddle point determinations is MINIT [155,156]. A search for a maximum is made along a quadratic line joining two minima, p(1), which is known to have negative curvature. A quasi-Newton minimisation is then made in the space of the (N-1) linearly independent directions conjugate to p(1). If the surface were quadratic, then during the minimisation in conjugate space, the gradient along p(1) would remain zero, and the optimisation would

converge to the saddle point. As the Hessian in conjugate space is constrained to be positive definite, and line searches are performed, the algorithm cannot converge to a minimum or maximum [152].

In reality the gradient along p(1) in conjugate space may depart from zero, so a test is made of the gradient along this quadratic path between the latest point and the two minima; if necessary a search for a maximum is made, and the process is repeated until convergence is obtained.

The algorithm is not so dependent as Schlegel's on either a suitable Hessian, or a good starting geometry. Difficulties may arise however in the definition of the two minima, or if additional minima intervene. The algorithm has a firm mathematical basis [152], but as it stands it is inefficient for several reasons:

a) Too many searches for minima can lead away from the saddle point on non-quadratic surfaces, and the criteria for performing another search for a maximum are not clearly defined.

b) An updated Hessian in real space is not calculated. Consequently, information is lost which could be used in future calculations, and there is no check that the algorithm has not drifted away from the saddle point.

c) The line searches, necessary for stability, are performed without gradients; this may be more efficient for an s, p basis set, but for an sp basis set in which gradient evaluation only takes 50% of the time for function evaluation, at both the RHF and MP2 levels, line searches with gradients would increase both speed and stability.

This method could benefit greatly from further development. One possible option which could be included in the program is to minimise in the space conjugate to an approximate direction of negative curvature. Initially this direction of negative curvature could be estimated using one of the methods given above, but in subsequent steps

it would need to be estimated using an updated Hessian. For this option to work, the starting geometry would have to be in a region of negative curvature. However, this may remove the necessity of defining two minima; in some cases this would be an advantage.

4.7 Allowed Barrier Heights

In studying various reaction pathways, part of the problem is to determine whether the barrier (for various possible mechanisms) is sufficiently low to allow the reaction to proceed. The barrier above which little or no reaction can proceed has been estimated for first order reactions

$$A \quad \text{---}> \quad A^{\ddagger} \quad \text{---}> \quad \text{product(s)}$$

by cautiously using the Eyring equation [157].

$$t_{1/2} = \ln 2 \; / \; (\; (\; kT \; / \; h \;) \exp (\; -\Delta G^{\ddagger} \; / \; RT \;) \;) \qquad (2.83)$$

The alkylation of DNA has been observed to be complete in a matter of hours [158], or about 20 minutes if no activation is required [158]. This process covers many steps such as absorption, diffusion, oxidation and decomposition, and individual steps may be complete in a matter of seconds [64,87,159]. The free energy barriers at 298.15K corresponding to half-lives of 1s, 10s, 1minute, 10 minutes and 1hour are 74, 80, 84, 90 and 94kJmol^{-1} respectively. At 310.55K the corresponding barriers are about 4kJmol^{-1} higher. Identical results are obtained for second order reactions which depend on the solvent (H_2O) and are therefore pseudo first order; for true second order reactions the corresponding barriers will be lower. Due to a number of factors, these will be minimum half-lives, and so in practice the barriers may be lower.

The range of barriers obtained from (2.83) is small, and probably less than the errors in any calculated barriers. As can be seen from tables A.5 and A.6 in the appendix, the Hartree-Fock energy difference

between A and $A^{\ddagger}$ is very similar to the free energy difference; it would seem useful to propose that RHF/4-21G energy barriers above $100 kJmol^{-1}$ effectively rule out reaction (by this mechanism), with the proviso that the effects of polarisation functions and electron correlation must be considered.

4.8 Basis Set Superposition Error

The basis set superposition error arises in calculating the interaction energy of two monomers A, B, in a complex AB. The interaction energy is normally given by

$$\Delta E = E_{AB} - E_A - E_B \qquad (2.84)$$

where E_C represents the (SCF) energy of A, B or the supermolecule AB. However, in the supermolecule AB, when truncated basis sets are used, A is able to improve its energy using the full basis set of B and vice versa. This gives an interaction energy which is too high, and the error is particularly prevalent with minimum basis sets.

It can be corrected for, using the counterpoise correction of Boys [145,160,161], in which E_A and E_B are also calculated using the full basis set of AB. This has been done for the $NO^+ - H_2O$ complex (see chapter 3), but because the counterpoise correction is small at the RHF/4-21G level, it has been ignored in other cases. Difficulties arise in applying this correction when the deformation of A and B in the complex AB is large, as determined by a full unconstrained geometry optimisation of AB, because the location for the full AB basis set for the calculation on A or B is not clearly defined.

4.9 Conformational Energy Maps

Flexible molecules do not possess a single conformation, but rather a variety of different conformations are populated. Conformational energies can be calculated using the PCILO method [162] (Perturbation Configuration Interaction using Localised Orbitals), which is based on the CNDO method of approximating integrals: $(mn|ls) = \delta_{mn}\delta_{ls}(mm|kk)$ [163]. The fully localised molecular orbitals are constructed from linear combinations of suitably hybridised atomic orbitals. Electron correlation is treated using the corresponding antibonding orbitals, using perturbation theory up to third order. The method is very fast due to the method of treating the orbitals, because there is no SCF procedure and because the number of terms in the CI expansion is small. Difficulties arise in the treatment of non-classical structures but this was not a problem in this work. The internal coordinates were fixed at either ab-initio values, or averages of ab-initio values, while the dihedral angles were varied. Where an internal coordinate may take several values, e.g. angle C-N-N in $CH_2OHNHNO$, the map was constructed from the lowest energy values for each point taken from several determinations. The contour maps were created on a grid of 169 points; the energy contours are plotted in $kJmol^{-1}$ above the lowest energy point. Enclosed depressions are hachured. The Pullmans have suggested that only conformations within $25kJmol^{-1}$ of the minimum will be populated [164]. This method has been successful in a number of conformational studies [164], though the results may differ qualitatively from ab-initio results [165].

4.10 Environmental Effects

Most of the calculations carried out have been on isolated molecules, and so the results are strictly speaking relevant only to the gas phase, and even then only at low temperature and pressure. The calculation of thermodynamic properties has shown that the neglect of the zero-point , thermal effects and entropy is not a serious error - see tables A.5 and A.6 in the appendix. However, the environment is likely to have a more profound effect. In biological systems, the environment is normally assumed to be an aqueous solution, but its exact nature in different parts of the cell is not known. There are two approximate methods of treating solutions: continuum models, which include the bulk effects of the solvent but which do not consider the effects of discrete molecules of solvent [166], and the supermolecule approach, which includes a small number of solvent molecules in the calculation. In this thesis the second approach has been followed, in line with the practice of the Pullmans [167]. The rationale is that in many potential energy surfaces the bulk effects are likely to be constant, whereas individual water molecules may change the mechanism. Cytochrome P450 is a membrane-bound enzyme. There is a continuous network of membranes from the endoplasmic reticulum to the nucleus [168]; calculations in the gas phase are likely to be relevant to this lipid phase [63].

A further approximation which is related to the effect of the environment is that non-functional groups, particularly methyl groups, have been replaced by hydrogens to save CPU time. The resulting potential energy surfaces have been found to parallel the surface for the methyl analogue [63] - see appendix. This approximation is probably valid only when the bulk effects of the solvent are ignored, or when discrete solvent molecules are not placed near the hydrogen replacing the hydrophobic methyl group.

5 COMPUTATIONAL ASPECTS

The majority of the ab-initio calculations performed in this thesis have used the methods described above as incorporated into the Gaussian 80 [153] and Gaussian 82 [169] programs.

Gaussian 80 has the facilities for entering the geometry for a given molecule in terms of bond lengths, bond angles and dihedral angles. A number of basis sets are stored internally (including the majority of the ones used in this thesis), but external basis sets may also be used. The program evaluates the integrals over gaussian functions. The program also has facilities for generating a guess at the wave function, for performing the SCF procedure [109,111], for carrying out the Mulliken population analysis [142] and for evaluating the Hartree-Fock energy derivatives [135]. Further facilities exist for transforming the integrals in order to evaluate post Hartree-Fock energies [113,114,115]. The Gaussian 80 program also contains the Murtaugh-Sargent minimisation algorithm and the minimum and saddle point algorithm of Schlegel [149]. Several options exist for reading in the starting Hessian besides the default diagonal guess based upon experimental force constants [150]. The version of Gaussian 80 used at St. Andrews has also been modified to include damping, to give more reliable convergence in the SCF procedure [170], and to include the program DENPOT [171] for determining the electrostatic potential [170].

Gaussian 82 is an improved version of Gaussian 80, which contains the additional features which are described below. It gives improved convergence in the SCF (through use of a better guess based upon semi-empirical calculations). It includes analytical second derivative calculations (which also provide the Møller-Plesset second order energy) and can therefore determine harmonic frequencies and thermodynamic parameters (these may also be determined numerically).

There is also a facility for evaluating the first derivatives of the Møller-Plesset energy [135]. The energy decomposition analysis [145,146] was performed using the algorithm incorporated into a modified version of the Gaussian 80 system of programs due to Kollman [172]. The PCILO calculations [162] were performed using a program supplied by A. Pullman. The INDO/2 calculations (see chapter 3) were performed using a program supplied by M. Zerner.

The above programs did not require any modification prior to the commencement of this thesis.

The saddle point (and minimisation) algorithm, MINIT [155,156], was supplied by S. Bell. This was used as a 'stand-alone' program in conjunction with Gaussian 82. It was modified by the author to run on the local computing facilities and to use internal coordinates rather than Cartesian coordinates. A series of service programs was written to transfer information between MINIT and Gaussian 82. These service programs create a command file in the correct format to run Gaussian 82, and also to read the output from Gaussian 82 to a service file in the correct format for MINIT. Communication between MINIT and Gaussian 82 was necessary because sometimes MINIT required the energy, and sometimes it required the energy and the energy derivatives; this communication was controlled by the use of command symbols within a command procedure.

The optimised geometries were plotted using a locally implemented [173] version of PLUTO [174].

The electrostatic potential maps were plotted on a rectangular plane defined by three points, as required by DENPOT. A program has been written so that these three points can be defined within the plane of any three atoms of a given molecule. The electrostatic potential maps are plotted as contour diagrams. These contours were generated and plotted using SURFACE II [175], which interfaces to the GINO-F graphics system [176]. A series of user-friendly programs has been

written which allows for the easy entry of atomic co-ordinates, to define the orientation and extent of the plane, to create the input date to be appended to the Gaussian 80 command file, to create a command file to use SURFACE II, to read the output from DENPOT to create a data file for SURFACE II and to provide input for a program which interfaces with GINO-F and plots the molecular structure upon the contour map. The use of command procedures greatly simplifies this process, enabling the output to be generated very efficiently. This would otherwise have been a very laborious process.

A user-friendly system of programs has also been written for the creation of command files to run PCILO, to store the output in a suitable format for use by SURFACE II, to merge data from several calculations to select the lowest energy data, and to create and run SURFACE II command files.

All the above programs have been run on the twin VAX11/780's of St. Andrews University computing laboratory. These facilities have been shared with other users in the University.

While computer hardware has advanced significantly in recent years, enabling an increase in the size of problems which can be tackled (and the accuracy which can be attained) using quantum chemical techniques, the limited speed and storage space of these computers have restricted the scope of this work. Because of the space restrictions, CI calculations using a large (6-31G**) basis set were effectively restricted to 3-heavy atom molecules (heavy atom molecules being C, N, O) while Møller-Plesset calculations using the smaller 6-31G* basis set were restricted to 4-heavy atom molecules. Analytical second derivative calculations also required a lot of disk space; these were restricted to 4-heavy atom systems using the 4-21G basis set. (While second derivative calculations could have been carried out numerically for larger systems, an unrealistically large amount of computer time would have been required). Even Hartree-Fock calculations using the

6-31G* or 6-31G** basis sets became prohibitive for molecules with more than four heavy atoms, particularly when optimisations were carried out. Much larger systems can be studied using smaller basis sets. However, as the basis set survey shows, the minimal STO-3G basis set is not always very reliable, whereas the (7s,3p/3s) minimal basis set required as much CPU time as the 4-21G basis set. Consequently, a compromise was reached, and the majority of this work used the 4-21G basis set, and most calculations were performed at the restricted Hartree-Fock level.

All energies are quoted in atomic units and distances are quoted in Ångstroms unless otherwise stated.

CHAPTER 3

THE NITROUS ACIDIUM ION AND ITS REACTIONS

1 INTRODUCTION

As described in chapter 1, there are at least two mechanisms for the nitrosation of amines in acidic solution. This chapter deals with the structure and reactions of the nitrosating agent in solutions of nitrite at pH 1 - 2. The rate equation (1.3) is consistent with nitrosation by $H_2NO_2^+$ or NO^+, and the nitrosating agent has been termed the nitrous acidium ion. The nitrous acidium ion has never been observed experimentally, and so it is a species for which a theoretical investigation may be of great predictive value. There have been mass spectral studies of $ON^+ - H_2O$ clusters in the gas phase [133], which enable a comparison to be made between the theoretical and experimental results. In strong acid there is evidence for the existence of NO^+ [7], but in most cases of interest to man, nitrosation in the presence of dilute acid is more likely. However, the acidity of the human stomach can be as high as pH = 1 [177] and it is clear that under these conditions the formation of the nitrous acidium ion can result in *in vivo* nitrosation.

There have been other *ab-initio* calculations on $ON(H_2O)_n^+$ but these have only considered the case for n = 1, or have used a minimum basis set without full geometry optimisation [89 - 93]. The latest three articles appeared during the progress of this work. The strategy adopted in determining the structure of the nitrous acidium ion was firstly to study the protonation of nitrous acid and then to study the hydration of the protonated derivatives.

The energies of all compounds studied in this chapter are given in table 3.1, and the structures are given in figures 3.1 - 3.8 and tables 3.7, 3.9 and 3.10.

2 STRUCTURE OF THE NITROUS ACIDIUM ION

2.1 Structure of $H_2NO_2^+$

There are three possible isomers of nitrous acid (1a,1b,1c) - see figure 3.1. Of the two most stable isomers, the anti isomer is found by experiment to be slightly more stable by about 2kJmol^{-1} [178,179], although Nguyen and Hegarty have suggested that there may be some doubt about the experimental results, because of the precision required in the measurements [92]. The study of the energy difference between these two isomers is an interesting theoretical problem: the RHF/4-21G and RHF/6-31G* methods predict the syn isomer to be the more stable, whereas the RHF/6-31G method predicts the anti isomer to be the more stable - see appendix. Other theoretical studies [180 - 182] have also reproduced the small energy difference between these two isomers [178,179]. All of these Hartree-Fock studies give reasonable agreement with the experimental structures [183,184]. However, at this level of theory any successful prediction of the most stable isomer can only be taken as fortuitous. The uncertainty arising from this problem does not have serious consequences in this work. The syn and anti isomers are likely to co-exist; the nitro form (1a), however, is 108kJmol^{-1} above the syn form. It has not been observed experimentally [178] and is unlikely to play a part in the chemistry of protonated nitrite.

In an early study of the protonation of nitrous acid, using the STO-3G basis set, Dargelos et. al. found that electrostatic potential maps did not predict the most favourable protonation site [89]. Edwards and Weinstein later showed that when the 4-31G basis set is used, the most favourable protonation site is correctly predicted [90]. Recently, Nguyen and Hegarty have shown that the failure of

Dargelos' work was due to incomplete optimisation of $ON(H_2O)^+$ rather than to limitations in the applicability of electrostatic potentials [92]. This work is in agreement with that of Nguyen and Hegarty in finding that electrostatic potential maps in the plane of the molecules - see figure 3.9 - correctly predict the most favourable protonation sites. Electrostatic potential maps perpendicular to the plane of the molecule (not shown) did not predict any non-planar minima and indeed none were found. The results are shown in figure 3.1. The most stable isomer of $H_2NO_2^+$ is $ON(H_2O)^+$ by 157kJmol^{-1}, so $ON(H_2O)^+$, (1m), is likely to be the only protonated structure of any significance, even allowing for the overestimation of the $ON^+ - H_2O$ interaction energy (see table A.2 in the appendix). It was suggested by Nguyen and Hegarty [92] that the non-planar structure (1l) was a minimum which was connected to the planar structure by a perpendicular form (saddle point). (These authors were probably misled by the failure of their optimisation algorithm [149] to generate a negative eigenvalue). The non-planar isomer has been confirmed by analytical second derivative calculations to be the transition structure for the rotation of the H_2O about the NO bond, by the presence of one negative eigenvalue of the Hessian and by inspection of the corresponding eigenvector; the energy barrier to rotation is 4kJmol^{-1}. No stationary point corresponding to Nguyen's perpendicular form could be found. The linear structures $H_2O.ON^+$ (1j) and $H_2O.NO^+$ (1k) were proposed as local minima [91]; they are stationary points on the surface of $ON(H_2O)^+$, but they each have one negative eigenvalue corresponding to inversion and a zero eigenvalue corresponding to rotation of the H_2O about the axis. (For the linear molecules, the analytical Hessian was calculated at the STO-3G level using the STO-3G geometry). These linear structures lie 79 and 65kJmol^{-1} respectively above (1m), and so they are accessible points on the surface.

There will be other stationary points on the surface of $ON(H_2O)^+$,

corresponding to rotation or inversion in structures (1e - 1i), and transition structures between these minima, but they will be of very high energy. Only one such stationary point is given, (1d); this is the transition structure for the interconversion of c,t-$HONOH^+$ and $ON(H_2O)^+$.

2.2 Binding in $ON(H_2O)^+$

All of the calculations on $ON(H_2O)^+$ (of C_{nv} symmetry), except for $ON(H_2O)^+$ at the RHF/STO-3G level, show that the Mulliken charge resides primarily on the NO^+ (table 3.2), indicating an electrostatic interaction between the NO^+ and the lone pairs of the H_2O. Jørgensen and Lawesson [93] have suggested that the long bond length between the nitrosyl cation and the oxygen in the water molecule may be an indication of a coulombic, rather than an orbital, interaction.

However, the energy decomposition analysis indicates that the electrostatic contribution to the binding in $ON(H_2O)^+$ is repulsive for all the basis sets studied (table 3.3). Moreover, the attractive components of the interaction are due to polarisation and an approximately equal charge transfer both ways between the two monomers. These results are partially obscured by a large MIX term. As the deformation energy is small, particularly with the large basis sets, but also with the 4-21G basis set, the molecule is best described as a complex.

It may be noted here that the isoelectronic H_3NNO^+ has many similarities with $ON(H_2O)^+$.

2.3 Structure of $ON(H_2O)_n^+$

The optimised structures are reported in figures 3.1 to 3.4 and also in tables 3.2 and A.3. Multiple hydration of NO^+ occurs very readily; up to four water ligands can be put around the NO^+ in C_{2v}, C_{3v} and C_{4v} symmetry. The four stepwise hydration energies decrease steadily for the addition of each molecule of water; they are 146, 102, 82 and 56kJmol^{-1}. In the C_{2v} structure, (2a), the staggered form (not shown) would correspond to a transition structure for the rotation of the ligand. However, the staggered form of the C_{3v} structure, (3b), is lower in energy than the parallel form (3a). Whereas the C_{3v} structure appears to be a local minimum, its staggered form probably corresponds to a transition structure for the interchange of two planar forms: namely (3c) and its mirror image; the energy barrier for this is 20kJmol^{-1}. The energy difference between these two C_{3v} based forms is low (about 0.5kJmol^{-1}), yet the structures are quite different, showing that the surface is very flat.

These C_{nv} forms, however, do not give the most stable arrangements; more stable arrangements of $ON(H_2O)_2^+$ can be obtained by letting the second molecule of water bind to the first, rather than to the nitrogen. Thus for n = 2 there are two possibilities (2b and 2c), with the cis isomer slightly more stable. For n = 3, all four isomers based on the cis cluster were studied. It can be seen that hydration on H (3d) is more favourable than hydration on N (3c), and that hydration at the end of the water chain gives the most stable structures (3e and 3f). Some researchers have expressed concern at the idea of a chain of three water molecules bound to a cation; however, the two most stable structures more resemble H_3O^+ ligated by H_2O and HONO than $NO^+_{(aq)}$. A fourth water ligand does not change this unless it binds to the end of the chain, in which case it shifts the H_3O^+ further away from HONO (4d). In an experimental mass-spectral study of NO^+ in

the gas phase in a limited amount of water [133], French et. al. were unable to observe $ON(H_2O)_4^+$, possibly because HONO in the second solvation layer of H_3O^+ is easily lost. (At higher temperatures they were unable to observe $ON(H_2O)_3^+$ either). In a similar study at 298K, $ON(H_2O)_3^+$ was observed, but $ON(H_2O)_4^+$ was not, and H_3O^+ and $H_5O_2^+$ did not achieve significant concentrations [185]. The results presented here are consistent with these observations. The structures of the proton hydrates are given in figure 3.6 for comparison (As there is only a small energy difference between the planar and the more stable staggered forms, only the planar forms for $H_2O.H_3O^+.OH_2$ and $H_3O^+(H_2O)_3$ are given).

The energetics of the equilibria involving $NO^+_{(aq)}$ and $HONO_{(aq)}$ are shown in table 3.4. (These values ignore the counterpoise correction as it is small at the 4-21G level, and it approximately cancels. For the monohydration of NO^+, H^+ and H_3O^+, it is approximately 15, 14 and 20kJmol^{-1} respectively). The best correlation of trends in the ΔE's with experiment is for the most stable ab-initio structures, rather than for the C_{nv} structures, so these are probably the ones observed by French et. al.. (Comparing the results in this form with the experimental values is better than comparing the stepwise hydration energies of H^+ and NO^+, due to a cancellation of the different errors in the treatment of cations, ligands and complexes by this method; this will be particularly true for reactions (3.4) and (3.5) where the HONO is already formed in the $ON(H_2O)_n^+$. Moreover, the zero-point, thermal and entropy effects are small: for reaction (3.2) ΔE = 23kJmol^{-1}, ΔH = 29kJmol^{-1}, ΔH_{298} = 26kJmol^{-1} and ΔG_{298} = 29kJmol^{-1}). The monohydration energies of the proton are taken from reference [186].

It would seem a reasonable conclusion that the nitrous acidium ion has a limited number of different structures which exist as $ON(H_2O)_n^+$ (rather than as HONO - $H_3O^+_{(aq)}$ clusters). This will include all structures with less than three molecules of water joined in a linear

chain, including the C_{nv} structures, (though the C_{nv} structures become more and more unlikely as n increases). The most likely structures are $ON.OH_2^+$ and $ON.OH_2.OH_2^+$.

2.3.1 Other work on $ON(H_2O)_n^+$

Although there have been a number of studies on $ON(H_2O)^+$, only one has considered multiple hydration. This was essentially a study of the formation of proton hydrates from NO^+ and water in the D-region of the earth's atmosphere [91], but the results are also applicable to the study of the nitrous acidium ion.

The results differ from the results presented in this thesis in several ways. Firstly, the experimental geometry for H_2O and the RHF/4-31G geometry for NO^+ is used throughout. Secondly, the staggered arrangement of water molecules around the NO^+ is used, rather than the planar one. Both of these constraints appear to give credence to the calculations as they result in a lengthening of the $NO^+ - OH_2$ bond length, giving results more in line with those obtained using large basis sets, even though a minimum basis set was used (compare structures (1l) and (1m) in figure 3.1). Thirdly, the most favourable structures were found to be the C_{nv} forms rather than the planar forms found in this work. This effect however is probably due partly to the use of a different scale factor on the oxygen of the water molecules - see below - and partly to the constrained optimisation. Because a chain of three water molecules based on the NO^+ was not considered (the maximum considered was two), and because full geometry optimisation was not carried out, it was proposed that the nitrous acid was regenerated by a proton transfer in the following molecule

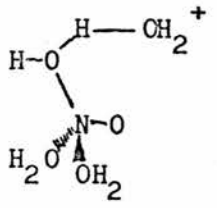

Although this molecule has the right conformation for the formation of anti HONO, it seems from the work outlined above that this mechanism is far less likely.

2.4 The Effect of Basis Set and Electron Correlation

2.4.1 The effect of basis set and electron correlation on $ON(H_2O)^+$

The structure of $ON(H_2O)^+$, particularly the overlap and the long NO bond length, is very dependent upon basis set, as can be seen from tables 3.2 and A.3. The more complete the basis set, the longer the NO bond. The STO-3G basis set is particularly poor for this molecule. The (7s,3p/3s) basis set has been successfully used in describing cation - ligand interactions by the Pullmans, but for NO^+ their scale factors must be used. The effect of varying the scale factors is shown in tables A.1 - A.3 in the appendix. For NO^+, increasing the scale factors from 1.00 to 1.08 on the valence orbitals results in a decrease in the total energy. For H_2O and $ON(H_2O)^+$, it results in an increase in the energy. For the complex, it results in an increase in the NO bond length and a decrease in the interaction energy of NO^+ and H_2O. This treatment is clearly variational for NO^+, but not for H_2O or $ON(H_2O)^+$. For this reason it is not valid as an ab-initio procedure,

in which confidence is obtained through the convergence of results as the method is refined. As a semi-empirical method it is well parameterised for $ON(H_2O)^+$, and possibly for the polyhydrates considered by Pullman et. al. [91], but it is not well parameterised for the fully relaxed $NO^+ - nH_2O$ system. The results for $ON(H_2O)_n^+$ using the (7s,3p/3s) basis set given in tables A.1 - A.3 were obtained using full geometry optimisation. The basis set superposition error is clearly important for the two minimal basis sets (table 3.3).

The effect of basis set on the monohydration of NO^+ is given in tables 3.3 and A.2. It appears that the RHF/4-21G method overestimates the interaction energy. The large basis sets give an interaction energy of about 90kJ/mol, which is not affected greatly when electron correlation is considered. This discrepancy between the 4-21G results and those for larger basis sets is not likely to affect the conclusions on the structure of the NO^+ in aqueous solution. Moreover, as the number of water molecules increases, the performance of the smaller basis sets improves, as can be seen from the close similarity of the results on the structure of C_{2v} $ON(H_2O)_n^+$ for the STO-3G and RHF/4-21G basis sets when n increases from 1 to 2 (table 3.2).

2.4.2 The effect of basis set on reactions (3.1) - (3.5)

The effect of basis set on the energetics of protonation of syn HONO is that increasing the basis set increases the tendency to form $NO^+_{(aq)}$ - ΔE for reaction (3.2) is 58kJmol^{-1} and 134kJmol^{-1} with the 6-31G and 6-31G* basis sets respectively. ΔE for reaction (3.3) at the RHF/6-31G* is greater than 21kJmol^{-1} (full optimisation of $ON.OH_2.OH_2^+$ was not carried out). However, increasing the number of water molecules favours HONO.

There is possibly some uncertainty over the extent of the

equilibria involved in reactions (3.1) - (3.5), and hence possibly over the length of the hydration chain required to generate H_3O^+ and HONO from $ON(H_2O)_n^+$ by stepwise hydration. At the 4-21G level n = 3 is required, but at more sophisticated levels of theory n may be 4 or more. (The experimental studies cannot determine whether $ON(H_2O)_3^+$ is a cluster based on NO^+ or on H_3O^+).

Table 3.5 compares the stepwise hydration energies of NO^+ and H^+ with those calculated using the INDO/2 method [163]. Clearly the INDO/2 results are far from satisfactory, and far worse than those obtained using the STO-3G basis set. In table 3.6 the corresponding comparison is given for reactions (3.1) - (3.4). This shows that these reactions do indeed result in an effective cancellation of errors, particularly as n increases; this suggests that information can be obtained for these reactions using minimal basis sets or semi-empirical methods. (Partly as a result of this observation, some calculations on an H_2O - H_3O^+ - ligand system with the STO-3G basis set will be presented in the next chapter).

It should also be noted that at the 4-21G level H_3O^+ is planar, but when polarisation functions are added it becomes pyramidal (the planar form being the transition structure for inversion) [187]; also the lowest energy form of $H_5O_2^+$ is not planar or staggered but pyramidal. (The staggered form is probably the transition structure for an H^+ shift between H_2O and H_3O^+; the planar form is probably a second order stationary point corresponding to rotation about the axis). The same effect may or may not occur in HONO - H_3O^+ - H_2O clusters, although this would have little effect on the conclusions presented here as the barrier for the proton shift, giving rise to H_3O^+ and HONO, is probably similar to that in $H_5O_2^+$ and would be less than the heat of monohydration.

3 NITROSATION BY THE NITROUS ACIDIUM ION

3.1 Nitrosation of Secondary Amines

3.1.1 The gas phase nitrosation reaction with NO^+

The simplest reaction leading to the formation of dimethylnitrosamine is

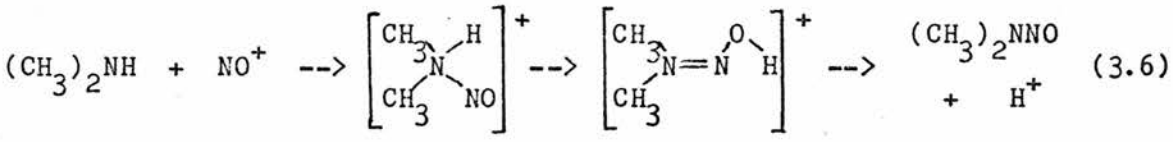

(I) (II)

The optimised geometries of $(CH_3)_2NH$, (I), (II) and $(CH_3)_2NNO$ are given in table 3.7, and figure 3.8. The dimethylnitrosoammonium ion, (I), appears to be a stable intermediate on the surface and forms without an energy barrier; the O-protonated form, (II), however, lies lower in energy by 59kJmol^{-1}. The final products could arise following a proton shift converting (I) to (II).

An approximate reaction pathway was studied by lengthening the N-N bond and the N-H bond in (I). The resultant energy profile is shown in figure 3.10. Also shown in figure 3.10 are two corresponding energy profiles for the model reaction

$$H_2NH + NO^+ \longrightarrow H_3NNO^+ \longrightarrow H_2NNOH^+ \longrightarrow H_2NNO + H^+ \qquad (3.7)$$

The one reaction profile was obtained by a very limited optimisation at each step, as was the case for the parent reaction (3.6) - the closeness of the results shows the similarity of the parent and model reactions. The other energy profile for the model reaction was

obtained by a more careful optimisation at each step, and shows that the reaction may go via the O-protonated form. The energy profile shows a discontinuity between R(N-H) = 2.0Å and R(N-H) = 2.5Å. This is due to the failings of the reaction coordinate method; the barrier for the proton shift is vastly overestimated. As reported in chapter 5, determination of the saddle point between H_3NNO^+ and H_2NNOH^+ shows that the barrier is only 280kJmol^{-1}.

It has been pointed out that ion-molecule reactions involving A + B^+, including those involved in carcinogenesis [188], cannot be described at the single determinant level. The condition for this occurs when the ionisation potential of A is less than that of B, and so an accurate wave function has to be able to describe the situation for both A + B^+ and A^+ + B. Kaufman has suggested that single excitations need to be included in the CI, although only a limited number of excitations need be considered, say from the five highest occupied orbitals to the ten lowest virtual orbitals. (The problem of considering limited CI, however, is that it ceases to be size-consistent).

These conditions clearly apply to reactions (3.6) and (3.7) - see table 3.8, where both theoretical ionisation potentials, calculated using Koopmans' theorem, and experimental ionisation potentials are given [95,189]. As shown in figure (3.10), the reaction coordinate clearly goes over correctly to both reactants and products at long intra-molecular distances. This is as expected because the reactions concerned all involve closed shell species, and no electron pairs are broken; for this reason one could expect the correlation energy errors to be small. The electronic interaction between the molecules at long bond lengths should also be small. Thus, while at intermediate bond lengths the potential energy curve may be lowered, the overall conclusion cannot be changed: that while formation of the intermediate - H_3NNO^+ - is favoured, the overall reaction is unfavourable. It may

be added here that due to the high ionisation potential of the H-atom one would expect that, according to Kaufman, all protonation reactions should be studied at the CI level, but Hartree-Fock theory is actually very successful in studying protonation reactions.

3.1.2 Nitrosation in the presence of water

As shown above, $NO^+_{(aq)}$ is readily destroyed by hydration; to be effective it must be created within the vicinity of the amine, so that it reacts on encounter, before being destroyed, as described by Ridd [7]. One detoxifying mechanism has been observed in a mass-spectral study [190]

$$ON(H_2O)^+_2 + NH_3 \longrightarrow NH_4.OH^+_2 + HNO_2 \qquad (3.8)$$

The efficacy of $NO^+_{(aq)}$ as a nitrosating agent is probably due to two factors. The first is that being planar in its most stable form, there is no steric hindrance for nucleophilic attack by an amine from either above or below the plane, even if the two hydration sites are occupied. Also, the surface of the C_{nv} forms is very flat, so they can easily distort as the amine approaches. The second factor is that it forms stronger bonds with amines than with water; ΔE for reactions (3.9, 3.10 and 3.11) is -48, -92 and -125kJmol^{-1} respectively.

$$ON(H_2O)^+ + NH_3 \longrightarrow H_2NHNO^+ + H_2O \qquad (3.9)$$

$$ON(H_2O)^+ + CH_3NH_2 \longrightarrow CH_3NH_2NO^+ + H_2O \qquad (3.10)$$

$$ON(H_2O)^+ + (CH_3)_2NH \longrightarrow (CH_3)_2NHNO^+ + H_2O \qquad (3.11)$$

(Jørgensen has given an expression, based on perturbation theory, for determining the interaction energy [93]). The effect of basis set and electron correlation on these reactions will be small - see table A.2. Hydration is also likely to have little effect on this equilibrium, as the resultant nitrosoammonium ion (if not derived from a tertiary amine) is almost as readily hydrated as the nitrous acidium ion - see

below and table A.2. ΔE for reactions (3.12) and (3.13) is -126 and $-118 kJmol^{-1}$ respectively.

$$H_3NNO^+ + H_2O \longrightarrow H_2O.HNH_2NO^+ \quad (3.12)$$

$$(CH_3)_2NHNO^+ + H_2O \longrightarrow (CH_3)_2N(NO)H.OH_2^+ \quad (3.13)$$

A reaction profile for the nitrosation reaction in which charged species are monohydrated is shown in figure (3.11). The reaction considered is

$$(CH_3)_2NH + ON(H_2O)^+ \longrightarrow (CH_3)_2N(H_2O)N{=}O^+ \quad (III)$$

$$(IV) \quad (CH_3)_2N(NO^+)H(OH_2) \longrightarrow (CH_3)_2NNO + H_3O^+ \quad (3.14)$$

The first part of the surface was obtained by increasing the N-N bond in III. However, IV is a more stable monohydrated form of I, and the second part of the energy profile was studied by lengthening the N-H bond in IV. (The corresponding model system was studied as before). The resultant ΔE for the overall reaction for the monohydrated system is $-42 kJmol^{-1}$, although accurate calculations on the model system - see table A.2 - indicate that the resultant ΔE may become positive. The inclusion of a second molecule of water shows that the overall ΔE will be negative, due to the greater hydration energy of the proton as compared to NO^+; the hydration of the neutral molecules will not have a great effect in comparison with the hydration of the cations. ΔE for reaction (3.15) is $-125 kJmol^{-1}$

$$(CH_3)_2NH + c\text{-}ON.OH_2.OH_2^+ \longrightarrow (CH_3)_2NNO + H_5O_2^+ \quad (3.15)$$

Reaction (3.14) may also proceed via the O-protonated form. (Whereas for the model compound there may be some doubt as to the most favourable protonation site of H_2NNO, for $(CH_3)_2NNO$ the most favourable site appears to be on the oxygen - see table A.2. There is an

experimental n.m.r. study which predicts the most favourable protonation site to be the oxygen [191]. Protonation on the nitroso-nitrogen is not likely, as the resultant protonated structure lies 124kJmol^{-1} above the O-protonated structure - see tables 3.1 and 3.9).

When just one molecule of water is considered, the nitrosoammonium ion intermediate appears to be a stable minimum, and there is a barrier of 164kJmol^{-1} to its destruction. The hydration of H_3NNO^+ can be treated in a similar manner to that of $ON(H_2O)^+$. The first molecule of water prefers to bind to a hydrogen (5b and 5c are more stable than 5a; 5f is more stable than 5e - see figure 3.5). A second molecule of water may bind to a second hydrogen of H_3NNO^+, but again binds preferentially to the first water molecule (see (5d) and also chapter 5). This yields an H_2O - H_3O^+ - nitrosamine cluster (5d) without an energy barrier. The possibility of forming only one amino-hydrogen based water chain (for secondary amines) may even be an advantage in that competing chains are not formed. As O-protonation of the nitrosamine is more likely than N-protonation, the nitrosamine thus formed will be stable. (In a mass-spectral experimental study it has been shown that H_3NNO^+ can be destroyed by NH_3 ligands to form H_2NNO and NH_4^+ in a similar manner [190]).

3.2 The Nitrosation of Tertiary Amines

Tertiary amines do not form nitrosamines as readily as do secondary amines, because the intermediate R_3NNO^+ does not posses an amino-hydrogen suitable for forming linear hydration chains. The reaction appears to be kinetically controlled, not thermodynamically controlled. The nitrosation of tertiary amines normally occurs at a pH greater than that at which the nitrous acidium ion is generated [17].

In this section, however, preliminary results are given on the nitrosation of tertiary amines by NO^+. As the nitrosation of amines by N_2O_3 has not been studied theoretically, it is difficult to say to what extent the intermediate R_3NNO^+ is involved, even though its occurrence in the mechanism is normally assumed [17].

3.2.1 Loss of CH_3^+ in the absence of water

Theoretical calculations show that $(CH_3)_3NNO^+$ loses CH_3^+ more readily than $(CH_3)_2NHNO^+$ loses H^+ - see table A.2. (The structure of $(CH_3)_3N$ is given in table 3.10). As before, an approximate energy profile was generated for the model compound

$$CH_3NH_2 + NO^+ \rightarrow CH_3NH_2NO^+ \rightarrow t\text{-}H_2NNOCH_3^+ \rightarrow H_2NNO + CH_3^+ \quad (3.16)$$

The results are plotted in figure (3.12). The overall energy of reaction is unfavourable, ΔE = 113kJmol^{-1} and 96kJmol^{-1} for the model and parent reactions respectively; the energy barrier for the CH_3^+ shift is also unfavourable. This barrier is only approximate; determination of the saddle point - see chapter 5 - shows that the barrier for the CH_3^+ shift is 264kJmol^{-1}. When zero-point effects and electron correlation are considered, the barrier may be lower. (The saddle point is only 27kJmol^{-1} above the reactants CH_3NH_2 and NO^+, although entropy affects this barrier considerably - see tables A.5 and A.6 for the corresponding proton shift results).

O-alkylated nitrosamines have been prepared and studied [192]. They can be formed by the action of electrophilic alkylating agents on nitrosamines, and are themselves alkylating agents; the usual products of alkylation reactions by O-alkylated nitrosamines are nitrosamines and alkylation products derived from all the alkyl groups. This gives experimental evidence for N->O alkyl shifts. O-alkyl nitrosamines are therefore likely to be carcinogenic, and would not need to be

metabolically activated. They may be intermediates in the formation of nitrosamines from tertiary amines.

3.2.2 Loss of CH_3^+ in the presence of water

When one molecule of water is considered, the overall reaction may become favourable - see table A.2

$$(CH_3)_3N + ON(H_2O)_n^+ \longrightarrow CH_3(H_2O)_n^+ + (CH_3)_2NNO \qquad (3.17)$$

ΔE for this reaction depends on both n, and on the hydration sites of NO^+ and CH_3^+.

The structures of hydrated CH_3^+ which have been studied are shown in figure 3.7. Clearly, hydration at the C-atom is more favourable than at the hydrogens. (7d) was found to be a rotational transition structure following an analytical determination of the Hessian. This is the structure given in tables A.1 - A.3 (except for the STO-3G basis set). The most stable structure (7e) is the one reported in table A.4, and differs from (7d) by rotation of the water molecule about the C-O axis by about 30^o; it lies about $0.5 kJmol^{-1}$ below (7d). By analogy, (7g) may also be a rotational transition structure. These molecules will be unstable in solution, and are likely to be detoxified by a hydration chain, giving rise to $H_2O - H_3O^+ - CH_3OH$ clusters. The term detoxification is used because CH_3^+ is a very powerful alkylating agent, and as such can act as an ultimate carcinogen.

The energies of these molecules are given in table 3.1. For the most stable isomers, (7a), (7e) and (7g), ΔE for reaction (3.17) becomes 96, -92, and -10 for n = 0, 1 and 2 respectively. The effect of basis set on this reaction has been considered - see table A.2. Without a much more thorough study it is impossible to say whether this reaction can proceed or not. This mechanism corresponds to mechanism (1.15) in chapter 1. Even if it is thermodynamically favourable, it is

unlikely to be kinetically favourable.

3.2.3 Radical mechanism

Mechanism (1.13) in chapter 1 has been ruled out by the stoichiometry. However, due to the relative ionisation potentials of NO and tertiary amines, the first part of (1.13) may contribute to some other mechanism.

3.2.4 Loss of HNO from R_3NNO^+

The other mechanisms given in chapter 1 involve the loss of HNO. The α-hydrogens in $(CH_3)_2NNO$ are labile and can undergo deuterium exchange with the solvent [193]. Consequently, a proton shift from $CH_3NH_2NO^+$ was considered

$$CH_3NH_2NO^+ \longrightarrow \left|\ H_2C\cdots H\cdots O\ \right|^+ \longrightarrow CH_2NH_2^+ + NOH \qquad (3.18)$$

The overall RHF energy change is 118kJmol^{-1}. Attempts to determine the transition structure were not successful. NOH is one molecule for which unrestricted Hartree-Fock theory gives a lower energy (for the singlet) by 101kJmol^{-1}, or 108kJmol^{-1} when the geometry is reoptimised. As the UHF energy includes a portion of the correlation energy, the actual correction on the true surface may be less than this. NOH is unstable to 1/2 H_2O and 1/2 N_2O; the RHF and UHF energy changes are -241 and -133kJmol^{-1} respectively. This mechanism is thermodynamically favoured, but because attempts to determine the transition structure were not successful, its importance cannot be

assessed.

3.3 Transnitrosation

H_3NNO^+ and $ON(H_2O)^+$ have many similarities: they are isoelectronic, the cation-ligand bond length is very basis set dependent, the molecules are best represented as complexes and the charge is primarily on the nitrogen. Although it is not normal practice to show electrostatic potential maps for cations, as they may be difficult to interpret due to the presence of hydrogen atoms [143], clearly in this respect the two molecules are very similar (figure 3.13). Therefore H_3NNO^+ and also its substituted analogues probably have very similar properties to $ON(H_2O)^+$ and could act as nitrosating agents. This is consistent with transnitrosation via a direct mechanism involving N-protonated nitrosamines.

4 SUMMARY

In the first part of this chapter the structure of $ON(H_2O)_n^+$ has been thoroughly studied, and it is concluded that the nitrous acidium ion exists in a number of different structures. These structures will be very unstable as they are destroyed by hydration. The nitrous acidium ion must be formed in the vicinity of its substrate in order to react. Hydration of the nitrous acidium ion - amine complex can result in the formation of a nitrosamine, without an energy barrier.

The nitrosation of tertiary amines has also been studied. It was discovered that the saddle point for an N->O CH_3^+ shift in $(CH_3)_3NNO^+$ is surprisingly not very high above the reactants $(CH_3)_3N$ and NO^+, and so a new mechanism for the nitrosation of tertiary amines involving

O-alkylated nitrosamines is presented. This mechanism may give rise to a carcinogenic alkylating agent. The mechanism appears to be thermodynamically favoured and may be aided by hydration. Moreover, there is experimental evidence for N->O alkyl shifts in O-alkylnitrosamines. It is difficult to determine at this stage, however, to what extent this mechanism may occur at the acidities involved in the nitrosation of tertiary amines.

The majority of this work has been accepted for publication [194,195].

Table 3.1a Energies of all structures considered at the 4-21G optimised geometry

Structure	Fig. Label	Energy	Structure	Figure Label	Energy
NO^+		-128.559070	$ON(H_2O)_4^+$	4a	-431.990563
HNO_2	1a	-204.081643	$HONO(OH_2).H_3O.OH_2^+$	4b	-432.018824
HONO	1b	-204.120206	$HONO(OH_2).H_3O.OH_2^+$	4c	-432.052503
HONO	1c	-204.122682	$HONO.OH_2.H_3O.OH_2^+$	4d	-432.052847
$H_2NO_2^+$	1d	-204.318062			
$HONOH^+$	1e	-204.348141	$ON.NH_3.OH_2^+$	5a	-260.534194
$H_2NO_2^+$	1f	-204.357852	$ON.NH_3.OH_2^+$	5b	-260.553463
$H_2NO_2^+$	1g	-204.368890	$ON.NH_3.OH_2^+$	5c	-260.554387
$HONOH^+$	1h	-204.374439	$H_2NNO.H_3O.OH_2^+$	5d	-336.421657
$HONOH^+$	1i	-204.375996	$ON.(CH_3)_2NH.OH_2^+$	5e	-338.441934
$NO.OH_2^+$	1j	-204.405645	$ON.(CH_3)_2NH.OH_2^+$	5f	-338.470709
$ON.OH_2^+$	1k	-204.411174			
$ON.OH_2^+$	1l	-204.434136	H_2O		-75.821207
$ON.OH_2^+$	1m	-204.435812	H_3O^+	6a	-76.125561
			$H_5O_2^+$	6b	-152.027674
$ON(H_2O)_2^+$	2a	-280.295820	$H_5O_2^+$	6c	-152.029229
$ON.OH_2.OH_2^+$	2b	-280.307308	$H_7O_3^+$	6d	-227.845042
$ON.OH_2.OH_2^+$	2c	-280.307856	$H_7O_3^+$	6e	-227.850872
			$H_7O_3^+$	6f	-227.856851
$ON(OH_2)_3^+$	3a	-356.148153	$H_2O.H_3O.OH_2^+$	6g	-227.903616
$ON(OH_2)_3^+$	3b	-356.148264	$H_3O.(OH_2)_3^+$	6h	-303.769323
$ON(OH_2)_2.OH_2^+$	3c	-356.155998			
$ONOH_2^+(OH_2)_2^+$	3d	-356.181178	NH_3		-56.052230
$HONO.H_3O.OH_2^+$	3e	-356.186454	CH_3NH_2		-94.995400
$HONO.H_3O.OH_2^+$	3f	-356.188006	$(CH_3)_2NH$		-133.942124

Table 3.1a (Continued)

CH_3^+	7a	-39.145047	$ONNH_3^+$	-184.685281
$CH_3.OH_2^+$	7b	-115.011517	$ONNH_2CH_3^+$	-223.644888
$CH_3.OH_2^+$	7c	-115.011884	$ONNH(CH_3)_2^+$	-262.604363
$CH_3.OH_2^+$	7d	-115.093331	$(CH_3)_2NNO$	-262.268219
$CH_3OH_2^+$	7e	-115.093419	$(CH_3)_3N$	-172.890848
$CH_3(OH_2)_2^+$	7f	-190.870369	HNO	-129.421762
$CH_3(OH_2)_2^+$	7g	-190.934181	HNO(UHF,opt)	-129.462906
$CH_3(OH_2)_3^+$	7h	-266.722649	N_2O	-183.205827

Table 3.1b Energies of molecules studied with the 6-31G* basis set

Molecule	Figure Label	4-21G geometry	6-31G geometry
$ON.OH_2.OH_2^+$	2c	-280.964117	<-280.987855
$H_5O_2^+$	6b		-152.348744
$H_5O_2^+$	6c	-152.349735	-152.350601
$H_5O_2^+$	6d		-152.352480

Table 3.2 The effect of basis set on the geometry of $ON(H_2O)^+$, the overlap between the N and the O on the H_2O and the charge on the NO. All the structures are minima, except that one saddle point is also given for $ON(H_2O)^+$.

No. of H_2O's	n = 1						n = 2		n = 3	n = 4
Basis	(73/3)	STO-3G	4-21G	4-21G	6-31G	6-31G*	STO-3G	4-21G	4-21G	4-21G
RNO1	1.162	1.185	1.063	1.061	1.060	1.044	1.166	1.062	1.059	1.058
RNO3	2.057	1.571	1.982	2.031	2.152	2.287	1.891	2.154	2.246	2.318
ROH4	1.019	0.992	0.973	0.972	0.953	0.953	0.986	0.970	0.969	0.968
ROH5	1.017	0.988	0.971	0.972	0.954	0.952	0.983	0.968	0.968	0.967
AONO	106.3	106.9	108.0	104.8	105.8	105.4	100.4	101.8	100.4	98.0
ANOH4	133.3	125.8	131.3	123.4	132.2	134.0	132.9	132.1	132.0	132.0
ANOH5	117.2	118.4	117.9	123.4	116.4	120.1	121.3	119.0	119.5	119.8
DONOH4	0.0	0.0	0.0	101.1	0.0	0.	0.0	0.0	0.0	0.0
DONOH5	180.0	180.0	180.0	-101.1	180.0	180.0	180.0	180.0	180.0	180.0
Overp.	0.019	0.110	0.026	0.029	-0.007	0.001	0.027	0.018	0.015	0.014
Charge	0.880	0.489	0.835	0.852	0.869	0.877	0.631	0.836	0.833	0.838

Table 3.3 $ON(H_2O)^+$ energy decomposition analysis, deformation energy and counterpoise correction. The deformation energy is the energy of isolated monomers minus the energy of the monomers at their geometry in the complex.

		BASIS SET			
Component	7s,3p	STO-3G	4-21G	6-31G	6-31G*
- Total Energy(au)	204.13902	202.25834	204.43581	204.83384	204.95662
Electrostatic Energy	1352	873	1295	1338	1442
Polarisation Energy	-1508	-1229	-1501	-1525	-1572
Charge Transfer En. A->B	-3702	-2657	-3505	-3601	-3727
Charge Transfer En. B->A	-3763	-2866	-3553	-3624	-3742
Exchange Energy	119	880	160	92	57
MIX	7382	4720	6955	7195	7446
Interaction Energy	-157	-279	-149	-125	-95
Deformation Energy	43	47	3	1	0
ΔE	-114	-232	-146	-124	-95
Counterpoise Correction	46	55	15	5	4
ΔE(Counterpoise Corrected)	68	-176	-131	-119	-92

Table 3.4 ΔE for the reaction: $NO^+_{(aq)} + H_2O \rightarrow H_3O^+_{(aq)} + HONO$. The most stable forms for $H(H_2O)^+_n$ from figure 6 are used. There is some doubt about ΔH for reaction (5) [185].

Reaction		No.	Expt[11]	C_{nv}	Hydration site (planar) N	1st H	Chn. end
$NO^+ + H_2O \rightarrow$ c-HONO $+ H^+$		(3.1)	643	676			
$ON(H_2O)^+ + H_2O \rightarrow$ c-HONO $+ H_3O^+$		(3.2)	99	23			
$ON(H_2O)^+_2 + H_2O \rightarrow$ c-HONO $+ H_5O^+_2$		(3.3)	23	-92		-61	-60
$ON(H_2O)^+_3 + H_2O \rightarrow$ c-HONO $+ H_7O^+_3$		(3.4)	8,-ve	-149	-129	-63	-45,-49
$ON(H_2O)^+_4 + H_2O \rightarrow$ c-HONO $+ H_9O^+_4$		(3.5)		-211	-136	-48	-47

Table 3.5 INDO/2 stepwise hydration energies for NO^+ and H^+

Reaction				ΔE(RHF/4-21G)	ΔE(INDO/2)
NO^+	$+ H_2O$	--->	$ON.OH^+_2$	-146	-901
NO^+	$+ 2H_2O$	--->	$ON.OH_2.OH^+_2$	-248	-1224
NO^+	$+ 3H_2O$	--->	$HONO.H_3O^+.OH_2$	-430	-1450
$ON.OH^+_2$	$+ H_2O$	--->	$ON.OH_2.OH^+_2$	-133	-323
$ON.OH_2.OH^+_2$	$+ H_2O$	--->	$HONO.H_3O^+.OH_2$	-151	-226
H^+	$+ H_2O$	--->	H_3O^+	-799	-1214
H^+	$+ 2H_2O$	--->	$H_5O^+_2$ (stag.)	-1011	-1553
H^+	$+ 3H_2O$	--->	$H_7O^+_3$	-1155	-1772
H_3O^+	$+ H_2O$	--->	$H_5O^+_2$ (stag.)	-216	-339
$H_5O^+_2$(planar)		--->	$H_5O^+_2$ (stag.)	-4	-1
$H_5O^+_2$(stag.)	$+ H_2O$	--->	$H_7O^+_3$	-140	-218

Table 3.6 INDO/2 ΔE's for the reaction: $NO^+_{(aq)} + H_2O \rightarrow H_3O^+ + HONO$. compared to RHF/4-21G ΔE's: $H_5O_2^+$ staggered is used.

Reaction							ΔE(RHF/4-21G)	ΔE(INDO/2)
NO^+	+	H_2O	->	c-HONO	+	H^+	(3.1) 676	278
$ON(H_2O)^+$	+	H_2O	->	c-HONO	+	H_3O^+	(3.2) 23	-36
$ON(H_2O)_2^+$	+	H_2O	->	c-HONO	+	$H_5O_2^+$	(3.3) -92	-52
$ON(H_2O)_3^+$	+	H_2O	->	c-HONO	+	$H_7O_3^+$	(3.4) -49	-44

Table 3.7 Optimised geometry of structures given in reaction (3.6)

Parameter	$(CH_3)_2NH$	I	$(CH_3)_2NNO$	hydration of I on H	hydration of I on N	II
RNC5	1.466	1.511	1.462	1.504	1.501	1.507
RNC4	1.466	1.522	1.458	1.514	1.510	1.506
RCH6	1.083	1.080	1.079	1.079	1.079	1.077
RCH7	1.092	1.079	1.083	1.079	1.080	1.080
RCH8	1.084	1.078	1.083	1.079	1.079	1.079
RCH9	1.084	1.078	1.081	1.078	1.079	1.079
RCH10	1.083	1.075	1.081	1.078	1.079	1.079
RCH11	1.092	1.079	1.079	1.079	1.080	1.075
ROH12						0.976
RHN	1.004	1.017		1.060	1.015	
RNN		1.645	1.333	1.582	1.731	1.227
RNO		1.150	1.241	1.166	1.130	1.383
RXO13				1.573	2.592	
ROH14				0.967	0.967	
ROH15				0.967	0.968	
ACNC	114.7	114.8	123.6	114.6	115.0	120.1
AH6CN	109.4	108.3	107.6	108.2	108.5	108.0
AH7CN	113.9	108.3	110.7	108.1	109.1	107.5
AH8CN	109.0	108.1	110.7	108.8	108.3	107.5
ANCH9	108.9	108.5	110.1	109.2	108.6	108.2
AH10CN	109.4	109.2	110.1	109.3	109.3	108.1
AH11CN	113.9	108.0	108.4	107.5	108.8	107.0
AHNC5	112.4	111.3		110.8	111.3	
ANNC5		112.5	119.3	112.9	112.1	123.2
AONN		110.7	114.3	111.5	109.3	110.9
AHON						106.9
AXOH14				125.3	125.3	
AXOH15				125.0	127.2	
ANXO13				179.7	166.1	
DH7NCH6	121.5	120.1	119.4	119.9	120.2	120.3
DH7CNC	58.4	64.5	60.6	64.2	65.3	59.8
DH8CNC	-62.1	-55.2	-60.6	-55.7	-54.5	-59.8
DCNCH9	61.9	58.7	120.4	58.2	58.9	120.4
DH9NCH10	117.8	120.4	119.2	120.6	120.2	119.3
DH11CNC	-58.7	-60.9	0.0	-61.6	-60.7	0.0
DHNCH10	-50.3	-55.7		-56.9	-54.9	
DNNCH9		-61.4	-59.6	-61.9	-60.6	-59.6
DONNC5		4.2	0.0	-5.6	0.9	0.0
DHONN						180.0
DH14OXN				0.0	-10.4	
DH15OXN				180.0	168.7	
DO13XNC5				59.1	-167.6	
				X = H12	X = N2	

Table 3.8 Ionisation Potentials (in electron volts)

Molecule	Experimental	RHF/4-21G	RHF/6-31G*
NH_3	10.3	10.7	11.4
CH_3NH_2	9.4	10.0	10.4
$(CH_3)_2NH$	9.1		
$(C_2H_5)_2NH$	8.4		
$(CH_3)_3N$	8.1	9.1	
NO	9.3		
H	13.6		
CH_3	9.9		
H_2NNO		11.2	11.2
c-CH_3NHNO		10.8	
t-CH_3NHNO		10.7	
$(CH_3)_2NNO$	9.1	10.2	
$(C_2H_5)_2NNO$	8.8		

Table 3.9 The RHF/4-21G structure of $(CH_3)_2NHNO^+$ - see figure 3.8

Parameter	Value	Parameter	Value	Parameter	Value
RCH9	1.081				
RNC5	1.489	ANCH9	108.9		
RNC4	1.494	ACNC	123.3	DCNCH9	120.3
RCH6	1.081	ANCH6	109.7	DH6NCH6	120.0
RCH7	1.079	ANCH7	108.2	DCNCH7	60.0
RCH8	1.079	ANCH8	108.2	DCNCH8	-60.1
RCH10	1.081	ANCH10	108.9	DH9NCH10	119.5
RCH11	1.076	ANCH11	107.4	DCNCH11	0.0
RNN	1.277	ANNC5	116.0	DNNCH9	-59.7
RNO	1.236	AONN	123.9	DONNC5	0.0
RNH	1.019	AHNN	117.8	DHNNC5	180.0

Table 3.10 The RHF/4-21G structure of Trimethylamine - see figure 3.8

Parameter	Value	Parameter	Value	Parameter	Value
RCH1	1.083				
RNC2	1.465	ANCH1	109.4		
RNC4	1.465	ACNC4	113.1	DCNCH1	55.6
RCH5	1.093	ANCH5	113.0	DCNCH5	65.5
RCH6	1.083	ANCH6	109.4	DCNCH6	-55.3
RCH7	1.083	ANCH7	109.4	DH6NCH7	120.7
RCH8	1.083	ANCH8	109.5	DH1NCH8	118.5
RCH9	1.093	ANCH9	112.9	DCNCH9	-65.1
RNC10	1.465	ACNC10	113.2	DC10NCH1	-174.0
RCH11	1.083	ANCH11	109.4	DCNCH11	55.9
RCH12	1.093	ANCH12	112.9	DCNCH12	-64.9
RCH13	1.083	ANCH13	109.4	DCNCH13	-185.7

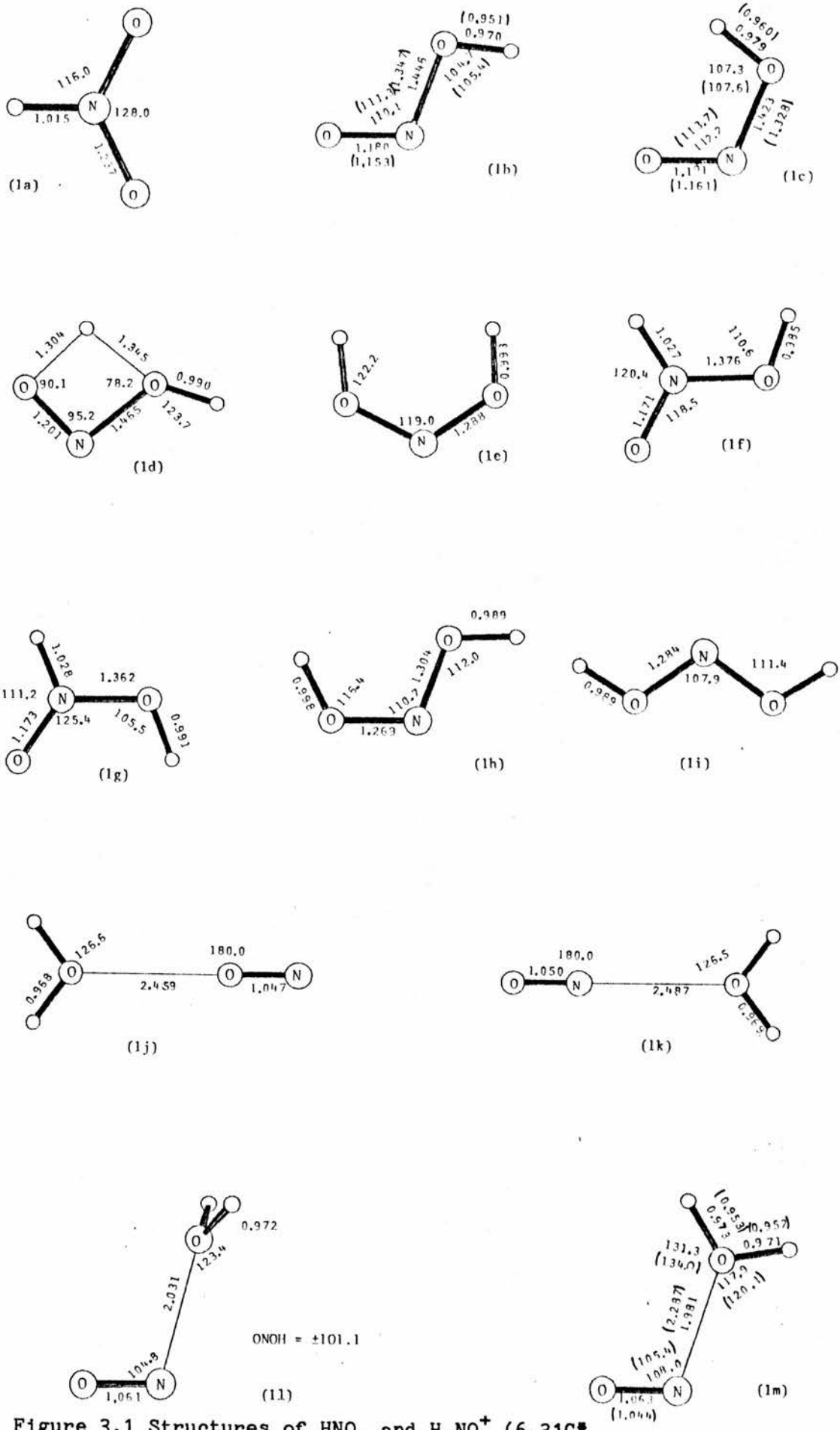

Figure 3.1 Structures of HNO_2 and $H_2NO_2^+$ (6-31G* values are in parenthesis). Hydrogen atoms are not labelled.

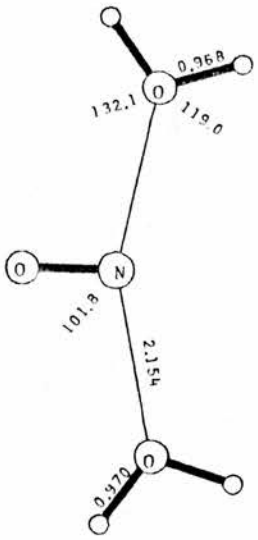

(2a)

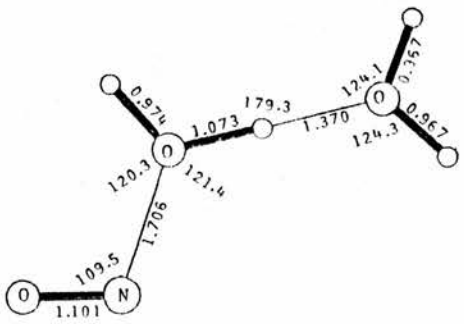

(2b)

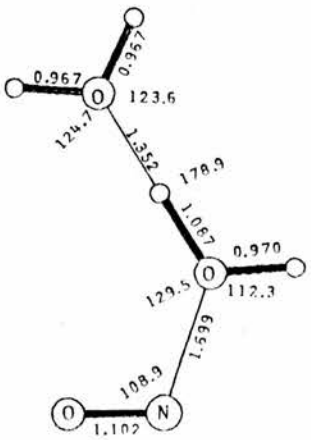

(2c)

Figure 3.2 Structures of $ON(H_2O)_2^+$

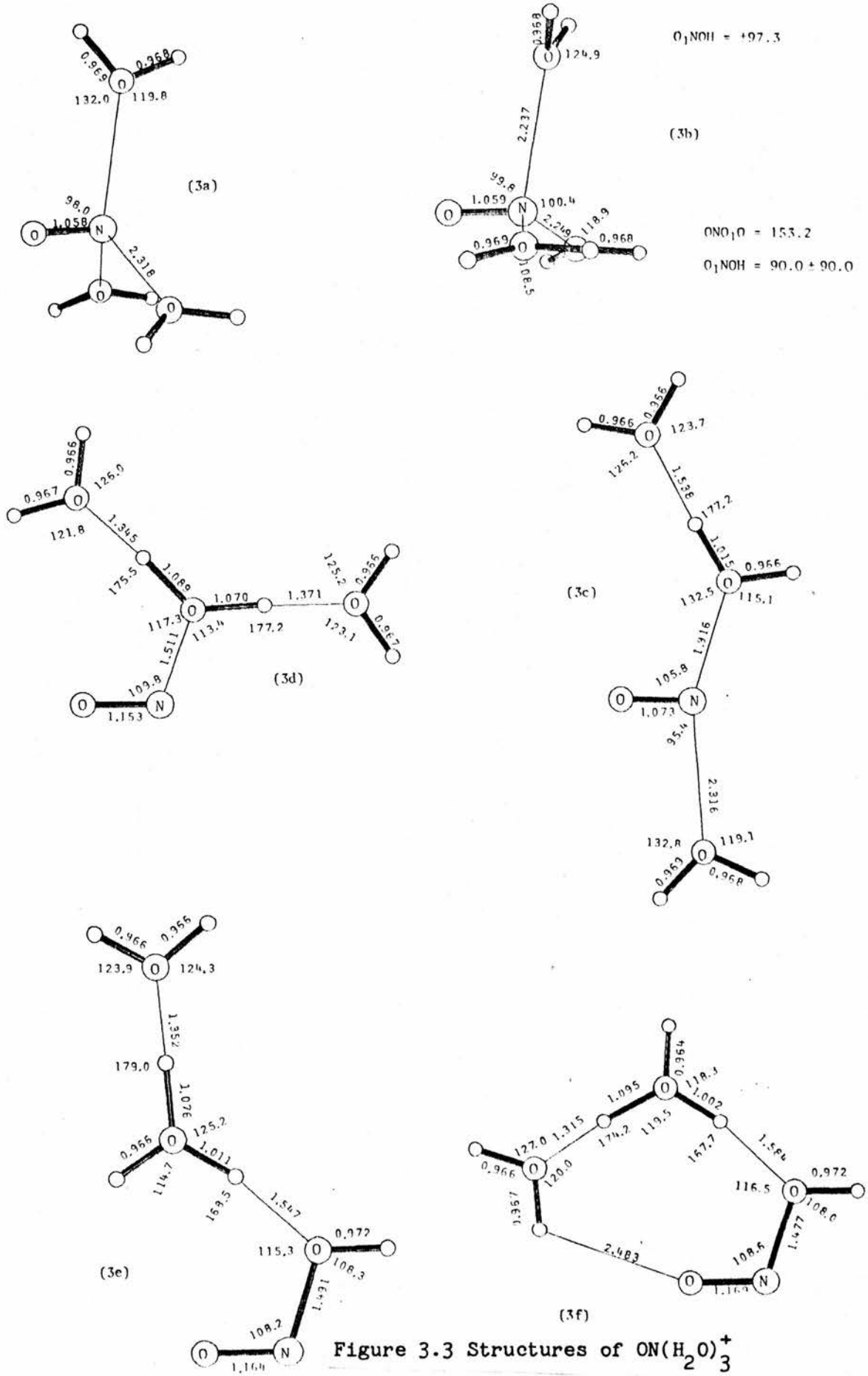

Figure 3.3 Structures of $ON(H_2O)_3^+$

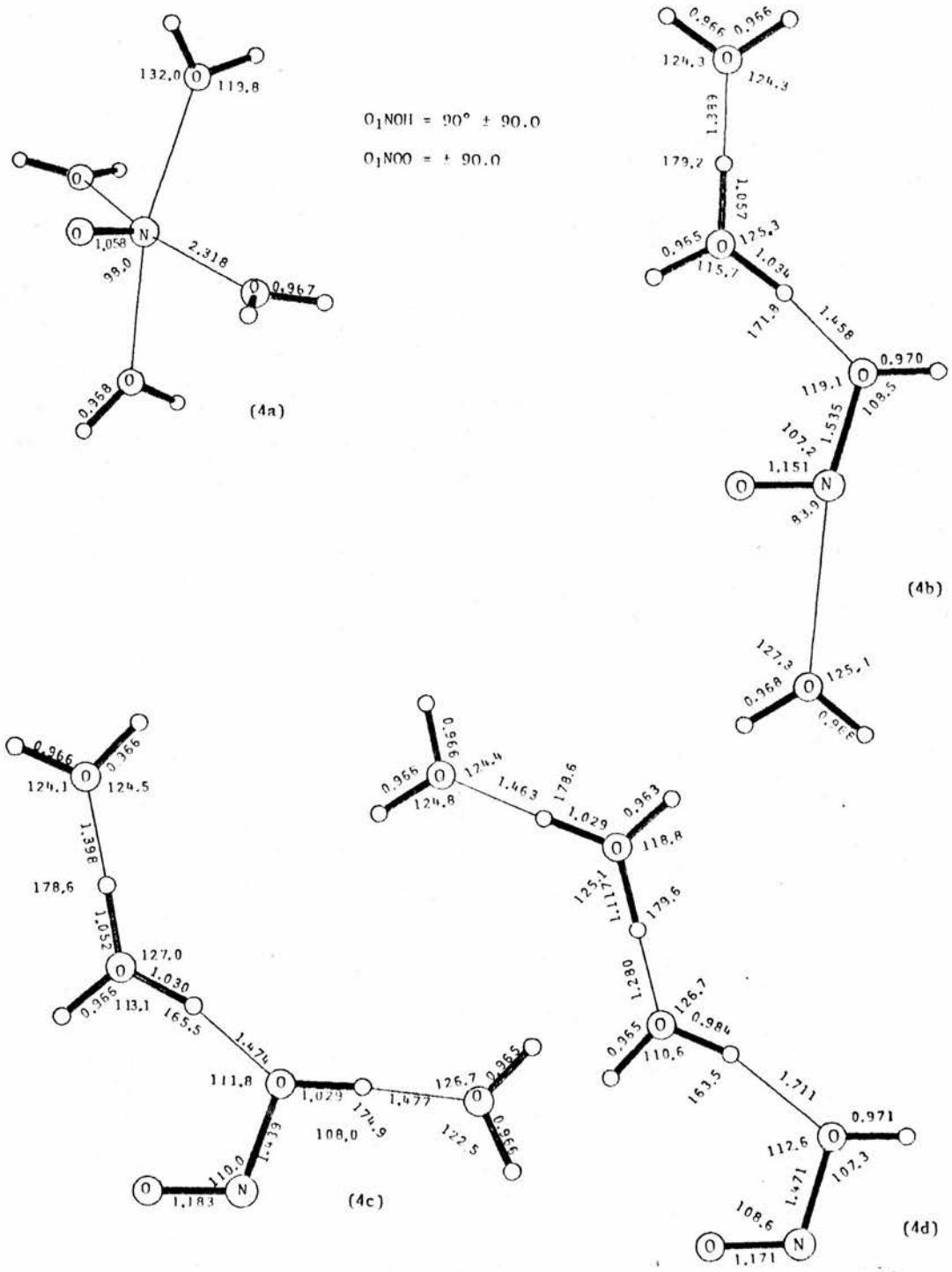

Figure 3.4 Structures of $ON(H_2O)_4^+$

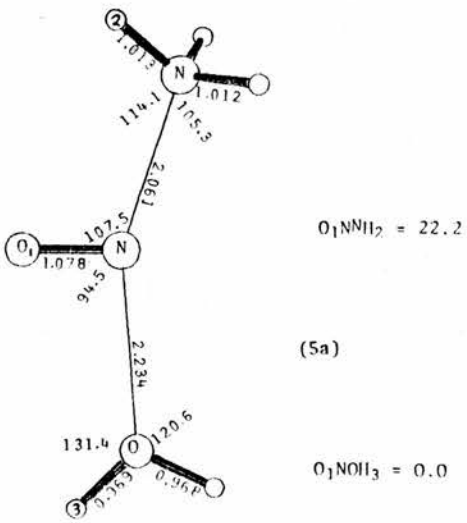

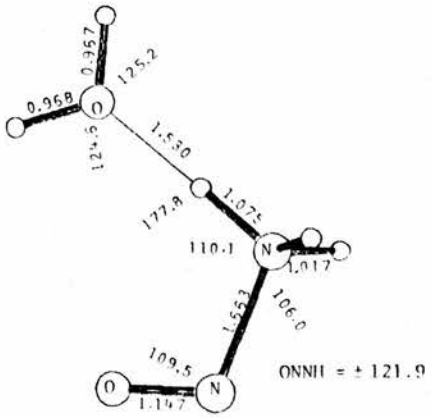

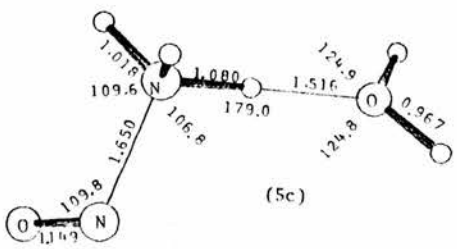

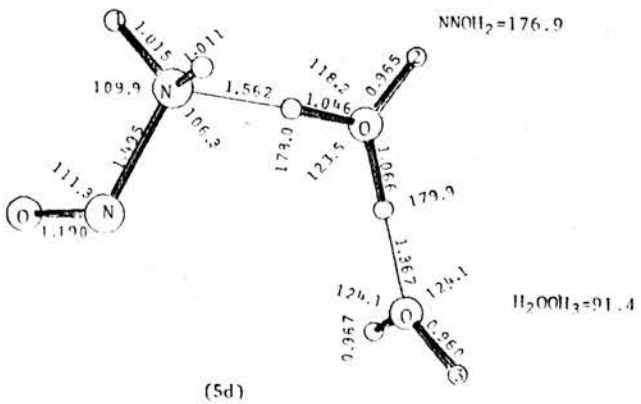

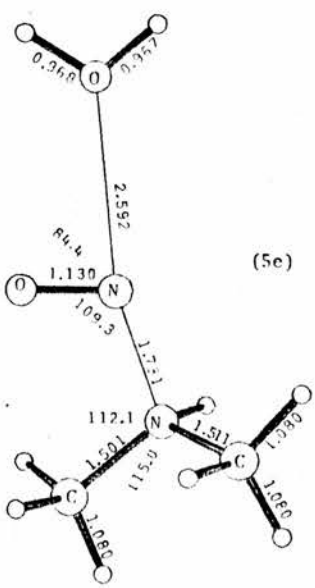

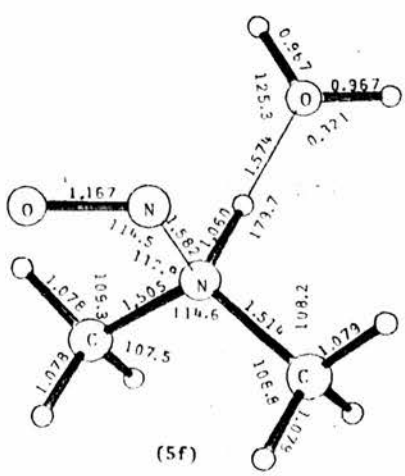

Figure 3.5 Structures of hydrated nitrosoammonium ions

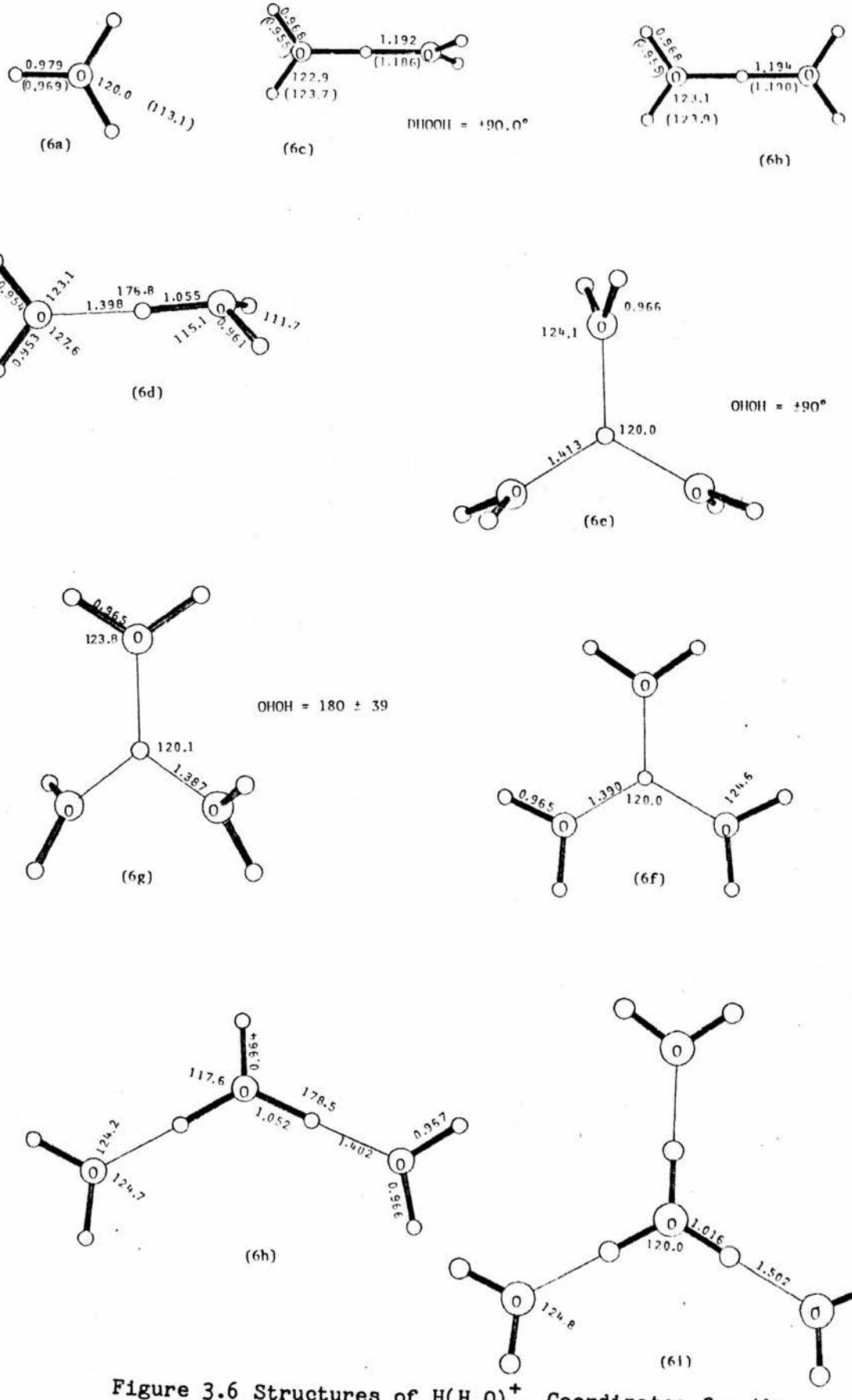

Figure 3.6 Structures of $H(H_2O)_n^+$. Coordinates for the 6-31G* geometry are in parenthesis.

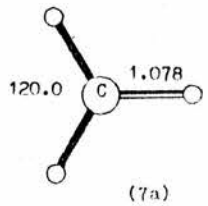

(7a)

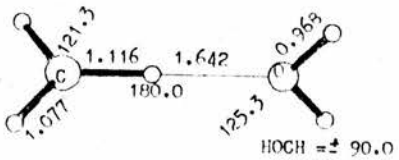

(7b)

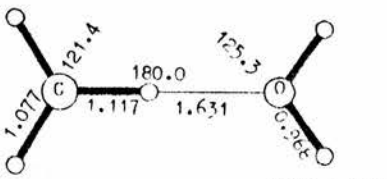

(7c)

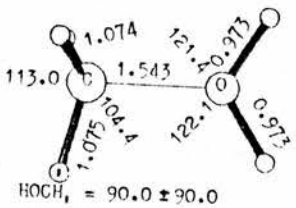

(7d)

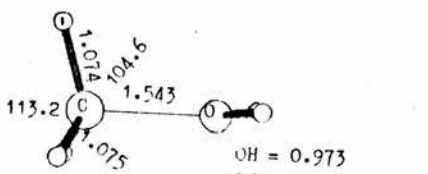

(7e) H,COH = 35.4, -153.9

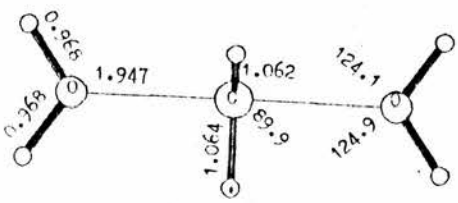

(7g)

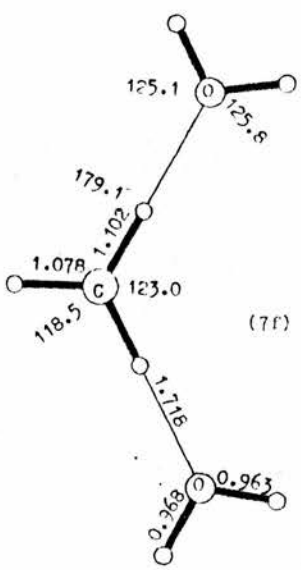

(7f)

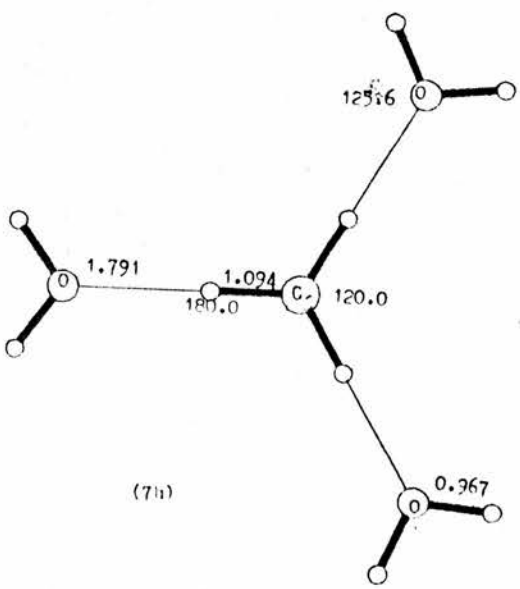

(7h)

Figure 3.7 Structures of hydrated CH_3^+

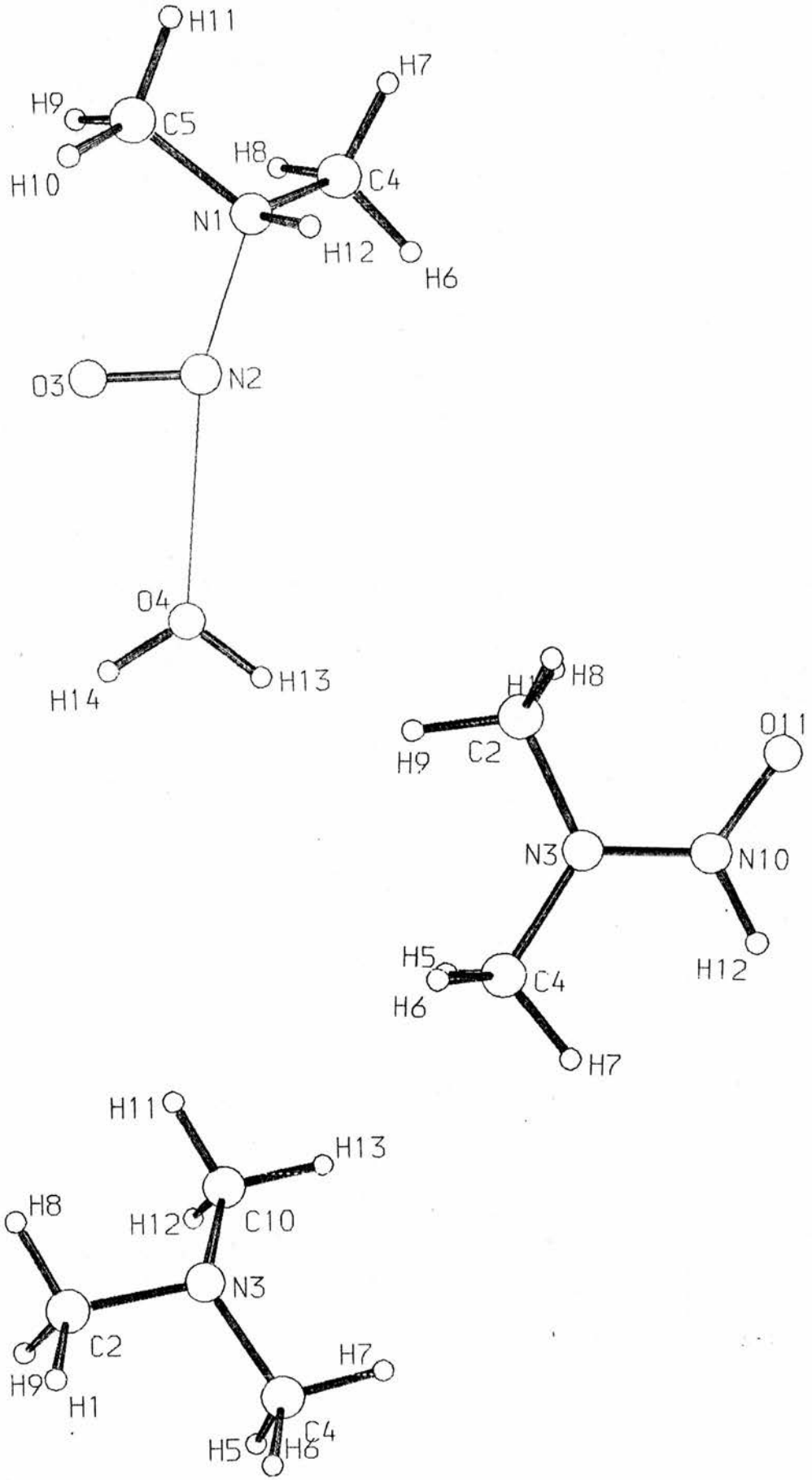

Figure 3.8 Basic numbering scheme for tables 3.7, 3.10 and 3.11

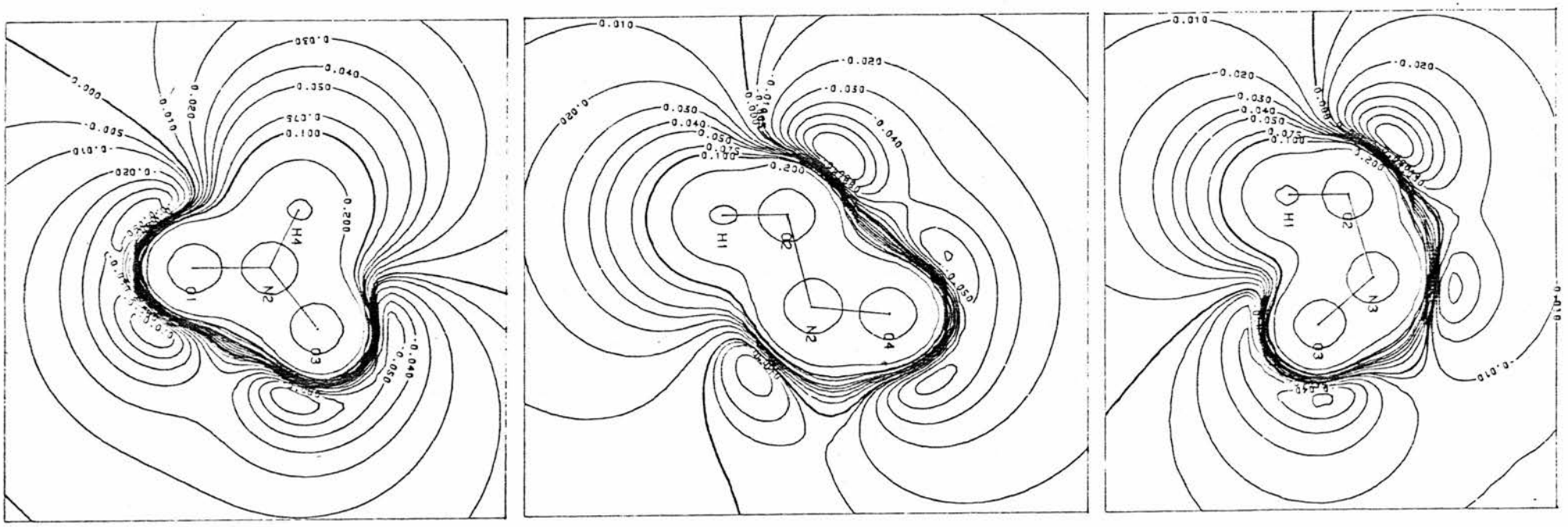

Figure 3.9 Electrostatic potential maps for (a) c-HONO, (b) t-HONO and (c) HNO_2

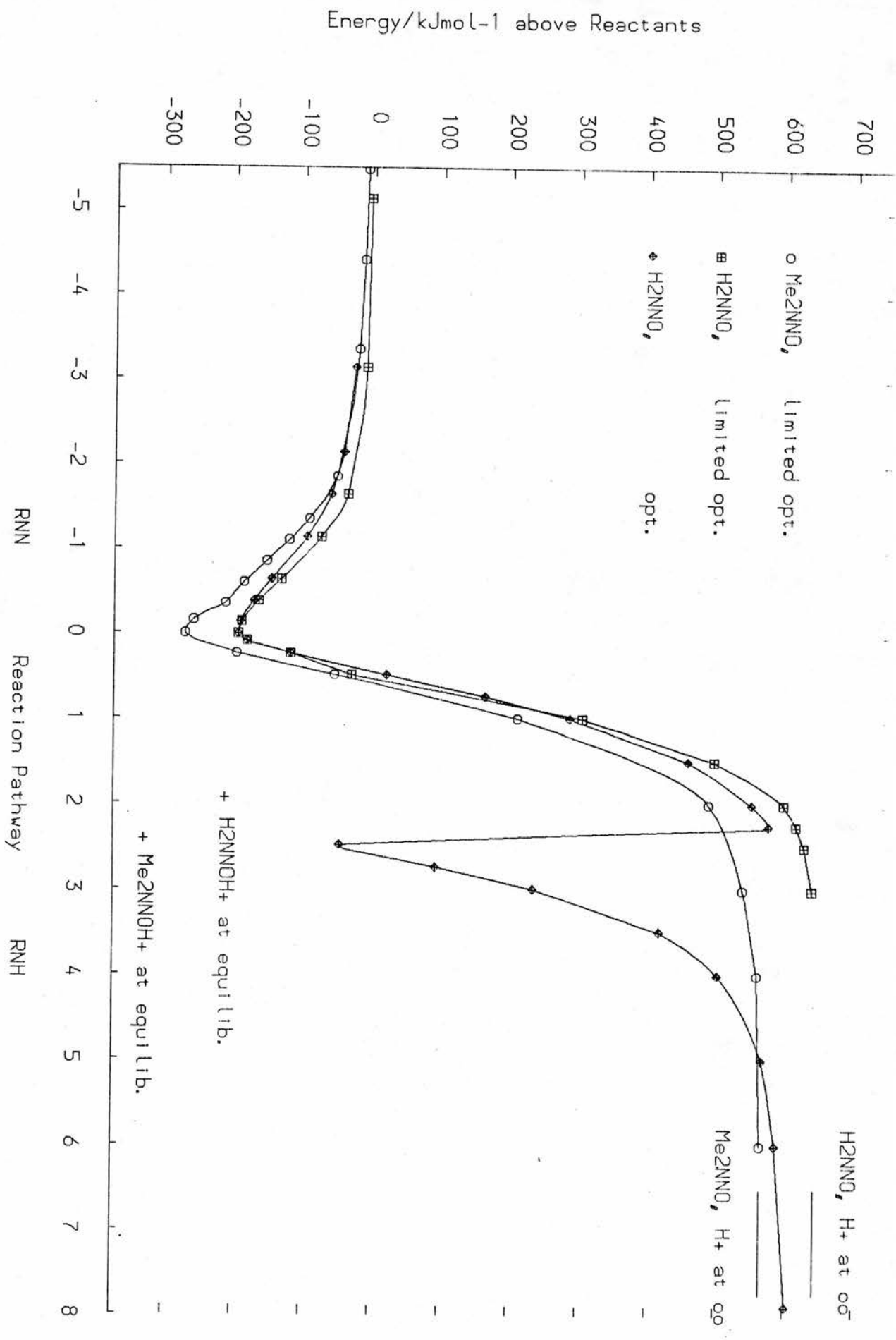

Figure 3.10 Reaction profile for nitrosation by NO^+

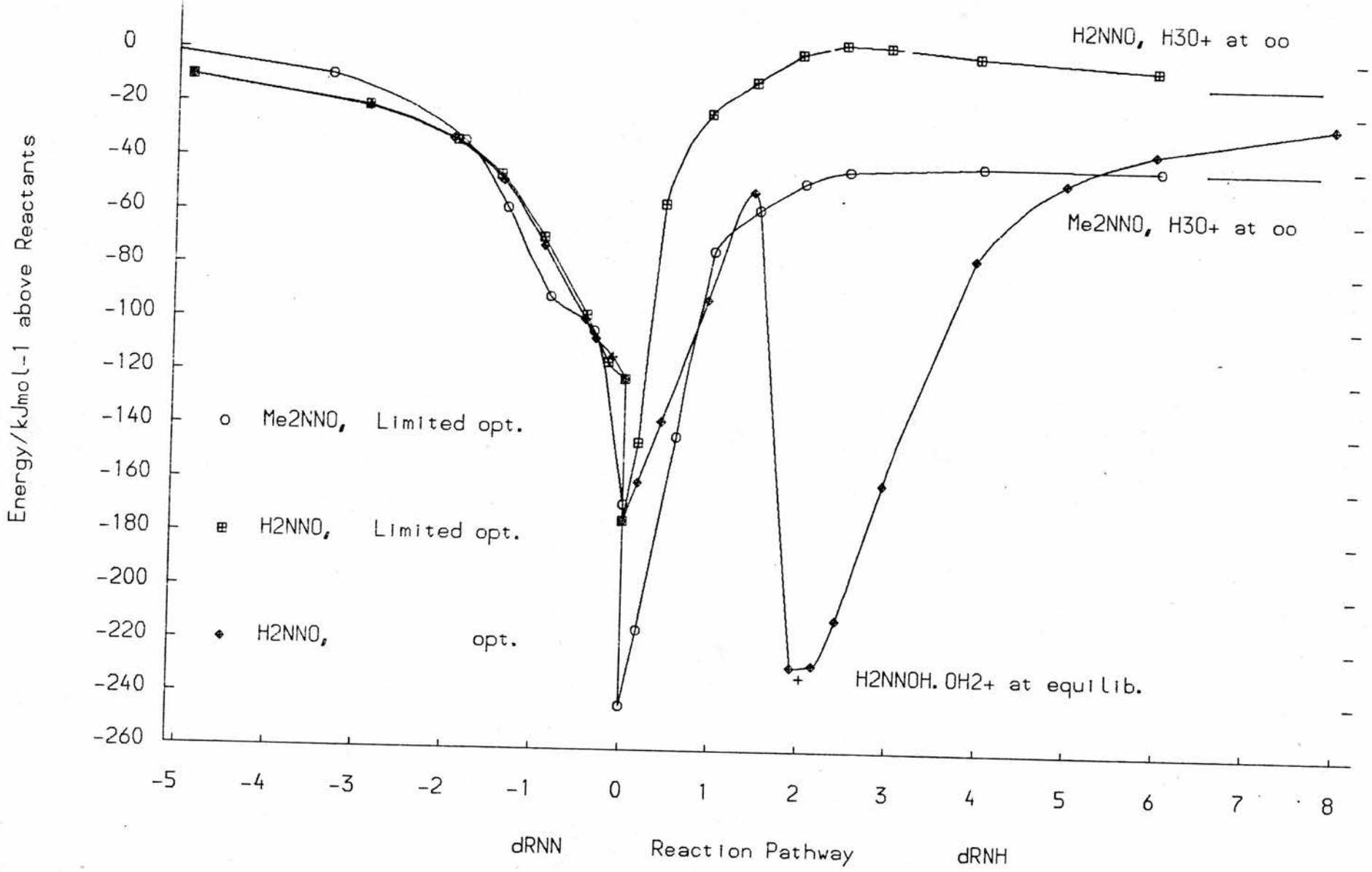

Figure 3.11 Reaction profile for nitrosation by $ON(H_2O)^+$

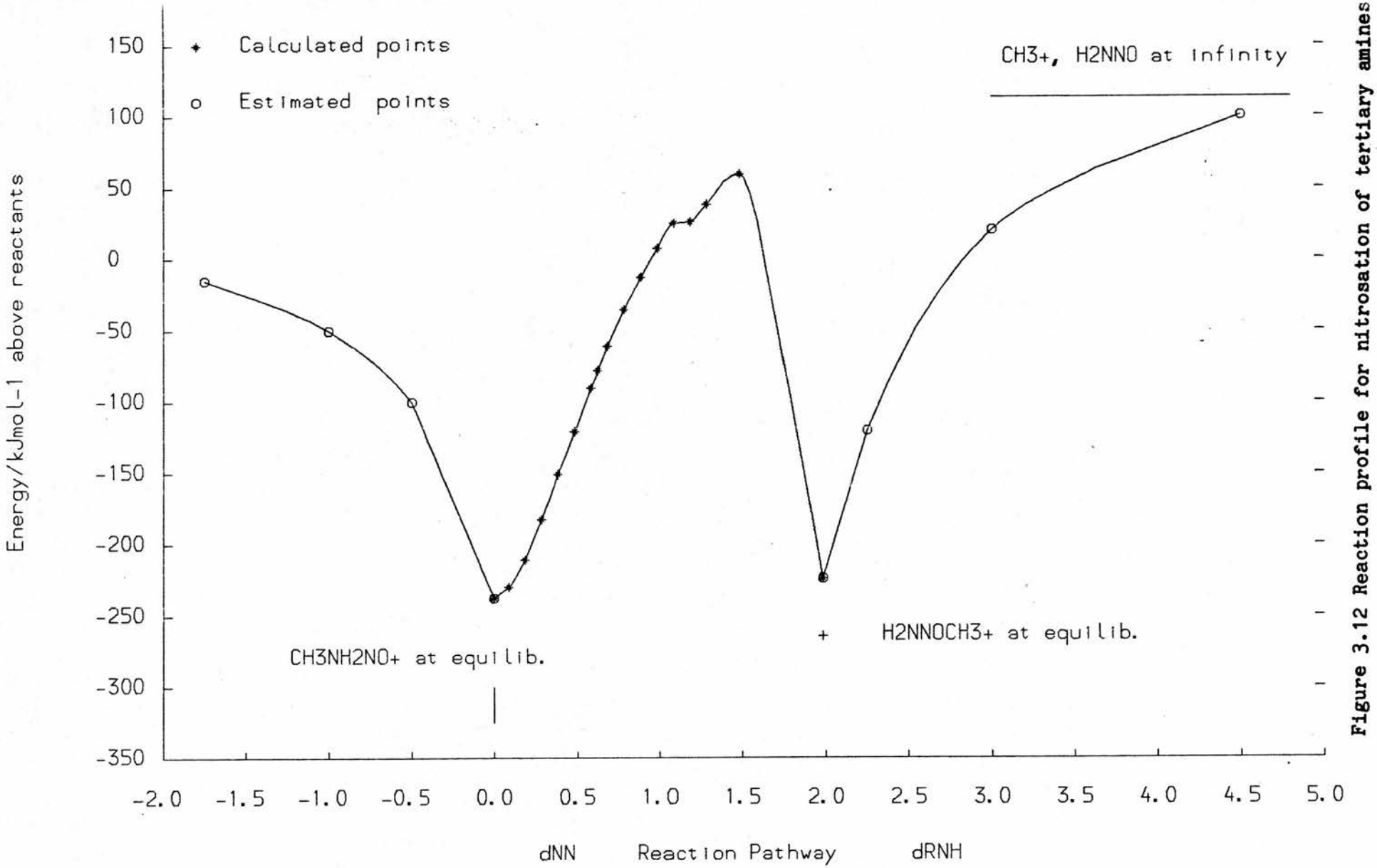

Figure 3.12 Reaction profile for nitrosation of tertiary amines

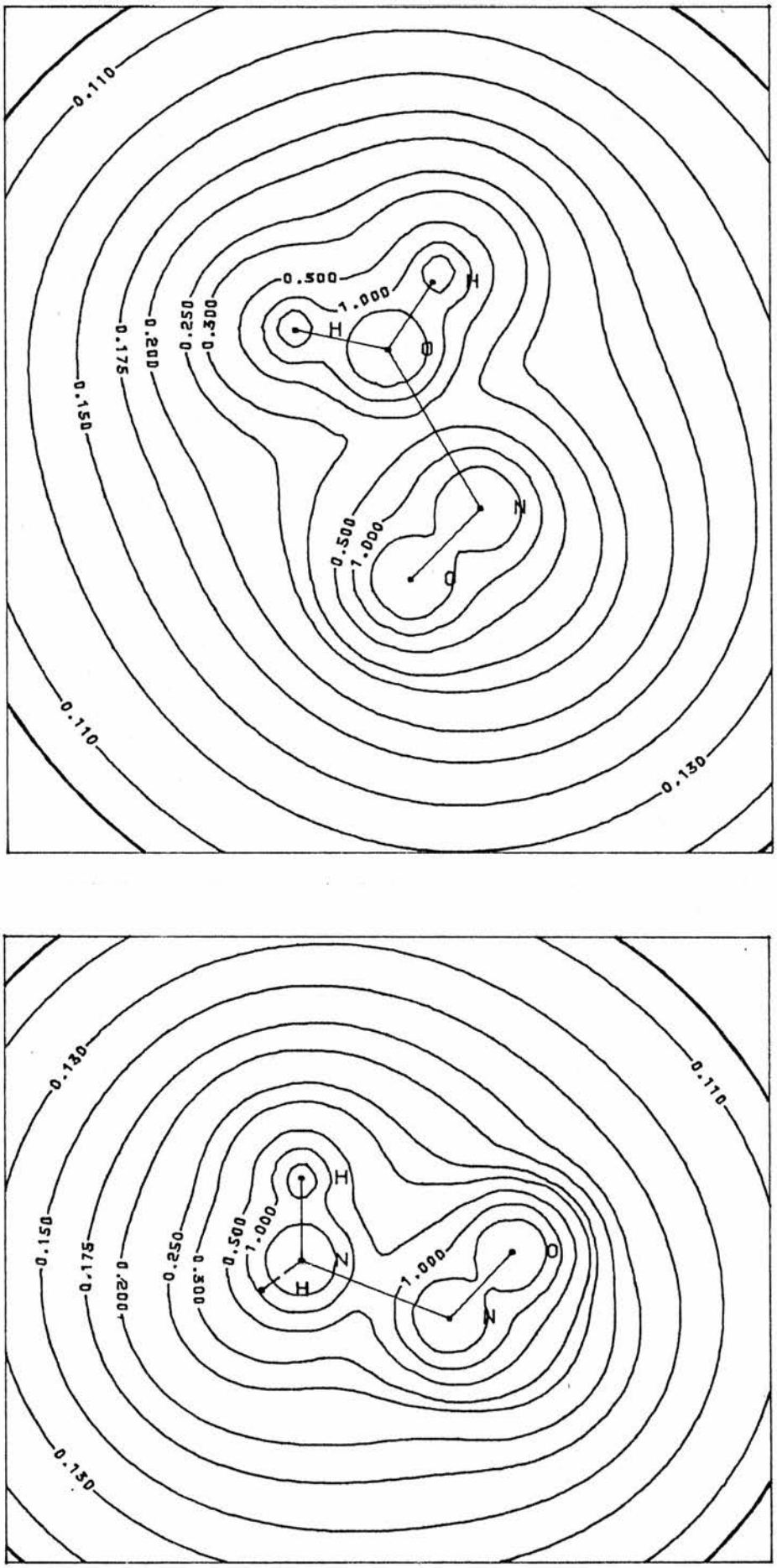

Figure 3.13 Electrostatic potential maps of H_3NNO^+ and $ON(H_2O)^+$

CHAPTER 4

THE DEMETHYLATION OF N,N-DIMETHYLNITROSAMINE

1 INTRODUCTION

The evidence for the metabolic activation of nitrosamines was discussed in chapter 1. Although there has been much controversy surrounding the nature of the activating enzyme, which is usually a demethylase, the evidence now suggests that the demethylase is a cytochrome P450.

1.1 Cytochrome P450

Cytochrome P450 actually refers to a group of enzymes which are monooxygenases; monooxygenases catalyse the addition of one atom of molecular oxygen to a substrate and simultaneously reduce the other atom of oxygen to water. The cytochromes are cell pigments with a molecular mass of around 50 000. They are present in organisms ranging from bacteria to man and are responsible for the activation of a range of carcinogens besides nitrosamines. (The designation 450 refers to an ultra-violet absorption band at 420nm which is displaced 30nm when the spectrum is recorded in the presence of carbon monoxide). The active site of cytochrome P450 is an iron porphyrin molecule. In the resting state, the iron is hexacoordinated; one axial ligand is a cysteine mercaptide ion, the other is probably an imidazole residue from histidine [39].

Binding of the substrate displaces one axial ligand to give a pentacoordinated complex. Molecular oxygen can bind to this complex following a one-electron reduction by NADH. A further one-electron reduction activates the oxygen, allowing oxidation to occur. The catalytic cycle is complete upon dissociation of the oxidised substrate. Disagreement exists, however, as to the exact nature of the activated oxygen complex [39,40].

In a recent review of cytochrome P450 catalysis [40], several different cytochrome P450 catalysed reactions have been discussed: carbon hydroxylation, heteroatom release (caused by hydroxylation α to a heteroatom), heteroatom oxidation, epoxidation, oxidative group transfer, olefinic suicide reactions and reductions. Moreover, a unified mechanism is presented in which the first step of the reaction is an electron abstraction (or a hydrogen atom abstraction) by a perferryl oxygen atom ($Fe^{V}O$) and the second step is an oxygen atom transfer. The mechanism is thus non-concerted; the experimental evidence for this comes from kinetic isotope studies and observations of the loss of stereospecificity. (Normally the reactions are stereospecific, and this is attributed to physical factors within the enzyme cage). The proposed mechanisms for hydroxylation, heteroatom release and heteroatom oxidation are given below.

a) $Fe^{V}O + H\text{-}\overset{|}{C}\text{-} \longrightarrow Fe^{IV}OH + \cdot\overset{|}{C}\text{-} \longrightarrow HO\text{-}\overset{|}{C}\text{-}$ (4.1)

b)

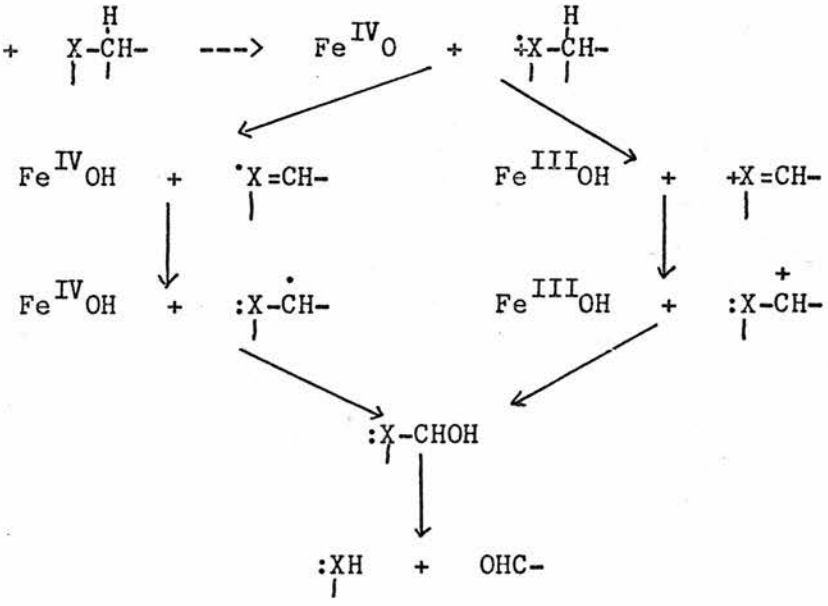

(4.2)

c) $Fe^{V}O + :\underset{|}{X}\text{-} \longrightarrow Fe^{IV}O + \cdot\underset{|}{X}\text{-} \longrightarrow {}^{-}O\text{-}\overset{+}{\underset{|}{X}}\text{-}$ (4.3)

The presence of a heteroatom can give rise to several alternative

reactions. It is found that hydroxylations occur preferentially α to a heteroatom, if a heteroatom is present. The proposed one-electron transfer from the heteroatom to the active oxygen could lead either to heteroatom oxidation or to hydroxylation α to the heteroatom. Heteroatom oxidation is apparently rare at nitrogen but is preferred on going down the non-metallic groups. It is suggested that the stability of the heteroatom radical cation, $(CH_3)_2\dot{N}NO^+$, versus the α-heteroatom radical, $CH_3(\dot{C}H_2)NNO$, is an important factor in determining whether heteroatom oxidation or heteroatom release is favoured. (It would be possible to investigate these criteria using ab-initio methods).

Two mechanisms are given for α-hydroxylations: one-electron removal from the heteroatom and hydrogen atom abstraction. Hydrogen atom abstraction is said to be favoured when the ionisation potential of the heteroatom is high. For dimethylnitrosamine the HOMO is composed mainly of basis functions centred on the amino nitrogen; the ionisation potential is less than that of methylamine but greater than that of dimethylamine or trimethylamine. Increasing the size of the alkyl groups in dialkylnitrosamines increases the ionisation potential - see table 3.8.

1.2 Other Theoretical Investigations

Andreozzi et. al. have investigated the possibility of enzymic hydroxylation at the amino-nitrogen atom of nitrosamines using OH^+ as the active oxidising species [100]. The oxidation is found to be favourable because OH^+ is highly unstable. The other proposed steps - elimination of water, followed by addition of hydroxide - result in the formation of the α-hydroxynitrosamine. These steps are also found to be favourable, though no transition structures for these steps were determined.

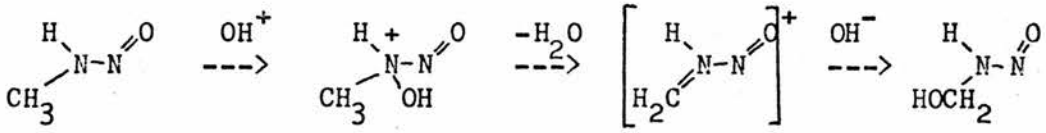

(4.4)

Andreozzi et. al. have also considered the possibility that α-hydroxylation may be governed by the electron density in the C-H bonds in the HOMO, and have predicted that the axial hydrogens of cyclic nitrosamines are preferentially oxidised [100]. This hypothesis has not, however, been tested against experiment. They have also suggested that besides the C-H bonds, other sites which might be susceptible to electrophilic attack can be measured by the relative proton affinities at the various protonation sites. They have suggested that these sites would lead to detoxification, and that the most likely site of attack leading to detoxification is the oxygen atom. This observation is in agreement with the results reported in the previous chapter on the preferred protonation site of dimethylnitrosamine. There is, however, very little experimental evidence for the nature of the detoxification pathways in the metabolism of nitrosamines.

In a series of articles which consider cytochrome P450 oxidation [41,141,196], G. Loew et. al. have modelled the active oxygen species by a triplet oxygen atom. It has been shown that this model does predict the oxidation to occur in a stepwise, rather than a concerted, manner [41] and that it is able to predict the observed oxidation products from $CHCl_3$ [196] (the actual numerical calculations in this article do not appear to be very reliable). It can also account for both the moderate (about 2-3) and the high (about 8-11) kinetic isotope effects that can be observed [141]. The model has also been applied to the oxidation of nitrosamines [197] in an attempt to rationalise the liver carcinogenicities of $(C_nH_{2n+1})_2NNO$ for n = 1 to 5. By comparing the stability of the radical, formed by the removal of an α-hydrogen, relative to the stability of the parent, it was found that

hydroxylation at all secondary carbon positions is greatly favoured over hydroxylation at primary carbon atoms, and that the α-position forms the most stable radicals. (It was suggested that these effects could explain the greater carcinogenicity of diethylnitrosamine relative to that of dimethylnitrosamine. This, however, is more likely to be connected with the preference of ethylating agents for the O-atoms of DNA - see chapter 1). The stability of the heteroatom radical (see above) was not investigated, neither were the transition structures for the initial oxidation, although these have been located for the oxidation of other substrates [41,141,196].

1.3 Strategy

The studies presented in this thesis consider only the decomposition of the α-hydroxynitrosamine. In particular, it is frequently assumed that the monomethylnitrosamine is involved in its decomposition (see figure 1.1). The work described in this chapter was initiated to determine both the products of the decomposition of the α-hydroxynitrosamine and the conditions under which this decomposition occurs. The articles by Andreozzi et. al [100] and Loew et. al [63,197] also consider this decomposition and will be discussed below. Two of the above articles [100,197], however, use semi-empirical methods. In particular, the article by Andreozzi et. al. gives several results which are qualitatively very different to those obtained by ab-initio methods. These are summarised in table 4.1. Given these large discrepancies, the semi-empirical results must be considered to be unreliable. The work presented in this chapter, like that of Andreozzi et. al., makes the approximation of replacing methyl groups by hydrogens. Loew has tested this approximation for several transition structures, using the MNDO method, and has found it to be

valid (i.e. minima, transition structures and enthalpies of activation are similar for both the dimethyl and monomethyl studies [63]). Work in this laboratory has also shown that the monomethyl and dimethyl ab-initio structures of the α-hydroxynitrosamines are similar [102].

The N-methyl-N-nitrosourea is already oxidised in the α-position and may decompose in a similar manner to the α-hydroxynitrosamine. For this reason, certain reactions of the nitrosourea are briefly considered.

2 DECOMPOSITION OF THE α-HYDROXYNITROSAMINE

The micro-environment in which the decomposition occurs is unknown. Loew has suggested that the enzyme pocket is hydrophobic [63], and that isolated molecule calculations are likely to be relevant to the lipid phase. The endoplasmic reticulum on which the cytochrome P450 is located is continuous with the nuclear membrane [168], providing a possible route to the nucleus by diffusion through the lipid phase. Normally, physiological conditions are assumed to imply a neutral aqueous solution. However, experiments with pH sensitive dyes have shown that membrane surfaces have a negative potential, implying basic conditions [168]. The histones surrounding DNA are basic proteins. The DNA itself, however, is acidic, due to the phosphate groups [198]. The calculations discussed below attempt to consider the decomposition under these different conditions.

The optimised geometries of all compounds studied are given in figures 4.1 - 4.4 (except where full geometry optimisation was not performed). The energies are reported in table 4.2. Conformational energy maps are given in figure 4.5, and electrostatic potential maps are given in figure 4.6.

2.1 Conformational Studies of the α-Hydroxynitrosamine

The three conformations of the α-hydroxymonomethyl nitrosamine are shown in figure 4.1 (1a,1b and 1c). One would expect the planar isomer, (1b), to be the most stable, due to the six-membered ring formed by hydrogen bonding between the nitroso-oxygen and the hydroxyl-proton. Although this structure, (1b), was obtained as a minimum by the optimisation algorithm, it is actually the highest energy conformation; it is probably a saddle point, the corresponding minima being forms of (1c). This is clearly illustrated in the PCILO conformational energy map (figure 4.5). The explanation for this appears to be that although there is a strong OH bonding overlap, which tends to form the planar ring, there is an even stronger anti-bonding overlap between the two oxygen atoms, and between the hydroxyl-proton and the nitroso-nitrogen. The deformation in the most stable Z-form and E-form serves to reduce this anti-bonding, which is more pronounced in the ab-initio calculations than in the PCILO calculations. This anti-bonding is apparent in (1b) through the exceptionally large CNN angle of 130.1°. (The PCILO conformational energy map was obtained by taking the lowest energy for each conformation, using the geometry of (1a), (1b) or an average of (1a) and (1b)).

This conformational phenomenon also appears in the conformation of dimethylnitrosamine. The most stable conformation is (I) - see table 3.7 - rather than (II). This surprising result has been observed in this laboratory [170], and also by Ha et. al. [103], although Ha did not comment on this.

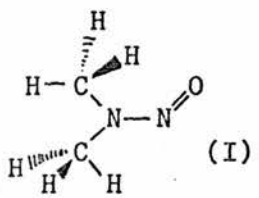

(I)

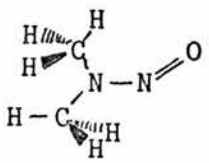

(II)

Although there is a strong bonding overlap between the nitroso-oxygen and the in-plane methyl hydrogen in (II), forming a five-membered ring, there is also a strong anti-bonding overlap between the C-atom and the nitroso-oxygen and between the in-plane methyl hydrogen and both nitrogens. These effects are minimised in (I), therefore (I) is the most stable form. The same effect may also be observed in the monomethylnitrosamines [170,103].

The Z-form of the α-hydroxynitrosamine, (1c), is more stable than the E-form (1a) by 11kJmol^{-1}. There is experimental evidence that the demethylase produces the E-form [62]. This will be connected to the most stable Z-form by rotation about the N-N bond. The RHF/4-21G energy barrier for rotation about the N-N bond in H_2NNO is 81kJmol^{-1} (see chapter 5). This compares favourably with the experimental energy barrier of 96kJmol^{-1} in $(CH_3)_2NNO$ [199], in which there will be increased steric hindrance. The energy barrier for rotation about the N-N bond in the α-hydroxynitrosamine is likely to be of a similar size. This barrier is sufficiently low to allow rotation to occur, and yet sufficiently high to allow the individual conformers to be studied [62].

While protonation has a dramatic effect on bond lengths, see below, the effect on conformation is not as great, although τNCOH does increase from 68° in (1c) to 90° in (1d) and then to 96° in (1e) on subsequent mono-hydration. The surfaces for the dihydrated molecules (2b) and (2c) are very flat. In these molecules τNNCO remains fairly constant, but τNCOH varies from 100° in (2b) to 177° in (2c) - see figure 4.2.

Protonation is likely to result in a substantial increase in the energy barrier for rotation about the N-N bond in (1d). The energy barrier for rotation about the N-N bond in H_2NNOH^+ is 244kJmol^{-1}. This is because the double bond character is shifted from the N-O to the N-N bond. This may contribute to the lower rate of decomposition of the

α-hydroxynitrosamine in acidic solution [64,200].

Only one conformation of the nitrosourea, (3e), was studied - see figure 4.3. Preliminary calculations using PCILO suggest that this is not the most stable conformation. This should not, however, affect any conclusions as conformational energy differences are usually small.

2.2 Acid Catalysed Decomposition

The possibility of acid catalysis has been investigated by studying protonation, and hydration of the protonated derivatives.

2.2.1 The effect of protonation and mono-hydration

The electrostatic potential map of (1b) (figure 4.6) suggests that the most likely protonation site is on the hydroxyl group. However, when attempts to optimise this protonated structure were made, one of the protons migrated to the nitroso-oxygen.

The protonated structure (1d) differs predictably from (1c) in that the double bond character shifts from the N-O bond to the N-N bond, as in the protonation of dimethylnitrosamines (see table 3.7). There is also a slight decrease in the C-O bond length, from 1.43Å (1c) to 1.38Å, but most significant is the change in the C-N bond length from 1.46Å to 1.58Å (for dimethylnitrosamine the corresponding change is 1.46Å to 1.51Å). Upon hydration the C-N bond length increases further to 1.63Å (1e).

The significance of these results can be seen in that a weakening of the C-N bond could result in the complete loss of CH_2OH^+, (1h), from (1d), or $CH_2OH.OH_2^+$, (1j), from (1e), giving rise to the anti-anti diazohydroxide. The energy barrier for these reactions is 206 and

105kJmol^{-1} respectively. It can be seen from figure 4.1 that $CH2OH.OH_2^+$ is better described as $CH_2O.H_3O^+$; there is no distinction between these two forms using the 4-21G basis set. Structure (1j) is 29kJmol^{-1} below $H_2O.CH_2OH^+$, (1i), at this level of theory.

However, the other main monohydration product of (1d), (1f), is more stable than (1e) by at least 50kJmol^{-1}; (1f) was not fully optimised.

2.2.2 Protonation and dihydration

The work on the protonation and hydration of nitrous acid - see chapter 3 - suggests that CH_2O, (1g), could be removed from (1d) by a chain of 2 molecules of water, without an energy barrier, as a $[CH_2O.H_3O.OH_2]^+$ complex. For these studies the STO-3G basis set has been used. The structures (2a), (2b) and (2c) were optimised to convergence on the gradient and gradient norm only, as full convergence was very slow, due to the flat nature of the surfaces. Surprisingly, two different structures for a hydration chain based on the hydroxyl proton were obtained - (2a) and (2b); (2b) is lower in energy by 11kJmol^{-1}, and there appears to be an energy barrier (which is probably small) between the two forms. The structure (2c) is 84kJmol^{-1} below (2a).

Protonation and hydration of the N-methyl-N-nitrosourea, (3e), could also lead to the formation of a diazohydroxide, provided that protonation occurred most readily at the nitroso-oxygen and that the most stable hydration chain was based on the amino proton. However, the electrostatic potential map, (figure 4.6), indicates that the most likely protonation site is at N6, closely followed by O5, suggesting that acid catalysed decomposition of the nitrosourea is unlikely; this is in agreement with experiment [58].

2.2.3 Summary

These results suggest that protonation and hydration will not cause the decomposition of the α-hydroxynitrosamine, as the two estimates of the energy barrier (from sections 2.2.1 and 2.2.2) are 155 and 84kJmol^{-1}; the acid catalysed decomposition can thus only occur slowly, if at all. These results are in agreement with experimental results which showed that increasing acidity had little effect on the decomposition of the α-hydroxynitrosamine [64,200]. Protonation and hydration are not expected to lead to the decomposition of the nitrosourea.

2.3 Base Catalysed Decomposition

The effects of base on the α-hydroxynitrosamine have been investigated by removing the hydroxyl proton from (1a) and (1b), and then carrying out a full optimisation on the resulting anions. The anions are unstable and fly apart during the optimisation to give the fragments CH_2O and $HNNO^-$. In the anions considered, all the electrons were bound - this is a test that a reasonable description of the anion is given; in unfavourable situations it is possible that some of the occupied orbitals may have a positive energy. However, just to confirm these studies, the first and last points of the optimisation of the anion derived from (1a) were repeated using the 6-31+G basis set. The initial result - that the anion falls apart to fragments - was confirmed, and again all the electrons were bound. The methyl diazotate anion, CH_3NNO^-, could be protonated to give either the monomethylnitrosamine or the diazohydroxide, there being very little energy difference between these two forms - see chapter 5. These results are consistent with the very short half-life of the

α-hydroxynitrosamine in alkali solution [64,200]. (Andreozzi et. al. also investigated this possibility; they found that the anion was stable and that the energy barrier for the removal of the CH_2O was 119kJmol^{-1}. These results are unreliable in the light of the ab-initio results).

The effect of base on the (model) nitrosourea could result in structure (3c), where a methyl group has been replaced by a hydrogen. This optimised structure, (3c), did not fly apart due to the large energy barrier of 107kJmol^{-1} for reaction (4.5). The CN bond of (3c) is long, being 1.55Å; all the electrons were bound.

$$HNCONHNO^- \longrightarrow HNCO + c\text{-}HNNO^- \qquad (4.5)$$

Nevertheless, the nitrosourea is unstable in base

$$H_2NCO(CH_3)NNO + OH^- \longrightarrow HNCO + H_2O + t\text{-}CH_3NNO^- \qquad (4.6)$$

ΔE for reaction (4.6) is -205kJmol^{-1}, and so nucleophilic attack by OH^- at the carbon atom would seem a more likely mode of decomposition than removal of the amino proton; HNCO would still be a likely product - PhNCO has been observed in the base catalysed decomposition of $PhNCON(CH_3)NO$ [201].

The hydrolysis of the α-hydroxynitrosamine

$$CH_2OHNHNO + OH^- \longrightarrow CH_2O + H_2O + t\text{-}HNNO^- \qquad (4.7)$$

is exothermic by 153kJmol^{-1}. For this reaction, the alternative mode of attack, by OH^- at the carbon atom, has also been considered. There appears to be an energy barrier for this reaction: when an OH^- fragment is placed near the carbon atom, and the supermolecule optimised, the hydroxide ion moves away from the carbon towards one of the α-hydrogens. However, when the hydroxide ion is bound to the carbon, the complex falls apart to give $CH_2(OH)_2$ and $HNNO^-$. The transition structure has not been located. $CH_2(OH)_2$ is an unstable molecule, and will be hydrolysed to give CH_2O and H_2O.

$$CH_2(OH)_2 \longrightarrow CH_2O + H_2O \qquad (4.8)$$

Base catalysed hydrolysis seems a likely mechanism for the

decomposition of the α-hydroxynitrosamine.

2.4 Decomposition in Lipid Solution

The decomposition of the α-hydroxynitrosamine, via a four-membered ring to the monomethyl nitrosamine, and via a six-membered ring to the diazohydroxide, has already been studied at the RHF/3-21G level [63]. The energy barriers above the E-hydroxymethylnitrosamine were found to be 277 and 118kJmol^{-1} respectively. We have repeated the transition structure for the six-membered ring, as the geometry was not fully reported, and find the energy barrier to be 141kJmol^{-1} above the Z-conformer at the 4-21G level (4a). The marked distortion in the transition structure is carried over from the geometry of the Z-conformer, (1c). Moreover, as the overall energy changes for reactions (4.9) and (4.10) are endothermic by 90 and 85kJmol^{-1} respectively, it appears that the inclusion of electron correlation or zero-point effects could not reduce the barriers sufficiently to enable the reactions to proceed.

$$Z\text{-}CH_2OHNHNO \longrightarrow CH_2O + t,c\text{-}HNNOH \qquad (4.9)$$

$$Z\text{-}CH_2OHNHNO \longrightarrow CH_2O + H_2NNO \qquad (4.10)$$

The endothermicities for the analogous reactions

$$E\text{-}CH_2OHNHNO \longrightarrow CH_2O + t,c\text{-}HNNOH \qquad (4.11)$$

$$E\text{-}CH_2OHNHNO \longrightarrow CH_2O + H_2NNO \qquad (4.12)$$

can be calculated using data from [63]. When the energy is calculated using the 6-31G** basis set at the 3-21G geometry, the overall energy changes are 61 and 70kJmol^{-1} respectively, therefore the barriers must be even higher. These high barriers are in agreement with the stability of the α-hydroxynitrosamines in aprotic solvents [64].

2.4.1 Reactions not leading to activation

In the next chapter several transition structures for N->O methyl shifts will be given, but the results will also be discussed here. The overall reaction

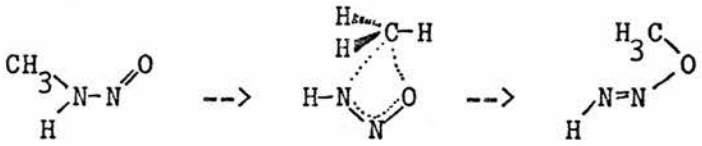

(4.13)

is slightly endothermic by 13kJmol^{-1}. (Note that the conformer of CH_3NHNO given is not the lowest energy conformer - see above). The formation of the diazomethoxide, $HNNOCH_3$, would be an activating step, as it would have similar properties to the diazohydroxide. However, the energy barriers for the forward and reverse steps are 294 and 281kJmol^{-1} respectively, so these reactions are clearly not favoured. The corresponding reaction for the O-protonated monomethylnitrosamine is

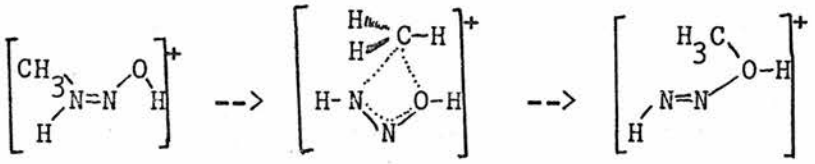

(4.14)

The overall energy change is -9kJmol^{-1}; the energy barriers for the forward and reverse reactions are 215 and 224kJmol^{-1} respectively. These calculations serve to illustrate the degree of activation required for the nitrosamines to be demethylated. (The nature of $HNN.CH_3OH^+$ will be discussed in chapter 6).

The possibility that the α-hydroxynitrosamine could decompose by an N->O shift was also investigated.

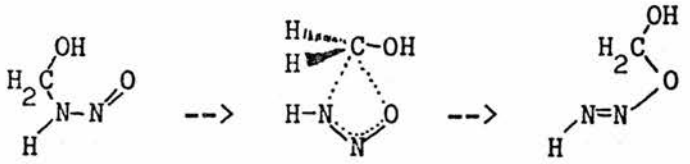

(4.15)

This would result in the formation of $HNNOCH_2OH$, which is likely to decompose to give HNNOH and $CH_2(OH)_2$, both of which would give rise to products normally expected from the metabolism of nitrosamines. The overall energy change for reaction (4.15), where (1c) is considered, is $24kJmol^{-1}$, so the overall reaction is not as unfavourable as reactions (4.9) - (4.12), but the forward energy barrier is far higher, being $264kJmol^{-1}$ above (1b).

2.5 Decomposition in Aqueous Solution

The decomposition of (1c) to the monomethylnitrosamine has been re-examined. Where the NO group is replaced by a hydrogen, the barrier is $206kJmol^{-1}$ (4b - 4c) (The barrier is $208kJmol^{-1}$ using the 3-21G basis set - results not shown). Moreover, the effect of solvent assistance in this reaction has also been investigated (4d - 4e); the barrier is reduced to $94kJmol^{-1}$. The transition structure (4e) was constrained to be planar, and although it is a stationary point, with zero forces, it is possibly a second order transition structure. If so, the true transition structure probably lies about $5kJmol^{-1}$ lower in energy, and is non-planar at the migrating H_3O^+ - see chapter 5. (The non-planar transition structure would be more difficult to locate).

The analogous transition structure to (4d) for the nitroso compound is (4g). This has been obtained by constraining the structure to be planar (likewise for (4f)); the energy barrier is approximately $163kJmol^{-1}$. (The maximum forces in (4f) and (4g) are 0.0076 and

0.0016hartree/bohr respectively). Replacing a hydrogen in either (4c) or (4e) by a nitroso group raises the energy barrier considerably; this has been attributed to the loss of conjugation [63]. It thus appears that decomposition of the α-hydroxynitrosamine to the monoalkylnitrosamine will not occur, even when aided by hydration. Moreover, full optimisation of (4f) gives conformation (3d) which is 204kJmol^{-1} lower in energy than (4g); the water molecule points towards the nitroso-oxygen, making the formation of the monoalkylnitrosamine even more unlikely. (3d) was optimised to convergence on the gradient norm and the r.m.s. displacement; the maximum force was 0.0006hartree/bohr. Solvent assistance in the formation of the diazohydroxide has not been investigated. The structure (3d) suggests that solvent assistance may lower the barrier for reaction (4.9) sufficiently to allow the reaction to proceed. Experiment shows that the rate of decomposition in neutral aqueous solution is not as great as in alkali solution [64,200].

3 CONCLUSIONS

Although protonation and hydration can significantly weaken the C-N bond, it would appear that the α-hydroxynitrosamine does not decompose by an acid catalysed mechanism. It also appears that the energy barriers for the decomposition in the gas or lipid phase are too high at physiological temperatures, partly due to the endothermicity of the reaction. Even when solvent assistance is possible, the barrier to the formation of the monoalkylnitrosamine (and probably the alkyldiazohydroxide) is sufficiently high to rule out this reaction. The loss of the hydroxyl-proton under basic conditions, however, gives rise to the expected products without an energy barrier. S_N2 attack at the α-carbon by hydroxide ions may also be important. Thus, base

catalysed decompositon would appear to be the most likely mechanism, and the resultant alkyldiazotate anion would yield either the monoalkylnitrosamine or the alkyldiazohydroxide upon reprotonation. These results are in agreement with experiment, and in addition indicate that the monomethylnitrosamine is not formed directly. The corollary is that in the absence of base, and particularly in the absence of an aqueous environment, the α-hydroxynitrosamine may have a sufficiently long life-time to diffuse across the cell.

One weakness in this work is that radical mechanisms have not been studied, even though the α-hydroxynitrosamine is formed by a radical mechanism. It may be possible to study the decomposition of the α-hydroxynitrosamine in an e.s.r. tube, but care would need to be exercised due to the large evolution of nitrogen [202].

The majority of the work in this chapter was presented at TOR85, an international conference on the theory of organic reactions, and has been submitted for publication [203]; other aspects have already been published [204].

Table 4.1 Qualitative differences between semi-empirical [100] and ab-initio results (this work)

Molecule	Semi-Empirical Results	Ab-initio Results
CH_2ONHNO^-	Stable molecule	Falls apart
$HNNO^-$	Syn and anti isomers differ by $99 kJmol^{-1}$	Syn and anti isomers differ by $38 kJmol^{-1}$
CH_3NHNO	Eclipsed CH and NO conformations preferred by MINDO/3 (but not by CNDO/2)	Staggered CH and NO conformations preferred
$CH_3NN.OH_2^+$	Geometry differs little from that of CH_3NNOH	Geometry very different to that of CH_3NNOH
$CH_3NN.OH_2^+$	Dissociates spontaneously to CH_3NN^+ and H_2O	Energy barrier to dissociation is $78 kJmol^{-1}$
t,t-CH_3NNOH	ACNN = 143°	ACNN = 113°
t,t-CH_3NNOH	Protonation is endothermic	Protonation is highly exothermic
HNNOH	c,c-isomer most stable	c,c-isomer least stable

Table 4.2. Energies, in hartrees, of compounds: (TS) denotes a transition structure, ~ denotes an approximate energy. The energies for (2a), (2b) and (2c) were determined using the STO-3G basis set, otherwise the 4-21G basis set was used.

Compound	Label	Energy	Compound	Label	Energy
E-$CH_2OHNHNO$	1a	-297.988977	HNCO	3a	-167.360128
Z-$CH_2OHNHNO$ (TS)	1b	-297.978481	$CH_2(OH)_2$	3b	-189.442106
Z-$CH_2OHNHNO$	1c	-297.993139	$HNCO.NHNO^-$	3c	-351.157377
Z-$CH_2OHNHNOH^+$	1d	-298.325012	$ONNH.CH_2OH.OH_2$	3d	-373.841583
Z-$CH_2OH.OH_2NHNOH^+$	1e	-374.185359	$CH_3N(NO)CONH_2$	3e	-390.693720
Z-$CH_2OHNHNOH.OH_2^+$	1f	<-374.204234	Z-$CH_2OHNHNO$ (TS)	4a	-297.939258
CH_2O	1g	-113.592448	H_2NCH_2OH	4b	-169.122422
CH_2OH^+	1h	-113.884598	H_2NCH_2OH (TS)	4c	-169.043227
$H_2O.CH_2OH^+$	1i	-189.772024	$H_2NCH_2OH.OH_2$	4d	-245.511189
$CH_2O.H_3O^+$	1j	-189.783238	$H_2NCH_2OH.OH_2$ (TS)	4e	-245.475507
$CH_2OHNHNOH.2H_2O^+$	2a	-445.194984	$HN(NO)CH_2OH.OH_2$	4f	<-373.825853
$CH_2OHNHNOH.2H_2O^+$	2b	-445.199120	$HN(NO)CH_2OH.OH_2$ (TS)	4g	-373.763731~
$CH_2OHNHNOH.2H_2O^+$	2c	-445.227020			

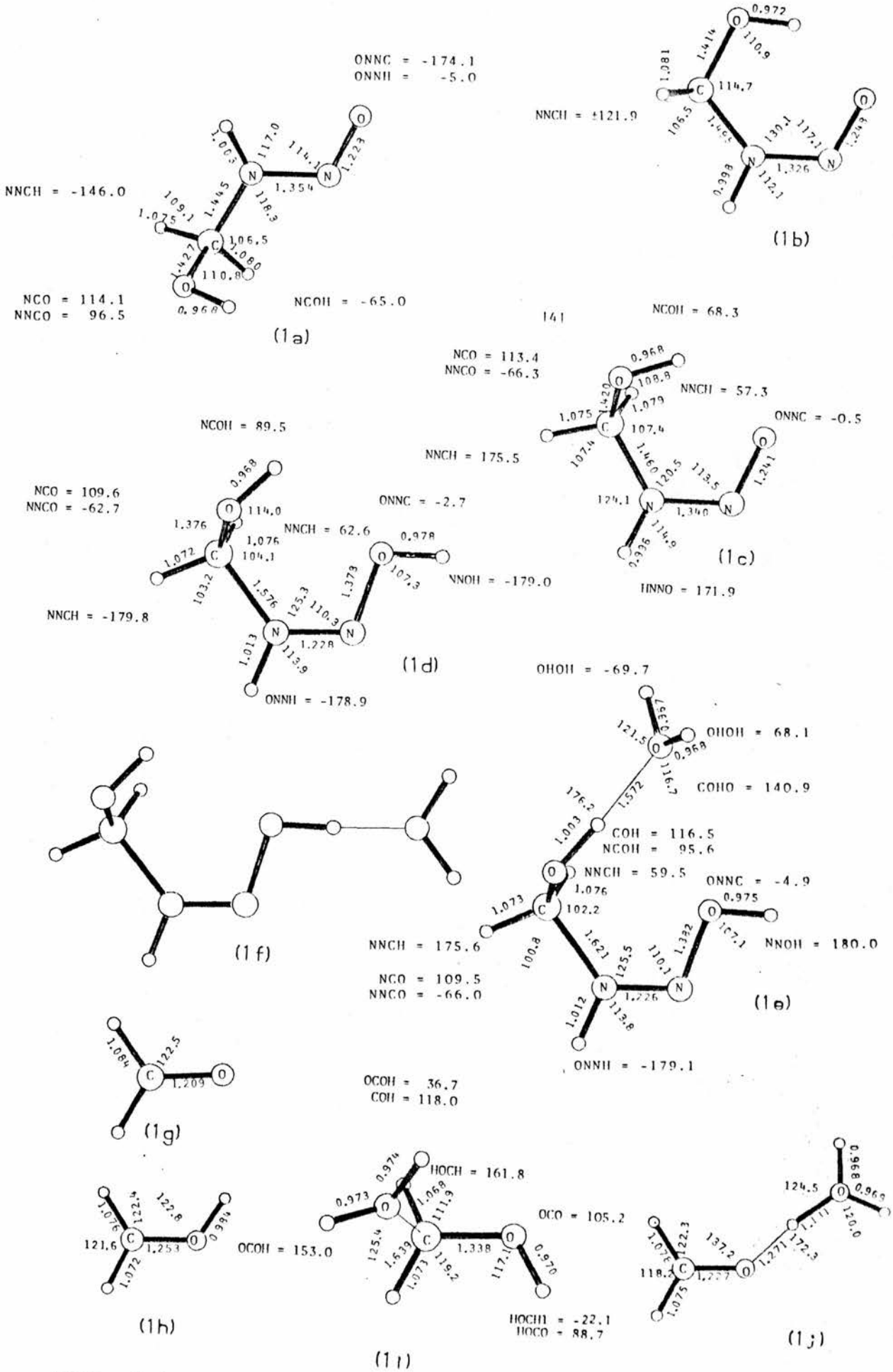

Figure 4.1 Fully optimised geometries of α-hydroxynitrosamine derivatives

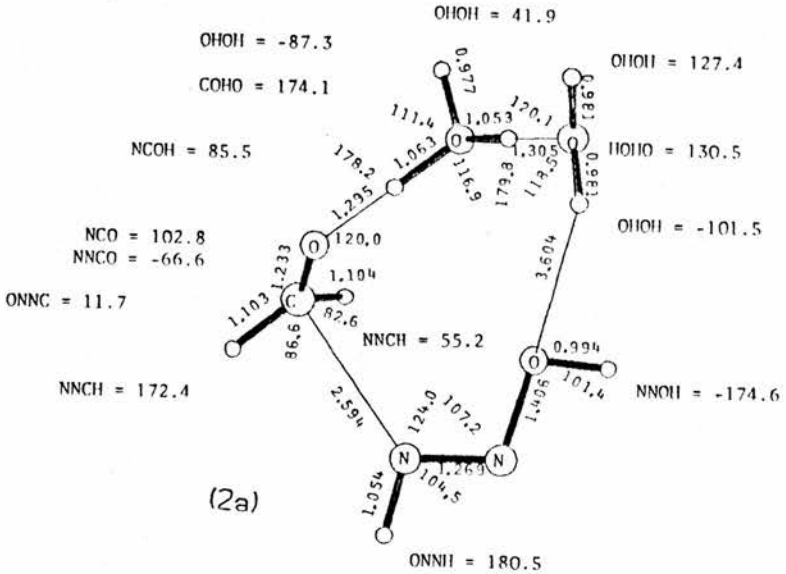

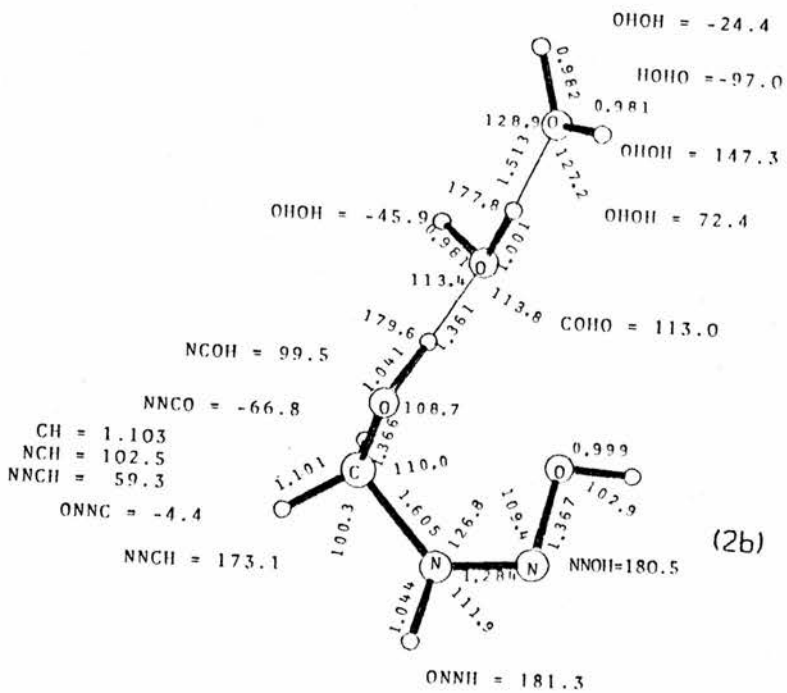

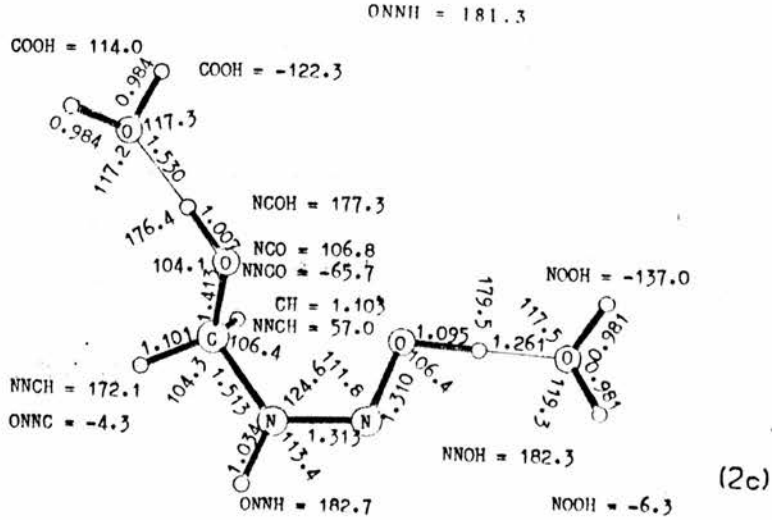

Figure 4.2 Fully optimised geometries of α-hydroxynitrosamine derivatives

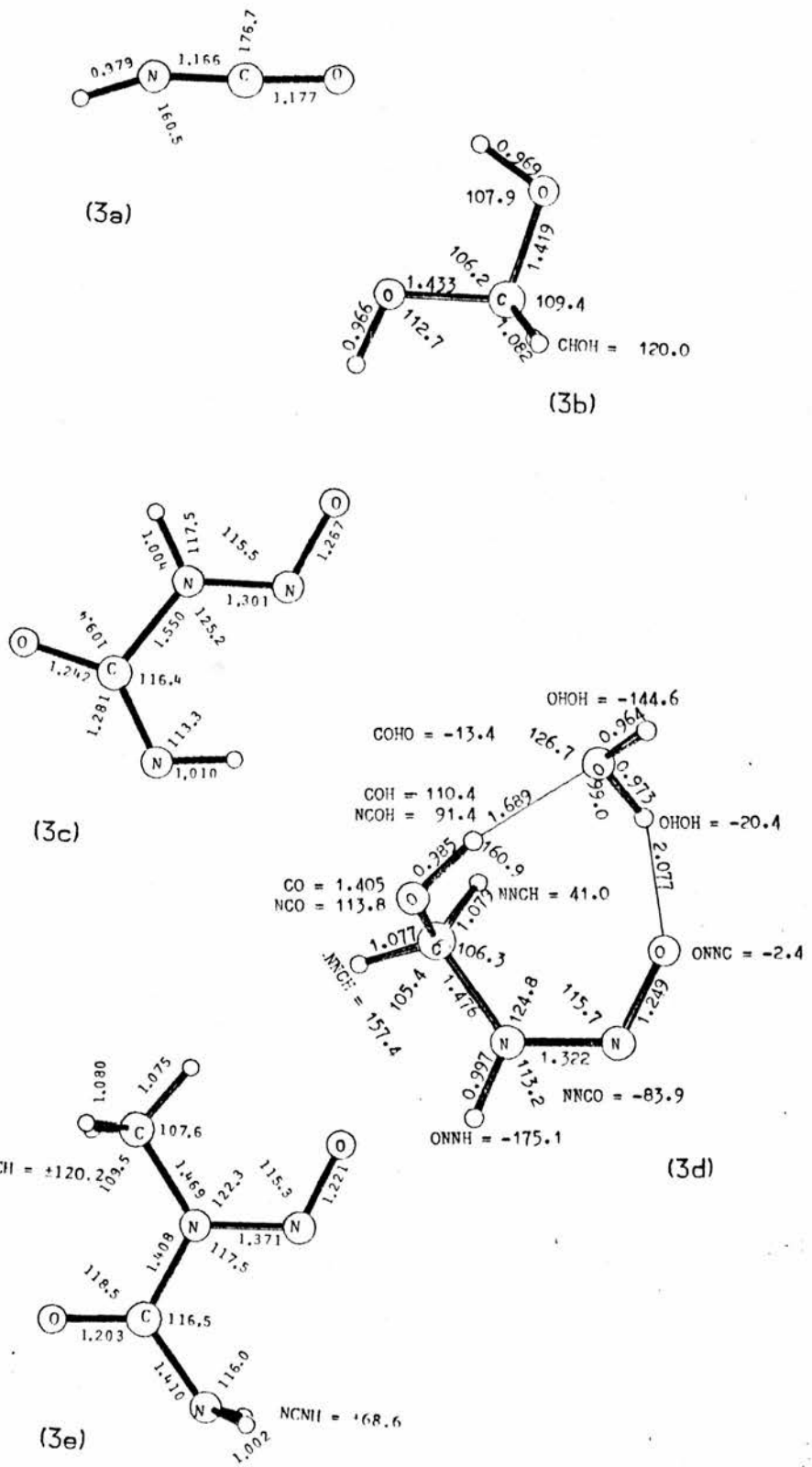

Figure 4.3 Fully optimised geometries of nitrosoureas and other species

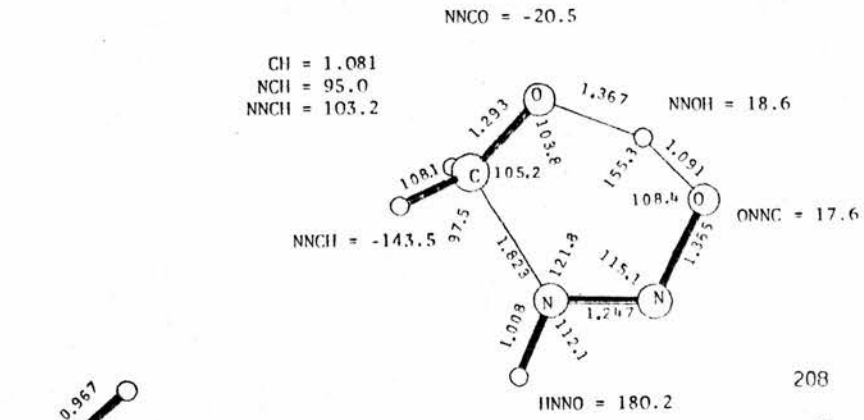

(4a)

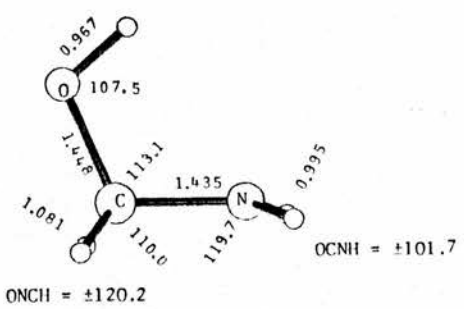

(4b)

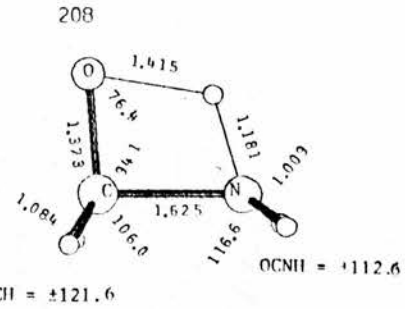

(4c)

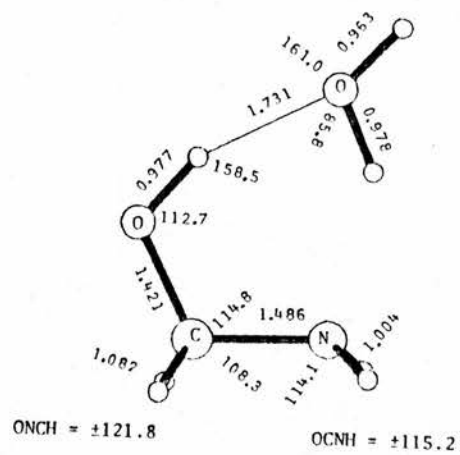

(4d)

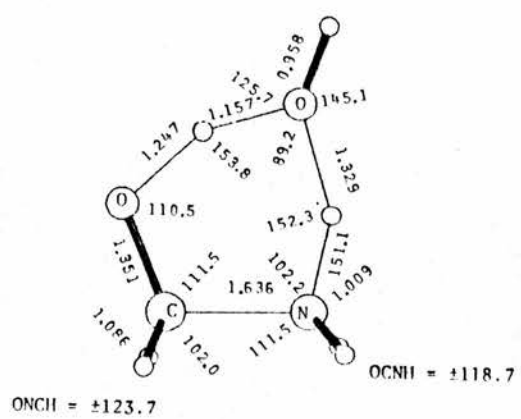

(4e)

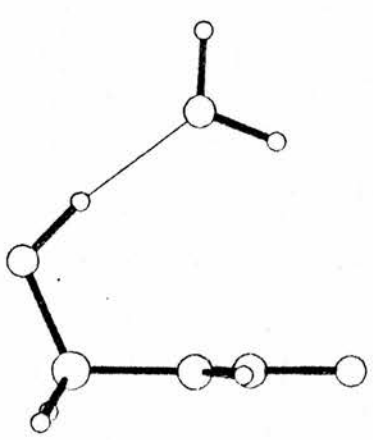

(4f)

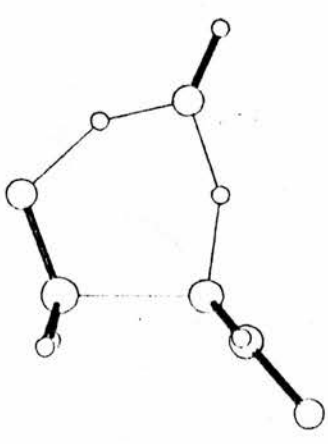

(4g)

Figure 4.4 Geometries of various minima and saddle points

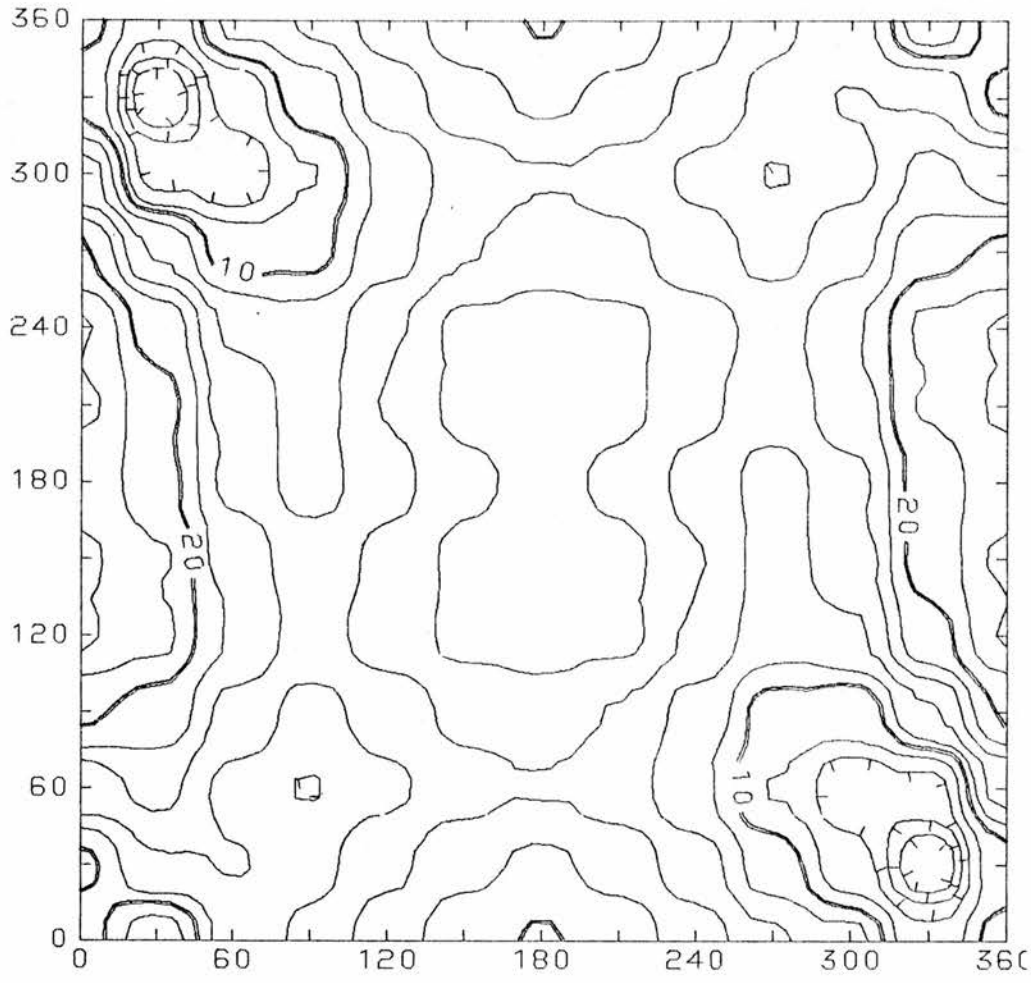

(a)

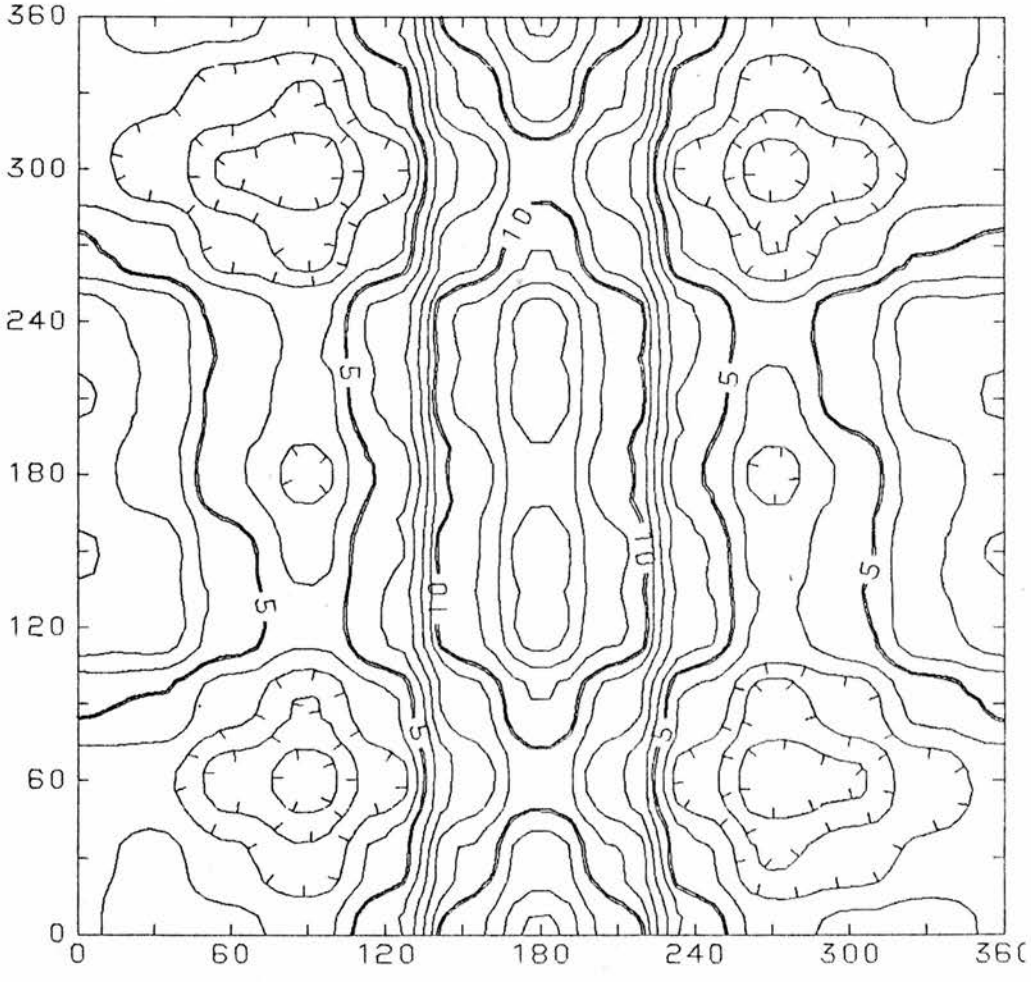

(b)

Figure 4.5 PCILO conformation energy maps τ-NCOH v. τ-OCNN
(a) Z-form, (b) E-form.

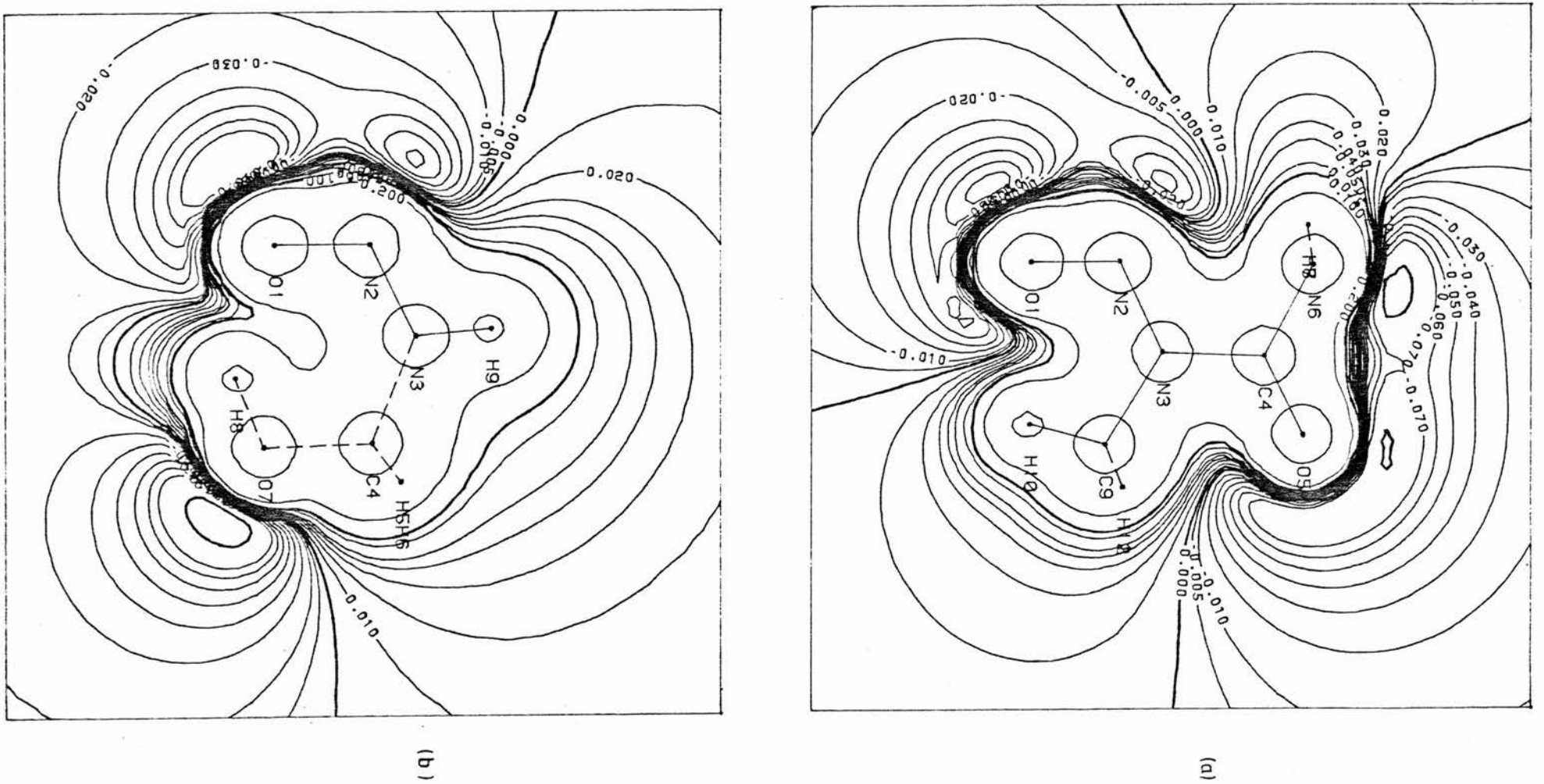

Figure 4.6 Electrostatic potential maps of (a) N-methyl-N-nitrosourea and (b) Z-$CH_2OHNHNO$

CHAPTER 5

TRANSFORMATIONS FOLLOWING DEMETHYLATION IN N-NITROSAMINES

1 INTRODUCTION

One of the main conclusions of the previous chapter was that the α-hydroxynitrosamine decomposes to give the diazohydroxide rather than the monomethylnitrosamine. This conclusion was not apparent at the outset of this work; moreover, as the two species are close in energy, it remains important to study their interconversion. The monomethylnitrosamine may be produced during the nitrosation of primary amines, and for this reason it remains an important intermediate in nitrosamine chemistry.

The monomethylnitrosamine is formally related to the diazohydroxide by an N->O H^+ shift

$$CH_3NHNO \quad \text{-->} \quad CH_3NNOH \qquad (5.1)$$

This transformation has been studied in detail using the model compounds H_2NNO and HNNOH. This reaction has been studied previously; in this laboratory [101], by Poulsen et. al. [63] and by Casewit and Goddard [205], but not in as much detail as is reported below. The O-protonated form of the nitrosamine, shown in reaction (5.1), can undergo an analogous model reaction

$$H_2NNOH^+ \quad \text{-->} \quad HNN.OH_2^+ \qquad (5.2)$$

The transition structure for this reaction is analogous to that in (5.1), and so the results are also reported in this chapter. Reaction (5.2) may represent the effect of acid catalysis on reaction (5.1). There are two more reactions similar to (5.1). The third reaction

$$H_3NNO^+ \quad \text{-->} \quad H_2NNOH^+ \qquad (5.3)$$

represents the effect of N-protonation on (5.1). It was referred to in chapter 3 in connection with the gas phase nitrosation of amines. It is reported in this chapter because of its similarity to reaction (5.1). The fourth model reaction

$$HNNO^- \quad \text{-->} \quad NNOH^- \qquad (5.4)$$

does not have any counterpart in nitrosamine chemistry, neither does it

have an analogous parent reaction. It is reported in this section for the sake of completeness.

In chapter 4, two reactions involving N->O methyl shifts were discussed. These reactions are analogous to reactions (5.1) and (5.2). In chapter 3, a mechanism for the nitrosation of tertiary amines involving an N->O methyl shift was suggested. This reaction is analogous to reaction (5.3) and is therefore discussed in this chapter.

Reactions (5.1) - (5.3) could also occur via a two-step N->N proton shift followed by an N->O proton shift. This possibility has been investigated.

All of the above reactions have been studied by locating the transition structures in the N-dimensional hyperspace. Ab-initio transition structures, for molecules with more than a few internal coordinates, have begun to appear frequently in the literature only in the last few years. The structures presented in this chapter thus comprise a significant number of fully optimised transition structures.

Systematic studies of minima using single determinant wave functions show that experimental geometries can be reproduced well. The situation for transition structures is not so clear. The transition structure cannot be determined experimentally, so no comparisons can be made. This means that theory is the only available method for determining the structures; moreover, absolute confidence in the results cannot be obtained unless the method is continually refined until there is convergence in the results. Very little work has done this using full geometry optimisation. However, it is often implied that SCF methods should give reasonable geometries for transition structures [141,206]. Enthalpies of activation are more likely to be affected by electron correlation than are energies of reaction, even in reactions for which the number of electron pairs is constant. There

are examples in the literature where the energy barrier is very dependent on electron correlation [207,208]. There are also cases where it is not [209]. The effects of basis set and electron correlation on the geometry and the energy barrier have been studied for reaction (5.1).

The effect of hydration on reaction (5.1) has been considered by incorporating one molecule of water and locating the saddle point for an H_3O^+ shift. Attempts to study reactions (5.2) and (5.3) in an analogous manner failed because the saddle point could not be located. However, the results of chapters 3 and 4 suggest that for such protonated molecules it may be more important to include at least two molecules of water. Results from this approach are also included in this chapter, although no saddle points are reported.

Many of the reactions given above involve species which are similar in energy. The sequence of events may involve conformational changes. The first section therefore considers the relative energies of nitrosamine and diazohydroxide species. It also includes the transition structures for various rotational and inversion isomerisations. The energies of all species studied in this chapter are given in tables 5.1, A.1 and A.4. Table 5.1 also shows the number of negative eigenvalues of the Hessian, where these have been determined analytically. The structures of the diazohydroxides are given in figure 5.1; the structures involved in CH_3^+ shifts, 1,3-H^+ shifts, 1,2-H^+ shifts and H_3O^+ shifts are given in tables 5.2, 5.3, 5.4 and 5.5 respectively. Other conformational transition structures are given in figure 5.6. Minima are shown on either the left or right of the figure, with the transition structure in the middle. Where a second order transition structure is also reported, it is shown above the first order transition structure. Where two minima may give rise to the same transition structure, the less stable minimum is shown above the more stable one. The numbers above the minima and second

order transition structures refer to the energy change to the first order saddle point. The structures involved in the acid catalysed pathway are shown in figures 5.7 and 5.8.

2 THE RELATIVE STABILITY OF NITROSAMINES AND DIAZOHYDROXIDES

2.1 Model Compounds

The three most stable isomers of the diazohydroxide are shown in figure 5.1. The c,t-isomer, (1c), and the t,c-isomer, (1b), are more stable than the t,t-isomer, (1a), by 17 and 8kJmol^{-1} respectively. The model nitrosamine, H_2NNO, (3a) in figure 3, is more stable than the t,t-isomer by 11kJmol^{-1}. The initial ab-initio study of these molecules using an STO-4G basis set predicted the same close ordering of the three diazohydroxides given above, with the c,c-isomer considerably less stable. It also predicted H_2NNO to be considerably less stable [101]. Limited studies have been carried out with the 6-31G* basis set, and it is found that the model nitrosamine, H_2NNO, is more stable than the t,t-isomer by 10kJmol^{-1}, see table A.2. Polarisation functions thus appear to have little effect on the relative energies of these molecules. Poulsen et. al. have calculated the relative energies of the trans and cis isomers, presumably (1a) and (1c), and find that there is an energy difference of 16kJmol^{-1} between the two forms at the 3-21G level. When the calculations are performed at the 6-31G** level, using the 3-21G geometry, there is no energy difference between these two forms; both forms remain 8kJmol^{-1} more stable than H_2NNO [63].

There is only a small energy difference between all these

molecules. The situation is analogous to that for the isoelectronic HONO, so the relative stability of all these molecules cannot be predicted reliably without further refinement of the methods; this has not been done.

2.2 Parent Species

The situation is analogous for the monomethyl derivatives, though there is a great increase in the number of isomers - four for the monomethylnitrosamines and eight for the methyldiazohydroxides. Consequently, not all of these have been studied. The most stable conformation of the t,c-CH_3NNOH, (1f), has the expected conformation of the methyl group. (This is not the situation for CH_3NHNO - see chapter 4). When this conformation is retained, the relative ordering of the diazohydroxides does not change - the c,t-isomer, (1g), and the t,c-isomer, (1f), are more stable than the t,t-isomer, (1d), by 8 and 7kJmol^{-1} respectively. The monomethylnitrosamine, (2a), is also more stable than the t,t-isomer by 3kJmol^{-1}. The most stable isomer, however, is the other conformation of the c-CH_3NHNO by 0.1kJmol^{-1} [170] - see table 5.1. It is clear that the relative stability of these molecules cannot by predicted reliably without further refinement of the methods.

2.3 The Effect of O-Protonation

The effect of O-protonation is to make the diazohydroxide derivatives more stable than the nitrosamine derivatives; thus $HNN.OH_2^+$, (3e), and $CH_3NN.OH_2^+$ (see chapter 6) are more stable than H_2NNOH^+, (3c), and CH_3NHNOH^+, (2d), by 69kJmol^{-1}, and 152kJmol^{-1} respectively. This latter observation was confirmed by Andreozzi et. al. using MINDO/3 [100]. However, they found the diazohydroxides to be considerably more stable than the monomethylnitrosamines, and found the sterically hindered c,c-CH_3NNOH to be the most stable isomer. This is contrary to other ab-initio results found in this laboratory.

2.4 Conformational Isomerisations in Diazohydroxide Derivatives

All three of the isomers of the diazohydroxide, (1a) - (1c), could result from the base catalysed decomposition of the α-hydroxymonomethylnitrosamine. Isomerisation by rotation about the N-O bond can occur readily; the energy barrier for the interconversion of (1b) to (1a) is only 34kJmol^{-1} - see figure 5.1. The isomerisation of (1a) to (1c) by formal rotation about the N-N bond will not occur because of the high energy barrier of 145kJmol^{-1}; this is to be expected. The isomerisation actually occurs by inversion, (1i); attempts to find a transition structure for rotation were unsuccessful. Moreover, (1i) has only one negative eigenvalue of the analytical Hessian matrix.

The situation is similar for the isomerisation of CH_3NNO^-, modelled by $HNNO^-$. The syn-isomer is the most stable by 38kJmol^{-1}. By analogy with the transition structure for inversion, (1i), (6e) was found as a first order transition structure using the algorithm of Schlegel - see figure 5.6. It is 226kJmol^{-1} above the anti-isomer.

Analytical second derivatives show that this is a second order transition structure, with one negative eigenvalue corresponding to inversion and one corresponding to rotation. The true first order transition structure (for rotation) lies 147kJmol^{-1} above the anti-isomer, and is therefore not accessible. The energy barriers for inversion or rotation in the parent molecules (of (1i) and (6f)) are likely to be even higher than in the model compounds.

2.5 Conformational Isomerisations in Nitrosamine Derivatives

The energy barrier for rotation about the N-N bond in H_2NNO is 81kJmol^{-1}. The transition structure, (6a), is shown in figure 5.6. There is considerable distortion at the amino-nitrogen, which serves to increase the H-O bonding overlap and to increase the single bond character of the N-N bond. The experimental barrier for rotation in the homologous $(CH_3)_2NNO$ is 96kJmol^{-1}. These results are in good agreement considering that $(CH_3)_2NNO$ will not be able to distort to the same extent as H_2NNO to reduce the energy of the transition structure. In the previous chapter, it was suggested that this energy barrier will be similar to that for rotation about the N-N bond in $CH_2OHNHNO$. This approximation is justified by comparing the N-N and N-O bond lengths in the series H_2NNO, CH_3NHNO (2a), $(CH_3)_2NNO$ and E-$CH_2OHNHNO$ - see table 5.2.

O-protonation increases this barrier considerably; the energy barrier for rotation about the N-N bond in H_2NNOH^+, see structure (6c), is 244kJmol^{-1}. This is to be expected as the double bond character is mainly in the N-N bond. This transition structure is also considerably distorted, more than may be possible in the parent molecule. The distortion helps both to spread the positive charge and to increase the single bond character of the N-N bond. This transition structure was

discussed in the previous chapter.

The possible involvement of N->O shifts occurring during nitrosation was discussed in chapter 3. An N->O H^+ shift would give rise to c-H_2NNOH^+, (3i); the trans isomer, (3c), is more stable by 66kJmol^{-1}, and can be reached by an energy barrier of only 17kJmol^{-1} - see structure (6b) in figure 5.6. In a similar manner, the N->O CH_3^+ shift, which may be involved in the nitrosation of tertiary amines, would give rise to the model compound c-$H_2NNOCH_3^+$. The trans isomer is more stable by 56kJmol^{-1} (the structure and energy are given in table 5.3); it can probably be reached by a similarly low energy barrier.

3 TRANSFORMATIONS OF MONOALKYLNITROSAMINES TO DIAZOHYDROXIDES

The transition structures discussed below are stationary points connecting (model) monomethylnitrosamines to methyldiazohydroxides. Some of these transition structures have already been discussed in the previous two chapters. These are not involved in reactions that can occur following the demethylation of nitrosamines. They are discussed in this section because of similarities in structure.

3.1 N->O Methyl Shifts

The transition structures are shown in figure 5.2. All these structures are similar. Analytical second derivative calculations were not performed. However, the structure (2b) was obtained using MINIT, which guarantees to converge to a first order saddle point by using line searches. By analogy to (2b), (2e) and (2i) would also appear to be first order saddle points. The barriers for the formation of (2b), (2e) and (2i) are 294, 215 and 264kJmol^{-1} respectively, so these

structures cannot be important *in vivo*. Two mechanisms for the formation of (2i) are shown: a CH_3^+ shift from $CH_3NH_2NO^+$ and insertion of NO^+ into CH_3NH_2.

Hydroxylation of the methyl group has little influence on either the transition structure geometry or the energy barrier.

CH_3^+ shifts occur more readily than does the complete loss of CH_3^+

$$c\text{-}CH_3NHNOH^+ \quad \text{-->} \quad t,t\text{-}HNNOH + CH_3^+ \qquad (5.5)$$

$$(CH_3)_2NHNOH^+ \quad \text{-->} \quad t,t\text{-}CH_3NNOH + CH_3^+ \qquad (5.6)$$

ΔE for reaction (5.5) and (5.6) is 401 and 436kJmol^{-1} respectively, whereas the energy of (2e) is only 215kJmol^{-1} above (2d). The complete loss of CH_2OH^+ from $CH_2OHNHNOH^+$ occurs even more readily; ΔE is only 206kJmol^{-1}, as discussed in chapter 4. Consequently, the energy barrier for a CH_2OH^+ shift from $CH_2OHNHNOH^+$ should be considerably less than this. Attempts to find this transition structure which is analogous to (2l) were, however, unsuccessful. This is partly because of the extra conformational flexibility introduced. Conformational changes in the migrating group, driven by Schlegel's algorithm, led to negative eigenvalues being generated by the formula for updating the Hessian. These negative eigenvalues did not correspond to the eigenvector for an N->O CH_3^+ shift and led to confusion in the search for a transition structure.

The structures (2e), (2i) and (2l) are the saddle points with the greatest number of atoms reported in this thesis; they each have 21 internal coordinates.

To describe these structures as CH_3^+ shifts may be a little misleading. The increases in charge from the minimum to the transition structure are given in table 5.4. The greatest increases are 0.2 and 0.4 from (2d) and (2f) to (2e); for (2i) and (2l) the increase is only 0.1, and for (2b) the increase is quite small. For the CH_3^+ shifts, the CH_3^+ part of the transition structure is almost planar. There appears to be a reduction in the energy barrier as both the charge on the

migrating group and the charge on the whole molecule increase - see table 5.4. For the charged molecules, the sum of the overlap populations in the bonds to the migrating group is less than that in the minima. This is not the case for the neutral molecules or the H^+ shift transition structures - see table 5.5.

For the N->O H^+ shift transition structures (which will also be discussed in the next sub-section), there appears to be some correlation between an increase in positive charge (on both the molecule as a whole and on the migrating hydrogen atom) and an increase in the energy barrier - see table 5.4. The increase in charge on the migrating H-atom is only 0.1. This effect, the overlap populations and the energy barrier compared to that for the complete loss of H^+ and CH_3^+ show that the transition structures cannot be considered as ion-pairs - compare reference [210].

3.2 N->O Proton Shifts

The transition structures for the N->O proton shifts are given in figure 5.3. All these structures were confirmed to be first order saddle points by analytical second derivative calculations. As the bonds being broken in (3b) are about 30% longer than those in the minima (3a) and (1b), there is a possibility that there is a UHF wave function lower in energy than the RHF wave function. The RHF wave function was, however, stable. The effect of basis set and electron correlation on the energy barrier for the formation of (3b) has been studied. Oie et. al. have pointed out that the effect of polarisation functions may be to increase energy barriers, whereas electron correlation may have the opposite effect [136]. This effect was observed here also - see tables A.2, A.5 and A.6. The effect on geometry is shown in table A.3 and discussed in the appendix. Due to

the similarity of the N->O H^+ shift transition structures, only (3b) was studied in greater detail. Assuming that the Møller-Plesset second order correction accounts for the majority of the correlation error, it would appear that these barriers cannot be crossed at physiological temperatures. This suggests that isolated H_2NNO would be a stable molecule, and automatically raises the question as to why it has never been observed experimentally. There are several possible reasons for this:

a) The second order Møller-Plesset correction does not account for the greater part of the correlation error, and a more refined treatment would reduce the barrier significantly.

b) A combination of a) and quantum tunnelling would enable the proton shift to occur. In this case, D_2NNO and T_2NNO but not H_2NNO would be observable.

c) A more refined treatment of H_2NNO would reveal that it has diradical character. H_2NNO could then catalyse its own decomposition by a radical mechanism.

d) H_2NNO is able to catalyse its own decomposition by a closed shell mechanism.

e) Poulsen et. al. have studied this reaction and obtained a similar RHF energy barrier, but implied that the reaction could still proceed [63].

f) Isolated H_2NNO cannot be formed; it can be created only in the presence of molecules such as H_2O and NH_3 which catalyse its decomposition.

Møller-Plesset theory is certainly less efficient at long bond lengths [110]. Radical mechanisms can play a part in nitrosamine chemistry [211] - see also chapter 1. (This point could be investigated further using multiconfigurational self-consistent-field theory). However, at present reason (f) seems the most likely.

The barrier for the formation of (3i) is only 86kJmol^{-1} above the

reactants (3f); the molecule (3i) may thus be formed by the insertion of NO^+ into an N-H bond in NH_3. Calculations, however, show that insertion into a C-N bond occurs more readily.

Some aspects of these transition structures related to the overlap populations were discussed in the previous sub-section.

3.3 N->N Proton Shifts

N->N proton shifts were studied as an alternative two-step route to the formation of the diazohydroxides from model nitrosamines. All the structures considered in this sub-section are shown in figure 5.4. While these barriers are more affected by basis set and electron correlation than the barriers for the N->O H^+ shifts, they are high and so this route does not seem feasible - see tables A.2 and A.6. For this reason, only one N->O 1,2-H^+ shift, (4i), was studied, and again a high barrier was obtained. Part of the reason for the high barrier is that the intermediate HNNHO, (4c), $HNNHOH^+$, (4f), and H_2NNHO^+, (4h), are already 103, 92 and 91kJmol^{-1} above H_2NNO, (3a), H_2NNOH^+, (3c), and H_3NNO^+, (3g) respectively. (In chapter 3 it was noted that $(CH_3)_2NNHO^+$ is 124kJmol^{-1} above $(CH_3)_2NNOH^+$).

These results are, however, interesting. The planar transition structure, (4a), was obtained as a first order transition structure by the algorithm of Schlegel; the true first order transition structure, (4b), lies 11kJmol^{-1} lower in energy. It appears to be stabilised by the overlap between the hydrogen 1s orbital and the p orbitals on the amino-nitrogen perpendicular to the plane of the molecule. An analogous situation applies to (4d) and (4e). For the transition structure between H_3NNO^+, (3g), and H_2NNHO^+, (4h), only one (first order) saddle point was found. The planar N->O 1,2-H^+ shift transition structure is a first order saddle point. The order of all the

transition structures given in figure 5.4 was confirmed by analytical second derivative calculations.

3.4 H_3O^+ Shifts

3.4.1 N->O H_3O^+ shift

The calculated dipole moments for H_2NNO, (3a), and H<NNOH>, (3b), are 3.73 and 3.67D respectively. While SCF dipole moments are not very reliable, [110], on the basis of these results one would expect the energy barrier to be little affected by going to a more polar solvent. The effect of solvent on the energy barrier was studied by the reaction coordinate method [101], at about the same time as the first ab-initio transition structure was determined using gradient methods [212]. A single water molecule was allowed to interact with the migrating proton in the following manner

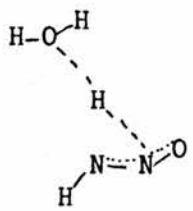

The migrating proton is conserved by this mechanism. A reduction of 10% in the energy barrier was obtained. Recently, it was suggested by Casewit and Goddard that this energy barrier was too high [205]. This problem was re-examined by considering H_3O^+ shifts in a concerted mechanism such that the migrating proton is not conserved - see figure 5.5. This amounts to a change in the mechanism for the reaction rather than a change in the dielectric constant of the medium. The barrier is reduced by 61%, and becomes low enough for facile reaction

in aqueous solution. The monohydration energies of H_2NNO in (5a) and (5d) are 62 and 68kJmol^{-1} respectively. Clearly, monohydration preserves the small energy difference between these two molecules; it also preserves their relative stability. The molecules (5a) and (5d) are very similar to each other (and to the saddle points (5b) and (5c)) in both geometry and energy. From these structures one could propose that the reaction (5a) -> (5d) will occur in solution through catalysis by only one molecule of water; thermodynamically, (5a) is the lowest energy species, as (5d) cannot isomerise to (monohydrated) c,t-HNNOH. Attempts to find the transition structure using MINIT were partially successful. It failed to converge to either of the stationary points, (5b) or (5c). The first order saddle point, (5c), was then found using Schlegel's algorithm, with the help of analytical second derivatives and a good starting geometry provided by MINIT. The structure (5b) is a second order saddle point, with two negative eigenvalues, one corresponding to the H_3O^+ shift, the other to inversion at the H_3O^+. The energy difference between the two transition structures is small, (5kJmol^{-1}), and is of the same order of magnitude as the 10kJmol^{-1} barrier for inversion in H_3O^+ [187].

3.4.2 N->N H_3O^+ shift

The minima, (5e) and (5g), and the saddle point, (5f), for the water-assisted N->N H^+ shift from H_2NNO to HNNHO are shown in figure 5.5. The structure (5f) was confirmed to be a first order saddle point by analytical second derivative calculations. Monohydration does not greatly affect the energy difference between H_2NNO and HNNHO; the energy difference is 88kJmol^{-1}, as opposed to 103kJmol^{-1} in the absence of monohydration. The reaction is thus endothermic, and this is a contributing factor to the high energy

barrier of 181kJmol^{-1}. Moreover, inspection of the minima, (5e) and (5g), suggests that there is room for the involvement of further water molecules. However, due to the endothermicity, this reaction will not proceed, even when aided by hydration.

In both of the H_3O^+ shift transition structures, the H_3O^+ prefers to be pyramidal. At the RHF/4-21G level, the H_3O^+ is planar, though it does become pyramidal when polarisation functions are included in the basis set - see table A.3. Definitive calculations show that H_3O^+ is indeed pyramidal [187]. The effect of the basis functions in the HNNO backbone in figure 5.5 is similar to that of polarisation functions.

3.4.3 Other work

Other researchers have reported H^+ shifts aided by water at the split-valence level [213,214,215]; one transition structure involving two molecules of water has been reported [214]. Transition structures with a non-planar H_3O^+ have also been reported [215].

3.4.4 H_3O^+ shifts involving H_2NNOH^+ and H_3NNO^+

Attempts to find the transition structures for the H_2O aided proton shifts for H_3NNO^+ and H_2NNOH^+ were unsuccessful. Regions of negative curvature and structures with low forces were found. It is likely that these transition structures possess considerable distortion. This is the case for the transition structure for the decomposition of the α-hydroxynitrosamine reported in the previous chapter. However, the results of chapter 3 (and the structures of the monohydrated species in figure 5.7) suggest that it may be more important to consider two molecules of water, rather than just one, as

the proton may be fully removed. This has been studied in the next section.

3.5 Acid Catalysed Pathways

The structures of the monohydrated isomers of H_3NNO^+, H_2NNOH^+ and $HNN.OH_2^+$ are shown in figures 5.7 and 5.8. The energies are given in table 5.1. Only a representative number of isomers has been studied. Moreover, the structures and energies of structures (7b), (7c) and (8b) are given in chapter 3.

3.5.1 Protonation and monohydration

The monohydration energies of H_3NNO^+, (3g), H_2NNOH^+, (3c), and $HNN.OH_2^+$, (3e), are about twice those of the neutral molecules H_2NNO, (3a), and HNNOH, (1b). The relative stabilities of the structures in figure 5.7 depend upon the protonated molecule, its conformation and the hydration site. Monohydration reverses the stability of H_2NNOH^+ and $HNN.OH_2^+$, as shown by the energies of (7e) and (7f). Monohydrated t-H_2NNOH^+ is more stable than monohydrated H_3NNO^+ by 61kJmol^{-1}. There appears to be an inverse relationship between the monohydration energy and the inter-molecular bond length.

3.5.2 Protonation and dihydration

The structure (8b) is the N-protonated model nitrosamine involved in the formation of nitrosamines from the nitrosation of secondary amines by the nitrous acidium ion. The parent molecule can form only one amino-proton based hydration chain. The structure (8a) could therefore be involved only in the nitrosation of model primary amines. However, the relative energies of (8a) and (8b) suggest that primary amine - nitrosonium ion complexes are also likely to be destroyed by a chain of two water molecules, to give the model monoalkylnitrosamine.

The structures (8c), (8d) and (8f) represent three different ways of forming water chains on H_2NNOH^+. Two of these structures, (8c) and (8d), result in the formation of HNNOH. However, (8f) is more stable than (8c) and (8d) by 23 and 16kJmol^{-1} respectively; the structure (8f) results in the regeneration of H_2NNO. Moreover, (8e) is also more stable than (8c) and (8d) by 15 and 8kJmol^{-1} respectively. Clearly, these energy differences are small, but it would appear that the conversion of H_2NNO to HNNOH is not catalysed by protonation and hydration. The structures (8c) and (8d) show that the relative stability of c,t-HNNOH and t,t-HNNOH may be reversed in acid solution. The structure (8d) is quite different from all the other ligand - H_3O^+-H_2O complexes studied in this thesis, as it is better represented as a ligand - $H_5O_2^+$ complex. This structure may be more sensitive to the inclusion of polarisation functions than the others.

3.6 Base Catalysed Pathways

Structure (5c) in figure 5.5 represents an H_2O aided transition structure. If the reaction were to occur in a basic medium, an OH^- aided transition structure could be proposed. However, as structure (5h) in figure 5.5 shows, the two possible minima and the proposed saddle point are all one structure. The pathway could thus occur without an energy barrier, and the product would be formed by re-protonation.

4 CONCLUSIONS

A large number of transition structures involving (model) monoalkylnitrosamines has been presented. Their relevance to the metabolism of nitrosamines is unclear because it now appears that the α-hydroxynitrosamine decomposes directly to the diazohydroxide. However, many of the species discussed in this chapter may be involved in the nitrosation of primary amines.

Apart from the possible occurrence of N->O shifts during nitrosation, it appears that the energy barriers for either N->O methyl shifts or N->O proton shifts are too high for these pathways to occur. The possible involvement of N->N proton shifts is even less likely. Protonation does not lower any of these barriers.

The combined effect of protonation and hydration could provide a low energy pathway between the nitrosamine and the diazohydroxide molecules (the most stable product would appear to be the nitrosamine). It is not necessary, however, to invoke the effects of protonation, or deprotonation, as the interconversion is also catalysed by a low energy transition structure involving one molecule of water.

The energy difference between H_2NNO and HNNOH is small and cannot

be determined with great confidence at this level of theory, particularly as the relative energies of H_2NNO and HNNOH may be affected by the environment. There is the possibility that radical pathways are involved in the interconversion of H_2NNO and HNNOH; this should be investigated further.

It is normally assumed that the alkylating species is derived from the alkyldiazohydroxide. The formation of the monoalkylnitrosamine from the alkyldiazohydroxide could lead to detoxifying reactions or to an effective increase in the life-time of the alkyldiazohydroxide. The nature of $HNN.OH_2^+$, (3e), and $CH_3NN.OH_2^+$ have not been discussed; this will be deferred to the next chapter, which discusses the nature of the alkylating agent. Figure 5.9 is a graphical representation of the relative energies of many of the species discussed in this chapter, and the energy barriers between them. Several aspects of the work discussed in this chapter have been submitted for publication [204,216].

Table 5.1. Energies and number of negative eigenvalues (N) for species studied at the RHF/4-21G level for which analytical second derivatives were evaluated. The symbols < > enclose the 'active' part of transition structures. '*' denotes that N was determined very close to the stationary point.

Compound	Label	N	Energy	Compound	Label	N	Energy
t,t-HNNOH	(1a)	0	-184.362004	H<NNH>O	(4a)	2	-184.212790
t,c-HNNOH	(1b)		-184.364992	H<NNH>O	(4b)	1	-184.217001
c,t-HNNOH	(1c)		-184.368388	HNNHO	(4c)		-184.327193
t,t-CH_3NNOH	(1d)		-223.315778	H<NNH>OH^+	(4d)	2	-184.540041
t,c-CH_3NNOH	(1e)		-223.316023	H<NNH>OH^+	(4e)	1	-184.541578
t,c-CH_3NNOH	(1f)		-223.318474	$HNNHOH^+$	(4f)		-184.656821
c,t-CH_3NNOH	(1g)		-223.318655	H_2<NNH>O^+	(4g)	1	-184.533368
HNN<OH>	(1h)		-184.352226	H_2NNHO^+	(4h)		-184.650496
<H>NNOH	(1i)	1	-184.306717	HN<NOH>	(4i)	1	-184.238293
c-CH_3NHNO	not shown		-223.318683	$H_2O.H_2NNO$	(5a)		-260.213200
c-CH_3NHNO	(2a)		-223.316857	H_2O, H_2NNO		0,0	-260.187468
H<NNOCH_3>	(2b)		-223.205003	H<NNO.H_3O>	(5b)	2*	-260.183139
t,c-HNNOCH_3	(2c)		-223.311889	H<NNO.H_3O>	(5c)	1	-260.184966
CH_3NHNOH^+	(2d)		-223.659702	t,c-HNNOH.OH_2	(5d)		-260.209711
H<NNOCH_3>H^+	(2e)		-223.577616	$H_2O.H_2NNO$	(5e)		-260.206487
c-HNN.CH_3OH^+	(2f)	1	-223.662944	$H_2O.H_2NNO$	(5e)		-260.205865
CH_3NH_2, NO^+	(2g)	0,0	-223.554470	H<NN.H_3O>O	(5f)	1	-260.136973
$CH_3NH_2NO^+$	(2h)		-223.644888	HNNHO.OH_2	(5g)		-260.173076
H_2<NNOCH_3>$^+$	(2i)		-223.544324	HNNO.HOH^-	(5h)		-259.614763
c-$H_2NNOCH_3^+$	(2j)		-223.633756				

Table 5.1 Continued

c-$CH_2OHNHNO$	(2k)		-297.978481	$H_2N<NO>$	(6a)	1	-184.335498
$H<NNO.CH_2OH>$	(2l)		-297.877786	$H_2NN<OH>$	(6b)	1	-184.660506
$HNNOCH_2OH$	(2m)		-297.982663	$H_2N<NOH>^+$	(6c)	1	-184.599134
				t-$HNNO^-$	(6d)		-183.742244
H_2NNO	(3a)	0	-184.366261	$<H>NNO^-$	(6e)	2	-183.656103
$H<NNOH>$	(3b)	1	-184.294691	$<HN>NO^-$	(6f)	1	-183.686092
t-H_2NNOH^+	(3c)	0	-184.691956				
$H<NNOH>H^+$	(3d)	1	-184.615746	$H_2NNOH.OH_2^+$	(7a)		-260.552448
$HNN.OH_2^+$	(3e)	1	-184.718071	$H_2O.H_3NNO^+$	(7b)		-260.553463
NH_3, NO^+	(3f)	0,0	-184.611301	$H_2O.H_3NNO^+$	(7c)		-260.554387
H_3NNO^+	(3g)	0	-184.685281	$H_2O.H_2NNOH^+$	(7d)		-260.569563
$H_2<NNOH>^+$	(3h)	1	-184.578699	$HNN.OH_2.OH_2^+$	(7e)		-260.571024
c-H_2NNOH^+	(3i)		-184.666870	$H_2NNOH.OH_2^+$	(7f)		-260.576535
c-$HNNO^-$	(3j)		-183.756541				
$<HNNO>^-$	(3k)		-183.704553	$H_3NNO.2H_2O^+$	(8a)		-336.419803
c-$NNOH^-$	(3l)		-183.786587	$H_2NNO.H_3O.OH_2^+$	(8b)		-336.421657
				$HNNOH.H_3O.OH_2^+$	(8c)		-336.437919
				$HNNOH.H_5O_2^+$	(8d)		-336.440580
				$H_2O.H_2NNOH.OH_2^+$	(8e)		-336.443489
				$H_2NNO.H_3O.OH_2^+$	(8f)		-336.446524

table 5.2 N-N and N-O bond lengths/Å in derivatives of H_2NNO and $HNNOH^+$

Species	N-N	N-O
H_2NNO (3a)	1.350	1.229
CH_3NHNO (2a)	1.345	1.234
$(CH_3)_2NNO$	1.333	1.241
E-$CH_2OHNHNO$	1.354	1.228
H_2NNOH^+ (3c)	1.235	1.357
CH_3NHNOH^+ (2d)	1.231	1.369
$(CH_3)_2NNOH^+$	1.227	1.383
Z-$CH_2OHNHNOH^+$	1.228	1.378

Table 5.3 The structure and energy of t-$H_2NNOCH_3^+$

Parameter	Value	Parameter	Value	Parameter	Value
RNH1	1.013				
RNN	1.245	ANNH1	120.8		
RNO	1.336	ANNO	110.8	DONNH1	0.0
RNH5	1.008	ANNH5	117.5	DONNH5	180.0
ROC	1.516	ANOC	114.2	DNNOC	180.0
RCH7	1.074	AOCH7	102.2	DNOCH7	80.0
RCH8	1.075	AOCH8	107.9	DNOCH8	60.2
RCH9	1.075	AOCH9	107.9	DNNOH9	60.2

Energy = -223.655201400a.u.

Table 5.4 Charges on migrating groups. The charge, Q, is given on the migrating group; δQ is the change in charge in the saddle point and ΔE is the energy barrier.

	Minimum 1			Saddle Point			Minimum 2
Saddle Point	Q	δQ	ΔE	Q	δQ	ΔE	Q
<NNOH>	0.1714	0.0561	136	0.2275	0.1332	215	0.0943
H<NNOH>	0.3703	0.1106	188	0.4813	0.0846	185	0.3967
H<NNOH>H^+	0.4887	0.0838	200	0.5725	0.0933	269	0.4792
H_2<NNOH>$^+$	0.4188	0.1182	280	0.5370	0.0576	297	0.4794
H<$NNOCH_3$>	0.3492	0.0437	294	0.3929	0.0138	281	0.3791
H<$NNOCH_3$>H^+	0.5496	0.2257	215	0.7753	0.3997	224	0.3756
H_2<$NNOCH_3$>$^+$	0.4630	0.1082	264	0.5712	0.0573	235	0.5139a
H<$NNOCH_2OH$>	0.3687	0.1023	264	0.4710	0.0682	275	0.4028
H<$NNOH_3O$>$_6$	0.3892	0.1721	74	0.5613	0.0526	65	0.5087

a) Approximate value

Table 5.5 Bonding overlap populations in transition structures. For the minima, the overlap for the bond which is broken is given. For the saddle point, two such values are given along with their total.

Saddle Point	Minimum 1	Saddle Point		(SP Total)	Minimum 2
<NNOH>$^-$	0.2502	0.1802	0.0946	(0.2748)	0.1648
H<NNOH>	0.3174	0.1360	0.1485	(0.2845)	0.2378
H<NNOH>H$^+$	0.2866	0.1386	0.1009	(0.2395)	0.2675
H_2<NNOH>$^+$	0.2972	0.0995	0.1425	(0.2420)	0.2433
H<NNOCH$_3$>	0.1482	0.0568	0.1010	(0.1578)	0.1842
H<NNOH>H$^+$	0.0632	0.0299	0.0275	(0.0574)	0.2006
H_2<NNOCH$_3$>$^+$	0.0922	0.0231	0.0432	(0.0663)	0.1400a
H<NNOCH$_2$OH>	0.1008	0.0593	0.1026	(0.1619)	0.1701
H<NNOH$_3$O>$_6$	0.5870			(0.4419)	0.5495

N.B. Only the total for the bonds which are broken or made is given for H<NNOH$_3$O>$_6$

a) Implies value is approximate

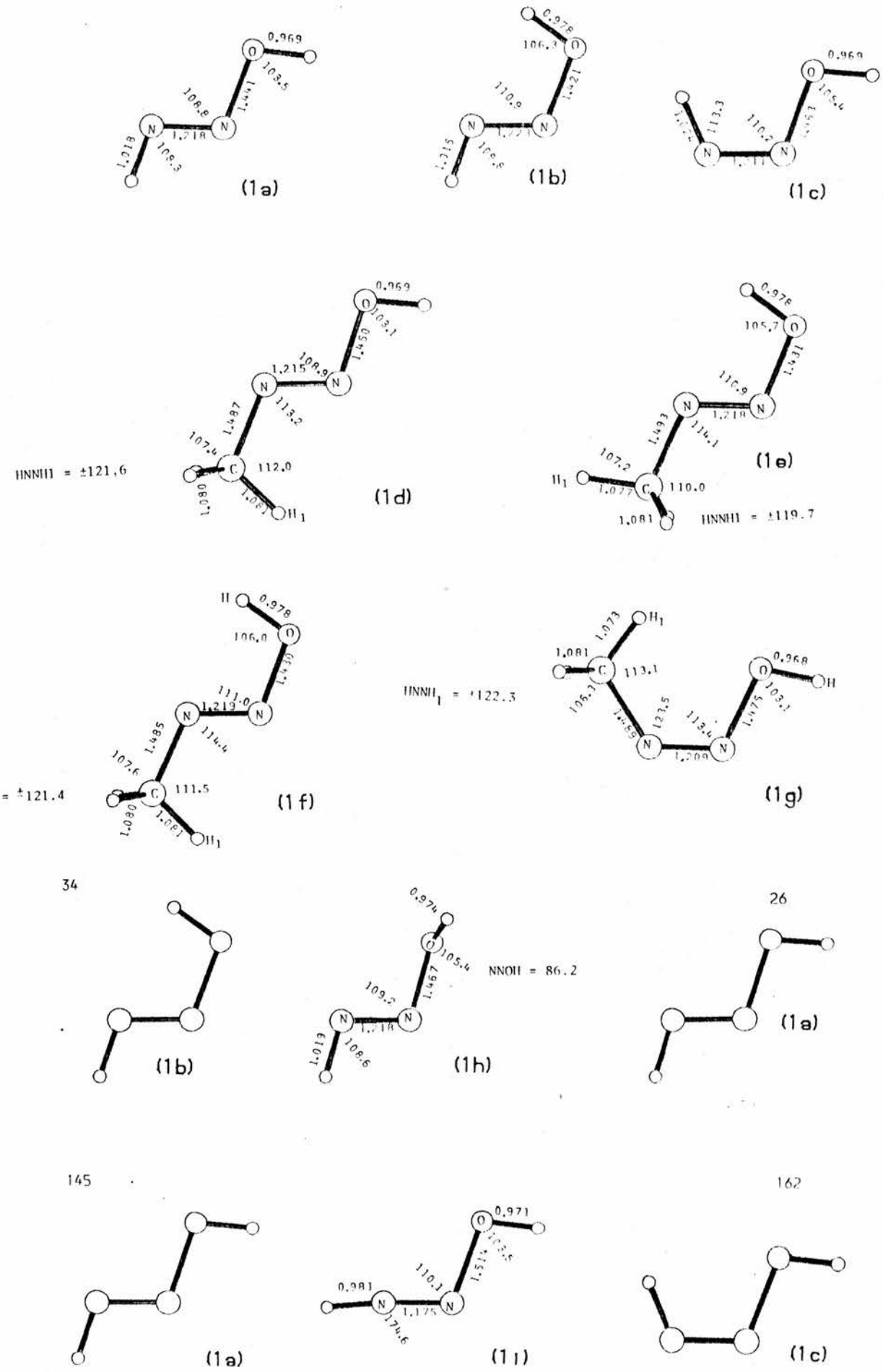

Figure 5.1 Geometries of alkyldiazohydroxides, and some transition structures between them (hydrogen atoms are not labelled)

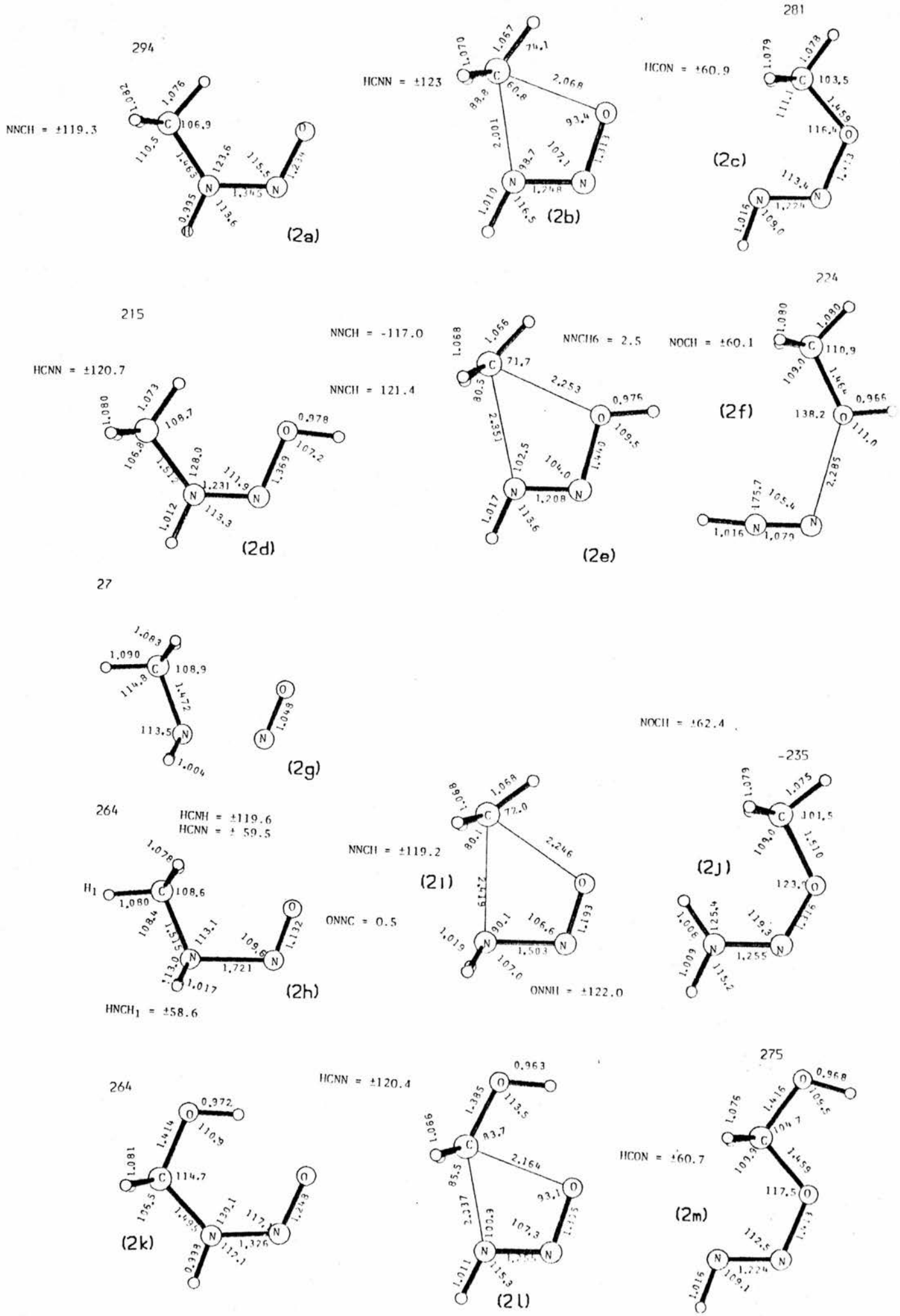

Figure 5.2 Minima and transition structure geometries for CH_3^+ shifts.

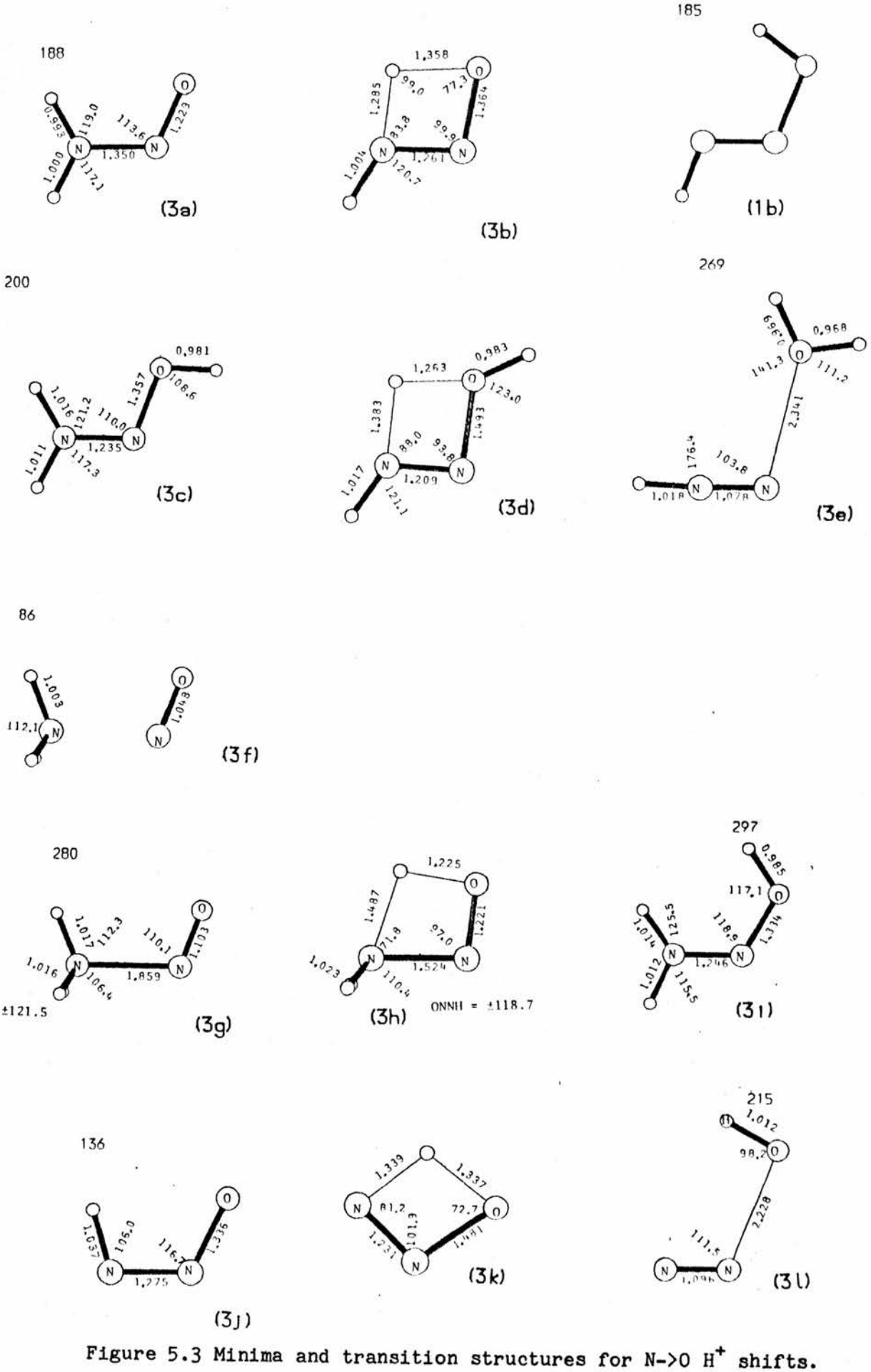

Figure 5.3 Minima and transition structures for N->O H^+ shifts.

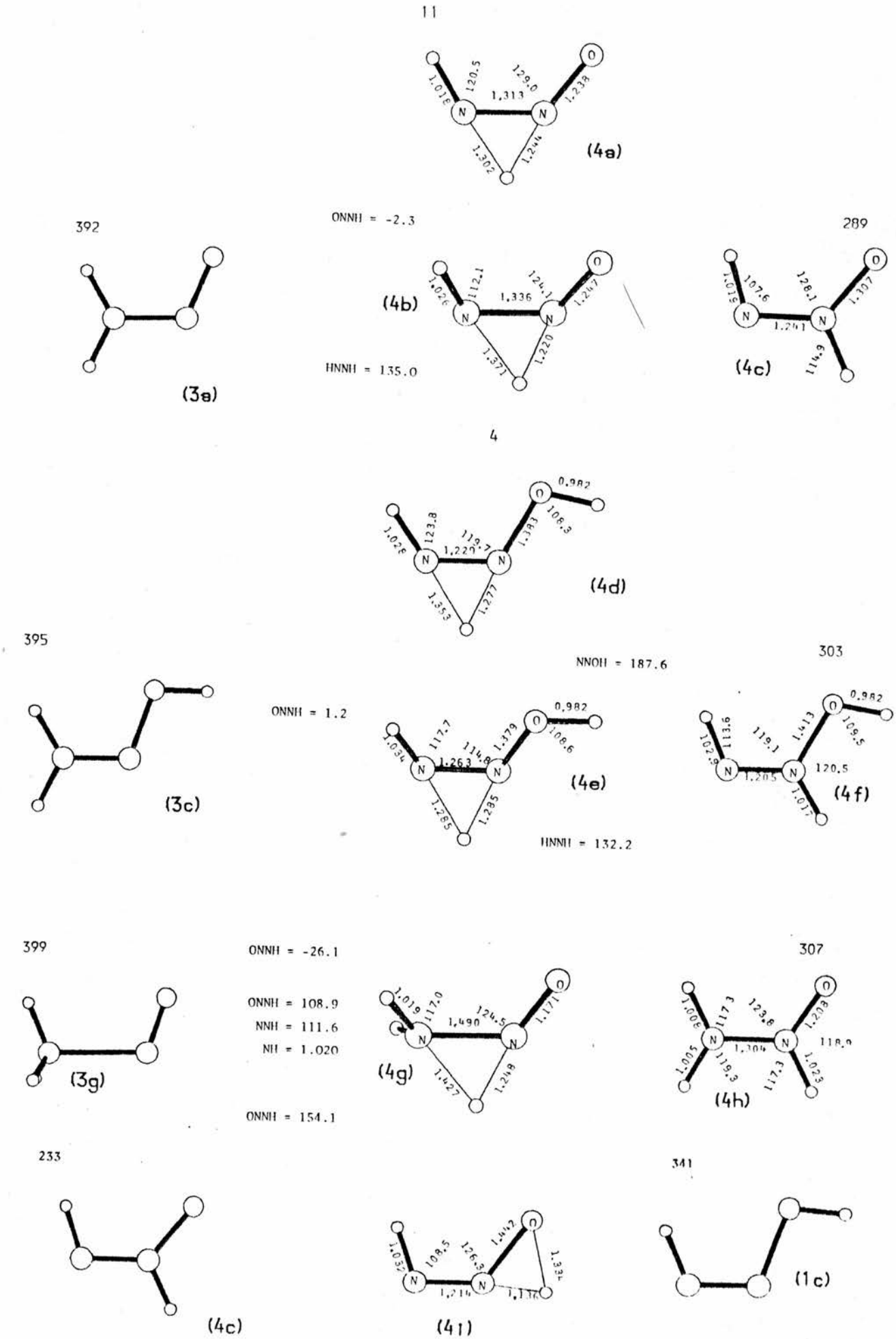

Figure 5.4 Minima and transition structures for N->N and N->O 1,2 H^+ shifts

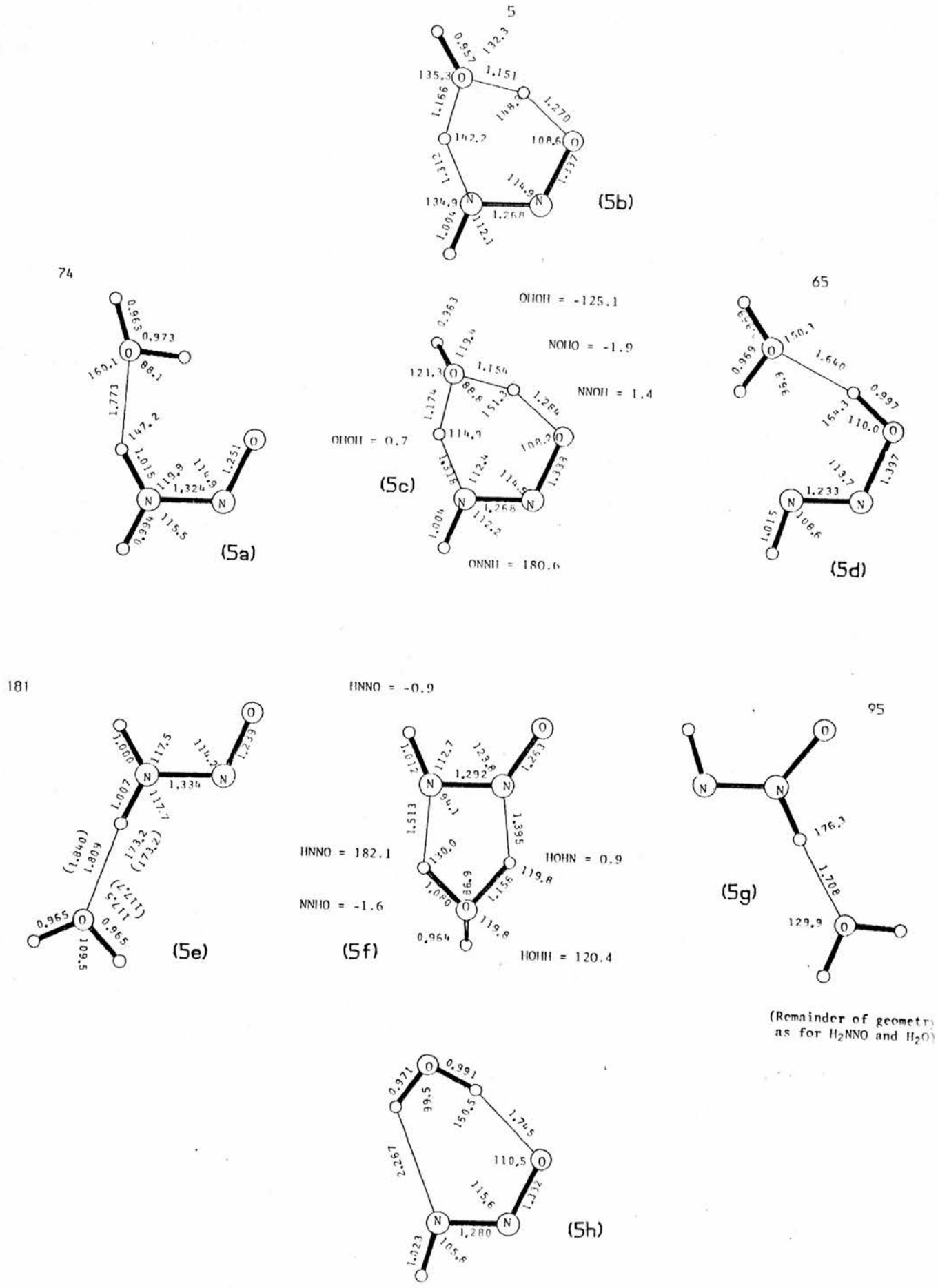

Figure 5.5 Minima and transition structure geometries for H_3O^+ shifts. The figures in parenthesis for (5e) were obtained with the monomers fixed at their equilib. geometr

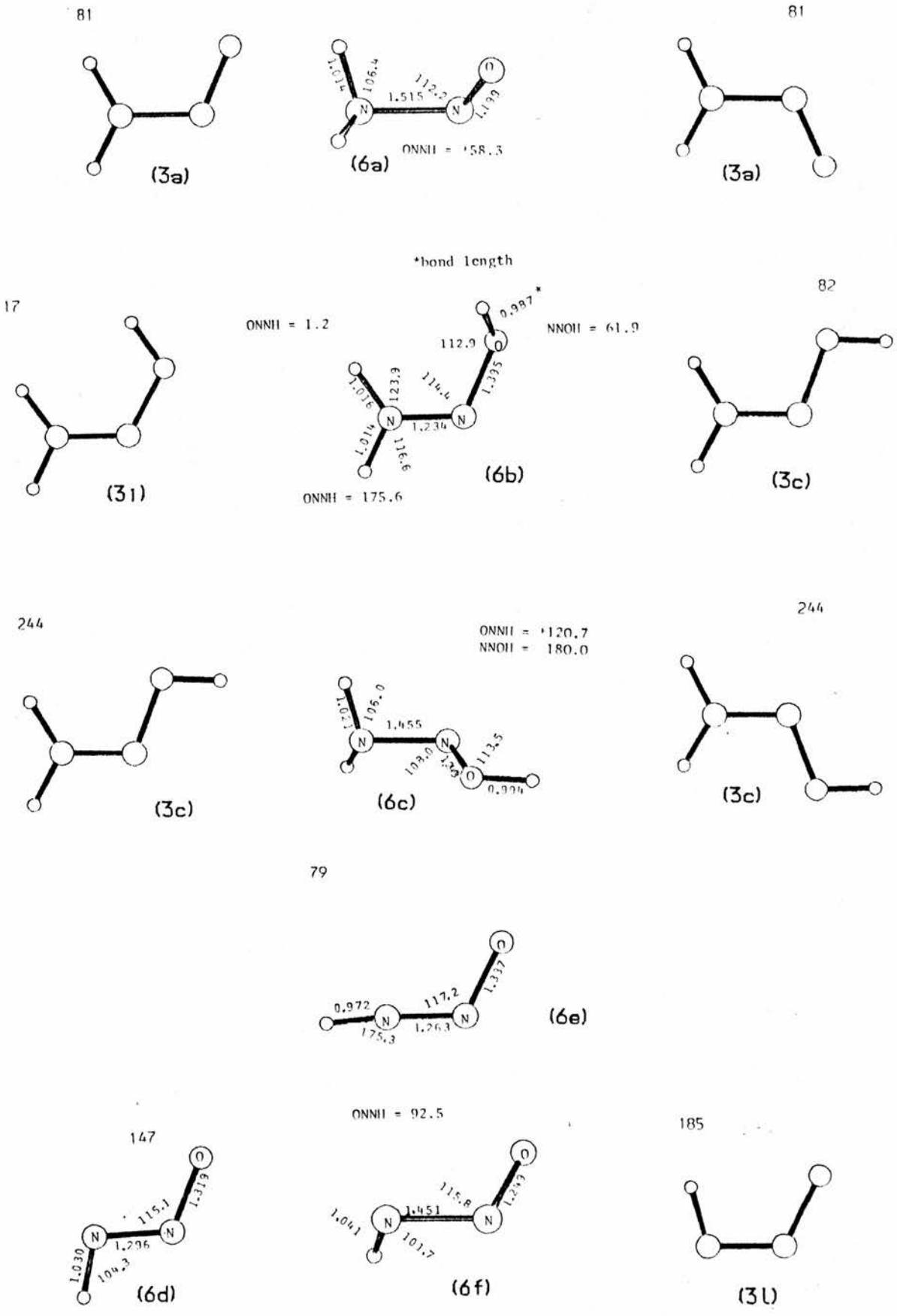

Figure 5.6 Minima and transition structure geometries for rotational and inversion transitions

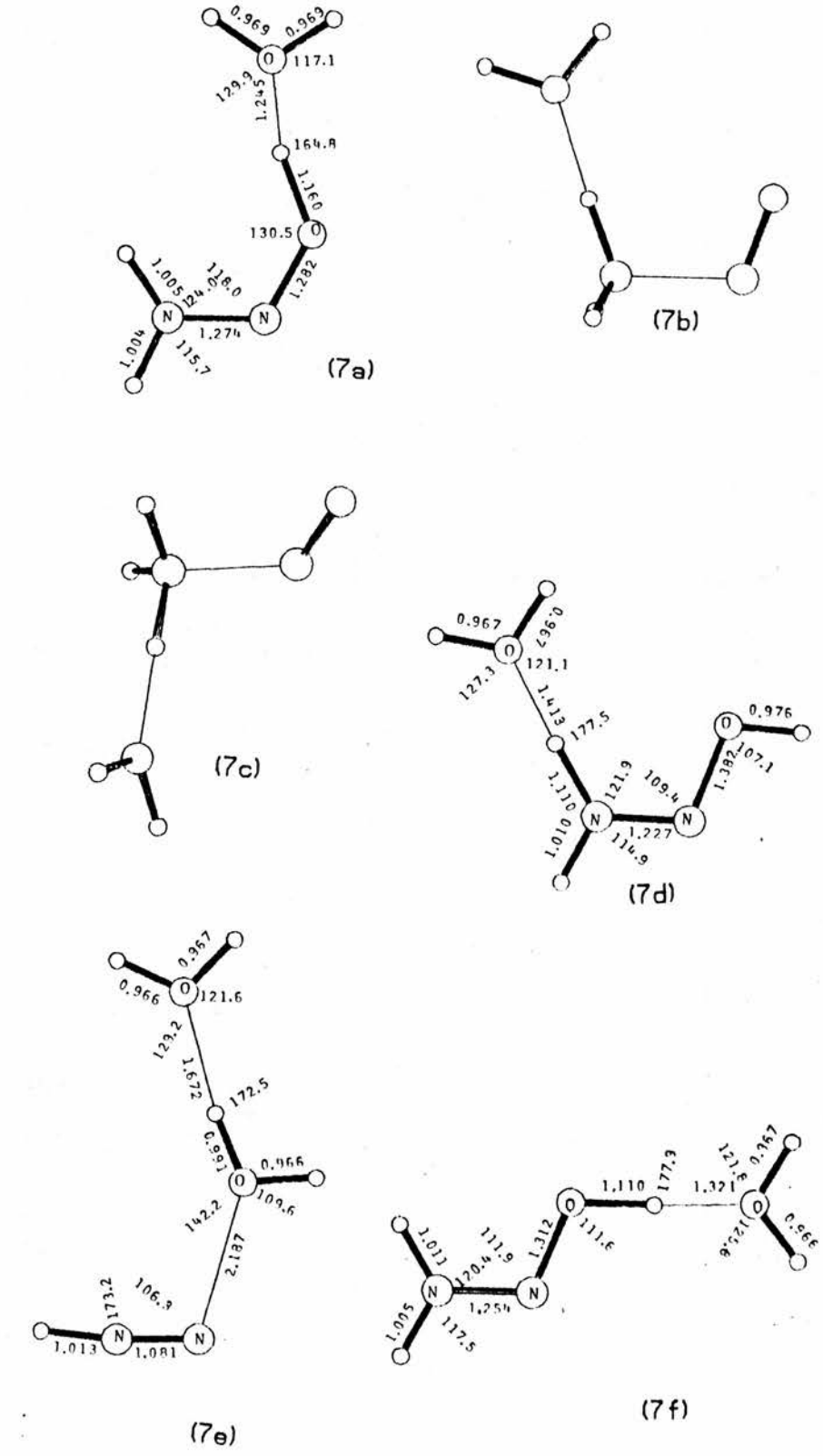

Figure 5.7 Structures of monohydrated H_3NNO^+, H_2NNOH^+ and $HNN.OH_2^+$

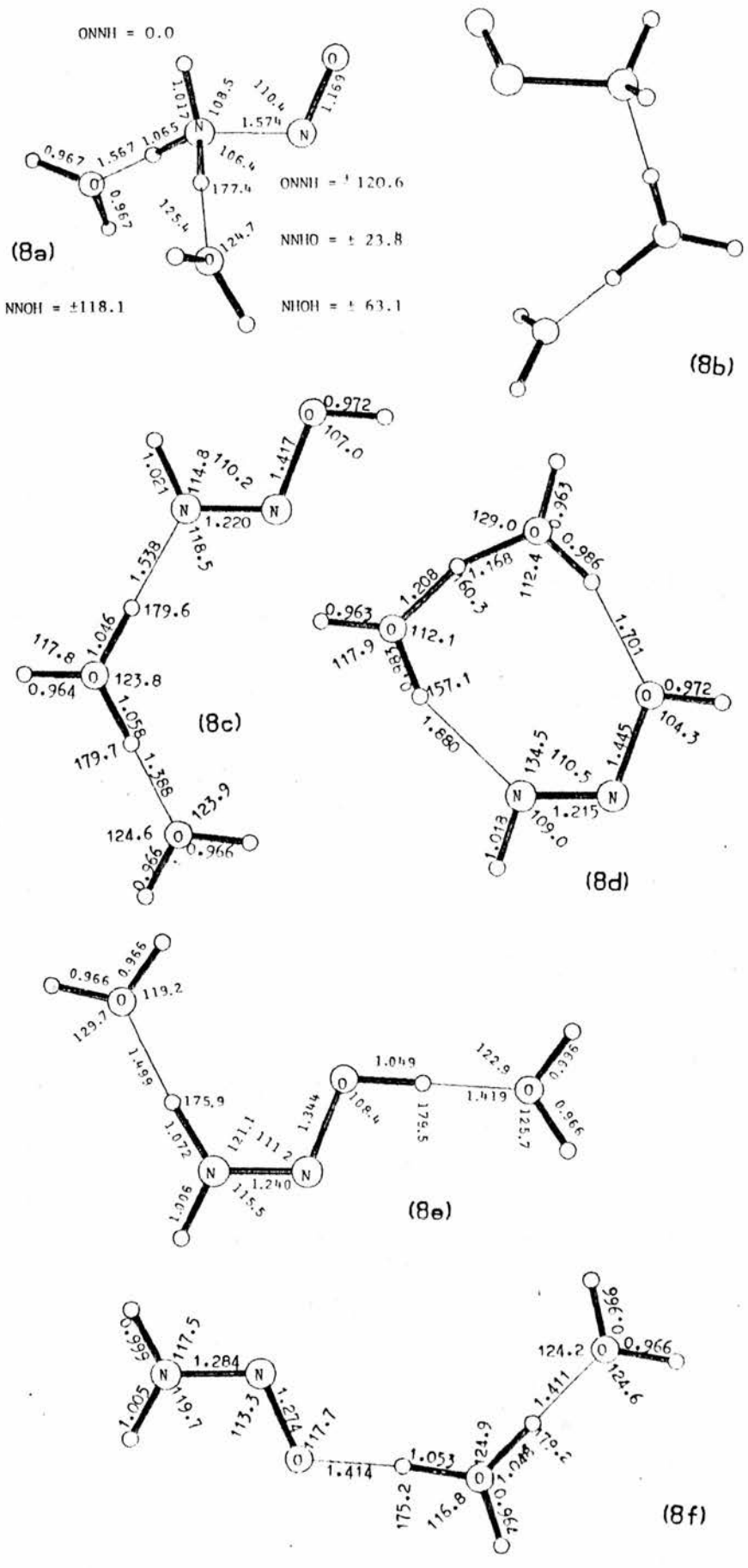

Figure 5.8 Structures of dihydrated H_3NNO^+, H_2NNOH^+ and $HNN.OH_2^+$

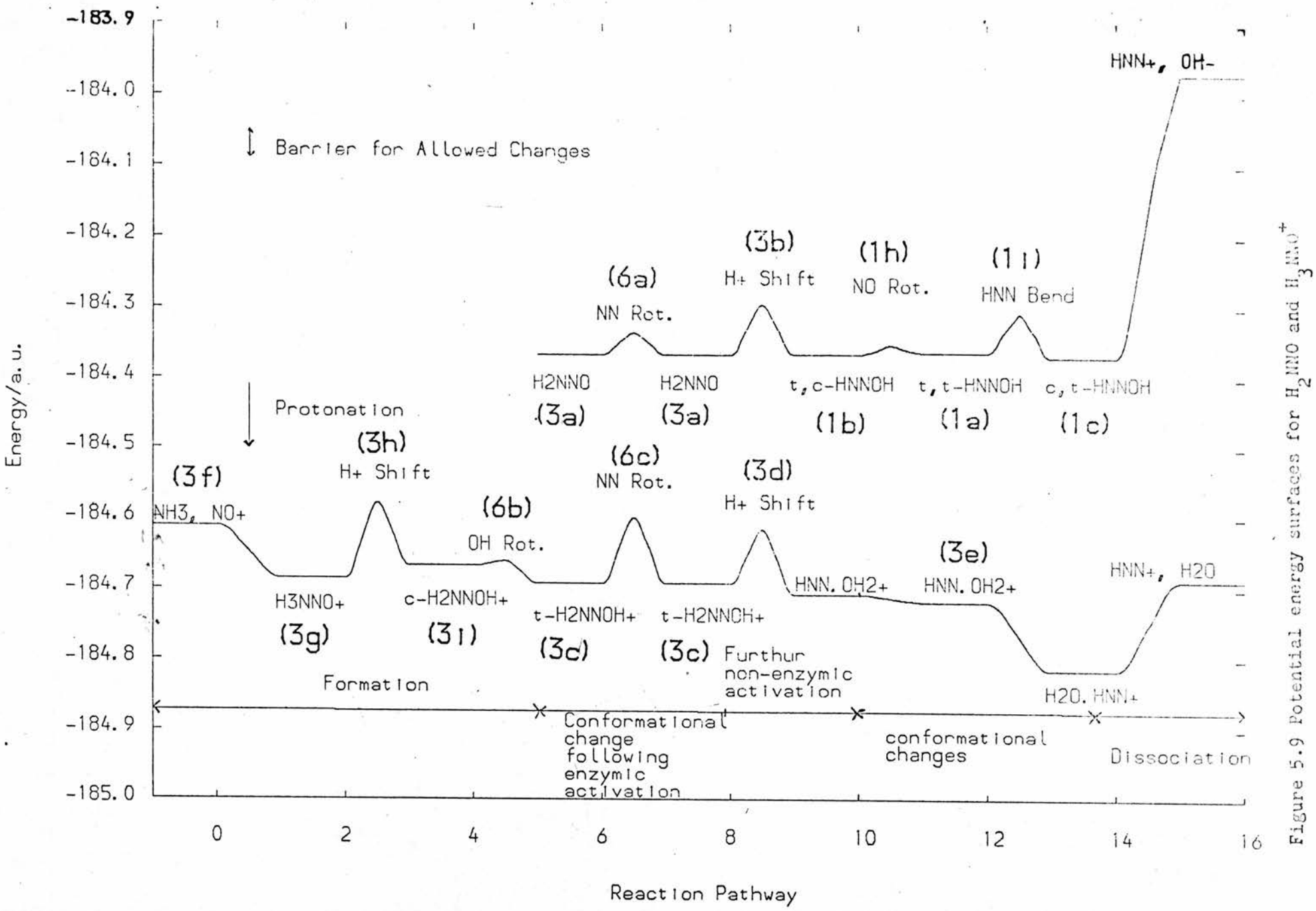

Figure 5.9 Potential energy surfaces for H_2NNO and H_3NO^+

CHAPTER 6

THE ALKYLATING AGENT

1 INTRODUCTION

The nature of the alkylating agent - the ultimate carcinogen - has been discussed many times in the literature [65,68,69,72,73,74]. Despite many experimental investigations, the exact chemical form of the alkylating agent has not been determined. Consequently, quantum chemical studies have attempted to determine the nature of the alkylating agent [99,100,104,105,106,204]. This was also one of the aims of this thesis.

The various possible alkylating agents which have been suggested in the literature - the α-hydroxynitrosamine, the diazohydroxide, the diazoalkane, diazonium ions and carbonium ions - were discussed in chapter 1. It would seem unlikely that the α-hydroxynitrosamine is the alkylating agent. The theoretical work carried out on the other molecules is discussed below. The evidence for their involvement as alkylating agents in nitrosamine carcinogenesis will also be discussed.

2 METHYLDIAZOHYDROXIDE

2.1 Methyldiazohydroxide as an Alkylating Agent

The formation of the diazohydroxide from the α-hydroxynitrosamine was discussed in chapter 4. The geometries of the various conformations and their relative energies were discussed in chapter 5.

The two earliest theoretical studies on the nature of the alkylating agent did not consider the diazohydroxide [99,100]. A semi-empirical study by Loew et. al. [104] concluded that RNNOH does

not appear to be a particularly electrophilic species by either simple electrophilic or covalent criteria. (The criteria considered were the positive charge on C_α of RNNOH, the overlap in the C-N bond and the electron density at C_α for the lowest virtual orbital with significant α-carbon character; this orbital was the LUMO + 1. The energy of LUMO + 1 did not appear to indicate electrophilic character). Loew studied a series of diazohydroxides where R = CH_3 - n-C_5H_{11}. However, she did not specify which conformers of the diazohydroxide were studied.

In a recent ab-initio study, using the 6-31G* basis set, Lown et. al. [106] have suggested that CH_3NNOH is the alkylating agent. The cis,cis isomer was found to be the least stable; it was found that the LUMO of this isomer had a large coefficient on the carbon atom. The trans,cis isomer has a zero LUMO coefficient on the carbon atom. The STO-3G HOMO of guanine was analysed in a similar way: O^6 was found to have a larger coefficient than N-7. From these results it was proposed that the cic,cis isomer would attack O^6, because the two reacting centres possess soft character, and that this would result in a loose transition structure due to the high reactivity of the reaction. Moreover, the loose transition structure could allow for rearrangement. In a similar way, it was argued that the carbon atom of the trans,cis isomer and N-7 both have hard character; the less reactive trans,cis isomer would thus tend to attack at N-7.

This observation is certainly interesting. However, it seems unwise to make this conclusion for several reasons. Four conformations of the diazohydroxide were studied, but only two of these are proposed as alkylating agents, including the least stable isomer which is $83 kJmol^{-1}$ less stable than the most stable conformation reported. The reactivity of the other two isomers is not discussed; moreover the two most stable conformations reported in this thesis were not even studied (Lown et. al. studied all the conformations of (1e) in figure 5.1,

but did not allow for rotation of the methyl group). In the isomers of CH_3NNOH studied in this work, the LUMO is a π-orbital extending over the O-N=N-C skeleton and also over the non-planar hydrogens. (This result was not obtained by Loew et. al., who found no carbon atom participation in the LUMO). None of the conformers studied in this work had a zero carbon atom coefficient in the LUMO. The least stable isomer of Lown et. al. was, however, not studied.

The criteria for site-selectivity proposed by Lown et. al. could be investigated in two ways: firstly, by locating the transition structures for attack by the different conformers at O^6 and N-7 of guanine; secondly, by studying C_2H_5NNOH (because ethylating agents prefer to attack oxygen). The second method would be considerably less expensive, but the first method would give more reliable information.

The electrostatic potential maps of c,t-CH_3NNOH and t,t-CH_3NNOH show that the molecules have large regions of negative potential - see figure 6.5. The electrostatic potential maps of the model compounds are similar; these are shown in figure 6.6. The similarity provides further evidence to justify the use of model compounds in this thesis.

This result suggests that the molecules are unlikely to be electrophilic; the same conclusion was also reached by Loew et. al. [104].

2.2 Methyldiazohydroxide as an Intermediate

Methyldiazohydroxide may undergo several reactions. These are listed below

$$t,t\text{-}CH_3NNOH \longrightarrow CH_3NNO^- + H^+ \qquad (6.1)$$

$$t,t\text{-}CH_3NNOH \longrightarrow CH_3^+ + N_2 + OH^- \qquad (6.2)$$

$$t,t\text{-}CH_3NNOH \longrightarrow CH_3^+ + NNOH^- \qquad (6.3)$$

$$t,t\text{-}CH_3NNOH \longrightarrow CH_3N_2^+ + OH^- \qquad (6.4)$$

$$t,t\text{-}CH_3NNOH \;\text{-->}\; CH_2N_2 + H_2O \qquad (6.5)$$

$$t,t\text{-}CH_3NNOH \;\text{-->}\; CH_2NNOH^- + H^+ \qquad (6.6)$$

Reaction (6.1) leads to the formation of methyldiazotate; reactions (6.2) - (6.4) lead to the formation of an electrophilic cation, either a diazonium ion or a carbonium ion. Reaction (6.5) leads to the formation of diazomethane; this could also be produced via reaction (6.6). The formation of the products of these reactions - alkanediazotates, cations and diazoalkane - will be discussed below.

Although the methyldiazohydroxide is extremely reactive, differences in reactivity of the conformers have been reported. Thus Lown et. al. claim to have detected the trans isomer by N.M.R., but were unable to detect the cis isomer [106].

3 METHYLDIAZOTATE

The action of base on the diazohydroxide is likely to produce the diazotate; reaction (6.1) is less endothermic than reaction (6.6). The structures of $t\text{-}CH_3NNO^-$, (1h), and CH_2NNOH^-, (2h), are shown in figures 6.1 and 6.2 respectively. Moreover, these reactions will be more favourable in aqueous solution, as shown by the following gas phase reactions

$$t,t\text{-}CH_3NNOH + OH^- \;\text{-->}\; t\text{-}CH_3NNO^- + H_2O \qquad (6.7)$$

$$t,t\text{-}CH_3NNOH + OH^- \;\text{-->}\; t,t\text{-}CH_2NNOH^- + H_2O \qquad (6.8)$$

ΔE for reactions (6.1), (6.6), (6.7) and (6.8) is 1630, 1675, -252 and -207kJmol^{-1} respectively. In either case, when the OH^- fragment is placed near the CH_3NNOH and the supermolecule is optimised, structures (4a) and (4b) in figure 6.4 result; there is no energy barrier for these reactions. (The processes are exothermic by -363 and -321kJmol^{-1} respectively). The preferred removal of a hydrogen by OH^- to form (4a) in the gas phase reaction shows that there is probably a barrier to

nucleophilic substitution at the carbon atom, even though substitution would give the most exothermic reaction

$$OH^- + t,t\text{-}CH_3NNOH \longrightarrow HOCH_3 + c\text{-}NNOH^- \qquad (6.9)$$

ΔE for reaction 6.9 is $-350 kJmol^{-1}$. (The energy of CH_3OH is given in table 6.1, but the structure is not shown). None of these energy changes has been calculated using a basis set which includes diffuse functions. This may lead to large errors in reactions (6.1) and (6.6), but in reactions (6.7) - (6.9) these errors are likely to cancel.

Reactions (6.1) and (6.7) are unlikely to result in the formation of an alkylating agent. They could lead either to detoxification or to an effective increase in the life-time of the diazohydroxide.

Although diazotates are unlikely to play a major part in the metabolism of nitrosamines, they may well prove to be useful experimental tools in elucidating the reactions of the diazohydroxide. Moss reports that the trans diazotate is more stable than the cis isomer [67]. The trans isomer can be dissolved in cold water without reaction. If it is heated, however, both diazoalkanes and carbonium ions are formed.

Moss has considered the hydrolytic partitioning of alkyldiazotates in strongly basic solutions

$$RNNO^- K^+ \xrightarrow{H^+} RNNOH \longrightarrow R^+ \longrightarrow \text{products} \qquad (6.10)$$

$$RNNOH \longrightarrow R'{=}N{=}N \qquad (6.11)$$

Moss finds that if R is a primary alkyl group, a rather even partitioning is observed. If R is methyl, benzyl or allyl the diazoalkane dominates; if R is a secondary alkyl group, very little diazoalkane is produced.

Lown et. al. have also observed that the trans diazotate is considerably more stable than the cis isomer [106]. A rapid exchange of the cation between the N and the O is detected in the cis isomer; this exchange is slow in the trans isomer. In CD_3OD, the cis isomer

rapidly forms diazoalkane, whereas the trans isomer is stable for up to 12 hours; the reaction can, however, be catalysed.

4 CATIONIC ALKYLATING AGENTS

4.1 Introduction

Reactions (6.2) - (6.4) give rise to CH_3^+ and $CH_3N_2^+$; both of these reagents are alkylating agents, and their possible involvement in nitrosamine induced alkylations has been studied previously using quantum chemical methods [99,100,104,105,204]. The search by experimentalists for the involvement of carbonium ions has centred around the detection of rearrangement products - see chapter 1. The evidence at present suggests that carbonium ions are not involved in alkylation at N-7; this is because rearrangement is not observed at this position [65]. However, Ford and Scribner did observe rearrangement at O^6 [74]; interestingly, they proposed that the alkylating agent is the diazonium ion and they attributed the rearrangement to a loose transition structure rather than to carbonium ions. They have subsequently carried out a semi-empirical study of the alkylation of various model nucleophiles by both $CH_3N_2^+$ and $C_2H_5N_2^+$ [105]. They find that the transition structures for ethylation are indeed looser than those for methylation. The energy barrier for O-methylation is higher than that for N-methylation by $33kJmol^{-1}$; for ethylation this energy difference is reduced to $2kJmol^{-1}$. They also find that the energy barrier for the S_N1 dissociation of the ethyldiazonium ion is $134kJmol^{-1}$ less than that for the S_N1 dissociation of the methyldiazonium ion.

Andreozzi et. al. [100] and Loew et. al. [104] considered the diazonium ion to be the most likely alkylating agent. Andreozzi et. al. reached this conclusion because of the high energy barrier to the formation of carbonium ions

$$CH_3N_2^+ \quad \text{-->} \quad CH_3^+ \quad + \quad N_2 \qquad (6.12)$$

An energy barrier of 436kJmol^{-1} was obtained for reaction (6.12). (The energy barrier obtained for reaction (6.12) in this work is 145kJmol^{-1}). Loew et. al. were, however, more cautious because their work indicated that only R^+ had substantial electrophilic properties. For example, neither the LUMO nor the LUMO + 1 of RN_2^+ was found to have significant α-carbon atom involvement, and the largest charge was located on the terminal nitrogen. The ab-initio calculations carried out during the course of this thesis at both the RHF/4-21G and RHF/6-31G* levels confirm this observation. LUMO and LUMO + 1 are degenerate orbitals centred mainly on the nitrogens, but also on the hydrogens. LUMO + 2 is, however, a low lying orbital and does have significant carbon atom character - the orbital energy is 0.0002 and 0.009hartrees respectively at the RHF/4-21G and RHF/6-31G* levels. There is, however, a negative charge on the carbon of about 0.35 by both methods, but the methyl group carries the bulk of the positive charge.

There have been other ab-initio calculations on the methyldiazonium ion [217 - 220].

Vincent and Radom showed, using the 4-31G basis set, that the linear form, (2f), given in figure 6.2 is more stable than the bridged forms in which both nitrogens are equidistant from the carbon atom [217]. They also determined the transition structure for the interchange of the two nitrogen atoms. They found that the carbon atom carried a small negative charge, but that the methyl group as a whole carried the majority of the positive charge. They obtained a value of 119kJmol^{-1} for the endothermicity of reaction (6.12).

Demontis et. al. [218] obtained similar results to Radom et. al. Using a double-zeta basis set, they found ΔE for reaction (6.12) to be 107kJmol^{-1} compared to the experimental value of 159kJmol^{-1}. (The result obtained in this work gives the best agreement with experiment, but this may be fortuitous). Using the CNDO/2 method, they studied the effect of hydration on reaction (6.12); nine molecules of water were included in a supermolecule approach. It was found that the dissociation occurred much more readily in solution. It was pointed out, however, that the actual CNDO/2 values for the endothermicity did not compare well with either the ab-initio or experimental values.

Griengl et. al. and Niemeyer found that protonation of diazoalkane occurred more readily at the carbon atom than at the terminal nitrogen [219,220]. This is in agreement with experiment [221] and with this work - see below; this is despite the fact that the largest potential well in the electrostatic potential map of diazomethane is near the terminal nitrogen - see figure 6.7. (The well above the carbon atom, perpendicular to the plane of the molecule, has a depth of only 0.2a.u.).

The relative importance of carbonium ions in the reactions of aliphatic diazonium ions is difficult to determine experimentally and at present the situation is far from clear [222]. For example, carbonium ions may react without rearrangement [223]. Thus no attempt will be made in this chapter to decide between the relative merits of diazonium ions and carbonium ions as the major alkylating agent.

Reactions (6.2), (6.3) and (6.4) are extremely endothermic in the gas phase; ΔE is 1050, 1087 and 905kJmol^{-1} respectively. Despite this, it is often inferred in the literature that the diazohydroxide dissociates spontaneously. These inferences are clearly in line with the known instability of the diazohydroxide, thus the following reaction is exothermic by 301kJmol^{-1}

$$t,t\text{-}CH_3NNOH \dashrightarrow CH_3OH + N_2 \qquad (6.13)$$

It is thus necessary to study reactions (6.2) and (6.4) in aqueous solution. Reaction (6.3) is similar to reaction (6.2) and will not be considered further.

4.2 Spontaneous Decomposition of the Diazohydroxide

Two methods of studying reactions (6.2) and (6.4) in aqueous solution have been used. The first of these is the supermolecule approach. The second method considers the bulk effects of hydration by estimating heats of solution using experimental values.

4.2.1 Supermolecule approach

The effect of solvent assistance in reactions (6.2) and (6.4) has been considered to a limited extent using the supermolecule method. The following reactions

$$t,t\text{-}CH_3NNOH + 2H_2O \longrightarrow H_2O.CH_3.N_2^+ + HOHOH^- \quad (6.14)$$

$$t,t\text{-}CH_3NNOH + nH_2O \longrightarrow CH_3(OH_2)_{n-1}^+ + N_2 + HOHOH^- \quad (6.15)$$

have been studied. These calculations assume that the major qualitative effects of hydration can be accounted for by monohydration and that the hydration energy of uncharged molecules is negligible compared to that of charged molecules. (This second approximation is justified by results presented in the next sub-section). ΔE for reaction (6.14) is $477 kJmol^{-1}$. The energy change for reaction (6.15) depends on the structure of $CH_3(OH_2)_n^+$ - see chapter 3. For n = 1 and 2, with hydration on the carbon atom, ΔE for reaction (6.15) is 493 and $442 kJmol^{-1}$ respectively; for n = 1, 2 and 3, with hydration on the hydrogen atoms, ΔE is 707, 609 and $528 kJmol^{-1}$ respectively.

The energies of reaction for (6.14) and (6.15) are large and

positive. Moreover, it should be noted that the RHF/4-21G method tends to overestimate cation - ligand interaction energies. The first hydration energy of CH_3^+ has been determined by experiment to be 276kJmol^{-1} [224]; this contrasts with the value of 334kJmol^{-1} reported in this work - see also table A.2 in the appendix. The monohydration energy of OH^- is also overestimated. Arshadi et. al. report the monohydration energy of OH^- to be 94kJmol^{-1} [225], but the RHF/4-21G method gives a monohydration energy of 223kJmol^{-1}.

These results are clearly approximate, but they do suggest that reactions (6.2) and (6.4) may not occur spontaneously in aqueous solution.

4.2.2 Empirical approach

In order to estimate the enthalpy and free energy change for the reaction

$$t,t\text{-}CH_3NNOH(aq) \longrightarrow CH_3^+(aq) + N_2(aq) + OH^-(aq) \qquad (6.16)$$

the following cycle can be considered

$$\begin{array}{ccccccc} t,t\text{-}CH_3NNOH(g) & \xrightarrow{a} & CH_3^+(g) & + & N_2(g) & + & OH^-(g) \\ \Big\downarrow b & & \Big\downarrow d & & \Big\downarrow e & & \Big\downarrow f \\ t,t\text{-}CH_3NNOH(aq) & \xrightarrow{c} & CH_3^+(aq) & + & N_2(aq) & + & OH^-(aq) \end{array}$$

where a, b, c, d, e and f represent ΔH or ΔG, the respective enthalpy and free energy changes. It is assumed that the solvent does not react chemically, i.e. that CH_3NNOH and CH_3^+ are inert in this scheme. The problem is to determine c, which is given by the equation below

$$c = a + d + e + f - b \qquad (6.17)$$

The value of a has been evaluated theoretically. In principle, b, d, e and f could be evaluated theoretically using one of the methods which includes bulk solvent effects [166]. However, such methods are likely to be either inaccurate or very expensive. Instead, the values have been estimated from experimental data.

The enthalpies of hydration of OH^- and F^- are -423 and -474kJmol^{-1} respectively [226]. Arshadi et. al. have considered the stepwise hydration energies of OH^- and compared these energies to those of F^- [225]. While the first two enthalpies of hydration of OH^- are less than those of F^-, the third and subsequent enthalpies of hydration of OH^- are greater than those of F^-. On this basis, it was suggested that the enthalpy of hydration of OH^- should be nearer -520kJmol^{-1}. The free energy of hydration of singly charged ions is generally less than the enthalpy of hydration; the free energy of hydration of F^- is -434kJmol^{-1} [226]. Applying a correction of a similar order of magnitude would make the free energy of hydration of OH^- equal to -480kJmol^{-1}. OH^- and F^- are isoelectronic and have similar enthalpies of hydration. The enthalpy and free energy of hydration of CH_3^+ may therefore be very similar to those of Na^+. The enthalpy and free energy of hydration of Na^+ are -444 and -411kJmol^{-1} respectively [226]. The enthalpy and free energy of solution of $N_2(g)$ are -11 and -7kJmol^{-1} respectively [227]. The enthalpy of solution of CH_3NNOH has clearly not been measured. However, some estimate of its magnitude can be obtained by considering the corresponding values for a series of alcohols. The heats of solution of CH_3OH, C_2H_5OH, n-C_3H_7OH, n-C_4H_9OH and t-C_4H_9OH are -45, -53, -58, -61 and -64kJmol^{-1} respectively [228]. CH_3NNOH is similar in size to n-C_3H_7OH and probably has a heat of solution of around -58kJmol^{-1}. The free energy change will be slightly less, say -50kJmol^{-1}. Alexander et. al. discuss the additivity of enthalpies of solution of groups within molecules [228].

The value of $-58kJmol^{-1}$ for CH_3NNOH is similar to the sum of the heats of solution of CH_3OH and N_2, which is $-56kJmol^{-1}$.

Equation (6.17) can now be solved using the RHF/4-21G values from tables A.5 and A.6 in the appendix.

$$\Delta H_{(c)} = 1050 - 444 - 11 - 520 + 58 = 97kJmol^{-1} \quad (6.18)$$

$$\Delta G_{(c)} = 934 - 411 - 7 - 480 + 50 = 86kJmol^{-1} \quad (6.19)$$

There are clearly several sources of errors in these calculations. The value of a could be calculated more accurately. The effect of electron correlation at the MP2/4-21G level increases ΔE by $84kJmol^{-1}$ - see appendix. The effect of polarisation functions on the model reaction

$$t,t\text{-}HNNOH \longrightarrow H^+ + N_2 + OH^- \quad (6.20)$$

is to reduce ΔE by $119kJmol^{-1}$; the effect of electron correlation at the MP2/4-21G level is to increase ΔE by $22kJmol^{-1}$. The model reaction is not strictly applicable in this case as H^+ is not comparable to CH_3^+. Moreover at the 4-21G level, $c,t\text{-}CH_3NNOH$ is more stable than $t,t\text{-}CH_3NNOH$ by $8kJmol^{-1}$; this increases a by $8kJmol^{-1}$. The values of b and d are estimated and may be subject to large errors. These errors are likely to increase ΔH for reaction (6.16) as d is probably overestimated, whereas CH_3NNOH is more polar than $n\text{-}C_3H_7OH$ so b may be underestimated.

4.2.3 Summary of above results

These calculations suggest that $CH_3NNOH(aq)$ will be stable unless its decomposition is catalysed. Although there is an overwhelming weight of evidence to suggest that CH_3NNOH is highly unstable, there is also experimental evidence to suggest that in certain cases $t,t\text{-}CH_3NNOH$ may possess a certain degree of stability. Such evidence may be sought from the relative stabilities of cis and trans alkyldiazotates.

These results imply that the diazohydroxide, along with the α-hydroxynitrosamine, may have a sufficient life-time to diffuse across the cell. The diazohydroxide may have added stability in the lipid phase. The results also suggest that catalysis may be important in the decomposition of the alkyldiazohydroxide.

4.3 Catalysed Decomposition of the Diazohydroxide

The above calculations suggest that the decomposition of the diazohydroxide may be catalysed. The observations of Moss and Lown (discussed above) suggest that this may indeed be the case. This is not unreasonable because OH^- is a poor leaving group [223]. The instability of the diazohydroxide suggests that there is no shortage of catalysts. Internal rearrangements may account for the reactivity of the cis isomers; some possibilities are suggested below, though the transition structures have not been located.

c,t-CH_3NNOH --> 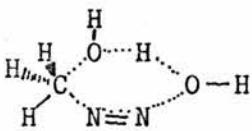 --> $CH_3OH + N_2 + H_2O$ (6.21)

c,t-CH_3NNOH --> 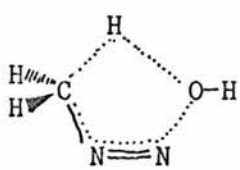 --> $CH_2NN + H_2O$ (6.22)

Moss proposed the involvement of nitrogen separated ion pairs in the chemistry of diazotates; this is similar to the idea of internal rearrangements. Alkylating agents derived from the trans diazohydroxide may have longer effective life-times, and may thus show a different spectrum of products to those derived from the cis

diazohydroxide. This may be open to experimental observation by low temperature studies using alkyldiazotates.

4.3.1 Acid catalysed decomposition of the diazohydroxide

Protonation of the diazohydroxide is an exothermic process that results in a large change in geometry; the monohydrated diazonium ion is formed. Similar results are obtained using the model system

$$t,t\text{-}CH_3NNOH + H^+ \longrightarrow CH_3NN.OH_2^+ \quad (6.23)$$

$$t,t\text{-}HNNOH + H^+ \longrightarrow HNN.OH_2^+ \quad (6.24)$$

ΔE for reactions (6.23) and (6.24) are -1054 and -935kJmol^{-1} respectively. In chapter 5, it was shown that $CH_3NN.OH_2^+$, (1e), and $HNN.OH_2^+$, (1c), or (3e) in figure 5.3, could be formed by a proton shift in CH_3NHNOH^+ and H_2NNOH^+ respectively. The geometries of these molecules, (1c) and (1e), are shown in figures 5.3 and 6.1. The nature of these molecules was not discussed in the previous chapter. The electrostatic potential maps (not shown) of $CH_3NN.OH_2^+$, (1e), and $CH_3N_2^+$ are similar, as are the geometrical structures and Mulliken charges. $CH_3NN.OH_2^+$, (1e), thus appears to be a monohydrated diazonium ion. Both $CH_3NN.OH_2^+$, (1e), and $HNN.OH_2^+$, (1c), were obtained as minima using the optimisation algorithms internal to Gaussian 80. However, analytical second derivative calculations show that these molecules are transition structures. The eigenvectors indicate that the transition state movement is an N=N-O-H torsional oscillation (rather than an N=N-O bending vibration) which for $HNN.OH_2^+$, (1c), would result in a structure (1d). The structure (1d) is not a stationary point, however, although it does have low forces; the true minima for $HNN.OH_2^+$, (1c), and $CH_3NN.OH_2^+$, (1e), are $H_3O.N_2^+$, (1b), and $H_2O.HCH_2N_2^+$, (1f). (Structure (2f) in figure 5.2 is also a transition structure. The situation is analogous to that for (1c) and (1e)). The linear structure, $HNN.OH_2^+$,

(1a), is higher in energy than (1c) by 29kJmol^{-1}; it has one negative eigenvalue corresponding to an N=N-O bending vibration, and one zero eigenvalue corresponding to rotation of the H_2O about the N-O bond.

The structure $H_2O.HCH_2N_2^+$, (1f), is thus the only monohydrated methyldiazonium ion. It is probably a local minimum; the global minimum is $H_2O.CH_3.N_2^+$. (Analytical second derivative calculations on $CH_3.OH_2^+$ suggest that (1g) is probably a saddle point for rotation of the H_2O about the O-C bond, and that the true minimum will lie about 0.5kJmol^{-1} lower in energy, with the H_2O rotated by about 30°). $H_2O.CH_3.N_2^+$, (1g), lies 117kJmol^{-1} lower in energy than $H_2O.HCH_2N_2^+$, (1f).

A study of the interconversion of $H_2O.HCH_2N_2^+$, (1f), and $H_2O.CH_3.N_2^+$, (1g), would be very interesting because the former is a hydrated diazonium ion, whereas the latter is essentially a hydrated carbonium ion; the C-N bond length in (1g) is 2.9Å.

Clearly, protonation initiates a sequence of events that initially results in the formation of a hydrated diazonium ion, which may then form a hydrated carbonium ion. A linear hydration chain based on $H_2O.CH_3.N_2^+$, (1g), would probably result in the formation of methanol and nitrogen, and regenerate the hydrated proton. Thus alkylation may occur only between the key events of protonation and detoxification. (Andreczzi et. al. also considered the effects of protonation on the diazohydroxide, but their method did not identify the nature of the products). This observation may be open to experimental verification by studying the distribution of alkylation products in macromolecules containing basic, acidic and neutral groups. A correlation between alkylated sites and the proximity of acidic groups would suggest that acid catalysis is important. This would shed light on the importance of the micro-environment in DNA alkylations. It may turn out that the acidic phosphate groups of DNA are involved [204]. In such an investigation it may be useful to use synthetic macromolecules. The

author is, however, unsure of the feasibility of such experiments.

5 THE DIAZOALKANE

The reasons for considering diazomethane as the alkylating agent, despite the fact that most researchers in this field state that it is not involved in nitrosamine carcinogenesis, were discussed in chapter 1.

5.1 Energetic Considerations

The structure of diazomethane and a number of its monohydrated derivatives are given in figures 6.2 and 6.3; the energies are given in table 6.1. Monohydrated diazomethane is formally related to methyldiazohydroxide by a proton shift, as shown in reaction (6.22); for this reason the structures of the various forms of monohydrated diazomethane are shown in figure 6.3 and the energies are given in table 6.1. The electrostatic potential map of diazomethane is shown in figure 6.7. The N-terminal end of $H_2C{=}N{=}N$ is surrounded by regions of negative potential. The binding of the oxygen atom of the water molecule to this region is repulsive; the water prefers to approach by its hydrogen atom - see (3a) and (3b). The electrostatic potential maps suggest that a stable arrangement may be achieved by both hydrogens of the H_2O approaching either end of $H_2C{=}N{=}N$, perpendicular to the plane. Such an approach, however, yields (3b). In the most stable arrangement the water molecule binds to the hydrogen atoms in a perpendicular arrangement, (3d). The structures (3a) - (3d) are more stable than c,t-$CH_3\dot{N}NOH$ by 5, 8, 13 and 14kJmol^{-1} respectively. The largest monohydration energy is 24kJmol^{-1}. Diazomethane cannot

therefore be ruled out on energetic grounds.

5.2 Formation of Diazomethane

Diazomethane could be formed via reaction (6.22); it could be formed by the effect of base on CH_3NNOH (reactions (6.6) and (6.8)) or on $CH_3N_2^+$

$$CH_3N_2^+ \longrightarrow CH_2N_2 + H^+ \qquad (6.25)$$

$$CH_3N_2^+ + OH^- \longrightarrow CH_2N_2 + H_2O \qquad (6.26)$$

ΔE for reaction (6.25) is 978kJmol^{-1}; Andreozzi et. al. discounted the involvement of the diazoalkane because of the high endothermicity compared to reaction (6.12). Reaction (6.26) is also endothermic, by 903kJmol^{-1}. However, as reaction (6.8) is exothermic by 207kJmol^{-1}, the formation of the diazomethane is clearly a possibility. The electrostatic potential maps of CH_2NNOH^- and CH_3NNO^- are shown in figure 6.8. The molecules are surrounded by regions of negative potential and could be reprotonated at a number of sites; not all of these sites have been investigated. The formation of CH_3NNO^- is more likely as it is more stable than CH_2NNOH^- by 45kJmol^{-1}; moreover (4b) is more stable than (4a) by 42kJmol^{-1}. The formation of CH_3NNO^- may be a detoxifying reaction as it is unlikely to lead to an alkylating agent. Re-protonation of CH_2NNOH^-, (2h), may, however, lead to the formation of diazomethane, especially as the regions of highest negative potential are not near the carbon atom. A linear hydration chain based on $H_2O.HCH_2.N_2^+$, (1f), could yield $[H_2O.H_3O.CH_2N_2]^+$, (4c). However, (4c) is 74kJmol^{-1} above (4d). The structure (4c) is not a stationary point; it collapses to (4d) upon optimisation. Diazomethane is therefore not formed by the hydration of (1f).

5.3 Other Theoretical Studies on Diazomethane

There have been other theoretical studies of diazomethane; the most significant of these, as far as this work is concerned, used the valence bond method and showed that diazomethane has diradical character [229]. The RHF method used in this work is unable to describe diradical behaviour. However, an error in the treatment of monohydrated diazomethane at the RHF level would suggest that $H_2O.CH_2NN$ becomes even more stable compared to CH_3NNOH. This would make the involvement of diazomethane even more likely.

5.4 Further Experimental Work

These results suggest that Lijinsky's original experiments [72,73] should be repeated on O^6-alkylguanine. Because the formation of the diazoalkane may require base, it would be interesting to study the distribution of alkylation products in macromolecules containing basic groups - see section 4.3.1.

6 CONCLUSIONS

This work does not provide sufficient evidence to identify the nature of the alkylating agent. It widens the range of molecules which need to be considered because it shows that on energetic grounds the diazoalkane cannot be excluded even if it is formed only as a minor product. It would be a relatively straightforward matter to determine the extent of diazoalkane involvement experimentally.

The diazohydroxide does not appear to be the alkylating agent. It seems more likely that the diazohydroxide decomposes to give a

diazonium ion. The importance of acid catalysis in this reaction has been discussed and it has been demonstrated that acid catalysis in the micro-environment can explain the involvement of diazonium ions and carbonium ions. An experiment is suggested which may reveal the importance of acid and base catalysis in nitrosamine induced alkylations. Catalysis, possibly via concerted reactions involving the solvent, may also play a part in detoxifying reactions.

Many theoretical studies on the nature of the alkylating agent have considered only indicators of reactivity such as Mulliken charges. Clearly, such approaches are unlikely to unravel the complexities of nitrosamine induced DNA alkylations. These approaches need to be supplemented by studies of the actual alkylation step; this has not been done in this thesis. The most fruitful approach may be to follow the lead of Ford and Scribner [105] and to determine the transition structures for alkylation by both methylating and ethylating agents. The experimental study of ethylations has certainly contributed a great deal to our understanding of tumour initiation; theoretical studies of ethylations may prove to be equally rewarding. It would thus be advantageous to extend Ford and Scribner's work to other alkylating agents, and if possible to use more reliable ab-initio methods. In order to use ab-initio methods it may be necessary to find suitable model systems for guanine. There have been many cases where semi-empirical methods have been shown to be unreliable in the study of nitrosamine metabolism. The work in this thesis, and by other researchers, has shown that much information may be obtained using model systems.

Table 6.1 Energies of various molecules studied in this chapter. The number of negative eigenvalues, N, is also shown

Molecule	Label	N	Energy
$HNN.OH_2^+$	(1a)	1	-184.707132
$H_3O.N_2^+$	(1b)	0	-184.814941
$HNN.OH_2^+$	(1c)	1	-184.718071
$HNN.OH_2^+$	(1d)	1	-184.719661
$CH_3NN.OH_2^+$	(1e)	1	-223.717426
$H_2O.HCH_2.N_2^+$	(1f)		-223.721189
$H_2O.CH_3.N_2^+$	(1g)		-223.765807
$t\text{-}CH_3NNO^-$	(1h)		-222.694884
OH^-	(2a)		-75.104378
N_2	(2b)		-108.666310
HN_2^+	(2c)		-108.866271
CH_3OH			-114.767062
CH_2NN	(2d)		-147.493865
CH_2NNH^+	(2e)		-147.752716
$CH_3N_2^+$	(2f)		-147.866512
$HOHOH^-$	(2g)		-151.010622
CH_2NNOH^-	(2h)		-222.677640
$CH_2NN.HOH$	(3a)		-223.320649
$CH_2NN.HOH$	(3b)		-223.321526
$H_2O.HCHNN$	(3c)		-223.323713
$H_2O.HCHNN$	(3d)		-223.324111
$CH_2NNOH.HOH^-$	(4a)		-298.542331
$CH_3NNO.HOH^-$	(4b)		-298.558279
$H_2O.H_3O.CH_2N_2^+$	(4c)		-299.546028
$H_2O.H_2O.HCHN_2^+$	(4d)		-299.574069

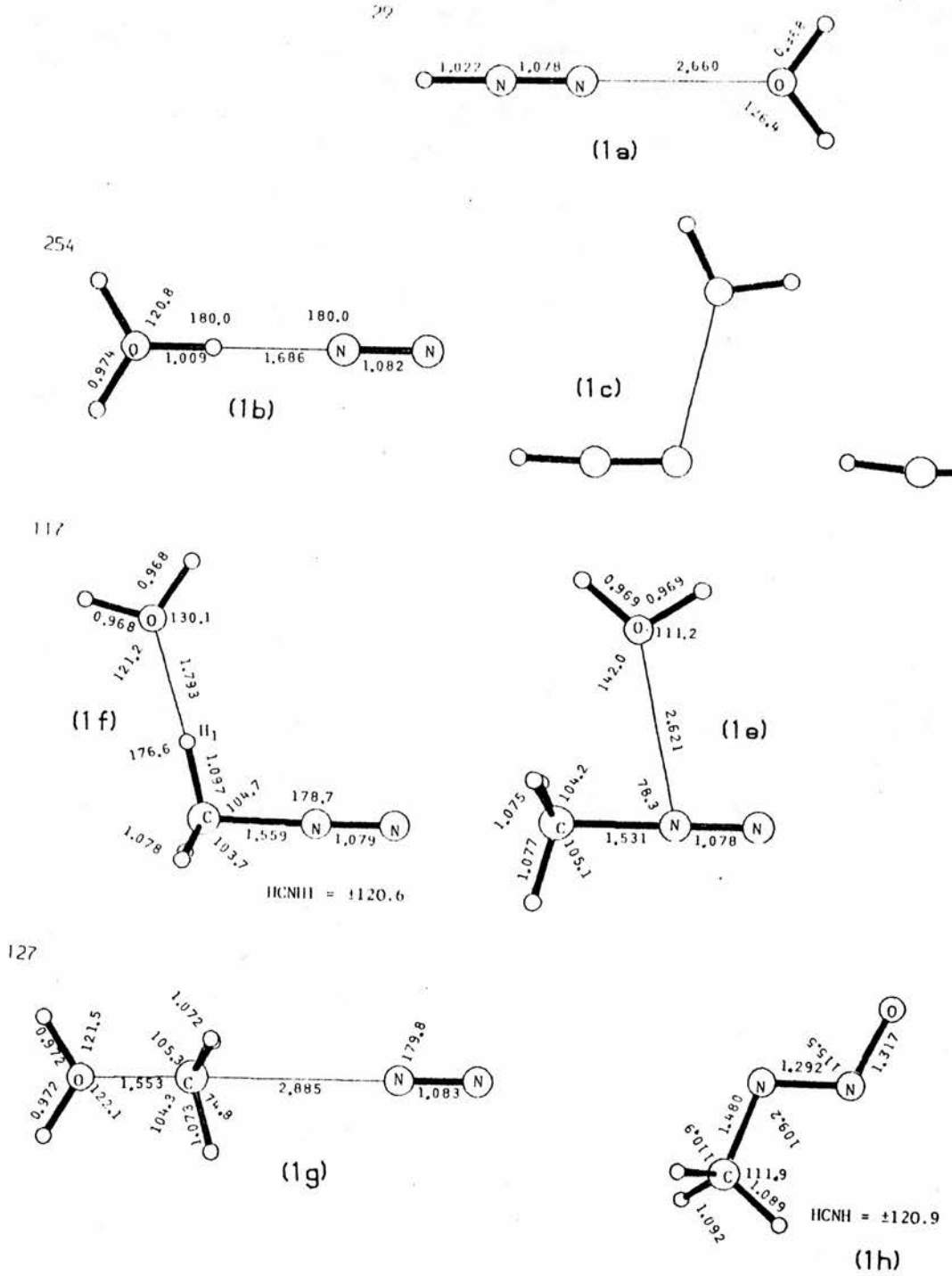

Figure 6.1 Structures of molecules studied in this chapter

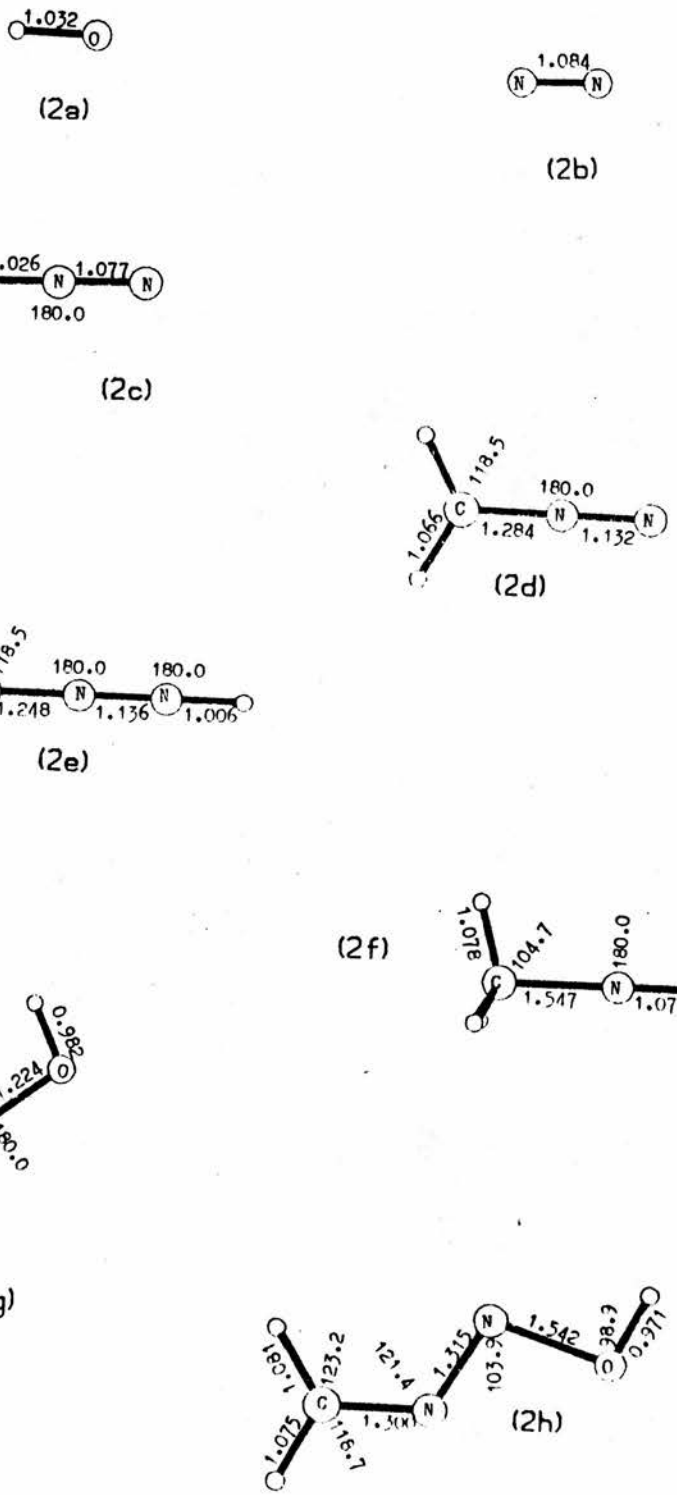

Figure 6.2 Structures of molecules studied in this chapter

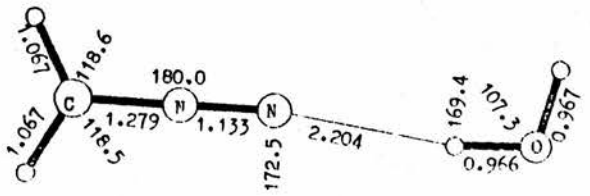

(3a)

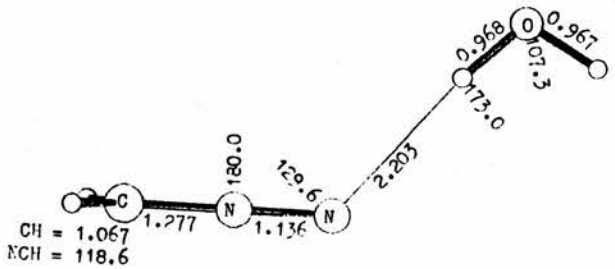

(3b)

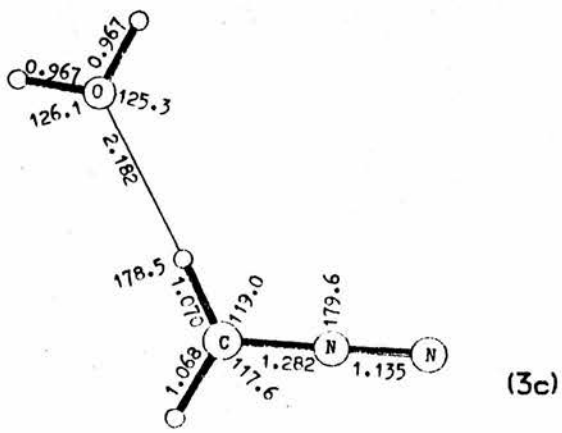

(3c)

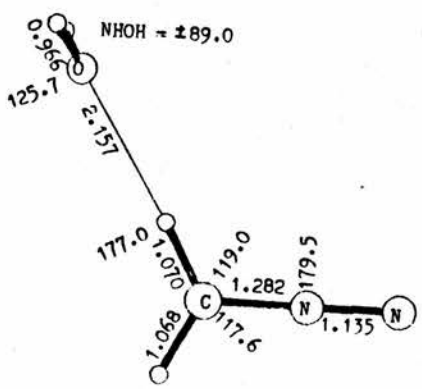

(3d)

Figure 6.3 Structures of monohydrated diazomethane

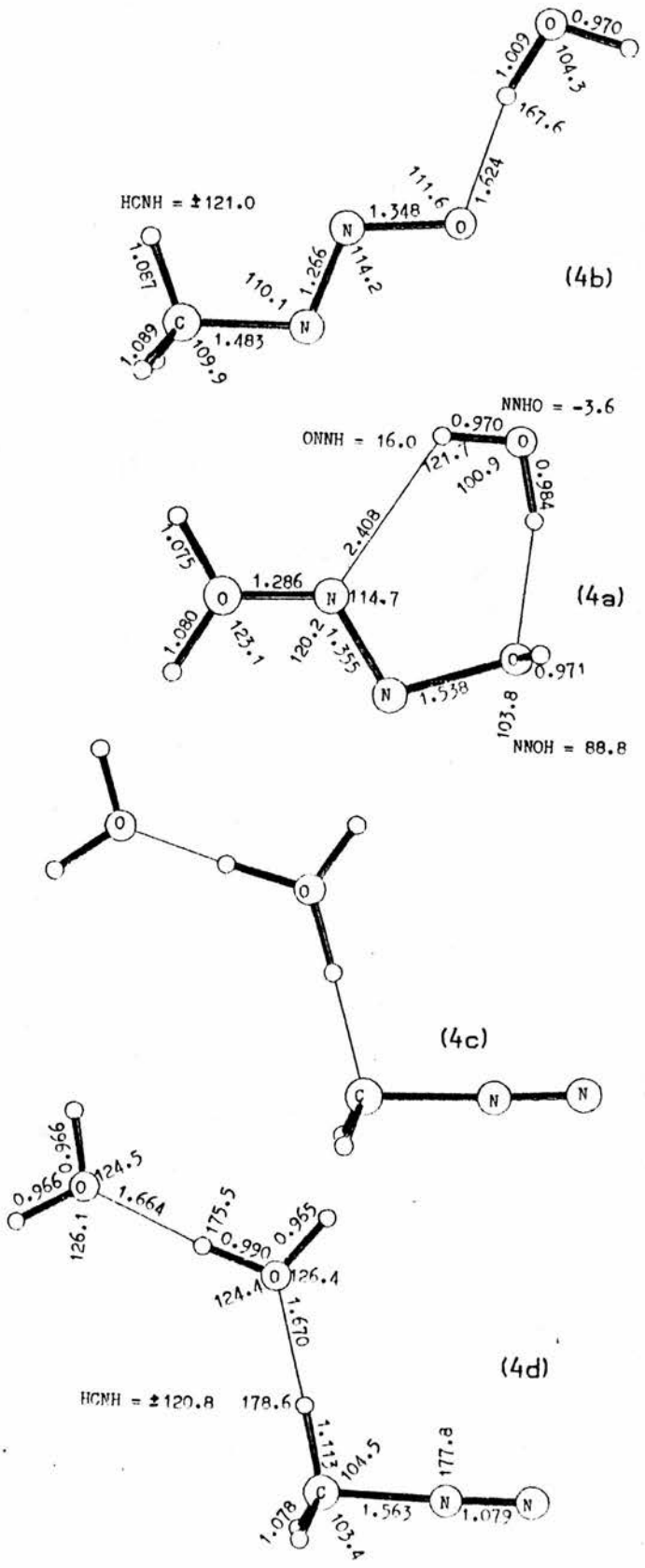

Figure 6.4 Structures of molecules studied in this chapter

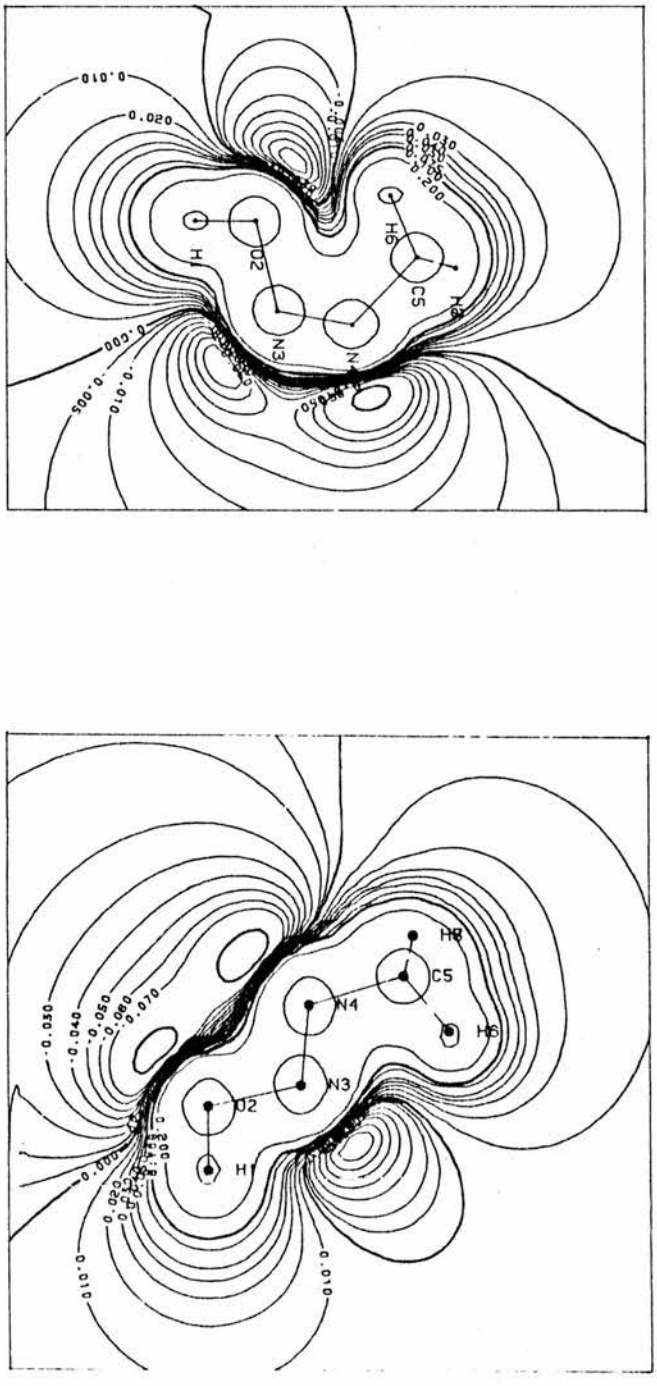

Figure 6.5 Electrostatic potential maps of CH_3NNOH

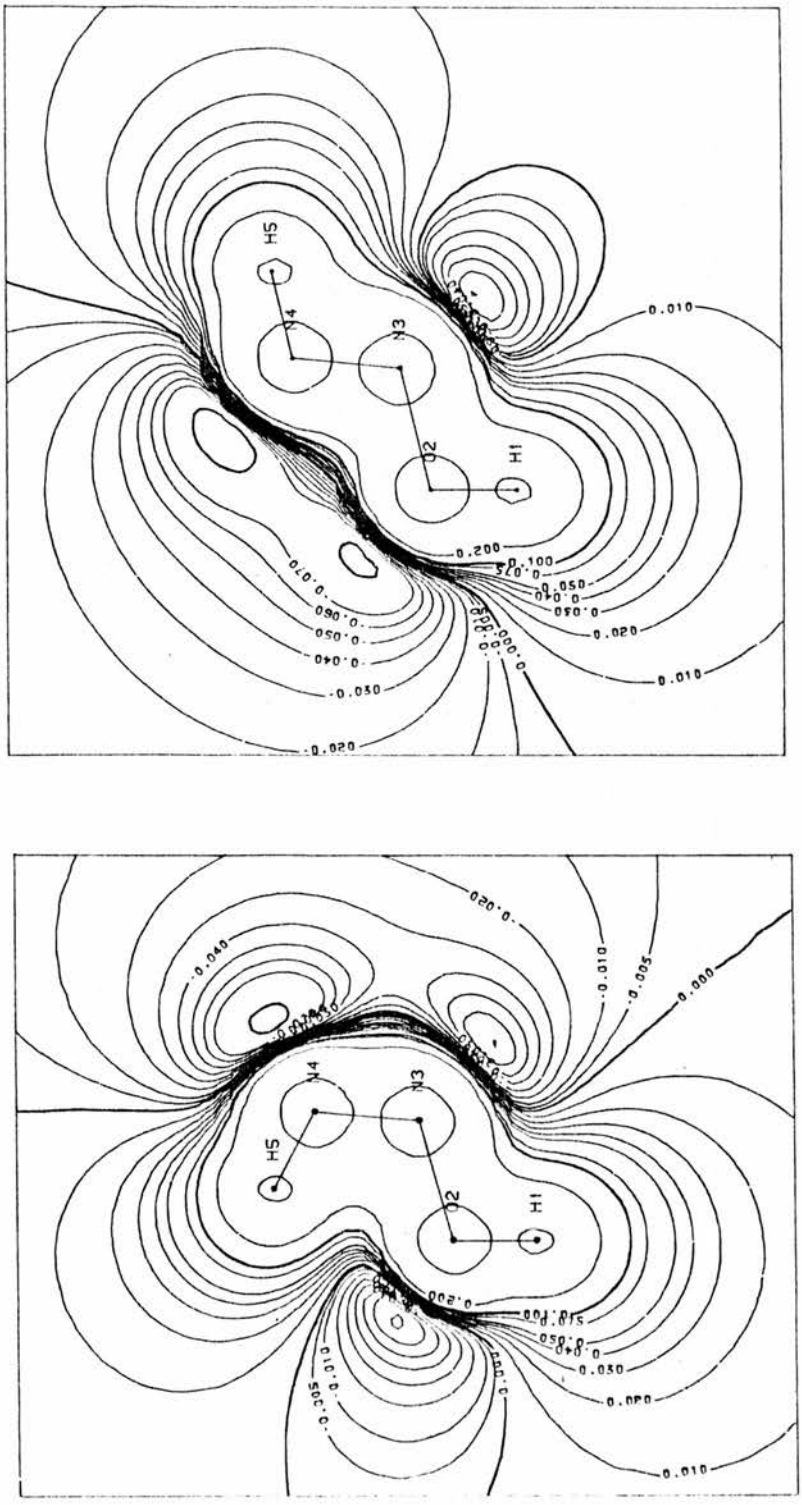

Figure 6.6 Electrostatic potential maps of HNNOH

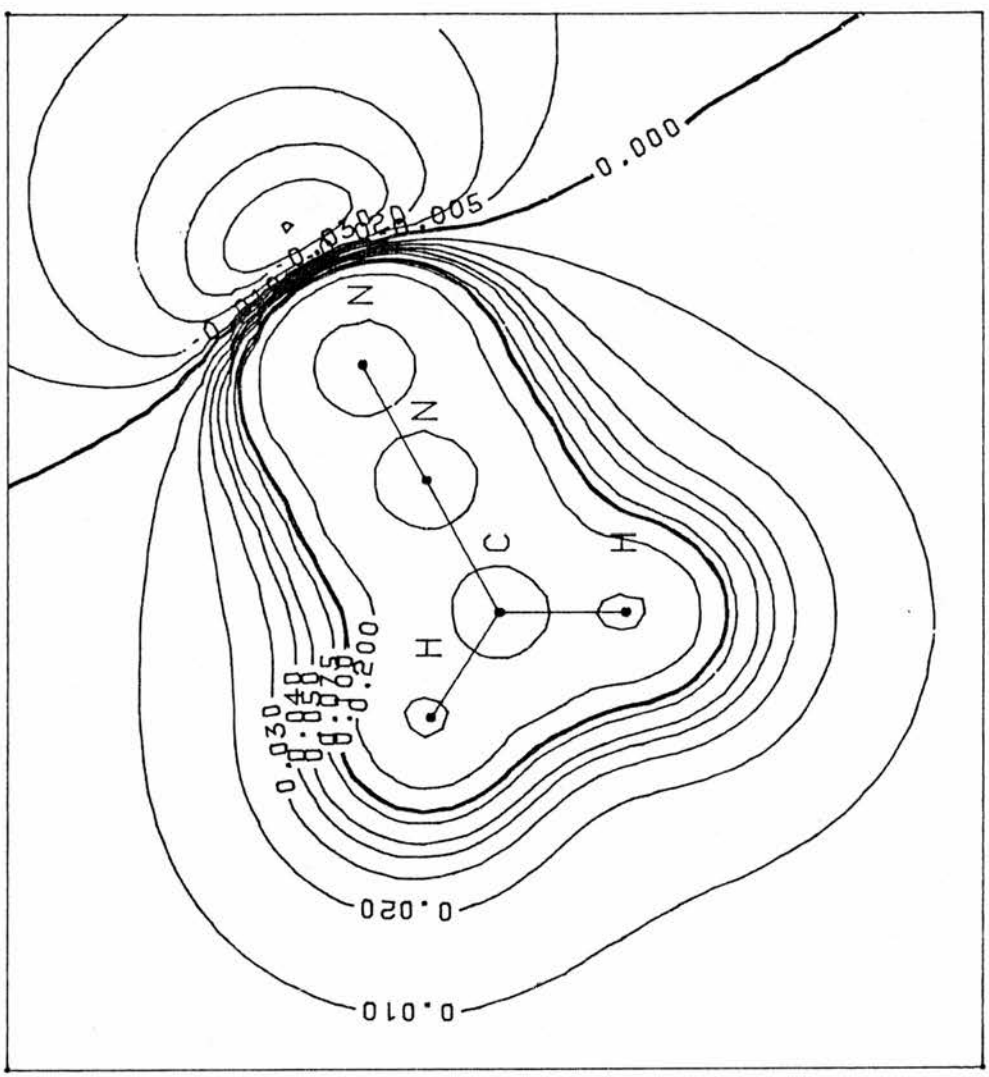

Figure 6.7 Electrostatic potential map of CH_2NN

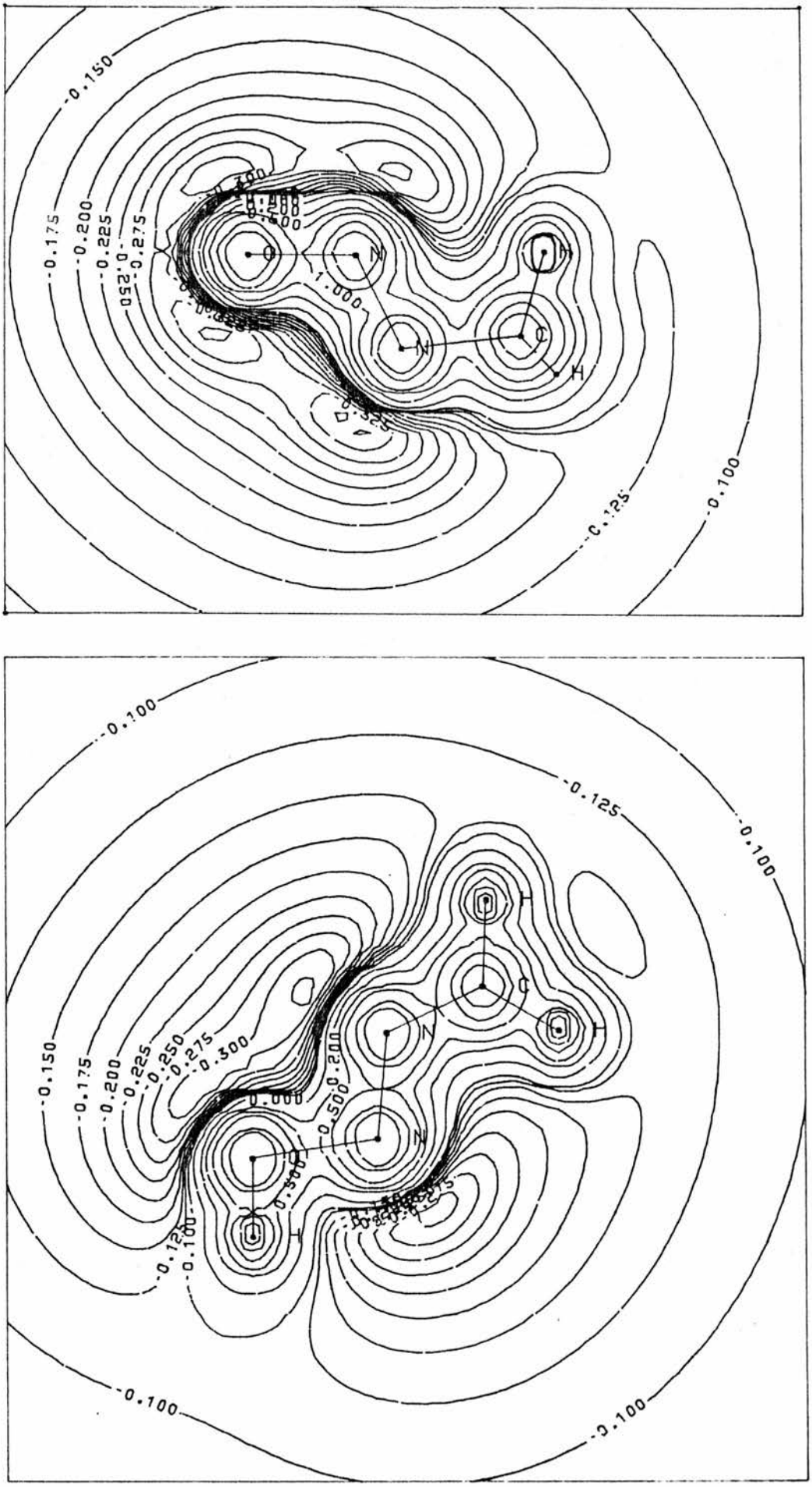

Figure 6.8 Electrostatic potential maps of CH_3NNO^- and CH_2NNOH^-

CHAPTER 7

STANDARD TRANSITION STRUCTURES

1 INTRODUCTION

The transition structures shown in figures 3.1, 4.4, 5.2, 5.3, 5.4, 5.5 and 7.1 have many common features. All the transition structures for 1,3 proton shifts appear to be very similar; the aim of this chapter is to determine the extent of this similarity. Consequently, an investigation of these common features has been carried out. This investigation has covered all stationary points which are believed to be either first or second order transition structures, regardless of whether or not the order of the stationary point has been determined analytically.

The concept of standard bond angles and bond lengths as applied to equilibrium structures is well known [230,231]. However, it is generally assumed that little can be known about the transition structure geometry unless is is determined by some theoretical procedure. The analysis presented below indicates otherwise. It suggests that it may be possible to propose standard transition structure bond lengths and bond angles. The Hammond postulate [232] is often used to discuss transition structure geometries. It implies that the transition structure for an endothermic reaction will more closely resemble the reactant geometry, whereas the transition structure for an endothermic reaction will more closely resemble the product geometry. If this postulate is widely applicable to ab-initio transition structure geometries, then it would appear wise to determine the standard features of transition structures from symmetrical saddle points for thermoneutral reactions. Such saddle points may be obtained very readily by a symmetry constrained minimisation. A number of saddle points obtained in this way are shown in figure 7.1, along with their minima; the energies are given in table 7.8. Having determined these standard features, it would then be useful to investigate asymmetrical transition structures to determine to what extent they

differ from the symmetrical structures. Such an analysis, coupled with improved saddle point optimisation algorithms and more efficient methods for determining second and higher energy derivatives, would greatly facilitate transition structure location which at present is far from routine.

Such an analysis may depend markedly on the choice of theoretical method and basis set. The fully optimised geometry for the saddle point denoted H<NNOH> in table A.2, for the N->O H^+ shift between H_2NNO and HNNOH, shows that the N-N and N-O bond lengths are very dependent on method and basis set. The O-H and N-H bond lengths and the N-N-H and N-O-H bond angles involved in the proton shift are, however, reasonably independent of method, as is the N-N-O bond angle. Thus in a study of the hypothetical transition structure $\langle X'XX''H\rangle_n$, the X'-X and X-X" bond lengths will not be investigated. However, the X'-H and X"-H bond lengths and all the bond angles will be investigated (n is the number of atoms in the ring structure). Similar features in the three-membered and six-membered ring transition structures will also be investigated. At present, the 3-21G basis set is widely used in transition structure studies, as the 6-31G* basis set is too expensive for many applications. The 4-21G basis set gives similar results to the 3-21G basis set.

2 TRANSITION STRUCTURE ANALYSIS

The largest number of transition structures presented are for 1,3 proton shifts and involve four-membered ring transition structures. The analysis of these structures is presented in tables 7.1 and 7.2. The O-H and N-H bond lengths and X'-X-X", X-O-H and X-N-H bond angles are given for a variety of saddle points. The corresponding internal coordinates for the minima are also given; the changes in these

internal coordinates in the transition structure, the charge on the molecule, the energy barrier for the reaction and the overall energy change for the reaction are also given. The three-membered ring N->N proton shift transition structures are treated in a similar way in table 7.3. The six-membered rings are treated in table 7.4. However, in table 7.5 additional information is given on the internal angles at the migrating hydrogen and oxygen atoms (X-H-O and H-H-H) and on the bond length between hydrogen and oxygen (X-H) in the migrating H_3O^+. Because the average values for X-X'-H and X'-H in tables 7.1 and 7.2 are similar for X' equal to both N and O, no distinction is made between X = N and X = O in tables 7.4 and 7.5. The results for structures in which the X-C bond is broken are shown in tables 7.6 and 7.7. For the three-membered ring N->O proton shift transition structures and the five-membered ring transition structure, tne reader is referred to figures 5.4 and 5.5 respectively. Also included in tables 7.1 - 7.7 are the mean and standard deviation of the various reported values.

If the Hammond postulate applies to the X-H bond length, then for exothermic reactions X-H should be shorter than average, while for endothermic reactions it should be longer than average. (In this analysis, the mean of all reactions has been used, rather than the more ideal mean taken from a large number of thermoneutral reactions). Likewise, for the bond angles in the structures with ring-strain (tables 7.1 - 7.3 and tables 7.6 - 7.7), an exothermic reaction should yield a more reactant like transition structure with a larger X'-X-X", X-X'-H or X-X'-C bond angle, whereas for an endothermic reaction the corresponding angles should be smaller. The results for O-H and N-H bonds are shown in tables 7.1 - 7.4; Large deviations (greater than the standard deviation) in line with the Hammond postulate (for $\Delta H >$ $65 kJmol^{-1}$) are denoted by H+. Those contrary to the Hammond postulate are denoted by H-; small deviations are denoted by + or -.

3 DISCUSSION

The results to emerge from this limited study may be summarised as follows.

The overall N-H transition structure bond length is 1.29±0.09Å. The value for three-membered and six-membered rings is slightly shorter than that for four-membered rings; the values are 1.29±0.08, 1.26±0.08 and 1.34±0.10Å respectively.

The overall O-H transition structure bond length is 1.32±0.05Å. The value for the six-membered ring structures is slightly shorter than that for four-membered rings; the values are 1.29±0.05 and 1.33±0.05Å respectively.

The range of these three and six-membered ring studies is however limited, and this difference may not be statistically significant.

A more careful analysis of the three-membered rings shows that the following standard structure emerges

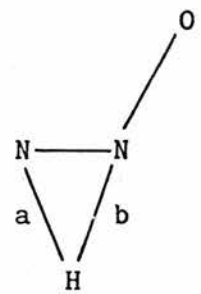

where a is 1.35±0.05Å and b is 1.25±0.02Å. These values clearly differ from the average values in the direction indicated by the Hammond postulate.

For the four-membered ring proton shift saddle points, the structure shown below emerges

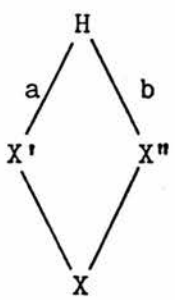

where a and b both equal 1.3±0.1Å, angles X' and X" equal 80°, and angle H equals 101° and angle X is 99°. Thus angle H is generally larger than angle X; angles X' and X" are usually approximately equal. The reduction in angle X in the transition structure is about 14°; the reduction in angles X' and X" is larger, being about 34°. This behaviour could have been predicted, but these results predict the magnitude of the changes that can be expected. The deviations from the above behaviour cannot be predicted from the Hammond postulate. Generally, large deviations occur only if the minima contain an unusually large X-X' or X-X" bond length. Further calculations would, however, be required to analyse how this affects a or b. Charge does not appear to have an effect.

Similar results are found for the CH_3^+ shift transition structures. The X'-C-X" bond angle is small, 57±3°. The reduction in the angle opposite X'-C-X", i.e. X, is 7±3°; the reduction in the X-X-C bond is larger, being 23±2° for the N-N-C angle and 26±8° for the N-O-C angle.

Overall, the N-C and O-C bond lengths are 1.9±0.3Å and 2.2±0.1Å respectively; the large difference in these values is probably due to the use of a small sample. As for the proton shift transition structures, long X-X' bond lengths in the minima are associated with longer and shorter X-C bond lengths. Further study may prove to be rewarding.

For the six-membered ring saddle points, the following structure emerges

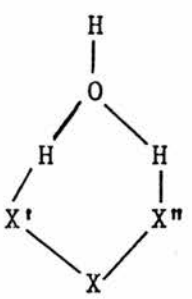

where X'-H and X"-H are 1.3Å, O-H (for the migrating protons) is 1.17Å,

angle H is 148°, angle O is 92° and angles X', X, X" are generally slightly smaller than their values in the equilibrium structures. It should be stressed, however, that these results have been obtained from a small sample of related structures, the majority of which are probably second order saddle points; in other structures, considerable deviations from planarity may be expected, particularly at the H_3O^+. Such a distortion from planarity may have an effect on the features noted above.

4 CONCLUSIONS

Considerable deviations from these structures may be expected. The Hammond postulate may not be very helpful in predicting these deviations; the failure of the Hammond postulate has been noted previously [152]. Further investigation of these deviations may be very useful in the search for reasonable starting geometries for transition structure location. Much useful information may already exist in the literature. One application of this idea may be that if the structure of a desired saddle point is completely unknown, it could be estimated from calculations on a more simple structure; if this saddle point is symmetrical, it could be located by a routine constrained minimisation.

Table 7.1 Standard transition structures of 1,3 O->X H^+ shifts

		O-H Bond length						
Saddle Pt.	Fig.	Min.	Sadl.	Diff.	Ham.	Ang. H	$\Delta E^{\ddagger}$	ΔH
H<NNOH>	5.3	0.978	1.358	0.380	-	99.0	185	-3
H<NNOH>$^+$	5.3	0.969	1.263	0.294	H-	96.9	269	69
H_2<NNOH>$^+$	5.3	0.985	1.225	0.240	-	97.3	297	17
<NNOH>$^-$	5.3	1.012	1.337	0.325	+	104.2	215	79
<ONOH>H^+	3.1	0.998	1.304	0.306	+	96.5	148	-161
<ONOH>H^+	3.1	0.973	1.345	0.372	+	96.5	309	161
<OC(H_2)NH>H_2	4.4	0.967	1.415	0.552		115.6	206	
<ONOH>	7.1	0.979	1.307	0.328		100.3	187	0
<OC(H)OH>	7.1	0.970	1.325	0.355		102.5	228	0
<ON(H)OH>$^+$	7.1	0.991	1.384	0.393		95.8	266	0
Mean		0.982	1.326	0.355		100.9	231	
Std. Dev.		0.014	0.053	0.079		5.8	50	
Number		10	10	10		9	10	

Table 7.1 (continued)

		Angle X'-O-X"			Angle X'-O-H"		
Saddle Pt.	Fig.	Min.	Sadl.	Diff.	Min.	Sadl.	Diff.
H<NNOH>	5.3	110.9	99.9	11.0	106.3	77.3	29.0
$H<NNOH>^+$	5.3	103.8	93.8	10.0	141.3	81.3	60.0
$H_2<NNOH>^+$	5.3	118.9	97.0	21.9	117.1	92.5	24.6
$<NNOH>^-$	5.3	111.5	101.9	9.6	98.2	72.7	25.5
$<ONOH>H^+$	3.1	110.7	95.2	15.5	116.4	90.1	26.3
$<ONOH>H^+$	3.1	108.0	95.2	12.8	131.3	78.2	53.1
$OC(H_2)NH)H_2$	4.4	113.1	94.1	19.0	107.5	76.4	31.1
<ONOH>	7.1	112.2	101.2	11.0	107.3	79.2	28.1
<OC(H)OH>	7.1	124.7	108.2	16.5	112.4	74.6	37.8
$<ON(H)OH>^+$	7.1	125.4	109.0	16.4	110.5	77.6	32.9
Mean		113.9	99.6	14.4	114.8	80.0	34.8
Std. Dev.		6.6	5.3	3.9	12.1	6.1	11.6
Number		10	10	10	10	10	10

Table 7.2 Standard transition structures of 1,3 N->X H^+ shifts

		N-H Bond length						
Saddle Pt.	Fig.	Min.	Sadl.	Diff.	Ham.	Ang. H	$\Delta E^{\ddagger}$	ΔH
H<NNOH>	5.3	0.993	1.285	0.292	-	99.0	188	3
H<NNOH>H^+	5.3	1.016	1.383	0.367	H-	96.9	200	-69
H_2<NNOH>$^+$	5.3	1.017	1.487	0.470	-	97.3	280	-17
<NNOH>$^-$	5.3	1.037	1.339	0.302	-	104.2	136	-79
<OC(H_2)NH>H_2	4.4		1.181	0.178		115.6		
Mean		1.016	1.335	0.322		102.6	201	
Std. Dev.		0.016	0.102	0.096		7.0	52	
Number		4	5	5		5	4	

Table 7.2 (continued)

		Angle X'-N-X"			Angle H-N-X		
Saddle Pt.	Fig.	Min.	Sadl.	Diff.	Min.	Sadl.	Diff.
H<NNOH>	5.3	113.6	99.9	13.7	119.0	83.8	35.2
H<NNOH>H^+	5.3	110.0	93.8	16.2	121.2	88.0	33.2
H_2<NNOH>$^+$	5.3	110.1	97.0	13.1	112.3	71.8	40.5
<NNOH>$^-$	5.3	116.7	101.9	14.8	106.0	81.2	24.8
<OC(H_2)NH>H_2	4.4		94.1			73.9	
Mean		112.6	97.3	14.5	114.6	79.7	33.4
Std. Dev.		2.8	3.2	1.2	6.0	6.1	5.6
Number		4	5	4	4	5	4

Table 7.3 Standard transition structures of 1,2 N->X H^+ shifts

		N-H Bond length					
Saddle Pt.	Fig.	Min.	Sadl.	Diff.	Ham.	$\Delta E^{\ddagger}$	ΔH
H<NNH>O(1)	5.4	1.000	1.371	0.371	+	392	103
H<NNH>O(1)	5.4	1.009	1.220	0.211	+	289	-103
H<NNH>O(2)	5.4	1.000	1.302	0.302	-	403	103
H<NNH>O(2)	5.4	1.009	1.244	0.235	+	300	-103
H<NNH>HO^+(1)	5.4	1.011	1.285	0.274	-	395	92
H<NNH>HO^+(1)	5.4	1.017	1.285	0.268	+	303	-92
H<NNH>HO^+(2)	5.4	1.011	1.353	0.342	+	399	92
H<NNH>HO^+(2)	5.4	1.017	1.277	0.260	+	307	-92
H_2<NNH>O^+	5.4	1.016	1.427	0.411	H+	399	92
H_2<NNH>O^+	5.4	1.023	1.248	0.225	+	307	-92
HNN<NOH>	5.4	1.009	1.136	0.127	H+	233	108
Mean		1.012	1.286	0.275		339	
Std. Dev.		0.007	0.075	0.076		57	
Number		7	11	11		11	

Table 7.4 Standard transition structures of 1,3 X'->X" H_3O^+ shifts

O-H Bond length

Saddle Pt.	Fig.	Min.	Sadl.	Diff.	Ham.	Ang. O	$\Delta E^{\ddagger}$	ΔH
H<NNO.H_3O>$_6$(1)	5.5	0.997	1.284	0.287	+	88.8	65	-9
H<NNO.H_3O>$_6$(2)	5.5	0.997	1.270	0.273	+	92.4	70	-9
<OC(H_2)N.H_3O>$_6H_2$	4.4	0.977	1.247	0.270		89.2	94	
<ONO.H_3O>$_6$	7.1	1.003	1.370	0.367		96.3	71	0
Mean		0.992	1.293	0.299		91.7	75	
Std. Dev.		0.011	0.047	0.040		3.0	11	
Number		3	4	4		4	4	

N-H Bond length

Saddle Pt.	Fig.	Min.	Sadl.	Diff.	Ham.	$\Delta E^{\ddagger}$	ΔH
H<NNO.H_3O>$_6$(1)	5.5	1.015	1.312	0.303	+	74	9
H<NNO.H_3O>$_6$(2)	5.5	1.015	1.318	0.297	+	79	9
<OC(H_2)N.H_3O>$_6H_2$	4.4		1.151				
Mean		1.015	1.260	0.300		77	
Std. Dev.		0.000	0.077	0.003		3	
Number		1	3	3		2	
Overall Mean		0.998	1.279	0.300		76	
Overall Std. Dev.		0.014	0.064	0.032		9	
Number		4	7	6		6	

Table 7.4 (continued)

		Angle O'-X-X"			Angle H-O-X		
Saddle Pt.	Fig.	Min.	Sadl.	Diff.	Min.	Sadl.	Diff.
$H\langle NNO.H_3O\rangle_6$(1)	5.5	113.7	114.5	-0.8	110.0	108.2	1.8
$H\langle NNO.H_3O\rangle_6$(2)	5.5	113.7	114.9	-1.2	110.0	108.6	1.4
$\langle OC(H_2)N.H_3O\rangle_6H_2$	4.4	114.8	111.5	3.3	112.7	110.5	2.2
$\langle ONO.H_3O\rangle_6$	7.1	113.9	115.5	-1.6	109.6	110.4	-0.8
Mean		114.1	114.1	-0.1	110.8	109.4	1.2
Std. Dev.		0.5	1.5	2.0	1.4	1.0	1.2
Number		3	4	4	3	4	4

		Angle N'-X-X"			Angle H-N-X		
Saddle Pt.	Fig.	Min.	Sadl.	Diff.	Min.	Sadl.	Diff.
$H\langle NNO.H_3O\rangle_6$(1)	5.5	114.9	114.5	0.4	119.8	112.4	7.4
$H\langle NNO.H_3O\rangle_6$(2)	5.5	114.9	114.9	0.0	119.8	113.0	6.8
$\langle OC(H_2)N.H_3O\rangle_6H_2$	4.4		111.5			102.2	
Mean		114.9	113.6	0.2	119.8	109.2	7.1
Std. Dev.		0.0	1.5	0.2	0.0	5.0	0.3
Number		1	3	2	1	3	2
Overall Mean		114.3	114.1	0.2	113.0	109.3	3.1
Overall Std. Dev.		0.5	1.5	1.6	4.1	3.3	3.0
Number		4	4	6	4	7	6

Table 7.5 Standard transition structures of 1,3 X'->X" H_3O^+ shifts.
In this table O refers to the oxygen of the migrating H_3O^+

		Bond length O-H			Angle O-H-X		
Saddle Pt.	Fig.	Min.	Sadl.	Diff.	Min.	Sadl.	Diff.
$H\langle NNO.H_3O\rangle_6$(1)	5.5	1.640	1.154	0.486	164.3	151.3	12.8
$H\langle NNO.H_3O\rangle_6$(2)	5.5	1.640	1.151	0.489	164.3	148.9	15.2
$\langle OC(H_2)N.H_3O\rangle_6H_2$	4.4	1.731	1.157	0.574	158.5	153.8	4.7
$\langle ONO.H_3O\rangle_6$	7.1	1.609	1.089	0.520	165.1	143.7	21.4
Mean		1.660	1.138	0.517	162.6	149.4	13.5
Std. Dev.		0.052	0.028	0.035	2.9	3.7	6.0
Number		3	4	4	3	4	4

		Bond length O-H			Angle N-H-X		
Saddle Pt.	Fig.	Min.	Sadl.	Diff.	Min.	Sadl.	Diff.
$H\langle NNO.H_3O\rangle_6$(1)	5.5	1.773	1.174	0.599	147.2	144.9	2.3
$H\langle NNO.H_3O\rangle_6$(2)	5.5	1.773	1.166	0.607	147.2	142.2	5.0
$\langle OC(H_2)N.H_3O\rangle_6H_2$	4.4		1.329			152.3	
Mean		1.773	1.223	0.603	147.2	146.5	3.7
Std. Dev.		0.0	0.075	0.004	0.0	4.3	1.4
Number		1	3	2	1	3	2
Overall Mean		1.688	1.174	0.546	158.8	148.2	10.2
Overall Std. Dev.		0.066	0.068	0.050	7.2	4.2	6.8
Number		4	7	6	4	7	6

Table 7.6 Standard transition structures of 1,3 O->X CH_3^+ shifts

		O-C Bond length					
Saddle Pt.	Fig.	Min.	Sadl.	Diff.	Ang. C	$\Delta E^{\ddagger}$	ΔH
H<NNO.CH_3>$_4$	5.2	1.459	2.068	0.609	60.8	281	-13
H<NNO.CH_3>$_4H^+$	5.2	1.464	2.253	0.789	54.0	224	9
H_2<NNO.CH_3>$_4^+$	5.2	1.510	2.246	0.736	55.3	235	- 29
H<NNO.CH_2OH>$_4$	5.2	1.459	2.164	0.705	58.7	275	11
Mean		1.473	2.183	0.710	57.2	254	
Std. Dev.		0.021	0.075	0.065	2.7	25	
Number		4	4	4	4	4	

Table 7.6 (continued)

		Angle N-N-O			Angle N-O-C		
Saddle Pt.	Fig.	Min.	Sadl.	Diff.	Min.	Sadl.	Diff.
H<NNO.CH_3>$_4$	5.2	113.4	107.1	6.3	116.4	93.4	23.0
H<NNO.CH_3>$_4H^+$	5.2	105.4	104.0	1.4	138.2	99.5	38.7
H_2<NNO.CH_3>$_4^+$	5.2	119.3	106.6	12.7	123.9	108.0	15.9
H<NNO.CH_2OH>$_4$	5.2	112.5	107.3	5.2	117.5	93.1	24.4
Mean		112.7	106.3	6.4	124.0	98.5	25.5
Std. Dev.		4.9	1.3	4.1	8.7	6.1	8.3
Number		4	4	4	4	4	4

Table 7.7 Standard transition structures of 1,3 N->X CH_3^+ shifts.
Also shown are a number of other C-N transition structure bond lengths.

		N-C Bond length					
Saddle Pt.	Fig.	Min.	Sadl.	Diff.	Ang. C	$\Delta E^{\ddagger}$	ΔH
H<NNO>$CH_3>_4$	5.2	1.463	2.001	0.537	60.8	294	13
H<NNO.$CH_3>_4H^+$	5.2	1.512	2.351	0.839	54.0	215	-9
H_2<NNO.$CH_3>_4^+$	5.2	1.515	2.419	0.904	55.3	264	29
H<NNO.CH_2OH$>_4$	5.2	1.495	2.037	0.542	58.7	264	-11
H<OC(H_2)NNOH$>_6$	4.4	1.460	1.823	0.363			
<OC(H_2)NH>H_2	4.4	1.435	1.625	0.190			
<OC(H_2)N.H_3O$>_6H_2$	4.4	1.486	1.636	0.150			
Mean		1.481	1.984	0.504	57.2	259	
Std. Dev.		0.027	0.293	0.272	2.7	28	
Number		7	7	7	4	4	

Table 7.7 (continued)

		Angle N-N-O			Angle N-N-C		
Saddle Pt.	Fig.	Min.	Sadl.	Diff.	Min.	Sadl.	Diff.
H<NNO.$CH_3>_4$	5.2	115.5	107.1	8.4	123.6	98.7	24.9
H<NNO.$CH_3>_4H^+$	5.2	111.9	104.0	7.9	128.0	102.5	25.5
H_2<NNO.$CH_3>_4^+$	5.2	109.6	106.6	3.0	113.1	90.1	23.0
H<NNO.CH_2OH$>_4$	5.2	117.1	107.3	9.8	120.5	100.9	19.6
Mean		113.5	106.3	7.3	121.3	98.1	23.3
Std. Dev.		2.9	1.3	2.6	5.4	4.8	2.3
Number		4	4	4	4	4	4

Table 7.8 Energies of molecules given in figure 7.1

Molecule	Energy/a.u.
HCOOH	-188.304777
HCOOH (TS)	-188.217930
HONO	-204.122692
HONO (TS)	-204.051578
$H_2NO_2^+$	-204.368890
$H_2NO_2^+$ (TS)	-204.267463
$ONOH.OH_2$	-297.971191
$ONOH.OH_2$ (TS)	-297.944297

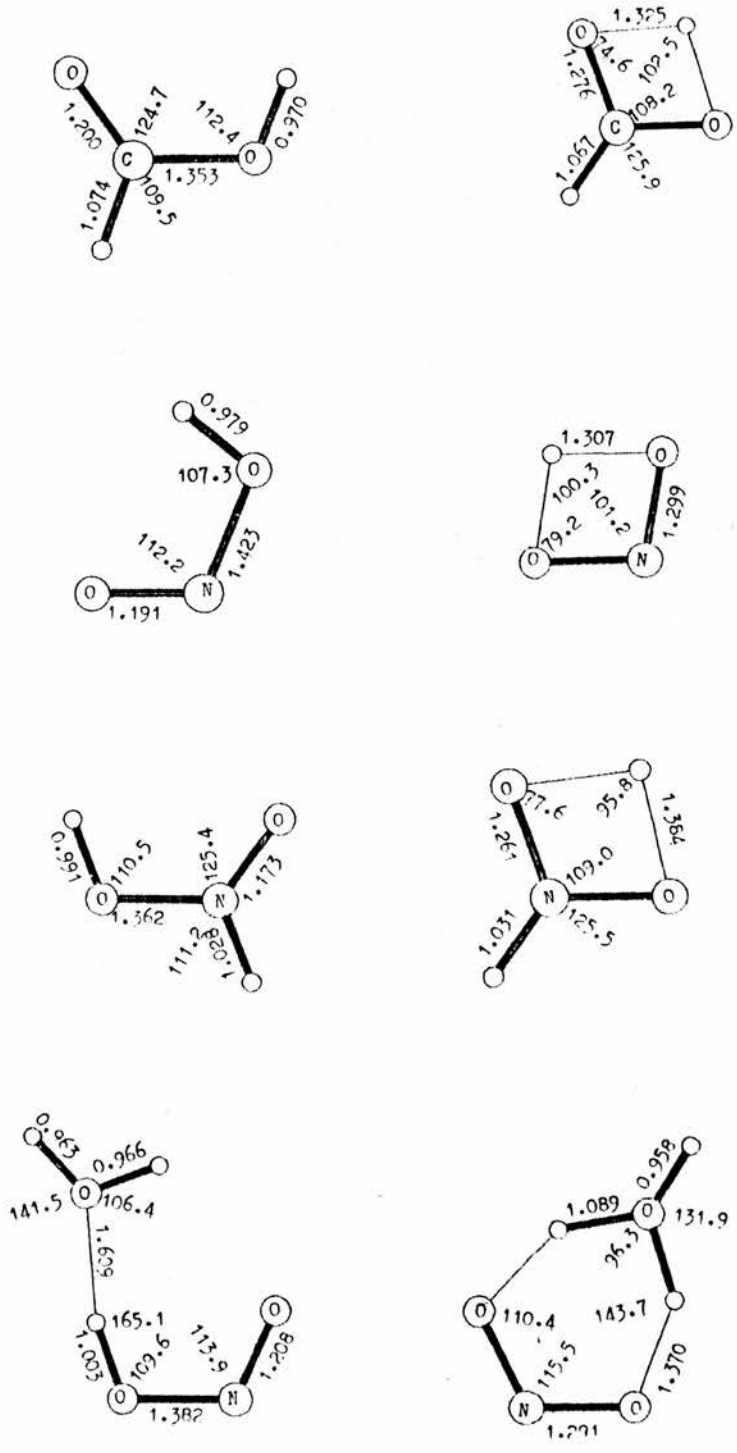

Figure 7.1 Transition structures obtained by constrained minimisation

CHAPTER 8

CONCLUSIONS

1 INTRODUCTION

The results presented in chapters 3 - 7 are summarised in this chapter; the limitations of the methods will also be discussed. It should be noted that the calculations presented in this thesis are approximate in that incomplete basis sets have been used and the correlation energy has generally been assumed to be constant. While it is believed that in many cases these approximations are justified, the results should be interpreted with care. In particular, the energies of transition structures may be subject to error; the correlation energy of many transition structures has been calculated using Møller-Plesset perturbation theory to second order. However, second order Møller-Plesset theory may not account for the largest part of the perturbation energy. The convergence of Møller-Plesset theory is poor at long bond lengths; it would be useful to investigate the convergence of this series for transition structures. It should also be noted that these calculations have been performed on isolated molecules or isolated clusters of molecules. The reactions of these molecules within the living cell may be quite different. Whereas some effort has been made to account for the effects of aqueous, lipid, acidic and basic micro-environments, these treatments have only been partial, and there may be many unknown factors in the cell. The specific conclusions are discussed below

2 THE NITROUS ACIDIUM ION (Chapter 3)

The calculations show that the nitrous acidium ion is formed by the protonation of nitrous acid. It exists as a number of structures, particularly $ON.OH_2^+$ and $ON.OH_2.OH_2^+$. The structures in which more than two molecules of water are bound to the nitrogen atom are unlikely, as these are unstable with respect to the planar structures. The most stable structures are those in which the water molecules are arranged in a linear chain. Moreover, a linear chain of three water molecules results in the destruction of the nitrous acidium ion and the regeneration of HONO and H_3O^+; there is no energy barrier for this process. Thus, in order to react, the nitrous acidium ion must be formed within the vicinity of its substrate so that it can react on encounter; its flat surface may aid this reaction. One possible extension to this work would be to repeat the calculations with a basis set which includes polarisation functions; such calculations may show that there is a small energy barrier to the destruction of the nitrous acidium ion and that it could also exist as $ON.OH_2.OH_2.OH_2^+$. The nitrous acidium ion forms complexes with secondary amines. The destruction of these complexes by a linear chain of two water molecules results in the formation of nitrosamines.

3 THE NITROSATION OF TERTIARY AMINES (Chapter 3)

The nitrosation of tertiary amines by the nitrous acidium ion would lead to the formation of R_3NNO^+ as an intermediate. Nitrosamines may be formed from R_3NNO^+ following either a proton shift or an R^+ shift. The latter would result in the formation of R_2NNOR^+; this is an alkylating agent, and its presence could be detected experimentally. It would be useful to detect the transition structure for the C->O

proton shift in the model system $CH_3NH_2NO^+$. This is a commonly accepted mechanism for the nitrosation of tertiary amines. However, the nitrosation of tertiary amines does not normally occur at the acidities at which the nitrous acidium ion is involved. It would therefore be useful to investigate the nitrosation of secondary and tertiary amines by nitrogen oxides to discover to what extent R_3NNO^+ is involved.

4 THE DECOMPOSITION OF THE α-HYDROXYNITROSAMINE (Chapter 4)

The effect of O-protonation in weakening the C-N bond of the α-hydroxynitrosamine was discussed. However, it was concluded that protonation is unlikely to catalyse the decomposition of the α-hydroxynitrosamine. Base catalysis - either the removal of hydroxyl proton or S_N2 attack by OH^- at the α-carbon - is likely to be important, and will result in the formation of the diazotate. The diazotate is likely to be reprotonated to form either the diazohydroxide or the monomethylnitrosamine. The α-hydroxynitrosamine may also decompose by a concerted mechanism, which may involve the solvent; this reaction is expected to be reasonably slow and will lead to the formation of the diazohydroxide rather than the monomethylnitrosamine. The α-hydroxynitrosamine may be one of the molecules with a sufficient stability to diffuse across the cell. It may be useful to determine the energy barrier for this S_N2 attack by OH^-, to determine the efficiency of $RNNO^-$ as a leaving group.

5 Transition Structures (Chapter 5)

The energy differences between monoalkylnitrosamines and diazohydroxides are small and cannot be determined reliably without carrying out more accurate calculations. Monoalkylnitrosamines and alkyldiazohydroxides readily interconvert by N->O H_3O^+ shifts. In the absence of water the reaction does not appear to occur. The stability of H_2NNO could be investigated further by carrying out more accurate calculations of the correlation energy, and by investigating whether radical mechanisms are important. If, following these further investigations, it still appears to be stable, then the calculated harmonic vibrational frequencies (not reported) may aid its experimental detection. It may be necessary to extend this investigation to HNNOH and other nitrosamine derivatives. The cis and trans isomers of diazotates and diazohydroxides do not readily interconvert.

6 THE ALKYLATING AGENT (Chapter 6)

In view of the complexities of nitrosamine metabolism, it appears unwise to make a firm statement as to the nature of the alkylating agent. Instead, it is proposed that a systematic ab-initio study be made of the transition structures for the alkylation of model nucleophiles for a variety of methylating and ethylating agents.

However, a number of features have emerged from this study. It appears that the diazohydroxide does not decompose spontaneously, either in lipid or in aqueous solution. It may therefore have sufficient stability to diffuse across the cell. Its decomposition may be catalysed by the action of acid, base or by internal rearrangements in the cis isomer. The importance of internal rearrangements in the

cis isomer could be investigated by studying the product distribution from cis and trans diazotates. It would be useful to locate the transition structure for a C->O proton shift in CH3NNOH, as this would lead to the formation of diazomethane. Diazoalkanes cannot be ruled out on energetic grounds. Their involvement should be re-investigated experimentally. Acid catalysis may be important in the formation of both diazonium ions and carbonium ions. An experiment is suggested which may help to determine the importance of acid and base catalysis within the micro-environment of the nucleophile.

7 STANDARD TRANSITION STRUCTURES (Chapter 7)

Many fully optimised transition structures have been reported in this thesis. It is noted that they have many common features. A detailed analysis of these features may be useful in aiding future transition structure determinations. It may be possible to suggest standard transition structure bond lengths and bond angles.

APPENDIX

BASIS SET SURVEY AND RESULTS OF THERMODYNAMICS CALCULATIONS

1 INTRODUCTION

In this appendix, the general results of the basis set survey and the thermodynamic calculations are presented. In the basis set survey and frequency calculations it was necessary to consider model compounds in which non-essential methyl groups were replaced by hydrogens; the various energies are presented in table A.1, the energy changes for various reactions are given in table A.2, and the geometries in table A.3. The results of the frequency calculations are given in tables A.4, A.5 and A.6. These results are discussed below. The notes are given at the end of tables A.3 and A.4.

2 STRUCTURAL COMPARISONS

NO^+ Complexes (2,6,8,9,11) For H_3NNO^+, $ON(H_2O)^+$ and $H_3NNO.OH_2^+$, the N-N bond length varies from 1.6 to 2.2Å. This is because these molecules are complexes of NO^+, and the variation arises out of the basis set superposition error. The N-N bond length in the parent is not as long as in the model compounds. In (9) the H_2O-H bond is more affected by the basis set superposition error than is the N-N bond length. In these molecules, comparisons of the other internal coordinates are probably not meaningful. Large errors can occur in the energy, particularly with the STO-3G basis set, unless it is calculated at the optimised geometry. The results for $ON(H_2O)^+$ using the (7s,3p) basis set show how the N-N bond length and total energy can depend upon the scale factors.

H_2NNO The geometry is fairly independent of basis set; the RHF/4-21G geometry differs from the RHF/6-31G* and MP2/6-31G* results by no more than 0.043Å and 1° and 0.018Å and 0.5° respectively. The

N-N bond is longer than the N-O bond by about 0.11Å throughout (this does not include the STO-3G results). The model and parent 4-21G geometries compare well.

H_2NNOH^+ The 4-21G basis set overestimates the N-N bond length by about 0.09Å compared to the RHF/6-31G* value. The model and parent geometries are in good agreement.

CH_3NH_2 Generally good agreement between the basis sets, and between model and parent, is obtained; the C-N bond lengths do not vary by more than 0.03Å.

$CH_3OH_2^+$ The CO intra-molecular bond length and consequently the other internal coordinates are fairly constant. The reason for the difference in the dihedral angles for the STO-3G basis set, compared to the others, is probably that in this case the optimisation algorithm found the global minimum, rather than a rotational transition structure. (This was confirmed for the 4-21G structure by analytical second derivative calculations).

HONO The N=O and H-O-N internal coordinates appear to be very sensitive to basis set.

t,t-HNNOH The 4-21G N-O bond length is greater than the 6-31G* N-O bond length by 0.1Å; it does, however, compare well with the parent compound.

$CH_3N_2^+$ and HN_2^+ Reasonable agreement between the 4-21G and 6-31G* basis sets is obtained, and the N-N bond length even compares favourably to the N-N bond length in HN_2^+.

H<NNOH> As the method is refined, the N-N and N-O bond lengths become more equal. (This is not the case for either H_2NNO or t,t-HNNOH). This trend is well described at the MP2/4-21G level, but the bond lengths are overestimated. The RHF/4-21G N-H and O-H bonds which are broken only vary by 0.025Å from the MP2/6-31G* values. The bond angles are fairly constant.

3 ENERGIES OF REACTION

The overall nitrosation reaction (3,10,14,16) Nitrosation by NO^+ clearly does not occur in the gas phase (3), and becomes even less likely as the calculation is refined. In the presence of just one molecule of water, (10), it becomes much more possible. With small basis sets, the reaction is favourable, but becomes unfavourable as the calculations are refined. The reaction for the parent is however slightly more exothermic. The comparable reactions for the loss of CH_3^+ are (14) and (16). In the absence of water, (14), this reaction is surprisingly not as unfavourable as the reaction for the loss of a proton. When monohydration is considered, (16), the reaction may be feasible. The reaction becomes less favourable as the method is refined, but convergence appears to be reached at the RHF level.

Protonation reactions (2,11,12) For these reactions, the RHF/4-21G results do not differ significantly from the more refined calculations. This is true for the formation of H_2NNOH^+ (12), even though for H_2NNOH^+ the N-N bond length is dependent upon basis set. The proton affinities of the parent molecules are similar to those of the model compounds.

Barriers for H^+ shifts (22,23,24) The RHF barriers are fairly

constant; they are reduced by about 25-30% by Møller-Plesset theory up to second order.

Cation-ligand complex formation (1,4,5,6,7,15,19) For reactions (1), (4), (7) and to a lesser extent (5), (15) and (19), the interaction energy decreases as the basis set increases. As the structure of the complex is very basis set dependent, the post Hartree-Fock calculations at the RHF/4-21G geometry may not be reliable. Although the structure of the complex in reaction (6) is not very basis set dependent, the interaction energy follows a similar trend. Reaction (6) is isoelectronic with reaction (5). The anomalous positive interaction energy for reaction (6) using the STO-3G basis set is partly due to the use of the 4-21G geometry. The other energy changes for this reaction are fairly independent of basis set - this is possibly due to a decrease in the H_3N-NO^+ interaction energy on the left-hand side being cancelled by a decrease in the H_3NNO^+-OH_2 interaction energy on the right-hand side, as the basis set is increased.

Isomerisation reactions (8,13,17,18) For reactions (17) and (18), the energy differences between the molecules is small, and probably cannot be determined accurately using MO theory. For reaction (13) a similar situation arises, even when electron correlation is included, making it difficult to predict the protonation site of H_2NNO. However, as the reaction for the dimethyl parent is more exothermic, the preferential protonation site is probably on the oxygen. Reaction (8) is exothermic when the changes are determined at the optimised geometry; the endothermic results for the larger basis sets are probably a result of using a poor geometry.

Reactions forming H_2NNO (2,9,15) Reactions (2) and (15) are very

basis set (and method) independent (excluding the STO-3G results). Reaction (9) is not so basis set independent due to the variation in the proton affinity of H_2O.

Ligand exchange reactions (20,21) Excluding the STO-3G results, the changes are fairly constant. This provides a more reliable method of studying cation-ligand interactions. Increasing methyl substitution increases the exothermicity.

4 THERMODYNAMIC CALCULATIONS

The effect of the various corrections to the Hartree-Fock energy change are discussed below.

The overall nitrosation reaction (A12,A13,A14,A15) The basic nitrosation reaction is so unfavourable that the refinements have little effect. When monohydration is taken into account, (A13), enthalpy and entropy have even less effect, and electron correlation becomes far more important. The corresponding reactions for the loss of CH_3^+, (A14,A15), are also far more affected by electron correlation than by the free energy correction.

Protonation reactions (A2,A11,A23,A27,A28) Generally there is a decrease in the exothermicity (which is of the same order of magnitude as the effect of electron correlation). In most cases this is due to zero-point effects. The percentage change in the exothermicity is, however, small.

Barriers for H^+ shifts (A6,A7,A19,A29,A30,A35,A39,A40) In each case, consideration of thermodynamic parameters reduces the energy barrier. Generally the reduction is greater for the three-membered

rings (average reduction 21kJmol^{-1}) than for the four-membered rings (average reduction 13kJmol^{-1}), the greatest reductions being 27 and 20kJmol^{-1} respectively. These reductions are mainly due to zero-point effects. When the barrier is high, the effect of such a reduction is negligible. Electron correlation has a greater effect; some barriers are reduced by more than 100kJmol^{-1}.

Barriers for bimolecular reactions (A8,A32,A33) Entropy has a large effect in these reactions, raising the barriers by about 40kJmol^{-1}. It acts against the effects of electron correlation. However, these reactions may be considered to take place in two steps: first of all the reactants come together to form a complex (exothermic reaction); this complex then reacts in a unimolecular fashion. The energy barrier for the second step is consequently increased, but the effects of entropy are far less important.

Barrier for inversion reaction (A20) There is a small decrease in the energy change, (9kJmol^{-1}), when the free energy, rather than the Hartree-Fock energy, is considered. This is due mainly to zero-point effects, and the reduction is of the same order as that due to electron correlation.

Barriers for rotation (A4,A10,A18,A34) In each case the free energy barrier is lower than the Hartree-Fock barrier by about 9kJmol^{-1}; again this is primarily due to zero-point effects. The MP2 barrier is higher by a similar amount.

Cation-ligand complex formation (A3,A5,A16,A24) There is an average decrease in the energy change of about 50kJmol^{-1}, the greater part of which is due to entropy. The correction is generally larger than the opposite effect of electron correlation.

Dissociation reactions (A21,A22,A23,A24,A25,A26) There is a decrease in the endothermicity, due to both zero-point effects and entropy, though the reactions remain extremely unfavourable. The effect of electron correlation has a less dramatic effect. Similar corrections are obtained for both model and parent molecules, even though the approximation of $CH_3N_2^+$ as HN_2^+ is pushing the model - parent approximation to its limits.

Isomerisation reactions (A1,A9,A17,A37,A38) Electron correlation appears to be more significant than thermodynamic effects.

5 CONCLUSIONS

The precise determination of molecular geometries is not the prime objective of this thesis. However, the 4-21G geometries are in reasonable agreement with the 6-31G* geometries, the notable exceptions being NO^+ complexes. As may have been expected, the RHF/4-21G transition structure (for H<NNOH>) does differ from the MP2/6-31G* structure, but even here the bonds which are broken do not vary by more than 0.03Å. There is generally good agreement between the model and parent geometries.

For many of the reactions studied, the energy changes for the model systems are similar to those for the parent reactions; this partly justifies the approximation of replacing non-functional groups with hydrogens. Many of the energy changes are also fairly basis set independent. In other reactions, however, the RHF/4-21G energy changes are usually overestimated, and allowances can be made for this, or reactions can be studied in which the errors cancel. For H^+ shift transition structures, the RHF/4-21G method overestimates the energy

barrier. However, when the barrier is large, this may not be significant.

The corrections to the Hartree-Fock energy changes due to thermodynamic parameters are generally smaller than those due to electron correlation. Except where there is a change in the number of molecules (so that entropy becomes important), the largest change is usually due to the zero-point correction. Allowances should be made for a reduction in the energy barriers for inversion, rotation and H^+ shifts.

Table A.1 ENERGIES OF SPECIES DETERMINED WITH DIFFERENT BASIS SETS (The energies are given in atomic units at both the optimised geometry and at the RHF/4-21G geometry, with the maximum and r.m.s. forces. The difference in the two energies is given in both atomic and S.I. units).

1 H_2NNO

METHOD	E(4-21G)	Max F	RMS F	E(Opt.)	ΔE/au	ΔE/SI
RHF/STO-3g	-182.382960	0.0568	0.0247	-182.387325	0.004365	11
RHF/4-21g	-184.366261					0
RHF/6-31g	-184.730133	0.0319	0.0146	-184.731915	0.001783	5
MP2/4-21G	-184.724172			-184.732054	0.007882	21
RHF/6-31g*	-184.820914	0.0796	0.0309	-184.826285	0.005371	14
RHF/6-31g**	-184.829089	0.0798	0.0309			
MP2/6-31G*	-185.337315a			-185.342692		
MP2/6-31G**	-185.351622					
MP3/6-31G**	-185.352178					
CI,S/6-31G**	-185.358126					

2 H_3NNO^+

METHOD	E(4-21G)	Max F	RMS F	E(Opt.)	ΔE/au	ΔE/SI
RHF/STO-3g	-182.753097	0.2202	0.0653	-182.781104	0.028007	174
RHF/4-21g	-184.685281					0
RHF/6-31g	-185.025260	0.0073	0.0040	-185.026144	0.000884	2
RHF/6-31g*	-185.132865	0.0649	0.0194	-185.140468	0.007603	20
RHF/6-31g**	-185.143368	0.0648	0.0195			
MP2/6-31G**	-185.678276					
MP3/6-31G**	-185.675088					
CI,S/6-31G**	-185.683938					

3 NO^+

METHOD	E(4-21G)	Max F	RMS F	E(Opt.)	ΔE/au	ΔE/SI
RHF/STO-3g	-127.176582	0.3793		-127.204262	0.027680	73
RHF/(7s,3p)b				-128.307636		
RHF/(7s,3p)c	-128.313719d			-128.331679	0.017961	47
RHF/4-21g	-128.559070					0
RHF/6-31g	-128.801161	0.0174		-128.801234	0.000072	0
RHF/6-31g*	-128.909416	0.0323		-128.909653	0.000237	1
MP2/6-31G**	-129.234425					
MP3/6-31G**	-129.221965					
CI,S/6-31G**	-129.230664					

4 NH_3

METHOD	E(4-21G)	Max F	RMS F	E(Opt.)	ΔE/au	ΔE/SI
RHF/STO-3g	-55.449650	0.0194	0.0134	-55.455420	0.005770	15
RHF/4-21g	-56.052230					0
RHF/4-31g	-56.105922	0.0067	0.0044	-56.106692	0.000770	2
RHF/6-31g	-56.164666	0.0064	0.0044	-56.165521	0.000855	2
RHF/6-31g*	-56.182690	0.0095	0.0060	-56.184356	0.001666	4
RHF/6-31g**	-56.194184	0.0081	0.0060	-56.195544	0.001361	4
MP2/6-31G**	-56.381256					
MP3/6-31G**	-56.393986					
CI,S/6-31G**	-56.396175					

5 H_3O^+

METHOD	E(4-21G)	Max F	RMS F	E(Opt.)	ΔE/au	ΔE/SI
RHF/STO-3g	-75.323134	0.0315	0.0200	-75.330439	0.007305	19
RHF/4-21g	-76.125561					0
RHF/6-31g	-76.251870	0.0536	0.0268	-76.276336	0.024466	64
RHF/6-31g*	-76.284235	0.0249	0.0128	-76.289338	0.005103	13
RHF/6-31g**	-76.303615	0.0259	0.0143	-76.310325	0.006710	18
MP2/6-31G**	-76.502288					
MP3/6-31G**	-76.510066					
CI,S/6-31G**	-76.512087					

6 $H_2O.NO^+$

METHOD	E(4-21G)	Max F	RMS F	E(Opt.)	ΔE/au	ΔE/SI
RHF/STO-3g	-202.207883	0.3491	0.1154	-202.258340	0.050457	132
RHF/(7s,3p)				-204.043971e		
RHF/(7s,3p)				-204.139016c		
RHF/(7s,3p)				-204.167523b		
RHF/4-21g	-204.435811					0
RHF/6-31g	-204.831347	0.0146	0.0077	-204.833838	0.002491	7
RHF/6-31g*	-204.948898	0.0568	0.0206	-204.956617	0.007718	20
RHF/6-31g**	-204.961360	0,0562	0.0209			
MP2/6-31G**	-205.492538					
MP3/6-31G**	-205.482881					
CI,S/6-31G**	-205.492306					

7 H_2O

METHOD	E(4-21G)	Max F	RMS F	E(Opt.)	ΔE/au	ΔE/SI
RHF/STO-3g	-74.962824	0.0332	0.0263	-74.965901	0.003077	8
RHF/(7s,3p)e				-75.651663		
RHF/(7s,3p)b	-75.756411d			-75.763755		
RHF/4-21g	-75.821207					0
RHF/6-31g	-75.984431	0.0160	0.0144	-75.985359	0.000929	2
RHF/6-31g*	-76.009710	0.0227	0.0191	-76.010746	0.001036	3
RHF/6-31g**	-76.022199	0.0277	0.0229	-76.023616	0.001417	4
MP2/6-31G**	-76.219332					
MP3/6-31G**	-76.225610					
CI,S/6-31G**	-76.227451					

8 $H_3NNO.OH_2^+$

METHOD	E(4-21G)	Max F	RMS F	E(Opt.)	ΔE/au	ΔE/SI
RHF/STO-3g	-257.712950	0.2875	0.0603	-257.758475	0.075525	198
RHF/4-21g	-260.534194					0
RHF/6-31g	-261.037945	0.0149	0.0059	-261.040392	0.002446	6
RHF/6-31g*	-261.169118	0.0555	0.0141			
RHF/6-31g**	-261.191887					

9 $H_2N(NO)H.OH_2^+$

METHOD	E(4-21G)	Max F	RMS F	E(Opt.)	ΔE/au	ΔE/SI
RHF/STO-3g	-257.788767	0.1294	0.0294	-257.810676	0.021909	60
RHF/4-21g	-260.554387					0
RHF/6-31g	-261.047753	0.0151	0.0064	-261.049502g	0.001756	5
RHF/6-31g*	-261.164040f	0.0748	0.0174			
RHF/6-31g**	-261.188192f					

10 H_2NNOH^+

METHOD	E(4-21G)	Max F	RMS F	E(Opt.)	ΔE/au	ΔE/SI
RHF/STO-3g	-182.769661	0.1141	0.0376	-182.779435	0.009778	26
RHF/4-21g	-184.691956					0
RHF/6-31g	-185.042102	0.0325	0.0123	-185.045027	0.002925	8
RHF/6-31g*	-185.137808	0.0721	0.0243	-185.145165	0.007357	19
RHF/6-31g**	-185.152219	0.0728	0.0248			
MP2/6-31G**	-185.667439					
MP3/6-31G**	-185.676492					
CI,S/6-31G**	-185.681968					

11 c-CH_3HNNO

METHOD	E(4-21G)	Max F	RMS F	E(Opt.)	ΔE/au	ΔE/SI
RHF/4-21g	-223.316857					
RHF/6-31g*	-223.852927	0.0778	0.0214			

12 CH_3^+

METHOD	E(4-21G)	Max F	RMS F	E(Opt.)	ΔE/au	ΔE/SI
RHF/STO-3g	-38.774854	0.0394	0.0279	-38.779477	0.004623	12
RHF/4-21g	-39.145047					0
RHF/6-31g	-39.216211	0.0001	0.0000	-39.216211	0.000000	0
RHF/6-31g*	-39.230638	0.0007	0.0005	-39.230640	0.000002	0
RHF/6-31g**	-39.236284	0.0019	0.0013	-39.236297	0.000001	0
MP2/6-31G**	-39.346501					
MP3/6-31G**	-39.364469					
CI,S/6-31G**	-39.368243					

13 CH_3NH_2

METHOD	E(4-21G)	Max F	RMS F	E(Opt.)	ΔE/au	ΔE/SI
RHF/STO-3g	-94.028308	0.0229	0.0099	-94.032862	0.004554	12
RHF/4-21g	-94.995400					0
RHF/6-31g	-95.170176	0.0092	0.0035	-95.170903	0.000726	2
RHF/6-31g*	-95.208450	0.0178	0.0058			
RHF/6-31g**	-95.220610					
MP2/6-31G**	-95.548559					
MP3/6-31G**	-95.572522					
CI,S/6-31G**	-95.576575					

14 $CH_3H_2NNO^+$

METHOD	E(4-21G)	Max F	RMS F	E(Opt.)	ΔE/au	ΔE/SI
RHF/STO-3g	-221.359750	0.1567	0.0358	-221.373921	0.014170	37
RHF/4-21g	-223.644888					0
RHF/6-31g	-224.047629	0.0076	0.0040	-224.048142	0.000513	1
RHF/6-31g*	-224.170492	0.0697	0.0160			

15 $CH_3.OH_2^+$

METHOD	E(4-21G)	Max F	RMS F	E(Opt.)	ΔE/au	ΔE/SI
RHF/STO-3g	-113.922165	0.0403	0.0147	-113.929594	0.007429	20
RHF/4-21g	-115.093331					0
RHF/6-31g	-115.305102	0.0153	0.0056	-115.305560	0.000459	1
RHF/6-31g*	-115.335777	0.0143	0.0065			
RHF/6-31g**	-115.354432	0.0267	0.0085			
MP2/6-31G**	-115.685054					
MP3/6-31G**	-115.705072					
CI,S/6-31G**	-115.709176					

16 c-HONO

METHOD	E(4-21G)	Max F	RMS F	E(Opt.)	ΔE/au	ΔE/SI
RHF/4-21g	-204.122692					
RHF/6-31g				-204.520615h		
RHF/6-31g*				-204.639938h		

17 t-HONO

METHOD	E(4-21G)	Max F	RMS F	E(Opt.)	ΔE/au	ΔE/SI
RHF/4-21g	-204.120206					
RHF/6-31g				-204.521940h		
RHF/6-31g*				-204.637676h		

18 t,t-HNNOH

METHOD	E(4-21G)	Max F	RMS F	E(Opt.)	ΔE/au	ΔE/SI
RHF/4-21g	-184.362004					0
RHF/6-31g*	-184.816211	0.052	0.025	-184.822464	0.006253	16

19 N_2

METHOD	E(4-21G)	Max F	RMS F	E(Opt.)	ΔE/au	ΔE/SI
RHF/4-21g	-108.666311					0
RHF/6-31g*	-108.943841	0.021	0.021	-108.943949	0.000109	0

20 HN_2^+

METHOD	E(4-21G)	Max F	RMS F	E(Opt.)	ΔE/au	ΔE/SI
RHF/4-21g	-108.866271					0
RHF/6-31g*	-109.131805	0.023	0.009	-109.131930	0.000125	0
RHF/6-31g**	-109.136106	0.021	0.009	-109.136216	0.000109	0

21 $CH_3.N_2^+$

METHOD	E(4-21G)	Max F	RMS F	E(Opt.)	ΔE/au	ΔE/SI
RHF/4-21g	-147.866512					0
RHF/6-31g*	-148.215567	0.024	0.007	-148.216055	0.000487	1

22 H_2NNO <> t,c-HNNOH ie H<NNOH>

METHOD	E(4-21G)	Max F	RMS F	E(Opt.)	ΔE/au	ΔE/SI
RHF/4-21g	-184.294691					0
MP2/4-21G	-184.670950	0.0871	0.0342	-184.678449	0.007499	20
RHF/6-31g*	-184.737097	0.0766	0.0353	-184.747581	0.010484	28
MP2/6-31G*	-185.282917	0.0486	0.0210	-185.288926	0.006009	16

23 H_2NNO <> HNHNO ie H<NNH>O(2) (2nd order saddle point)

METHOD	E(4-21G)	Max F	RMS F	E(Opt.)	ΔE/au	ΔE/SI
RHF/4-21g	-184.212790					
MP2/4-21G	-184.612134					
RHF/6-31g*	-184.672158					
MP2/6-31G*	-185.227321					

24 H_2NNO <> HNNHO ie H<NNH>O(1) (1st order saddle point)

METHOD	E(4-21G)	Max F	RMS F	E(Opt.)	ΔE/au	ΔE/SI
RHF/4-21g	-184.217001					
MP2/4-21G	-184.614636					
RHF/6-31g*	-184.681565					
MP2/6-31g*	-185.232043					

Table A.2 ENERGIES OF REACTION

(The energies of reaction are given in both atomic and S.I. units for both the optimised and RHF/4-21G geometries. In some cases the comparable energy change is given for either the parent system or the H^+ system, where H^+ replaces CH_3^+).

1 $H_2NH + NO^+ \rightarrow H_3NNO^+$

METHOD	ΔE/au	ΔE/SI	ΔE(parent)	ΔE(opt,au)	ΔE(opt,SI)
RHF/STO-3G	-0.126865	-330		-0.121422	-319
RHF/4-21G	-0.073981	-194	-271	-	-194
RHF/6-31G	-0.059433	-156		-0.059389	-156
RHF/6-31G*	-0.040759	-107		-0.046459	-122
RHF/6-31G**	-0.039769	-104			
MP2/6-31G**	-0.062595	-164			
MP3/6-31G**	-0.059137	-155			
CI,S/6-31G**	-0.057099	-150			

2 $H_3NNO^+ \rightarrow H_2NNO + H^+$

METHOD	ΔE/au	ΔE/SI	ΔE(parent)	ΔE(opt,au)	ΔE(opt,SI)
RHF/STO-3G	0.370137	972		0.393779	1034
RHF/4-21G	0.319021	837	882	-	0
RHF/6-3.1G	0.295127	775		0.294229	772
RHF/6-31G*	0.311951	819		0.314183	825
RHF/6-31G**	0.314280	825			
MP2/6-31G**	0.326654	857			
MP3/6-31G**	0.322910	848			
CI,S/6-31G**	0.325812	855			

3 $NH_3 + NO^+ \rightarrow H_2NNO + H^+$

METHOD	ΔE/au	ΔE/SI	ΔE(parent)	ΔE(opt,au)	ΔE(opt,SI)
RHF/STO-3G	0.243272	639		0.272357	715
RHF/4-21G	0.245040	643	612		643
RHF/6-31G	0.235695	619		0.234840	616
RHF/6-31G*	0.271192	712		0.267724	703
RHF/6-31G**	0.274511	721			
MP2/6-31G**	0.264060	693			
MP3/6-31G**	0.263773	692			
CI,S/6-31G**	0.268713	705			

4 $H_2O + NO^+ \rightarrow H_2O.NO^+$

METHOD	ΔE/au	ΔE/SI	ΔE(parent)	ΔE(opt,au)	ΔE(opt,SI)
RHF/STO-3G	-0.068477	-180		-0.088177	-231
RHF/(7s,3p)e				-0.060629	-159
RHF/(7s,30)c				-0.043581	-114
RHF/(7s,3p)b				-0.096132	-252
RHF/4-21G	-0.055534	-146			-146
RHF/6-31G	-0.045755	-120		-0.047245	-124
RHF/6-31G*	-0.029772	-78		-0.036217	-95
RHF/6-31G**	-0.029745	-78			
MP2/6-31G**	-0.038781	-102			
MP3/6-31G**	-0.035306	-93			
CI,S/6-31G**	-0.034191	-90			

5 $NH_3 + H_2O.NO^+ \rightarrow H_2O.H_3NNO^+$ (H_2O bonded to N)

METHOD	ΔE/au	ΔE/SI	ΔE(parent)	ΔE(opt,au)	ΔE(opt,SI)
RHF/STO-3G	-0.055417	-145		-0.044715	-117
RHF/4-21G	-0.046152	-121	-168		-121
RHF/6-31G	-0.041933	-110		-0.041032	-108
RHF/6-31G*	-0.037530	-99			
RHF/6-31G**	-0.036344	-95			

6 $H_2O + H_3NNO^+ \rightarrow H_3NNO.OH_2^+$ (H_2O bonded to N)

METHOD	ΔE/au	ΔE/SI	ΔE(parent)	ΔE(opt,au)	ΔE(opt,SI)
RHF/STO-3G	0.002971	8		-0.011470	-30
RHF/4-21G	-0.027705	-73	-43		-73
RHF/6-31G	-0.028255	-74		-0.028888	-76
RHF/6-31G*	-0.026543	-70			
RHF/6-31G**	-0.026320	-69			

7 $H_2O + H_3NNO^+ \rightarrow H_2O.H_3NNO^+$ (H_2O bonded to H)

METHOD	ΔE/au	ΔE/SI	ΔE(parent)	ΔE(opt,au)	ΔE(opt,SI)
RHF/STO-3G	-0.072847	-191		-0.063671	-167
RHF/4-21G	-0.478987	-126	-118	-	-126
RHF/6-31G	-0.038063	-100		-0.037999	-100
RHF/6-31G*	-0.021465	-56			
RHF/6-31G**	-0.022625	-59			

8 $H_3NNO.H_2O^+$ --> $H_2O.H_3NNO^+$ (H_2O bonded to H)

METHOD	ΔE/au	ΔE/SI	ΔE(parent)	ΔE(opt,au)	ΔE(opt,SI)
RHF/STO-3G	-0.075817	-199		-0.052201	-137
RHF/4-21G	-0.020194	-53	-76	-	-53
RHF/6-31G	-0.009808	-26		-0.009110	-24
RHF/6-31G*	+0.005078	+13			
RHF/6-31G**	+0.003695	+10			

9 $H_2O.H_3NNO^+$ --> $H_2NNO + H_3O^+$ (H_2O bonded to H)

METHOD	ΔE/au	ΔE/SI	ΔE(parent)	ΔE(opt,au)	ΔE(opt,SI)
RHF/STO-3G	0.082673	217		0.092912	244
RHF/4-21G	0.062566	164	202	-	164
RHF/6-31G	0.065750	173		0.041251	108
RHF/6-31G*	0.058891	154			
RHF/6-31G**	0.055489	146			

10 $H_2NH + H_2O.NO^+$ --> $H_2NNO + H_3O^+$

METHOD	ΔE/au	ΔE/SI	ΔE(parent)	ΔE(opt,au)	ΔE(opt,SI)
RHF/STO-3G	-0.048561	-127		-0.004004	-11
RHF/4-21G	-0.003780	-10	-42	-	-10
RHF/6-31G	+0.014010	+37		-0.008892	-23
RHF/6-31G*	+0.026440	+69		+0.025349	+67
RHF/6-31G**	+0.022840	+60			
MP2/6-31G**	+0.019884	+52			
MP3/6-31G**	+0.014623	+38			
CI,S/6-31G**	+0.018268	+50			

11 $H_2O + H^+$ --> H_3O^+

METHOD	ΔE/au	ΔE/SI	ΔE(opt,au)	ΔE(opt,SI)
RHF/STO-3G	-0.360310	-946	-0.364538	-959
RHF/4-21G	-0.304354	-799	-	-799
RHF/6-31G	-0.267440	-702	-0.290977	-764
RHF/6-31G*	-0.274525	-721	-0.278592	-731
RHF/6-31G**	-0.281416	-739	-0.286709	-753
MP2/6-31G**	-0.282957	-743		
MP3/6-31G**	-0.284455	-747		
CI,S/6-31G**	-0.284637	-747		

12 $H_2NNO + H^+ \rightarrow H_2NNOH^+$

METHOD	ΔE/au	ΔE/SI	ΔE(parent)	ΔE(opt,au)	ΔE(opt,SI)
RHF/STO-3G	-0.386702	-1015		-0.392110	-1029
RHF/4-21G	-0.325695	-855	-942		-855
RHF/6-31G	-0.311969	-819		-0.313111	-822
RHF/6-31G*	-0.316894	-832		-0.313880	-837
RHF/6-31G**	-0.323131	-848			
MP2/6-31G**	-0.315817	-829			
MP3/6-31G**	-0.324314	-851			
CI,S/6-31G**	-0.323841	-850			

13 $H_3NNO^+ \rightarrow H_2NNOH^+$

METHOD	ΔE/au	ΔE/SI	ΔE(parent)	ΔE(opt,au)	ΔE(opt,SI)
RHF/STO-3G	-0.016565	-43		+0.001669	4
RHF/4-21G	-0.006674	-18	-59		-18
RHF/6-31G	-0.016842	-44		-0.018882	-50
RHF/6-31G*	-0.004943	-13		-0.004697	-12
RHF/6-31G**	-0.008851	-23			
MP2/6-31G**	+0.010837	+28			
MP3/6-31G**	-0.001404	-4			
CI,S/6-31G**	+0.001971	+5			

14 $CH_3NH_2 + NO^+ \rightarrow H_2NNO + CH_3^+$

METHOD	ΔE/au	ΔE/SI	ΔE(H^+ loss)	ΔE(opt)	ΔE(opt)	ΔE(H^+)
RHF/STO-3G	0.047076	124	639	0.070322	185	715
RHF/4-21G	0.043163	113	643	-	113	643
RHF/6-31G	0.024995	66	619	0.009582	25	616
RHF/6-31G*	0.060668	159	712	0.062556	164	703
RHF/6-31G**	0.057307	150	721			
MP2/6-31G**	0.084861	223	693			
MP3/6-31G**	0.077839	204	692			
CI,S/6-31G**	0.080870	212	705			

15 $CH_3H_2NNO^+ \rightarrow H_2NNO + CH_3^+$

METHOD	ΔE/au	ΔE/SI	ΔE(H^+ loss)	ΔE(opt)	ΔE(opt)	ΔE(H^+)
RHF/STO-3G	0.201936	530	972	0.207119	554	1034
RHF/4-21G	0.133580	351	837	-	351	837
RHF/6-31G	0.101286	266	775	0.855872	225	772
RHF/6-31G*	0.118940	312	815			825
RHF/6-31G**			825			

16 CH_3NH_2 + $H_2O.NO^+$ --> H_2NNO + $CH_3.OH_2^+$

METHOD	ΔE/au	ΔE/SI	ΔE(H^+ loss)	ΔE(opt)	ΔE(opt)	ΔE(H^+)
RHF/STO-3G	-0.068934	-181	-127	-0.025717	-68	-11
RHF/4-21G	-0.028381	-74	-10	-	-74	-10
RHF/6-31G	-0.033711	-88	+37	-0.032734	-86	-23
RHF/6-31G*	+0.000657	+2	+69			
RHF/6-31G**	-0.001550	-4	+60			
MP2/6-31G**	+0.004420	+12	+52			
MP3/6-31G**	-0.001848	-5	+38			
CI,S/6-31G**	+0.001579	+4	+50			

17 c-HONO --> t-HONO

METHOD	ΔE/au	ΔE/SI	ΔE(opt,au)	ΔE(opt,SI)
RHF/4-21G	0.002486	7		7
RHF/6-31G			-0.001326	-3
RHF/6-31G*			0.002262	6

18 H_2NNO --> t,t-HNNOH

METHOD	ΔE/au	ΔE/SI	ΔE(parent)	ΔE(opt,au)	ΔE(opt,SI)
RHF/4-21G	0.004256	11	-2		11
RHF/6-31G*	0.004703	12		0.003821	10

19 CH_3^+ + H_2O --> $CH_3.OH_2^+$

METHOD	ΔE/au	ΔE/SI	ΔE(parent)	ΔE(opt,au)	ΔE(opt,SI)
RHF/STO-3G	-0.184487	-484		-0.184216	-484
RHF/4-21G	-0.127077	-334			-334
RHF/6-31G	-0.104460	-274		-0.103990	-273
RHF/6-31G*	-0.095429	-251			
RHF/6-31G**	-0.095949	-252			
MP2/6-31G**	-0.119221	-313			
MP3/6-31G**	-0.114993	-302			
CI,S/6-31G**	-0.113482	-298			

20 $ON(OH_2)^+ + NH_3 \rightarrow H_3NNO^+ + H_2O$

METHOD	ΔE/au	ΔE/SI	ΔE(parent)	ΔE(opt,au)	ΔE(opt,SI)
RHF/STO-3G	-0.058388	-153		-0.033245	-87
RHF/4-21G	-0.018447	-48	-125		-48
RHF/6-31G	-0.013678	-36		-0.012144	-32
RHF/6-31G*	-0.010987	-29		-0.010241	-27
RHF/6-31G**	-0.010023	-26			
MP2/6-31G**	-0.023814	-63			
MP3/6-31G**	-0.023831	-63			
CI,S/6-31G**	-0.022908	-60			

21 $ON(OH_2)^+ + CH_3NH_2 \rightarrow CH_3NH_2NO^+ + H_2O$

METHOD	ΔE/au	ΔE/SI	ΔE(parent)	ΔE(opt,au)	ΔE(opt,SI)
RHF/STO-3G	-0.086383	-227		-0.048620	-128
RHF/4-21G	-0.034884	-92	-125		-92
RHF/6-31G	-0.030537	-80		-0.028760	-75
RHF/6-31G*	-0.022854	-60			

22 $H_2NNO \rightarrow H<NNOH>$

METHOD	ΔE/au	ΔE/SI	ΔE(parent)	ΔE(opt,au)	ΔE(opt,SI)
RHF/4-21G	0.071570	188			188
MP2/4-21G	0.053222	140		0.053605	141
RHF/6-31G*	0.083817	220		0.078704	207
MP2/6-31G*				0.053766	141

23 $H_2NNO \rightarrow H<NNH>O(2)$

METHOD	ΔE/au	ΔE/SI	ΔE(parent)	ΔE(opt,au)	ΔE(opt,SI)
RHF/4-21G	0.153471	403			403
MP2/4-21G	0.112038	294			
RHF/6-31G*	0.148756	390			
MP2/6-31G*a	0.109994	289			

24 H_2NNO --> H<NNH>O(1)

METHOD	Δ E/au	ΔE/SI	ΔE(parent)	ΔE(opt,au)	ΔE(opt,SI)
RHF/4-21G	0.149260	392			
MP2/4-21G	0.109536	288			
RHF/6-31G*	0.239349	366			
MP2/6-31G*a	0.110649	290			

Table A.3 BASIS SET STUDIES - GEOMETRIES

(In some cases, the geometry is compared to that for the corresponding fragment of the parent).

1 H_2NNO

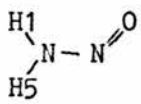

Model for: $(CH_3)_2NNO$ parent:

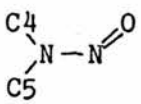

Parameter	RHF/ STO-3G	RHF/ 4-21G	RHF/ 6-31G	RHF/ 6-31G*	MP2/ 4-21G	MP2/ 6-31G*	RHF/ parent
RNH1	1.020	1.000	0.996	0.999	1.017	1.018	
RNN	1.402	1.350	1.312	1.307	1.406	1.336	1.333
RNO	1.235	1.229	1.214	1.186	1.301	1.237	1.241
RNH5	1.016	0.993	0.988	0.992	1.009	1.009	
ANNH1	120.9	119.0	120.0	119.4	119.2	119.2	119.3
AONN	111.6	113.6	115.4	114.6	111.2	113.1	114.3
ANNH5	117.9	117.1	117.4	117.4	116.9	117.3	117.1
DONNH1	0.0	0.0	0.0	0.0	0.0	0.0	0.0
DONNH5	180.0	180.0	180.0	180.0	180.0	180.0	180.0

2 H_3NNO^+

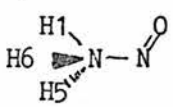

Model for: $(CH_3)_2NHNO^+$ parent:

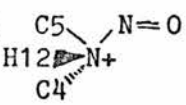

Parameter	RHF/STO-3G	RHF/4-21G	RHF/6-31G	RHF/6-31G*	parent
RNH1	1.046	1.017	1.007	1.008	
RNN	1.623	1.859	1.979	2.214	1.646
RNO	1.199	1.103	1.090	1.054	1.150
RNH5	1.045	1.016	1.006	1.007	1.017
RNH6	1.045	1.016	1.006	1.007	
ANNH1	113.8	112.3	113.5	116.4	112.6
AONN	108.1	110.1	110.5	109.9	110.7
ANNH5	108.2	106.4	105.5	109.6	102.8
ANNH6	108.2	106.4	105.5	109.6	105.0
AH1NH5	109.4	110.8	110.9	107.1	114.8
DONNH1	0.0	0.0	0.0	0.0	4.2
DONNH5	121.8	121.5	121.7	121.6	124.0
DONNH6	-121.8	-121.5	-121.7	-121.6	-121.4

3 NO^+

Parameter	RHF/ STO-3G	RHF/ (7s,3p)c	RHF/ (7s,3p)b	RHF/ 4-21G	RHF/ 6-31G	RHF/ 6-31G*
RNO	1.133	1.120	1.217	1.048	1.053	1.041

4 NH_3

Model for: $(CH_3)_2NH$ parent: 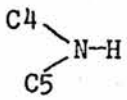

Parameter	STO-3G	4-21G	4-31G	6-31G	6-31G*	6-31G**	parent
RNH	1.033	1.003	0.991	0.991	1.003	1.001	1.004
AHNH	104.2	112.1	115.9	116.2	107.2	107.6	

5 H_3O^+

Parameter	RHF/STO-3G	RHF/4-21G	RHF/6-31G	RHF/6-31G*	RHF/6-31G**
ROH	0.990	0.979	0.963	0.969	0.961
AHOH	113.8	120.0	120.0	113.1	114.7

6 $H_2O.NO^+$

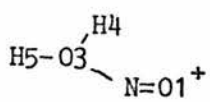

Parameter	RHF/ STO-3G	RHF/ (7s,3p)e	RHF/ (7s,3p)c	RHF/ (7s,3p)b	RHF/ 4-21G	RHF/ 6-31G	RHF/ 6-31G*
RNO1	1.185	1.154	1.126	1.272	1.063	1.060	1.044
RNO3	1.571	1.735	2.057	1.663	1.982	2.152	2.287
RO3H4	0.992	0.987	1.019	1.042	0.973	0.955	0.953
RO3H5	0.988	0.985	1.017	1.040	0.971	0.954	0.952
AONO	106.9	109.0	106.3	106.9	108.0	105.8	105.4
ANOH4	125.8	126.9	133.3	123.7	131.3	132.2	134.0
ANOH5	118.4	116.8	117.2	116.3	117.9	116.4	120.1
AHOH	115.9	116.3	109.5	119.9	110.8	111.4	105.9
DONOH4	0.0	0.0	0.0	0.0	0.0	0.0	0.0
DONOH5	180.0	180.0	180.0	180.0	180.0	180.0	180.0

7 H_2O

Parameter	RHF/ STO-3G	RHF/ (7s,3p)e	RHF/ (7s,3p)b	RHF/ 4-21G	RHF/ 6-31G	RHF/ 6-31G*	RHF/ 6-31G**
ROH	0.989	0.977	1.012	0.968	0.950	0.948	0.943
AHOH	100.0	107.9	107.2	107.4	111.5	105.5	106.0

8 $H_3NNO.OH_2^+$

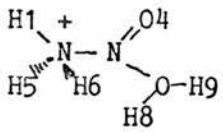

Model for: $(CH_3)_2NHNO.H_2O^+$ parent:

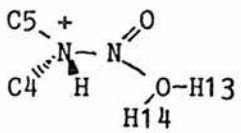

Parameter	RHF/STO-3G	RHF/4-21G	RHF/6-31G	parent
RNH1	1.044	1.013	1.004	
RNH5	1.043	1.012	1.003	1.015
RNH6	1.043	1.013	1.004	
RNN	1.650	2.061	2.215	1.731
RNO	1.195	1.078	1.071	1.130
RNO7	2.563	2.324	2.388	2.592
ROH8	0.987	0.968	0.952	0.968
ROH9	0.987	0.969	0.953	0.968
ANNH1	114.1	114.1	114.6	112.1
ANNH5	108.2	105.3	103.6	102.7
ANNH6	108.1	108.3	107.4	104.8
AO4NN	107.3	107.5	107.3	109.3
ANNO7	172.7	159.3	158.9	166.1
ANOH8	123.6	120.6	117.7	125.3
ANOH9	136.0	131.4	131.6	127.2
AH1NH5	109.2	109.9	110.5	115.0
DONNH1	0.2	22.2	22.1	1.0
DONNH5	122.0	142.8	142.6	120.6
DONNH6	-121.5	-100.3	-100.9	-124.5
DNNOH8	1.4	-0.4	-0.5	-10.4
DNNOH9	180.3	179.8	179.7	168.7
DO7N3NO	-181.4	-179.9	-179.4	-168.6

9 $H_2O.H_3NNO^+$

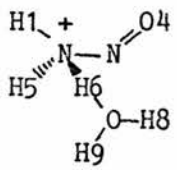

Model for: $(CH_3)_2N(NO)H.H_2O^+$ parent:

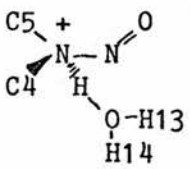

Parameter	RHF/STO-3G	RHF/4-21G	RHF/6-31Gg	parent
RNH1	1.041	1.018	1.011	
RNH5	1.039	1.016	1.009	
RNH6	1.205	1.081	1.054	1.060
RNN	1.541	1.650	1.598	1.582
RNO	1.213	1.149	1.147	1.167
ROH6	1.211	1.516	1.598	1.574
ROH8	0.980	0.968	0.953	0.967
ROH9	0.980	0.967	0.953	0.967
ANNH1	110.4	109.6	111.4	112.9
ANNH5	106.4	106.3	106.6	105.0
ANNH6	109.7	106.8	106.3	103.5
AONN	108.9	109.9	111.1	114.5
AOHN	179.6	179.1	178.4	179.7
AHOH8	118.5	124.8	124.3	125.3
AHOH9	119.1	124.9	124.2	125.0
AHNH	108.1	111.2	111.1	114.6
DONNH1	12.4	14.7	14.5	-5.6
DONNH5	129.5	135.0	135.9	-131.1
DONNH6	-111.2	-106.9	-107.1	114.2
DNHOH8	-16.1	-1.8	-0.9	128.8
DNHOH9	-149.1	182.2	181.4	-83.9
DOHNH1	-147.6	-175.3	-176.9	59.1

10 H_2NNOH^+

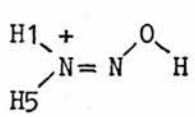

Model for: $(CH_3)_2NNOH^+$ parent:

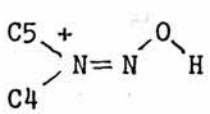

Parameter	RHF/STO-3G	RHF/4-21G	RHF/6-31G	RHF/6-31G*	parent
RNH1	1.045	1.016	1.009	1.012	
RNN	1.296	1.235	1.228	1.222	1.227
RNO	1.349	1.357	1.299	1.271	1.383
RNH5	1.041	1.011	1.003	1.006	
ROH	1.003	0.981	0.963	0.961	0.976
AHON	104.0	108.6	112.2	108.3	106.9
ANNH1	121.9	121.2	121.8	121.7	123.2
AONN	109.4	110.0	112.7	112.4	110.9
ANNH5	116.9	117.3	117.4	116.8	116.7
DONNH1	0.0	0.0	0.0	0.0	0.0
DONNH5	180.0	180.0	180.0	180.0	180.0
DHONN	180.0	180.0	180.0	180.0	180.0

11 $CH_3NH_2NO^+$

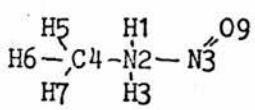

Model for: $(CH_3)_3NNO^+$

Parameter	RHF/STO-3G	RHF/4-21G	RHF/6-31G
RNN		1.721	1.717
RNO		1.132	1.128
RCN		1.515	1.494
RNH1		1.017	1.010
RNH3		1.017	1.010
RCH5		1.078	1.078
RCH6		1.078	1.078
RCH7		1.080	1.080
ANNC		113.1	114.8
AONN		109.6	110.5
AHNH		108.6	108.3
ACNH1		113.0	113.2
ANCH5		108.6	109.2
ANCH6		108.6	109.3
ANCH7		108.4	108.9
DNNCH5		-59.5	-59.7
DONN		0.5	0.4
DCNHH3		126.2	126.3
DH5CNH1		58.6	58.7
DH5CNH6		120.3	120.5
DH5CNH7		-119.9	-119.8

12 CH_3^+

Parameter	RHF/STO-3G	RHF/4-21G	RHF/6-31G	RHF/6-31G*	RHF/6-31G**
RCH	1.120	1.078	1.077	1.079	1.080
AHCH1	120.0	120.0	120.0	120.0	120.0

13 CH_3NH_2

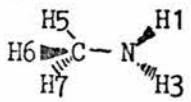

Model for: $(CH_3)_3N$

Parameter	RHF/STO-3G	RHF/4-21G	RHF/6-31G	RHF/6-31G*	parent
RCN	1.486	1.473	1.451	1.453	1.465
RNH1	1.033	1.004	0.994	1.002	
RNH3	1.033	1.004	0.994	1.002	
RCH5	1.089	1.082	1.082	1.084	1.083
RCH6	1.089	1.083	1.082	1.084	1.083
RCH7	1.093	1.090	1.090	1.091	1.093
AHNH	104.4	111.0	113.3	106.8	113.1
ACNH1	107.4	113.5	116.6	110.7	
ANCH5	109.1	108.9	109.5	109.2	109.4
ANCH6	109.2	108.9	109.4	109.2	109.4
ANCH7	113.7	114.8	114.6	114.8	112.9
DCNHH3	113.7	129.2	139.4	120.5	
DH5CNH1	65.0	57.7	52.4	62.2	65.5
DH5CNH6	118.2	117.1	117.3	117.2	
DH5CNH7	-120.8	-121.5	-121.4	-121.4	

14 $CH_3.OH_2^+$

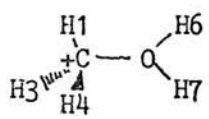

Parameter	RHF/STO-3G	RHF/4-21G	RHF/6-31G
RCH1	1.095	1.075	1.074
RCH3	1.095	1.074	1.073
RCH4	1.097	1.074	1.073
RCO5	1.484	1.543	1.542
ROH6	0.990	0.973	0.958
ROH7	0.990	0.973	0.958
AH1CH3	111.4	113.0	113.1
AH1CH4	112.2	113.0	113.1
AH1CO5	106.0	104.4	104.3
ACOH6	115.6	122.1	122.0
ACOH7	115.6	121.4	121.5
DH4CH1H3	-126.7	-131.6	-132.1
DO5CH1H3	114.8	114.2	113.9
DH1COH6	54.4	1.0	0.7
DH1COH7	186.2	179.7	180.2

15 HONO

	c-HONO			t-HONO		
Parameter	RHF/4-21G	RHF/6-31G	RHF/6-31G*	RHF/4-21G	RHF/6-31G	RHF/6-31G*
RHO1	0.979	0.964	0.960	0.970	0.953	0.951
RO1N	1.423	1.368	1.328	1.446	1.387	1.347
RNO2	1.191	1.182	1.161	1.180	1.171	1.153
AHON	107.3	112.2	107.6	104.7	108.4	105.4
AONO	112.2	114.0	113.7	110.1	111.6	111.3
DHONO	0.0	0.0	0.0	180.0	180.0	180.0

16 t,t-HNNOH

Parameter	RHF/4-21G	RHF/6-31G*	parent
RHN	1.018	1.008	
RNN	1.218	1.203	1.215
RNO	1.441	1.351	1.450
ROH	0.969	0.949	0.969
AHNN	108.3	105.9	113.2
ANNO	108.8	110.4	108.8
ANOH	103.5	104.6	103.1
DHNNO	180.0	180.0	180.0
DNNOH	0.0	180.0	180.0

17 HN_2^+

Parameter	RHF/4-21G	RHF/6-31G*	RHF/6-31G**	parent
RHN	1.026	1.026	1.025	
RNN	1.077	1.071	1.071	1.079
AHNN	180.0	180.0	180.0	180.0

18 N_2

Parameter	RHF/4-21G	RHF/6-31G*
RNN	1.084	1.087

19 $CH_3N_2^+$

Parameter	RHF/4-21G	RHF/6-31G*
RNN	1.079	1.073
RNC	1.547	1.510
RCH	1.078	1.078
ANNC	180.0	180.0
ANCH	104.7	105.1
DHNCH	120.0	120.0

20 H_2NNO <> t,c-HNNOH ie H<NNOH>

Parameter	RHF/4-21G	MP2/4-21G	RHF/6-31G*	MP2/6-31G*
RNH1	1.285	1.325	1.285	1.310
RNN	1.261	1.348	1.240	1.286
RNO	1.364	1.363	1.260	1.290
RNH5	1.004	1.027	1.002	1.023
ROH1	1.358	1.404	1.327	1.380
ANNH1	83.8	82.0	80.8	81.3
ANNO	99.9	100.2	103.4	103.1
ANNH5	120.7	118.7	118.6	117.5
DONNH1	0.0	0.0	0.0	0.0
DONNH5	180.0	180.0	180.0	180.0

Notes:

a) H_2NNO at RHF/6-31G* optimised geometry

b) scale factor = 1.00 om all N, O

c) scale factor = 1.08 on NO^+

d) experimental geometry [91]

e) scale factor 1.08 on all N, O

f) geometry differs slightly to the RHF/4-21G geometry

g) convergence criteria multiplied by four

h) calculations by C. Thomson

TABLE A.4 THERMODYNAMIC PROPERTIES AT 298.15K, ATMOSPHERIC PRESSURE

Reactant	E/au	EMP2/au	U_{298}/au	H_0/au	S/Jmol^{-1}
H^+	0.000000	0.000000	0.001416	0.000000	108.840
CH_3^+	-39.145047	-39.213125	-39.109034	-39.111881	186.198
NH_3	-56.052231	-56.164353	-56.013339	-56.016233	201.469
OH^-	-75.104378	-75.215869	-75.095442	-75.097803	173.344
H_2O	-75.821207	-75.943959	-75.796691	-75.799525	188.680
H_3O^+	-76.125561	-76.253035	-76.087600	-76.090626	203.814
CH_3NH_2	-94.995400	-95.197634	-94.924042	-94.927445	239.994
N_2	-108.666311	-108.898181	-108.658019	-108.660379	191.239
HN_2^+	-108.866271	-109.104950	-108.846028	-108.848499	200.673
$CH_3.OH_2^+$	-115.093419	-115.304225	-115.022785	-115.026773	253.262
NO^+	-128.559070	-128.825909	-128.550778	-128.553138	197.835
$CH_3N_2^+$	-147.866512	-148.190753	-147.814467	-147.818147	253.177
H<NHN>O(2)	-184.212790	-184.612134	-184.183356	-184.186447	246.733
H<NHN>O(1)	-184.217001	-184.614636	-184.186176	-184.189402	248.744
HN<NHO>	-184.238293	-184.618378	-184.206610	-184.209947	250.512
H<NNOH>	-184.294691	-184.670950	-184.261632	-184.264637	245.772
HNNOH(B)	-184.306717	-184.662237	-184.271957	-184.275376	251.764
H_2NNO(R)	-184.320498	-184.678069	-184.286227	-184.289703	253.767
t,t-HNNOH	-184.362004	-184.713492	-184.324099	-184.327443	50.295
H_2NNO	-184.366262	-184.724172	-184.328552	-184.331960	250.843
H_2<NHN>O	-184.533368	-184.921292	-184.488803	-184.492438	257.128
H<NHN>OH^+(2)	-184.540041	-184.923719	-184.497662	-184.501014	251.865
H<NHN>OH^+(1)	-184.541578	-184.913189	-184.498531	-184.502123	255.240
H_2<NNOH>$^+$	-184.578699	-184.960506	-184.532814	-184.536049	250.984
H_2NNOH^+(R)	-184.599134	-184.948760	-184.550842	-184.554032	249.955
H<NNOH>H^+	-184.615746	-184.986888	-184.570429	-184.573962	255.529

H_2NNOH^+(I)	-184.660506	-185.011558	-184.610512	-184.613658	249.259
H_3NNO^+	-184.685285	-185.071845	-184.634077	-184.638392	273.121
t-H_2NNOH^+	-184.691956	-185.045676	-184.639695	-184.642970	250.144
HNN.OH_2^+(L)	-184.707132	-185.068947	-184.661207	-184.665453	261.319
HNN.OH_2^+	-184.718071	-185.080380	-184.670931	-184.675551	277.297
$H_3O.N_2^+$	-184.814942	-185.179548	-184.765895	-184.771070	282.475
t-HONO	-204.120208	-204.499159	-204.096328	-204.099568	248.612
c-HONO	-204.122693	-204.502994	-204.098810	-204.101948	247.472
ON.OH_2^+(T)	-204.434136	-204.826001	-204.399009	-204.402947	263.116
$H_2O.NO^+$	-204.435812	-204.827945	-204.399671	-204.404176	272.398
t,t-CH_3NNOH	-223.315778	-223.759091	-223.246738	-223.251440	283.198
$CH_3NN.OH_2^+$	-223.717430	-224.167033	-223.637649	-223.643673	313.077
H<NN.H_3O>O	-260.136973	-260.649777	-260.075781	-260.080011	280.640
H<NNO.H_3O>	-260.184966	-260.680419	-260.124178	-260.128276	278.313

Notes:

H_2NNO(R)	saddle point for rotation about N-N
HNNOH(B)	saddle point for inversion at amino N
H_2NNOH^+(R)	saddle point for rotation about N-N
HNN.OH_2^+(L)	linear isomer
ON.OH_2^+(T)	saddle point for rotation of H_2O about N O
(1)	first order saddle point
(2)	second order saddle point
H_2NNOH^+(I)	saddle point for c-H_2NNOH^+ <> t-H_2NNOH^+
A <> B	signifies the saddle point between A and B
<NNOH>	signifies a ring transition structure containing N-N-O-H
<NN.H_3O>	signifies a ring transition structure containing N-N-H-O-H
<NNO.H_3O>	signifies a ring transition structure containing N-N-O-H-O-H

TABLE A.5 REACTIONS STUDIED USING RESULTS FROM FREQUENCY CALCULATIONS

(A1)	c-HONO	->	t-HONO				
(A2)	c-HONO	+ H^+		->	$H_2O.NO^+$		
(A3)	NO^+	+ H_2O		->	$H_2O.NO^+$		
(A4)	$H_2O.NO^+$	->	$ON.OH_2^+$(T)				
(A5)	NO^+	+ NH_3		->	H_3NNO^+		
(A6)	H_3NNO^+	->	H_2<NNOH>$^+$				
(A7)	H_3NNO^+	->	H_2<NHN>O				
(A8)	NO^+	+ NH_3		->	H_2<NNOH>$^+$		
(A9)	H_3NNO^+	->	t-H_2NNOH^+				
(A10)	t-H_2NNOH^+	->	H_2NNOH^+(I)				
(A11)	t-H_2NNOH^+	->	H_2NNO(M)	+ H^+			
(A12)	NO^+	+ NH_3		->	H_2NNO(M)	+ H^+	
(A13)	$H_2O.NO^+$	+ NH_3		->	H_2NNO(M)	+ $H_3\overset{+}{O}$	
(A14)	CH_3NH_2	+ NO^+		->	CH_3^+	+ H_2NNO(M)	
(A15)	CH_3NH_2	+ $H_2O.NO^+$		->	H_2NNO(M)	+ $CH_3.OH_2^+$	
(A16)	CH_3^+	+ H_2O		->	$CH_3.OH_2^+$		
(A17)	H_2NNO	->	t,t-HNNOH				
(A18)	H_2NNO	->	H_2NNO(R)				
(A19)	H_2NNO(M)	->	H<NNOH>				
(A20)	t,t-HNNOH	->	HNNOH(B)				
(A21)	t,t-HNNOH	->	HN_2^+	+ OH^-			
(A22)	t,t-CH_3NNOH	->	$CH_3N_2^+$	+ OH^-			
(A23)	HN_2^+	->	N_2	+ H^+			
(A24)	$CH_3N_2^+$	->	CH_3^+	+ N_2			
(A25)	t,t-HNNOH	->	N_2	+ OH^-		+ H^+	
(A26)	t,t-CH_3NNOH	->	CH_3^+	+ N_2		+ OH^-	
(A27)	t,t-CH_3NNOH	+ H^+		->	$CH_3NN.OH_2^+$		
(A28)	t,t-HNNOH	+ H^+		->	$HNN.OH_2^+$		

(A29) H_2NNO -> $H\langle NHN\rangle O(1)$

(A30) H_2NNO -> $H\langle NHN\rangle O(2)$

(A31) t,t-HNNOH -> $HN\langle NHO\rangle$

(A32) $H_2NNO + H_2O$ -> $H\langle NNO.H_3O\rangle$

(A33) $H_2NNO(M) + H_2O$ -> $H\langle NN.H_3O\rangle O$

(A34) $t\text{-}H_2NNOH^+$ -> $H_2NNOH^+(R)$

(A35) $t\text{-}H_2NNOH^+$ -> $H\langle NNOH\rangle H^+$

(A36) $t\text{-}H_2NNOH^+$ -> $HNN.OH_2^+$

(A37) $HNN.OH_2^+$ -> $HNN.OH_2^+(L)$

(A38) $t\text{-}H_2NNOH^+$ -> $H_3O.N_2^+$

(A39) $t\text{-}H_2NNOH^+$ -> $H\langle NHN\rangle OH^+(1)$

(A40) $t\text{-}H_2NNOH^+$ -> $H\langle NHN\rangle OH^+(2)$

TABLE A.6 THERMODYNAMIC PARAMETERS FOR VARIOUS REACTIONS

Reaction	ΔE	ΔEMP2	ΔH^{θ}_{298}	ΔH^{θ}_{0}	ΔS^{θ}_{298}	ΔG^{θ}_{298}
(A1)	7	10	7	6	1	6
(A2)	-822	-853	-790	-793	25	-797
(A3)	-146	-152	-140	-135	-114	-106
(A4)	4	5	2	3	-9	5
(A5)	-194	-214	-186	-181	-126	-149
(A6)	280	292	266	269	-22	272
(A7)	399	395	381	383	-16	386
(A8)	86	78	79	87	-148	124
(A9)	-18	69	-15	-12	-23	-8
(A10)	83	90	77	77	-1	77
(A11)	855	844	817	816	1	817
(A12)	643	698	616	623	-148	660
(A13)	-10	40	-8	-6	-19	-3
(A14)	113	226	98	96	-1	98
(A15)	-75	-7	-73	-71	-8	-70
(A16)	-334	-386	-310	-303	-122	-274
(A17)	11	28	12	12	-1	12
(A18)	120	121	111	111	3	110
(A19)	188	140	176	177	-5	177
(A20)	145	135	137	137	1	136
(A21)	1027	1031	1007	1000	124	970
(A22)	905	925	887	881	143	844
(A23)	525	543	494	494	-9	496
(A24)	145	209	127	120	124	90
(A25)	1552	1574	1501	1494	114	1467
(A26)	1050	1134	1014	1001	268	934
(A27)	-1054	-1071	-1033	-1030	-79	-1009
(A28)	-935	-963	-910	-914	27	-918
(A29)	392	952	374	374	-2	374
(A30)	403	294	381	452	-4	382
(A31)	325	250	308	308	0	308
(A32)	7	-32	0	8	-161	48
(A33)	133	48	127	135	-159	174
(A34)	244	254	233	233	0	233
(A35)	200	154	182	181	5	180
(A36)	-69	-91	-82	-86	27	-90
(A37)	29	30	26	27	-16	30
(A38)	-323	-351	-331	-336	32	-341
(A39)	395	348	371	370	5	369
(A40)	399	320	373	373	2	372

REFERENCES

[1] P.N. Magee, J.M. Barnes, Br. J. Cancer, 10 (1956) 114 -122

[2] J.D. Scribner, J. Natl. Cancer. Inst., 55 (1975) 1035 - 1038

[3] B.C. Challis, in Safety Evaluation of Nitrosatable Drugs Chemistry, Ed. G.G. Gibson, C. Ioannides, Francis and Taylor (London) 1981 p16-55

[4] D.L.H. Williams, Adv. Phys. Org. Chem., 19 1983 381 - 428

[5] S.S. Mirvish, Toxicol. Appl. Pharmacol., 31 (1975) 325 - 351

[6] S.S. Mirvish, J. Natl. Cancer Inst., 44 (1970) 633 - 639

[7] J.H. Ridd, Adv. Phys. Org. Chem., 16 (1978) 1 - 49

[8] A.F. Croisy, J.C. Fanning, L.K. Keefer, B.W.Slavin, S.-J. Uhm, IARC Sci. Pub. 31, Lyon, 1980 83 - 93

[9] P.P. Roller, L.K. Keefer, IARC Sci. Pub. 9, Lyon, 1975, 86 - 89

[10] J.D. Okun, M.C. Archer, IARC Sci. Pub. 14, Lyon, 1976, 147 - 151

[11] J.J. Kamm, T. Dashman, A.H. Conney, J.J. Burns, IARC Sci. Pub. 9, Lyon, 1975, 200 - 204

[12] H.L. Newmark, W.J. Mergens, in Inhibition of Tumor Induction and Development, Ed. M.S. Zedeck, M. Lipkin, Plenum (1981) p127 - 168

[13] S.S. Singer Sci. Pub. IARC 31, Lyon, 1980, 111 - 117

[14] R. Preussmann, B.W. Stewart, in Chemical carcinogens Volume 2, ACS Monograph 182, Ed. C.E. Searle, American Chemical Society, Washington, 2nd. Ed., 1984, p643 - 828

[15] B.G. Gowenlock, R.J. Hutchinson, J. Little, J. Pfab, J.C.S. Perkin II, (1979) 1110 - 1114

[16] W. Fiddler, J.W. Pensabene, R.C. Doerr, A.E. Wasserman, Nature, 236 (1972) 307

[17] P.A.S. Smith, R.N. Loeppky, J. Am. Chem. Soc., 89 (1967) 1147 - 1157

[18] G.M. Singer, IARC Sci. Pub. 31, Lyon, 1980, 139 - 153

[19] W. Lijinsky, L. Keefer, E. Conrad, R.v.d. Bogart, J. Natl. Cancer Inst., 49 (1972) 1239 - 1249

[20] R.N. Loeppky, J.R. Outram, W. Tomasik, J.M. Faulconer, Tet. Lett., 24 (1983) 4271 - 4274

[21] S.S. Hecht, C.B. Chen, R.M. Ornaf, E. Jacobs, J.D. Adams, D. Hoffmann, J. Org. Chem., 43 (1978) 72 - 76

[22] W. Lijinsky, M. Greenblatt, Nature New Biology, 236 (1972) 177 - 178

[23] W. Lijinsky, G.M. Singer, IARC Sci. Pub. 9, Lyon, 1975, 111-114

[24] R. Preussmann, G. Eisenbrand, in Chemical Carcinogenesis, ACS Monograph 182, Ed. C.E. Searle, American Chemical Society, Washington, 2nd. Ed., 1984, p829 - 868

[25] D.H. Fine, in Banbury Report 12 Nitrosamines and Human Cancer, Ed. P.N. Magee, Cold Spring Harbour Laboratory, 1982 p199 - 209

[26] D. Hoffmann, K.D. Brunnemann, J.D. Adams, A. Rivenson, S.S. Hecht, in Banbury Report 12 Nitrosamines and Human Cancer, Ed. P.N. Magee, Cold Spring Harbour Laboratory, 1982, p211 - 225

[27] D. Hoffmann, J.D. Adams, K.D. Brunnemann, S.S. Hecht, in N-Nitroso Compounds, ACS Symposium Series 174, Ed. R.A. Scanlan, S.R. Tannenbaum, American Chemical Society, Washington, 1981, p247 - 273

[28] W. Lijinsky, in Banbury Report 12 Nitrosamines and Human Cancer, Ed. P.N. Magee, Cold Spring Harbour Laboratory, 1982 p257 - 269

[29] D.H.Fine, in Banbury Report 12 Nitrosamines and Human Cancer, Ed. P.N. Magee, Cold Spring Harbour Laboratory, 1982 p271 - 281

[30] B.C.Challis, S.J. Lomas, H.S. Rzepa, P. Michael, G. Bavin, D.W. Darkin, N.J. Viney, P.J. Moore, in Banbury Report 12 Nitrosamines and Human Cancer, Ed. P.N. Magee, Cold Spring Harbour Laboratory, 1982 p243 - 256.

[31] B.C. Challis, J.A. Challis, in The chemistry of amino, nitroso and nitro compounds and their derivatives Part 2, Ed. S. Patai, Wiley, Chichester, 1982, p1174 -1198

[32] W. Lijinsky, A.M. Losikoff, E.B. Sansone, J. Natl. Cancer Inst., 66 (1981) 125 - 127

[33] P.N. Magee, in Microsomes, Drug Oxidations, and Chemical Carcinogenesis 2, , Ed., M.J. Coon, A.H. Conney, R.W. Estabrook, Academic Press, 1980, p1081 - 1092

[34] W. Lijinsky, in Banbury Report 12 Nitrosamines and Human Cancer, Ed. P.N. Magee, Cold Spring Harbour Laboratory, 1982 p561 - 576

[35] A.H. Dutton, D.F. Heath, Nature (London), 178 (1956) 644

[36] P.N. Magee, M. Vendekar, Biochem. J., 70 (1958) 600 - 605

[37] P. Czygan, H. Greim, A.J. Garro, F.Hutterer, F. Schaffner, H. Popper O. Rosenthal, D.Y. Cooper, Cancer Res., 33 (1973) 2983 - 2986

[38] A.N. Saprin, J. Ramseyer, J. McConn, L.H. Piette, Biochemical and Biophysical Research Communications, 77 (1977) 789 - 796

[39] L.S. Alexander, H.M. Goff, J. Chem. Ed., 59 (1982) 179 - 182

[40] F.P. Guengerich, T.L. Macdonald, Acc. Chem. Res., (1984) 17 9 - 16

[41] A.T. Pudzianowski, G.H. Loew, J. Am. Chem. Soc., 102 (1980) 5443 - 5449

[42] S.R. Koepke, Y. Tondeur, J.G. Farrelly, M.L. Stewart, C.J. Michejda, M.B. Kroeger-Koepke, Biochem. Pharmacol., 33 (1984), 1509 - 1513

[43] C.J. Michejda, M.B. Kroeger-Koepke, S.R.Koepke, P.N.Magee, C. Chu, in Banbury Report 12 Nitrosamines and Human Cancer, Ed. P.N. Magee, Cold Spring Harbour Laboratory, 1982 p69 - 85

[44] R.C. Cottrell, B.G. Lake, J.C. Phillips, S.D. Gangolli, Biochem. Pharmacology, 26 (1977) 809 - 813

[45] C. Ioannides, G.G. Gibson, Safety evaluation of Nitrosatable Drugs Chemistry, Ed. G.G. Gibson, C. Ioannides, Francis and Taylor (London) 1981 p257 - 267

[46] S.D. Gangolli, Safety evaluation of Nitrosatable Drugs Chemistry, Ed. G.G. Gibson, C. Ioannides, Francis and Taylor (London) 1981 p157 - 171

[47] B.G. Lake, I.R. Rowland, R.A. Harris, M.A. Collins, J.C. Phillips, R.C. Cottrell, S.D. Gangolli. Adv. Exp. Med. Biol., 136B (1982) 1143 - 1147

[48] T. Kawanishi, Y. Ohno, A. Takahashi, A. Takanaka, Y. Kasuya, Y. Omori, Biochem. Pharmacol., 34, (1985), 919 - 924

[49] Y.Y. Tu, C.S. Yang, Cancer Res., 43, (1983) 623 - 629

[50] D.M. Kokkinakis, D.R. Koop, D.G. Scarpelli, M.J. Coon, P.F. Hollenberg, Cancer Res., 45 (1985) 619 - 624

[51] C.S. Yang, Y.Y. Tu, D.R. Koop, M. J. Coon, Cancer Res., 45 (1985) 1140 - 1145

[52] C.E. Phillipson, C. Ioannides, Biochem. Pharmacol., 34 (1985) 441 - 442

[53] L.K. Keefer, W. Lijinsky, H. Garcia, J. Natl. Cancer Inst., 51 (1973) 299 - 302

[54] W. Lijinsky, H.W. Taylor, L.K. Keefer, J. Natl. Cancer Inst., 57 (1976) 1311 - 1313

[55] H. Autrup, G.D. Stoner, Cancer Res., 42 (1982) 1307 - 1311

[56] G.E. Labuc, M.C. Archer, Cancer Res., 42 (1982) 3181 - 3186

[57] B. Singer, J. Natl. Cancer Inst., 62 (1979) 1329 - 1339

[58] P.N. Magee, R. Montesano, R. Preussmann, in Chemical Carcinogens, ACS Monograph 173, Ed. C.E. Searle, American Chemical Society, Washington, 1976, p573 - 574

[59] P.P. Roller, D.R. Shrimp, L.K. Keefer, Tet. Lett., 25 (1975) 2065 - 2068

[60] O.G. Fahmy, M.J. Fahmy, Cancer Res., 35 (1975) 3780 - 3785

[61] P.N. Magee, D.E. Jensen, E.E. Henderson, Safety evaluation of Nitrosatable Drugs Chemistry, Ed. G.G. Gibson, C. Ioannides, Francis and Taylor (London) 1981 p118 - 140

[62] C.J. Michejda, M.B. Kroeger-Koepke, S.R. Koepke, R.J. Kupper, in N-Nitrosamines, ACS Symposium Series, 101, Ed. J.-P. Anselme, American Chemical Society, 1979, p78 - 89

[63] M. Poulsen, D. Spangler, G.H. Loew, J. Am. Chem. Soc., (in press)

[64] M. Mochizuki, T. Anjo, M. Okada, Tet. Lett., 21 (1980) 3693 - 3696

[65] K.K. Park, M.C. Archer, J.S. Wishnok, Chem.-Biol. Interactions, 29 (1980) 139 - 144

[66] E. Müller, H. Haiss, W. Rundel, Chem. Ber., 93 (1960) 1541 - 1552

[67] R.A. Moss, Acc. Chem. Res., 7 (1974) 421 - 427

[68] D.F. Heath, Biochem. J., 85 (1962) 72 - 91

[69] D.F. Heath, Nature, 192 (1961) 170

[70] P.N. Magee, E. Farber, Biochem. J., 83 (1962) 114 - 124

[71] A. Streitwieser, C.H. Heathcock, Introduction to Organic Chemistry, MacMillan, New York, 1976, p798

[72] W. Lijinsky, J. Loo, A.E. Ross, Nature, 218 (1968) 1174 - 5

[73] A.E. Ross, L. Keefer, W. Lijinsky, J. Natl. Cancer Inst., 47 (1971) 789 - 795

[74] J.D. Scribner, G.P. Ford, Cancer Letters, 16 (1982) 51 - 56

[75] P.N. Magee, T. Hultin, Biochem. J., 83 106 - 114

[76] D.N. Mhaskar, M.J.W. Chang, R.W. Hart, S.M. D'Ambrosio, Cancer Res., 41 (1981) 223 - 229

[77] A. Loveless, Nature, 223 (1969) 206 - 207

[78] P.F. Swann, P.N. Magee, Biochem. J., 110 (1968) 39 - 47

[79] R. Schoental, Br. J. Cancer, 28 (1973) 436 - 439

[80] P.D. Lawley, C.J. Thatcher, Biochem. J., 116 (1970) 693 - 707

[81] P.F. Swann, P.N. Magee, Biochem. J., 125 (1971) 841 - 847

[82] J.V. Frei, D.H. Swenson, W. Warren, P.D. Lawley, Biochem. J., 174 (1978) 1031 - 1044

[83] J.D. Watson, F.H.C. Crick, Nature, 171 (1953) 964 - 967

[84] L.L. Gerchman, D.B. Ludlum, Biochim. Biophys. Acta, 308 (1973) 310 -316

[85] B. Singer, H. Fraenkel-Conrat, J.J. Kusimerek, Proc. Natl. Acad. Sci. USA, 75 (1978) 1722 - 1726

[86] M.F. Argus, C. Hoch-Ligeti, J.C. Arcos, A.H. Conney, J. Natl. Cancer Inst., 61 (1978) 441 - 449

[87] D.R. Umbenhauer, A.E. Pegg, Cancer Res., 41 (1981) 3471 - 3474

[88] G.P. Margison, P. Kleihues, Biochem. J., 148 (1975) 521 - 525

[89] A. Dargelos, S.El Ouadi, D. Liotard, M. Chaillet, Chem. Phys. Lett., 51 (1977) 545 - 551

[90] W.D. Edwards, H. Weinstein, Chem. Phys. Lett., 56 (1978) 582 - 584

[91] A. Pullman, S. Ranganathan, Chem. Phys. Lett., 107 (1984) 107 - 111

[92] M.T. Nguyen, A.F. Hegarty, J.Chem. Soc. Perkin II, (1984) 2037 - 2041

[93] K.A. Jørgensen, S.O. Lawesson, J. Chem. Soc. Perkin II, (1985) 231 - 235

[94] L. Herzig, A.M. Sapse, G. Snyder, J. Comput. Chem., 4 (1983) 68 - 72

[95] D.R. Battiste, L.P. Davis, R.V. Nauman, J. Am. Chem. Soc., 97 (1975) 5071 - 5078

[96] A.R. Farminer, G.A. Webb, J. Mol. Struct., 27 (1975) 417 - 421

[97] K. Kirste, P. Rademacher, J. Mol. Struct., 73 (1981) 171 - 180

[98] O. Gropen, P.N. Skancke, Acta. Chem. Scand., 25 (1971) 1241 - 1249

[99] C. Nagata, A. Imamura, Gann, 61 (1970) 169 - 176

[100] P. Andreozzi, G. Klopman, A.J. Hopfinger, Cancer Biochem. Biophys., 4 (1980) 209 - 220

[101] C. Thomson, D. Provan, S. Clark, Int. J. Quantum Chem. Quantum Biol. Symp., 1977, 4, 205 - 215

[102] A. Skancke, C. Thomson, Int. J. Quant. Chem., 21 (1982) 431 - 443

[103] T.K. Ha, M.T. Nguyen, P. Ruelle, Theochem., (In press)

[104] G.Loew, M.T. Poulsen, D. Spangler, E. Kirkjian, Int. J. Quant. Chem. Quant. Biol. Symp., 10 (1983) 201 - 213

[105] G.P. Ford, J.D. Scribner, J. Am. Chem. Soc., 105 (1983) 349 - 354

[106] J.W.Lown, S.M.S. Chauhan, R.R. Koganty, A.-M. Sapse, J. Am. Chem. Soc., 106 (1984) 6401 - 6408

[107] P.W. Atkins, Quanta, Clarendon Press, Oxford, 1974, p11

[108] P.W. Atkins, Physical Chemistry, O.U.P., Oxford, 1st. Ed. 1978

[109] C.C.J. Roothaan, Rev. Mod. Phys., 23 (1951) 69 - 89

[110] A. Szabo, N.S. Ostlund, Modern Quantum Chemistry, MacMillan, New York, 1982

[111] J.A. Pople, R.K. Nesbet, J. Chem. Phys., 22 (1954) 571 - 2

[112] A.W. Salotto, L. Burnelle, J. Chem. Phys., 52 (1970) 2936 - 2945

[113] J.A. Pople, R. Seeger, R. Krishnan, Int. J. Quant. Chem., S11 (1977) 149 - 163

[114] J.S. Binkley, J.A. Pople, Int. J. Quant. Chem., 9 (1975) 229 - 236

[115] J.A. Pople, J.S. Binkley, R. Seeger, Int. J. Quant. Chem., S10 (1976) 1 - 19

[116] R.F.W. Bader, R.A. Gangi, in Theoretical Chemistry 2, Ed. R.N. Nixon, C. Thomson, Chemical Society, London, 1975 p1 - 65

[117] C. Møller, M.S. Plesset, Phys. Rev., 46 (1934) 618 - 622

[118] T.H. Dunning, jr., P.J. Hay, in Modern Theoretical Chemistry 3, Ed. H.F. Schaefer III, Plenum Press, New York, 1977 p1 - 27

[119] S.F. Boys, Proc. R. Soc. London Ser. A., 200 (1950) 542 - 554

[120] J.S. Binkley, J.A. Pople, W.J. Hehre, J. Am. Chem. Soc., 102 (1980) 939 - 947

[121] P. Pulay, G. Fogarasi, F. Pang, J.E. Boggs, J. Am. Chem. Soc., 101 (1979) 2550 - 2560

[122] W.J. Hehre, R.F. Stewart, J.A. Pople, J. Chem. Phys., 51 (1969) 2657 - 2664

[123] R. Ditchfield, W.J. Hehre, J.A. Pople, J. Chem. Phys., 54 (1971) 724 - 728

[124] W.J. Hehre, R. Ditchfield, J.A. Pople, J. Chem. Phys., 56 (1972) 2257 - 2261

[125] P.C. Hariharan, J.A. Pople, Theor. Chim. Acta, 28 (1973) 213 - 222

[126] L. Radom, in Modern Theoretical Chemistry 4, Ed. H.F. Schaefer III, Plenum Press, New York, 1977, p333 - 356

[127] G.W. Spitznagel, T. Clark, J. Chandrasekhar, P.v.R. Schleyer, J. Comput. Chem., 3 (1982) 363 - 371

[128] T. Clark, J. Chandrasekhar, G.W. Spitznagel, P.v.R. Schleyer, J. Comput. Chem., 4 (1983) 294 - 301

[129] J.G. Chandrasekhar, J.G. Andrade, P.v.R. Schleyer, J. Am. Chem. Soc., 103 (1981) 5609 - 5612

[130] A. Pullman, H. Berthod, N. Gresh, Int. J. Quant. Chem. Symp., 10 (1976) 59 - 76

[131] B. Pullman, N. Gresh, H. Berthod, A. Pullman, Theor. Chim. Acta, 44 (1977) 151 - 163

[132] E. Clementi, J.M. André, M.Cl. Andre, D. Klint, D. Hahn, Act. Phys. Acad. Sci. Hung., Tomus 27 (1969) 493 - 551

[133] M.A. French, L.P. Hills, P. Kebarle, Can. J. Chem., 51 (1973) 456 - 461

[134] P. Pulay, Mol. Phys., 17 (1969) 197 - 204

[135] J.A. Pople, R. Krishnan, H.B. Schlegel, J.S. Binkley, Int. J. Quant. Chem. Quant. Chem. Symp., 13 (1979) 225 - 241

[136] T. Oie, G.H. Loew, S.K. Burt, J.S. Binkley, R.D. MacElroy, Int. J. Quant. Chem. Quant. Biol. Symp., 9 (1982) 223 - 245

[137] E.B. Wilson, J.C. Decius, R.C. Cross, in Molecular Vibrations, McGraw-Hill, New York 1955, p11 - 33, 54 - 76

[138] J.A. Pople, H.B. Schlegel, R. Krishnan, D.J. DeFrees, J.S. Binkley, M.J. Frisch, R.A. Whiteside, Int. J. Quant. Chem. Quant. Chem. Symp., 15 (1981) 269 - 278

[139] R.F. Hout, Jr., B.A. Levi, W.J. Hehre, J. Comput. Chem., 3 (1982) 234 - 250

[140] G. Herzberg, Molecular Spectra and Molecular Structure II Infrared and Raman Spectra of Polyatomic Molecules, Van Nostrand Reinhold, New York, 1945, p501 - 530

[141] A.T. Pudzianowski, G. Loew, J. Phys. Chem., 87 (1983) 1081 - 1085

[142] R.S. Mulliken, J. Chem. Phys., 23 (1955) 1833 - 1840

[143] P. Politzer, K.C. Daiker, in The Force Concept in Chemistry, Ed. B.M. Deb, Van Nostrand Reinhold, New York, 1981 p294 - 387

[144] R. Bonaccorsi, E. Scrocco, J. Tomasi, J. Chem. Phys., 52 (1970) 5270 - 5284

[145] K. Morokuma, K. Kitaura, in Chemical Applications of Atomic and Molecular Electrostatic Potentials, Ed. P. Politzer, D.G. Truhlar, Plenum, New York, 1981 p215 - 242

[146] K. Kitaura, K. Morokuma, Int. J. Quant. Chem., 10 (1976) 325 - 340

[147] J.A. Pople, in Modern Theoretical Chemistry 4, Ed. H.F. Schaefer III, Plenum Press, New York, 1977, p1 - 27

[148] K. Müller, Angew. Chemie, 19 (1980) 1 - 13

[149] H.B. Schlegel, J. Comput. Chem., 3 (1982) 214 - 218

[150] H.B. Schlegel, Theor. Chim. Acta, 66 (1984) 333 - 340

[151] R. Fletcher, Practical Methods of Optimisation Vol 1, John Wiley, Chichester, 1980 p10 - 45

[152] S. Bell, Department of Chemistry, University of Dundee, Personal communication

[153] J.S. Binkley, R.A. Whiteside, R. Krishnan, R. Seeger, D.J. DeFrees, H.B. Schlegel, S. Topiol, L.R. Kahn, J.A. Pople, GAUSSIAN 80, Carnegie-Mellon University, 1980

[154] K. Jug, Theor. Chim. Acta, 54 (1980) 263 - 300

[155] S. Bell, J.S. Crighton, R. Fletcher, Chem. Phys. Lett., 82 (1981) 122 - 126

[156] S. Bell, J.S. Crighton, J. Chem. Phys., 80 (1984) 2464 - 2475

[157] J. Nicholas, Chemical Kinetics, Harper and Row, London, 1976, p102 - 111

[158] D.R. Umbenhauer, A.E. Pegg, Chem.-Biol Int., 33 (1981) 229 - 238

[159] A.E. Pegg, W. Perry, Cancer Res., 41 (1981) 3128 - 3132

[160] S.F. Boys, F. Bernardi, Mol. Phys., 19 (1970) 553 - 566

[161] W. Kolos, Theor. Chim. Acta, 51 (1979) 219 - 240

[162] S. Diner, J.P. Malrieu, F. Jordan, M. Gilbert, Chem. Phys. Lett., 2 (1968) 319 - 323

[163] J.A. Pople, D.L. Beveridge, Approximate Molecular Orbital Theory, McGraw-Hill, New York, 1970, p57 - 84

[164] B. Pullman, in The World of Quantum Chemistry, Ed. R. Daudel, B. Pullman, D. Reidel, Boston, USA, p61 - 89

[165] P.R. Laurence, C. Thomson, Theor. Chim. Acta, 58 (1981) 121 - 4

[166] W.G. Richards, Quantum Pharmacology, 2nd Ed., Butterworths, London, 1983, p203 - 213

[167] A. Pullman, in The World of Quantum Chemistry, Ed. R. Daudel, B. Pullman, D. Reidel, 1974, p239 - 251

[168] M.I.S. Hunter, Dept. of Biochemistry and Microbiology, University of St. Andrews, personal communication

[169] M. Frisch, GAUSSIAN 82 Release A, Carnegie-Mellon University, 1983

[170] J. Ball, unpublished work

[171] D. Peters, M. Sana, QCPE 360 (1978) DENPOT

[172] U.C.Singh, P. Kollman, QCPE Bulletin 2 (1982) 117 QCPE 446

[173] J.R. Bews, Dept. of Chemistry, University of St. Andrews

[174] S. Motherwell, Crytallographic Data Centre, University Chemical Laboratories, Lensfield Lane, Cambridge

[175] R.J. Sampson, SURFACE II, 1978, Kansas Geological Survey, Lawrence, Kansas, USA

[176] GINO-F, Computer-Aided-Design Centre, Madingley Road, CAMBRIDGE

[177] P.I. Reed, K. Haines, P.L.R. Smith, F.R. House, C.L. Walters, The Lancet, (1981) 550 - 552

[178] L.H. Jones, R.M. Badger, G.E. Moore, J. Chem. Phys., 19 (1951) 1599 - 1604

[179] G.E. McGraw, D.L. Bernitt, I.C. Hisatsune, J. Chem. Phys., 45 (1966) 1392 - 1399

[180] L. Farnell, J.F. Ogilvie, Proc. R. Soc. Lond. A 381 (1982) 443 - 455

[181] P. Benioff, G. Das, A.C. Wahl, J. Chem. Phys. 64 (1976) 710 - 717

[182] S. Skaarup, J. E. Boggs, J. Mol. Struct. 30 (1976) 389 - 398

[183] A.P. Cox, A.H. Brittain, D.J. Finnigan, Trans. Faraday Soc., 67 (1971) 2179 - 2194

[184] D.J. Finnigan, A.P. Cox, A.H. Brittain, J.G. Smith, J. Chem. Soc. Faraday Trans. II, 68 (1972) 548 - 565

[185] F.C. Fehsenfeld, M. Mosesman, E.E. Ferguson, J. Chem. Phys., 55 (1971) 2120 - 2125

[186] M.S.B. Munson, J. Am. Chem. Soc., 87 (1965) 2332 - 2336

[187] W.R. Rodwell, L. Radom J. Am. Chem. Soc. 103 (1981) 2865 - 2866

[188] J. Kaufman, Int. J. Quant. Chem. Quant. Biol. Symp., 6 (1979) 503 - 510

[189] V.I. Vedenyev, L.V. Gurvich, V.N. Kondrat'yev, V.A. Medvedev, Ye. L. Trankevich, Bond Energies, Ionisation Potentials and Electron Affinities (English translation), Arnold, 1966

[190] F.C. Fehsenfeld, E.E. Ferguson, J. Chem. Phys., 54 (1971) 439 - 440

[191] S.J. Kuhn, J.S. McIntyre, Can. J. Chem., 44 (1966) 105 - 109

[192] C.J. Michejda, S.R. Koepke, R. Kupper, IARC Sci. Pub. 31 (1980) 155 - 167

[193] B.C. Challis, J.A. Challis, The chemistry of amino, nitroso and nitro compounds and their derivatives part 2, Ed., S. Patai, Wiley, 1982, p1177

[194] C.A. Reynolds, C. Thomson, Int. J. Quant. Chem. Quant. Biol. Symp., 11 (1984) 167 - 181

[195] C.A. Reynolds, C. Thomson, Int. J. Quant. Chem. Quant. Biol. Symp., 12 (1985), (In press)

[196] A.T. Pudzianowski, G.H. Loew, B.A. Mico, R.V. Branchflower, L.A. Pohl, J. Am. Chem. Soc., 105 (1983) 3434 - 3438

[197] G.Loew, M.T. Poulsen, D. Spangler, E. Kirkjian, Int. J. Quant. Chem. Quant. Biol. Symp., 10 (1983) 201 - 213

[198] G.A.J. Goodlad, Dept. of Biochemistry and Microbiology, University of St. Andrews, Personal Communication

[199] K.H. Abramson, P.T. Inglefield, E. Krakower, L.W. Reeves, Can. J. Chem., 1966, 44, 1685 - 1698

[200] M. Mochizuki, T. Anjo, K. Takeda, E. Suzuki, N. Sekiguchi, G.-F. Huang, M. Okada, IARC Sci. Publ., 41, Lyon, 1982, 553 - 559

[201] K. Yoshida, K. Yano, Bull. Chem. Soc. Jpn., 55 (1982) 2200 - 2203

[202] M. Mochizuki, Kycritsu College of Pharmacy, Japan, personal communication

[203] C.A. Reynolds, C. Thomson, Theochem., (submitted)

[204] C.A. Reynolds, C. Thomson, in Molecular Basis of Cancer, Ed. R. Rein, Alan R. Liss, Inc., New York, 1985, p239 - 248

[205] C.J. Casewit, W.A. Goddard III, J. Am. Chem. Soc., 104 1982 3280 - 3287

[206] R. Daudel, G. Leroy, D. Peters, M. Sana, Quantum Chemistry, Wiley, Chichester, 1983, p322

[207] R.H. Nobes, L. Radom, W.R. Rodwell, Chem. Phys. Lett., 74 1980 269 - 272

[208] J.A. Pople, K. Raghavachari, M. Frish, J.S. Binkley, P.v. R. Schleyer, J. Am. Chem. Soc.,105 1983 6389 - 6398

[209] A. Komornicki, C.E. Dykstra, M.A. Vincent, L. Radom, J. Am. Chem. Soc., 103 1981 1652 - 1656

[210] K. Krogh-Jespersen, C.M. Young, R.A. Moss, M. Wiostowski, Tet. Lett., 23 (1982) 2339 - 2342

[211] D.M.G. Lloyd, Department of Chemistry, University of St. Andrews, personal communication

[212] A. Komornicki, K. Ishida, K. Morokuma, R. Ditchfield, M. Conrad, Chem. Phys. Lett., 45 (1977) 595 - 602

[213] C. Dijkgraaf, A.D. Buckingham, N.C. Handy, J.E. Rice, Faraday Symposium 19, Molecular Electronic Structure Calculations - Methods and Applications, Cambridge, 1984 (Poster)

[214] M.J. Field, I.H. Hillier, M.F. Guest, J. Chem. Soc., Chem. Commun., 1984 1310-1311

[215] I.H. Williams, D. Spangler, D.A. Femec, G.M. Maggiora, R.L. Schowen, J. Am. Chem. Soc., 105 1983 31 - 40

[216] C.A. Reynolds, C. Thomson, (to be submitted)

[217] M.A. Vincent, L. Radom, J. Am. Chem. Soc., 100 (1978) 3306 - 3312

[218] P. Demontis, R. Ercoli, A. Gamba, G.B. Suffritti, M. Simonetta, J. Chem. Soc. Perkin II, (1981) 488 - 493

[219] H. Griengl, R. Janoschek, Tetrahedron, 33 (1977) 445 - 448

[220] H.M. Niemeyer, Helv. Chim. Acta, 59 (1976) 1133 - 1139

[221] J.F. McGarrity, D.P. Cox, J. Am. Chem. Soc., 105 (1983) 3961 - 3966

[222] A.R. Butler, Chemistry Department, University of St. Andrews, Personal communication

[223] J. March, Advanced Organic Chemistry: Reactions, Mechanisms and Structure, McGraw-Hill, 1968 p290 - 293

[224] K. Hiraoka, P. Kebarle, J. Am. Chem. Soc., 99 (1977) 360 - 366

[225] M. Arshadi, P. Kebarle, J. Phys. Chem., 74 (1970) 1483 - 1485

[226] J.E. Desnoyers, C. Jolicoeur, in Modern Aspects of Electrochemistry 5, Ed. J.O'M. Bockris, B.E. Conway, Butterworths, London, 1969 p17 - 25

[227] C.E. Klots, B.B. Benson, J. Phys. Chem., 67 (1963) 933 - 934

[228] D.M. Alexander, D.J.T. Hill, Aust. J. Chem., 22 (1969) 347 - 356

[229] S.P. Walch, W.A. Goddard III, J. Am. Chem. Soc., 97 (1975) 5319 - 5330

[230] J.A. Pople, M.S. Gordon, J. Am. Chem. Soc., 89 (1967) 4253 - 4261

[231] J.A. Pople, D.L.Beveridge, Approximate Molecular Orbital Theory, McGraw-Hill, New York, 1970 p110 - 113

[232] G.S. Hammond, J. Am. Chem. Soc., 77 (1954) 334 - 338